



Durham E-Theses

Novel Antimicrobial Coatings

COX, HARRISON,JOHN

How to cite:

COX, HARRISON,JOHN (2022) *Novel Antimicrobial Coatings*, Durham theses, Durham University.
Available at Durham E-Theses Online: <http://etheses.dur.ac.uk/14285/>

Use policy

The full-text may be used and/or reproduced, and given to third parties in any format or medium, without prior permission or charge, for personal research or study, educational, or not-for-profit purposes provided that:

- a full bibliographic reference is made to the original source
- a [link](#) is made to the metadata record in Durham E-Theses
- the full-text is not changed in any way

The full-text must not be sold in any format or medium without the formal permission of the copyright holders.

Please consult the [full Durham E-Theses policy](#) for further details.

Novel Antimicrobial Coatings

PhD Thesis
Department of Chemistry
University of Durham
Harrison John Cox

August 2021

Statement of Copyright

The copyright of this thesis rests with the author. No quotation from it should be published without prior written consent and information derived from it should be acknowledged.

Declaration

The work contained within this thesis was carried out at the Department of Chemistry, University of Durham, between October 2017 and May 2021. It is the original work of this author (except when otherwise stated) and has not been submitted for a degree at this or any other higher education establishment.

Tracey Davey (Electron Microscopy Services, University of Newcastle) performed all electron microscopy within this thesis (Chapters 3 & 4). Joy Paterson acquired Figure 3.8, Figure 3.10, and Figure 3.11 in Chapter 3. Graham Christie (Department of Chemical Engineering and Biotechnology, University of Cambridge) performed antiviral testing (Chapter 4). Emily Unsworth (Department of Chemistry, Durham University) performed ICP-OES analysis (Chapter 4). Gary Oswald (Department of Chemistry, Durham University) performed XRD analysis (Chapter 4). Colin Gibson (Department of Chemistry, Durham University) performed AFM analysis (Chapter 5). Henry Kasper and Mike Packer (Cawthron Institute, New Zealand) performed microalgae biofouling and toxicity testing, and took photographs in Chapter 6. Hayley Andrews (Department of Chemistry, Durham University) prepared coatings, except poly(vinyl pyridine), in Chapter 6. Egemen Ozcelik, Mustafa Karaman, and Mustafa Tabakci (Chemical Engineering Department, Konya Technical University) synthesised the DMAM-calixarene in Appendix 1. Vera Bieber performed chromium filtration in Appendix 1. Preeti Garg and Gurpreet Kaur (Department of Chemistry, Panjab University) synthesised the metallosurfactant in Appendix 3. The switchable surface coating in Appendix 4 was originally created and developed by Angus Ritchie (Department of Chemistry, Durham University).

List of publications

Work in this thesis has been published, has been submitted for publication or is in preparation for publication as follows:

Articles

1. Cox, H. J.; Li, J.; Saini, P.; Paterson, J. R.; Sharples, G. J.; Badyal, J. P. S. Bioinspired and Eco-Friendly High Efficacy Cinnamaldehyde Antibacterial Surfaces. *J. Mater. Chem. B* **2021**, *9*, 2918–2930.
2. Cox, H. J.; Sharples, G. J.; Badyal, J. P. S. Tea–Essential Oil–Metal Hybrid Nanocoatings for Bacterial and Viral Inactivation. *ACS Appl. Nano Mater.* **2021**, *4*, 12619–12628.
3. Cox, H. J.; Gibson, C. P.; Sharples, G. J.; Badyal, J. P. S. Nature-Inspired Substrate-Independent Omniphobic and Antimicrobial Slippery Surfaces. *Adv. Eng. Mater.* **2021**, 2101288.
4. Cox, H. J.; Cooper, I.; Kaspar, H. F.; Packer, M. A.; Badyal, J. P. S. Anti-Biofouling Functional Surfaces for Marine Aquaculture. *Colloids Surfaces A Physicochem. Eng. Asp.* **2022**, 128313.

Patents

1. Cox, H. J.; Hatfield, C.; Badyal, J. P. S. Liquid-Enriched Slippery Surfaces, *patent application filed*, 2021.
2. Cox, H. J.; Li, J.; Badyal, J. P. S. Liquid-Enriched Solid Surfaces, *patent application filed*, 2021.

Collaborative Articles

1. Ritchie, A. W.; Cox, H. J.; Barrientos-Palomo, S. N.; Sharples, G. J.; Badyal, J. P. S. Bioinspired Multifunctional Polymer–Nanoparticle–Surfactant Complex Nanocomposite Surfaces for Antibacterial Oil–Water Separation. *Colloids Surfaces A Physicochem. Eng. Asp.* **2019**, *560*, 352–359.
2. Bieber, V. S.; Ozcelik, E.; Cox, H. J.; Ottley, C. J.; Ratan, J. K.; Karaman, M.; Tabakci, M.; Beaumont, S. K.; Badyal, J. P. S. Capture and Release Recyclable Dimethylaminomethyl-Calixarene Functional Cloths for Point-of-Use Removal of Highly Toxic Chromium Water Pollutants. *ACS Appl. Mater. Interfaces* **2020**, *12*, 52136–52145.
3. Ritchie, A. W.; Cox, H. J.; Gonabadi, H. I.; Bull, S. J.; Badyal, J. P. S. Tunable High Refractive Index Polymer Hybrid and Polymer–Inorganic Nanocomposite Coatings. *ACS Appl. Mater. Interfaces* **2021**, *13*, 33477–33484.

Youtube Video

Antibacterial Surfaces video presentation; <https://youtu.be/sbQ3cq7uCUM>.

Acknowledgements

Many thanks to the following: Professor Jas Pal Badyal, for all of his guidance and support; to all of the members of Lab 98, who made it such a welcoming and friendly place to work; to all of the members of the electrical, mechanical, and glassblowing workshops, who provided plenty of help making and fixing various things for me; to Dr Gary Sharples and Joy Paterson, for allowing me to work in the biology lab and for all the guidance and support they have provided.

Abstract

Antimicrobial coatings play an important role in stopping the spread of pathogens and diseases. This thesis is about the synthesis of novel antimicrobial coatings *via* wet chemical methods and plasmachemical deposition methods.

Chapter 1 provides an overview of the threat posed by bacteria, and the various methods used to stop the spread of pathogens. It also briefly reviews the different types of coating systems used throughout this thesis.

Chapter 2 provides a brief synopsis of the analytical and experimental techniques used in this thesis.

Chapter 3 details the synthesis of a coating that combines polydopamine and cinnamaldehyde. The coating is characterised, including its antibacterial activities. The coating method is extended to tannic acid and polyethyleneimine, both of which also produce antibacterial coatings. The use of porous substrates to absorb cinnamaldehyde to produce long-lasting antibacterial surfaces is also described.

Chapter 4 describes coatings that are produced by combining tea, cinnamaldehyde, and a metal salt. Both copper and silver salts are utilised. The coatings are found to have strong antibacterial efficacies, and are also found to be antiviral against murine coronavirus (mouse hepatitis virus A59), a potential surrogate for SARS-CoV-2.

Chapter 5 describes how pulsed plasma polymer coatings can be combined with liquid lubricants to produce slippery surfaces. A range of different monomers and lubricants are tested, with many forming slippery surfaces that exhibit excellent water repellency. Fluorinated systems are used to produce omniphobic slippery surfaces. Use of cinnamaldehyde as a lubricant endows the slippery surfaces with strong antibacterial efficacy.

Chapter 6 details how pulsed plasma coatings may be used to prevent (or encourage) fouling of microalgae on surfaces. Hydrophilic coatings produce the best anti-biofouling results, and are non-toxic towards the microalgae species tested.

Contents

1	Introduction and Literature Review	15
1.1	Bacteria	15
1.2	Why Antimicrobial Coatings?	17
1.2.1	Antibiotics	17
1.2.2	Vaccines	19
1.2.3	Natural Remedies	20
1.2.4	Social Measures	21
1.2.5	Sterilization	22
1.2.6	Antimicrobial Coatings	22
1.3	Literature Review	28
1.3.1	Cinnamaldehyde	29
1.3.2	Polydopamine	30
1.3.3	Tannic Acid	31
1.3.4	Polyethyleneimine	32
1.3.5	Tea	32
1.3.6	Slippery Liquid Infused Porous Surfaces	33
1.4	Scope of Thesis	34
1.5	References	37
2	Experimental Methods	54
2.1	Plasma Deposition	54
2.2	Infrared Spectroscopy	57
2.3	Antibacterial Testing	58
2.4	Film Thickness Measurements	60
2.5	Contact Angle Measurements	61
2.5.1	Contact Angle	61
2.5.2	Contact Angle Hysteresis	62
2.5.3	Sliding Angle	63
2.6	UV-Vis Spectroscopy	63
2.7	X-Ray Photoelectron Spectroscopy	64
2.8	Scanning Electron Microscopy	65
2.9	Transmission Electron Microscopy	66
2.10	X-Ray Diffraction	66
2.11	Raman Spectroscopy	67
2.12	Mass Spectrometry	67

2.13	Inductively Coupled Plasma Optical Emission Spectroscopy.....	68
2.14	Atomic Force Microscopy.....	68
2.15	References.....	70
3	Cinnamaldehyde Antibacterial Surfaces.....	71
3.1	Introduction	71
3.2	Experimental	72
3.2.1	Coating Preparation	72
3.2.2	Coating Characterisation	74
3.2.3	Antibacterial Testing.....	74
3.3	Results.....	74
3.3.1	Polydopamine–Cinnamaldehyde Coating.....	74
3.3.2	Poly(norepinephrine)–Cinnamaldehyde Coating	84
3.3.3	Polyethyleneimine–Cinnamaldehyde Coating	86
3.3.4	Tannic Acid–Cinnamaldehyde Coating	89
3.3.5	Cinnamaldehyde–Porous Substrates	92
3.4	Discussion.....	94
3.5	Conclusions	96
3.6	References.....	97
4	Antimicrobial Tea Coatings.....	100
4.1	Introduction	100
4.2	Experimental	101
4.2.1	Materials.....	101
4.2.2	Tea Coatings Preparation.....	102
4.2.3	Coating Characterisation	103
4.2.4	Metal Leaching	104
4.2.5	Antibacterial Testing.....	104
4.2.6	Antiviral Testing.....	104
4.3	Results.....	105
4.3.1	Tea–Cinnamaldehyde Coating	105
4.3.2	Tea–Cinnamaldehyde–Copper Coating	108
4.3.3	Tea–Cinnamaldehyde–Silver Coating	112
4.3.4	Antibacterial Testing.....	116
4.3.5	Antiviral Testing.....	116
4.4	Discussion.....	117
4.5	Conclusions	120

4.6	References.....	121
5	Slippery Lubricant Infused Surfaces.....	126
5.1	Experimental.....	129
5.1.1	Pulsed Plasmachemical Deposition.....	129
5.1.2	Polystyrene Surfaces.....	130
5.1.3	Formation of Slippery Lubricant-Infused Surfaces.....	130
5.1.4	Coating Characterisation.....	131
5.1.5	Contact Angle Analysis.....	131
5.1.6	Sliding Angle Analysis.....	131
5.1.7	Foodstuffs Repellency.....	132
5.1.8	Antibacterial Testing.....	132
5.2	Results.....	133
5.2.1	Control Studies.....	133
5.2.2	Pulsed Plasma Poly(Hexyl Acrylate).....	135
5.2.3	Pulsed Plasma Poly(Styrene).....	137
5.2.4	Pulsed Plasma Poly(Benzyl Acrylate).....	138
5.2.5	Pulsed Plasma Poly(Vinylbenzaldehyde).....	139
5.2.6	Pulsed Plasma Poly(Vinylbenzyl Chloride).....	141
5.2.7	Pulsed Plasma Poly(Perfluoroallylbenzene).....	143
5.2.8	Pulsed Plasma Poly(Vinylaniline).....	144
5.2.9	Pulsed Plasma Poly(Vinylpyridine).....	150
5.2.10	Pulsed Plasma Poly(Glycidyl Methacrylate).....	152
5.2.11	Pulsed Plasma Poly(Pentafluorostyrene).....	154
5.2.12	Pulsed Plasma Poly(1H, 1H, 2H, 2H-Perfluorooctyl Acrylate).....	155
5.3	Discussion.....	156
5.4	Conclusions.....	159
5.5	Videos.....	160
5.6	References.....	161
6	Anti-Biofouling Coatings for Marine Aquaculture.....	165
6.1	Introduction.....	165
6.2	Experimental.....	167
6.2.1	Pulsed Plasma Deposition.....	167
6.2.2	Coating Characterisation.....	168
6.2.3	Immersed Coating Stability.....	168
6.2.4	Biofouling Testing.....	168

6.2.5	Toxicity Testing	169
6.3	Results	172
6.3.1	Biofouling.....	172
6.3.2	Toxicity	175
6.4	Discussion.....	176
6.5	Conclusions	178
6.6	References.....	179
7	Conclusions and Further Work.....	182
7.1	Conclusions	182
7.2	Further Work.....	184
Appendix 1	185
A1.1	Introduction	185
A1.2	Experimental	186
A1.2.1	Pulsed Plasma Deposition.....	186
A1.2.2	DMAM-Calixarene Immobilisation	186
A1.2.3	Characterisation	187
A1.2.4	Antibacterial Testing.....	187
A1.3	Results.....	187
A1.3.1	Characterisation	187
A1.3.2	Antibacterial Testing.....	189
A1.3.3	Chromium Filtration	190
A1.4	Conclusions	190
A1.5	References.....	192
Appendix 2	193
A2.1	Introduction	193
A2.2	Experimental	193
A2.2.1	Pulsed Plasma Deposition.....	193
A2.2.2	Quaternization	194
A2.2.3	Characterisation	194
A2.2.4	Antibacterial Testing.....	194
A2.3	Results.....	194
A2.3.1	Characterisation	194
A2.3.2	Antibacterial Testing.....	195
A2.4	Discussion.....	196

A2.5	Conclusions	196
A2.6	References.....	197
Appendix 3	198
A3.1	Introduction	198
A3.2	Experimental	199
A3.2.1	Atomised Spray Plasma Deposition of Nanocomposite Layers	199
A3.2.2	Characterisation	200
A3.3	Results	200
A3.4	Discussion.....	201
A3.5	Conclusions	201
A3.6	References.....	203
Appendix 4	207
A4.1	Introduction	207
A4.2	Experimental	207
A4.2.1	Polymer–Particle–Fluorosurfactant Complex Coatings	207
A4.2.2	Antibacterial Testing.....	208
A4.3	Results	208
A4.4	Discussion.....	209
A4.5	Conclusions	209
A4.6	References.....	210

List of Figures

Figure 1.1: Structure of trans-cinnamaldehyde	29
Figure 1.2: Structure of dopamine	30
Figure 1.3: Structure of polydopamine	30
Figure 1.4: Structure of tannic acid	31
Figure 1.5: Structure of polyethyleneimine	32
Figure 1.6: Structures of tea polyphenols	33
Figure 2.1: Pulsed plasma deposition apparatus	55
Figure 2.2: Schematic of pathways of incident light on a thin film	60
Figure 2.3: Schematic demonstrating surface tensions and contact angle for a droplet	62
Figure 2.4: XPS emission of a photoelectron from core energy level into vacuum	64
Figure 3.1: Deposition of antibacterial coatings	71
Figure 3.2: Photographs of polydopamine coating solutions and coatings	76
Figure 3.3: FTIR spectra of cinnamaldehyde and polydopamine coatings	77
Figure 3.4: UV-Vis spectra of cinnamaldehyde and polydopamine coatings	78
Figure 3.5: Reaction of cinnamaldehyde with phenethylamine to form imine product	79
Figure 3.6: ASAP mass spectrum of product of phenethylamine and cinnamaldehyde reaction.	79
Figure 3.7: Antibacterial recycling of polydopamine–cinnamaldehyde; polyethyleneimine– cinnamaldehyde; and tannic acid–cinnamaldehyde	81
Figure 3.8: Bacteria plate counts of untreated PET	81
Figure 3.9: SEM images of uncoated and polydopamine–cinnamaldehyde coated PET surfaces	82
Figure 3.10: Bacteria plates after sample treatment.	82
Figure 3.11: Bacteria plates after sample treatment	83
Figure 3.12: UV-Vis spectroscopy of coating cinnamaldehyde release	84
Figure 3.13: Structure of norepinephrine	84
Figure 3.14: Photographs of polynorepinephrine coatings	85
Figure 3.15: FTIR spectra of polynorepinephrine coatings	86
Figure 3.16: FTIR spectra of polyethyleneimine coatings	88
Figure 3.17: Photographs of tannic acid coatings	89
Figure 3.18: FTIR spectra of tannic acid coatings	91
Figure 3.19: Antibacterial recycling of cinnamaldehyde impregnated polypropylene cloth	92
Figure 3.20: Antibacterial recycling of polydopamine–cinnamaldehyde coated polypropylene cloth	93
Figure 4.1: Photographs of tea coatings	106
Figure 4.2: Photographs of tea coatings with larger cinnamaldehyde quantities	106
Figure 4.3: Coating thickness of tea coatings	107

Figure 4.4: FTIR spectra of tea coatings.....	108
Figure 4.5: Photographs of tea–copper coatings with larger copper quantities	108
Figure 4.6: XRD patterns for tea coatings.....	110
Figure 4.7: TEM images of tea–cinnamaldehyde–metal coatings	110
Figure 4.8: Raman spectra tea coatings	111
Figure 4.9: ICP-OES of metal leaching of tea–cinnamaldehyde–metal coatings	112
Figure 4.10: Photographs of tea–silver coatings with larger silver quantities	113
Figure 4.11: Photographs of glass slides with tea–cinnamaldehyde–metal coatings.....	114
Figure 4.12: Photographs of PTFE with tea–cinnamaldehyde–metal coatings	115
Figure 4.13: Photographs of hydrophilic non-woven polypropylene cloth with tea– cinnamaldehyde–metal coatings	115
Figure 4.14: Photographs of cotton gloves with tea–cinnamaldehyde–metal coatings	115
Figure 4.15: Photographs of tennis balls with tea–cinnamaldehyde–metal coatings	116
Figure 4.16: Personal protection face masks with tea–cinnamaldehyde–metal coatings.....	117
Figure 5.1: Pulsed plasma deposited slippery lubricant-infused nanocoatings	127
Figure 5.2: Lubricant chemical structures	127
Figure 5.3: Chemical structures of pulsed plasma functional nanolayers.....	128
Figure 5.4: FTIR spectra of pulsed plasma poly(hexyl acrylate).....	135
Figure 5.5: AFM images of pulsed plasma poly(hexyl acrylate) coated silicon wafer.....	136
Figure 5.6: FTIR spectra of pulsed plasma poly(styrene)	137
Figure 5.7: FTIR spectra of pulsed plasma poly(benzyl acrylate).....	139
Figure 5.8: FTIR spectra of pulsed plasma poly(vinylbenzaldehyde)	140
Figure 5.9: FTIR spectra of pulsed plasma poly(vinylbenzyl chloride).....	142
Figure 5.10: FTIR spectra of pulsed plasma poly(perfluoroallylbenzene)	143
Figure 5.11: FTIR spectra of pulsed plasma poly(vinylaniline)	145
Figure 5.12: Time lapse photographs of foodstuffs on slippery surfaces.....	147
Figure 5.13: Antibacterial tests for pulsed plasma poly(vinylaniline)–cinnamaldehyde lubricant infused coating.....	148
Figure 5.14: FTIR spectra of pulsed plasma poly(vinylpyridine)	151
Figure 5.15: FTIR spectra of pulsed plasma poly(glycidyl methacrylate)	153
Figure 5.16: FTIR spectra of pulsed plasma poly(pentafluorostyrene)	154
Figure 5.17: FTIR spectra of pulsed plasma poly(1H,1H,2H,2H-perfluorooctyl acrylate).....	155
Figure 6.1: Functional nanocoatings	166
Figure 6.2: Photographs of microalgal biofouling apparatus	169
Figure 6.3: Photographs of microalgal toxicity apparatus	171
Figure 6.4: Photographs of microalgal biofouling on samples	173
Figure 6.5: Pulsed plasma poly(vinylpyridine) coating thickness variation with time of immersion in water	174
Figure 6.6: FTIR spectra of samples immersed in microalgae.	175
Figure 6.7: Growth and photosynthetic health of microalgae treated with coated samples.....	176

Figure A1.1: Structure of DMAM-calixarene	185
Figure A1.2: Mechanism of immobilisation of DMAM-calixarene onto poly(vinylbenzyl chloride)	186
Figure A1.3: Antibacterial test results for DMAM-calixarene immobilised cloths	190
Figure A2.1: Schematic for coating of pulsed plasma poly(vinylbenzyl chloride) and quaternisation with butylimidazole.....	193
Figure A2.2: XPS spectra of pulsed plasma poly(vinylbenzyl chloride) and quaternised pulsed plasma poly(vinylbenzyl chloride)–butylimidazole	195
Figure A2.3: Antibacterial test results for quaternised pulsed plasma poly(vinylbenzyl chloride)– butylimidazole coated cloths.....	196
Figure A3.1: ASPD poly(di(ethylene glycol) ethyl ether acrylate) nanocomposite layers with Cu(DDA) metallosurfactant.....	199
Figure A3.2: Structure of bis(dodecylamine) copper dichloride (Cu(DDA)).	199
Figure A3.3: Antibacterial test results of ASPD poly(di(ethylene glycol)ethyl ether acrylate)– Cu(DDA) coated cloth.....	200
Figure A4.1: Antibacterial test results of poly(diallyldimethylammonium)–anionic fluorosurfactant complex spray coated non-woven polypropylene cloth and poly(diallyldimethylammonium)–3% w/v silica (7 nm)–anionic fluorosurfactant spray coated non-woven polypropylene cloth	208

List of Tables

Table 1.1: Common bacteria that cause infections in the UK, and their societal impact.	15
Table 3.1: Mass increases for cinnamaldehyde surfaces	76
Table 3.2: Antibacterial activities for cinnamaldehyde coatings.....	80
Table 4.1: Experimental parameters for fabrication of tea–cinnamaldehyde–metal coatings. .	103
Table 4.2: Thickness values for tea-based coatings	106
Table 4.3: XPS atomic percentages of tea-based coatings	109
Table 4.4: Antibacterial test results for tea-based coatings	116
Table 4.5: Antiviral test results for tea-based coatings	117
Table 5.1: Pulsed plasma deposition parameters for deposited polymer coatings, film thicknesses values and deposition rates.	130
Table 5.2: Water contact angle values and sliding angle values for control substrates	133
Table 5.3: Water contact angle values and sliding angle values for slippery surfaces.....	134
Table 5.4: Water contact angle values following lubricant impregnation of pulsed plasma poly(hexyl acrylate) coated substrates	136
Table 5.5. Water droplet sliding angle values for pulsed plasma poly(vinylbenzaldehyde) coated porous polypropylene cloth substrates.	141
Table 5.6: Antibacterial test results for pulsed plasma poly(vinylaniline)–cinnamaldehyde coating	148
Table 5.7: Water droplet sliding angle values for pulsed plasma poly(vinylaniline) coated porous polypropylene cloth substrates	150
Table 5.8: Water contact angle values for pulsed plasma poly(vinylpyridine) coating.....	152
Table 5.9: Water contact angle values for pulsed plasma poly(glycidyl methacrylate) coating	153
Table 5.10: Water contact angle values for pulsed plasma poly(pentafluorostyrene) coating..	155
Table 5.11: Water contact angle values for pulsed plasma poly(1H, 1H, 2H, 2H-perfluorooctyl acrylate) coating	156
Table 6.1: Pulsed plasma deposition parameters and nanocoating growth rates.	167
Table A1.1: XPS compositions for pulsed plasma deposited poly(vinylbenzyl chloride) and pulsed plasma-deposited poly(vinylbenzyl chloride) functionalized with DMAM-calixarene	188
Table A2.1: XPS compositions pulsed plasma deposited poly(vinylbenzyl chloride) and pulsed plasma-deposited poly(vinylbenzyl chloride) functionalized with butylimidazole.	195

CHAPTER 1

1 Introduction and Literature Review

1.1 Bacteria

The name 'Bacteria' refers to one of the kingdoms of prokaryotic organisms. Most bacteria are single-celled organisms, with sizes ranging from 0.5 to 4 μm .¹ There are a large number of bacterial species known, many of which are non-pathogenic.¹ However, there are several species that are pathogenic and have negative impacts on the host, and cause diseases. Several of the most common pathogenic bacteria that cause infection found in the UK, and their impact on society, are shown in Table 1.1.

Table 1.1: Common bacteria that cause infections in the UK, and their societal impact.

Name of Bacteria	Societal Impact
<i>Campylobacter</i> spp.	<ul style="list-style-type: none"> • <i>Campylobacter</i> is the most common cause of food poisoning in the UK.² • 56,279 laboratory reports in 2017 (England & Wales), equates to 96.57 cases per 100,000 population.³ • <i>Campylobacter</i> is estimated to have caused 76 deaths in the UK in 2008.² • Food Standards Agency estimates that <i>Campylobacter</i> costs the UK economy £900 million per year.⁴
<i>Escherichia coli</i>	<ul style="list-style-type: none"> • 40,580 reported cases from 2019/20 (England), which equates to 73.9 cases per 100,000 population. An increase of 34% from 2012/13 (n = 32,309).⁵ • Treatment of <i>E. coli</i> infections costs the UK an estimated £14 million per annum.⁶ • From 2011 to 2015, there were 89 deaths in Wales attributed to <i>E. coli</i>.⁷ (Total population Wales roughly 3 million).
<i>Streptococcus</i> spp.	<ul style="list-style-type: none"> • 18,057 reports of streptococcal infections in 2019 (England, Wales & N. Ireland).⁸ An increase of 39% from 2015 (n=13,012). • In 2016, there were 19,206 reports of Scarlet Fever in England & Wales (a rate of 33.2 cases per 100,000 population). The highest it has been since 1967.⁹ • The cost of Invasive Group A Streptococcal infections are estimated to be “£1,984-£2,212 per case, totalling £4.43-£6.34 million per year in England.”¹⁰ • Group B <i>Streptococcus</i> (<i>S. agalactiae</i>) resistance to clindamycin and erythromycin was 23 and 29% respectively in 2016 (an increase from 17 & 18% in 2011). Tetracycline resistance in this group was 84% in 2016.

	Group A <i>Streptococcus</i> (<i>S. pyogenes</i>) resistance was at 5, 7 & 10% for the three drugs in 2016. ⁸
<i>Clostridium difficile</i>	<ul style="list-style-type: none"> • 13,177 cases were reported from 2019/20 (England). This equates to a rate of 23.4 cases per 100,000 population.⁵ • The cost to the NHS for treating a <i>C. difficile</i> infection is roughly £10,000.¹¹ • In 2012, there were 1,646 deaths involving <i>C. difficile</i> infection in England and Wales.¹²
Methicillin-resistant <i>Staphylococcus aureus</i> (MRSA)	<ul style="list-style-type: none"> • 814 reported cases from 2019/20 (England), which equates to 1.5 cases per 100,000 population.⁵ • In 2012, <i>S. aureus</i> caused 557 deaths (England & Wales), 292 of which were attributed to MRSA.¹³ • The cost to the NHS for treating a MRSA infection is roughly £7000.¹¹
Methicillin-susceptible <i>Staphylococcus aureus</i> (MSSA)	<ul style="list-style-type: none"> • 12,193 reported cases from 2019/20 (England), which equates to 20.9 cases per 100,000 population.⁵ This is an increase of 39.1% from 2011/12 (n = 8,767).
<i>Mycobacterium tuberculosis</i>	<ul style="list-style-type: none"> • 4,725 cases reported in 2019 (England), which equates to 8.4 cases per 100,000 population.¹⁴ • 231 people were reported to have died of tuberculosis in the UK in 2018.¹⁴ • The costs to the NHS of treating 'normal' and 'drug-resistant' tuberculosis are estimated at £5000 and £50,000–£70,000 per case respectively.¹⁵
<i>Salmonella</i> spp.	<ul style="list-style-type: none"> • 8,630 cases reported in 2016 (England & Wales), which equates to a rate of 14.8 cases per 100,000 population.¹⁶
<i>Enterococcus</i> spp.	<ul style="list-style-type: none"> • 8,136 cases reported in 2018 (England, Wales & N. Ireland), which equates to a rate of 13.3 cases per 100,000 population.¹⁷
<i>Pseudomonas aeruginosa</i>	<ul style="list-style-type: none"> • 4,336 cases reported in 2019/20 (England), which equates to a rate of 7.7 cases per 100,000 population.⁵

In developing countries, the situation is often worse, as nations are less able to help prevent infections, and people may be more vulnerable (due to being malnourished, immunocompromised, or HIV-positive).^{18, 19} For example, *Campylobacter* infections in developed countries such as Germany or the USA were found to have a case-fatality ratio of $\leq 0.1\%$, whilst in Kenya the case-fatality ratio was 8.8%.^{20, 21} There is therefore a need to combat the threat of bacterial infection on the global scale.

1.2 Why Antimicrobial Coatings?

Humans have developed several methods to deal with the threat of bacteria and pathogenic diseases, which includes antibiotics, vaccines, natural remedies, social measures, and antimicrobial coatings. Here, we will examine each one, and consider their advantages and disadvantages.

1.2.1 Antibiotics

Antibiotics are a type of drug, medicine or substance that are used to treat an infection caused by bacteria, either by killing the bacteria (bactericidal) or inhibiting their growth (bacteriostatic).²² Since the early twentieth century and the discovery of penicillin, significant research into antibiotics has resulted in a variety of medicines, allowing for the treatment of a whole range of diseases, thus having the clear advantage of increasing humans' expected lifespans and decreasing mortality rates against these pathogens²³, as well as uses in preventing infections in animals and in plants.^{24, 25} However, there are some disadvantages associated with the usage of antibiotics, namely, side effects and antibiotic resistance. Side effects are the lesser of these two problems—side effects occur when a person's body has an unwanted reaction to a medicine, and common symptoms can include vomiting, nausea, and diarrhoea, or allergic reactions such as rashes or breathing difficulties.²⁶ The more serious problem is the evolution of antibiotic resistance (also called antimicrobial resistance). Antibiotic resistance occurs when a population of bacteria, some of which have random mutations, are treated with an antibiotic. These mutations may confer upon the bacteria the necessary changes required to prevent the mechanism of action of the drug molecule, such as blocking the drug molecule from its target, or altering the antibiotic target site.^{27, 28} Therefore, when treated with the antibiotic, bacteria without the mutation will be killed, leaving the mutant bacteria alive. This mutant strain can then proliferate, unaffected by the drug, to produce a population of which all (or a considerable proportion) now have the mutation that endows them with antibiotic resistance, meaning that the antibiotic is rendered inactive for treating the infection. To further exacerbate matters, bacteria are capable of 'horizontal gene transfer', a process where bacteria are able to transfer DNA from one cell to another.^{28, 29} In this way, drug resistant bacteria can transfer antibiotic resistance

genes to non-resistant bacteria that may have never even been exposed to antibiotics.

Some form of resistance has been observed for nearly all antibiotics that have been produced.³⁰ Antimicrobial resistance has been described by the World Health Organization as “one of the top 10 global public health threats facing humanity”.³¹ The emergence of antimicrobial resistance has been caused by several different factors: (i) Overuse—in many countries, particularly developing ones, there is little or no regulation regarding antibiotics, they are readily available to purchase, and with no prescriptions needed (or prescriptions are readily given out). This has led a high-level of over-prescriptions and overuse.³² Even in developed countries, for example the U.S., overuse is a problem, and in some states the number of antibiotic courses prescribed in a year exceeds the population of that state.³³ The result is that antibiotic resistant bacteria kill 23,000 people per year in the U.S.³³

(ii) Misuse—many people may lack an understanding of what antibiotics are and what they used for.^{34, 35} This can lead to people taking antibiotics for illnesses that antibiotics are completely ineffective against. For example, it has been reported that, during the COVID-19 pandemic, sales of antibiotics in India increased, and many patients were given strong antibiotics, despite evidence that they are ineffective against the disease.^{36, 37}

(iii) Environmental pollution—antibiotics can enter the environment through multiple different routes, including waste from pharmaceutical factories, from excrement after usage (i.e. sewage), and disposal of unused medicines.³⁸ Many sewage treatment plants are unable to effectively completely remove antibiotics from waste water, meaning that much of the excreted antibiotics ultimately end up being released into the environment.³⁹ The result is that antibiotics have been detected in river water⁴⁰, seawater⁴¹, and even in tap water.^{40, 42} Once in the environment, antibiotics are able to transfer from water to soil, and on to plants, including vegetables and crops, where they can produce negative effects on the growth of the plants.^{43, 44} Certain antibiotics, for example penicillin, will degrade rapidly once released into the environment⁴⁵, whereas others, for example tetracycline and roxithromycin, can persist in soil for weeks and even months before degradation to non-detectable levels.^{46, 47}

(iv) Lack of development—over the past several decades, research into drug discovery and the development of new antibiotics has declined (although it has

picked up again in recent years).⁴⁸ There are numerous reasons for this, including reduced academic funding, strict regulations, long development times leading to reluctance by pharmaceutical companies/investors due to a potential lack of return or profit on the large sums of money required throughout the development pipeline.⁴⁸

1.2.2 Vaccines

Vaccines are inactivated or attenuated pathogens, or a subunit of a pathogen such as a protein or a nucleic acid, or a toxin, or RNA. A vaccine administered to an individual is designed to not infect the individual with the disease, but to invoke a response from the immune system, which will then fight off the vaccine, and subsequently, the body will ‘remember’ how to fight the infection, leading to the production of antibodies, and immunisation against the pathogen.⁴⁹ Vaccines are therefore used to prevent individuals from becoming infected and protect against diseases. It is undeniable that vaccines are highly effective, and have been very important in massively reducing the number of cases and the mortality rates of several diseases, as well as in eradicating diseases completely (e.g. smallpox).⁵⁰ ⁵¹ Vaccines have been described by the U.S. Centre for Disease Control and Prevention (CDC) as one of the ‘ten great public health achievements’.⁵²

There are however also several disadvantages associated with vaccines:

(i) Waning immunity—as time progresses after someone has had a vaccination, the efficacy of the vaccine, and the ability of the immune system to effectively fight the disease, may diminish leading to increased susceptibility towards infection.^{53, 54} For example, influenza virus vaccinations have been observed to decrease in effectiveness by about 6%–11% per month.⁵⁵ This effect can be offset by offering ‘booster’ vaccinations to help improve and prolong immunisation.

(ii) Shortages—there have been several examples in recent years of countries experiencing shortages of vaccines due to suppliers being unable to meet the levels of demand, which ultimately means that, even if the vaccine itself is highly efficacious, people do not receive it and thus can become infected and become hospitalised or die.^{56, 57, 58, 59}

(iii) Development cost—the total lifetime development costs for vaccines can be very large (several hundred million U.S. dollars), with pharmaceutical companies

needing to recoup the costs.⁶⁰ Historically, the average time required to develop a new vaccine is about 10 years, and only 6% of new vaccine ultimately would enter the market.⁶¹

(iv) Lack of vaccine—there are still several infectious and deadly diseases which do not have any effective vaccine available, including HIV-AIDS, Ebola, and *E. coli* (to name but a few).⁶²

(v) Hesitancy—there exists a number of people in the world whom are hesitant or reluctant to take vaccines.^{63, 64} The reasons for this are generally complex and multi-faceted, and a detailed explanation is outside the scope of this review. However, in simple broad terms, it is generally due to the perception that there are negative effects caused by the vaccine(s), and that the benefits of taking the vaccine(s) are outweighed by these potential negative effects.⁶³ Often there is little or no plausible or peer-reviewed scientific evidence to support the claims of negative effects (for example, claims that the measles, mumps, and rubella (MMR) vaccine causes autism in young children).⁶⁵

1.2.3 Natural Remedies

Traditional medicine has been used to treat illnesses for thousands of years.⁶⁶ Natural or herbal remedies typically consist of a plant extract containing many different chemical compounds, one or more of which works as an active ingredient to help treat the disease.⁶⁷ Even today, for many people around the world, traditional medicine is often the primary or sole source of healthcare.⁶⁸

Over 50% of commercially available drugs contain (or at one point contained) compounds derived from (or patterned from) biological sources (e.g. plants).⁶⁹

However, there are several issues associated with traditional medicines, including:

(i) Regulation—in many parts of the world, there is little or no regulation regarding herbal remedies, meaning that people are free to sell them without needing to provide any evidence of their quality, safety, or efficacy.⁶⁷

(ii) Toxicity—many traditional medicines are sold with no evaluation of their toxicological properties. Many such medicines have been found to cause side effects and even be poisonous.⁶⁷

(iii) Unscientific—some concepts found in traditional medicine (such as yin and yang in Chinese traditional medicine) are considered by some to be “pseudoscience” and are inaccurate and “verge on imagination”.⁷⁰ Many of these

are deeply rooted in culture, and people are often unwilling to let go of these ideas in favour of modern concepts.⁷⁰

1.2.4 Social Measures

Social measures are methods of stopping the spread of pathogens and infections that do not involve the use of drugs, medicines, or vaccines, and instead consists of providing instructions for people to follow. One of the most important of these is hand-washing.⁷¹ Many pathogens are able to survive on fomites (objects that are likely to carry infection, such as touch surfaces, e.g. door handles, tabletops, etc.) for several hours⁷², and once transferred to hands, are again able to survive for hours—for example, *Pseudomonas aeruginosa* and *Burkholderia cepacia* strains were found to be transmissible *via* hand-shaking for up to 180 min.⁷³ Hand-washing therefore is a simple easy method to reduce infection.⁷⁴ This is particularly important in hospital and healthcare settings where patients are more vulnerable, and hand-washing has been shown to reduce the number of nosocomial infections.⁷⁵ Hand-washing is also vital for preventing the spread of pathogens on foodstuffs⁷⁶, preventing communicable illness in schoolchildren⁷⁷, and in the prevention of diarrhoea (which is caused by bacteria, viruses, and parasites, and causes an estimated 1.8 million deaths in children in low- and middle-income countries).⁷⁸ Soap is able to destabilise the lipid membranes of bacteria and viruses, rupturing the system, thus killing bacteria and inactivating viruses.

After the outbreak of the COVID-19 global pandemic, countries and governments around the world introduced various measures to help contain the spread of the SARS-CoV-2 virus, including mandatory wearing of face masks.⁷⁹ ⁸⁰ Masks can help to reduce the transmission of airborne pathogens from person to person, and whilst the level of protection may not be perfect, it is generally better than no face mask at all.^{80, 81, 82} Other measures include mandatory quarantines⁸³, travel bans⁸³, and social distancing.⁸⁰

The main disadvantage of all of these measures is that of compliance—in order for these measures to be effective, everyone must follow the rules and do what is asked of them in order to help limit the spread of disease. However, people may resist these rules, particularly where they are perceived to infringe on an individual's independence, or because the rules are considered

uncomfortable or inconvenient.^{84, 85} Failure to comply with the mandatory social measures may ultimately lead to further infections and spread of disease.

1.2.5 Sterilization

There are several different sterilization techniques used, including heat sterilization, radiation (ultraviolet, ionising) sterilization, and disinfectants (e.g. sodium hypochlorite (bleach), ethanol), in order to kill bacteria contaminants on a surface.¹ These techniques may be effective at killing pathogens, but their main disadvantage is that treated surfaces are not rendered permanently antimicrobial, and are potentially free for bacteria to re-contaminate the surface.

1.2.6 Antimicrobial Coatings

Many pathogenic bacteria are able to survive for months on dry surfaces, which can result in increased transmission *via* people's hands coming into contact with the surface.⁸⁶ This is of particular concern in hospitals where patients may be more susceptible to infection, and transmission may occur either directly to patients, or initially to healthcare workers who then pass it on to patients.⁸⁶ Another issue is that of biofilm formation—this is a process where bacteria attach themselves to a surface using an extracellular polymer matrix.⁸⁷ Biofilm allows bacteria to adhere to surfaces much more strongly than they would otherwise be able to, and once bacteria become encapsulated within a biofilm, they are much less susceptible to antimicrobial agents.⁸⁷ Bacterial adhesion is a constant problem with regards to medical devices and implants, where colonization of bacteria can lead to serious infections.⁸⁸ Pathogenic bacteria are able to contaminate a range of common touch surfaces, whereupon they can spread to people, either directly *via* hand/skin contact, or indirectly *via* contamination of foods or water.^{89, 90, 91, 92}

Therefore, surfaces that are capable of killing bacteria (bactericidal) are key for the reduction and prevention of infections.⁹³ Antimicrobial coatings, as the name suggests, are coatings that are applied to surfaces which are capable of killing microbes such as bacteria, and thus can help prevent the spread of infection and biofilm formation. In general, antibacterial coatings can be categorised into three groups, depending on their mode of action: (i) repellent surfaces; (ii) leachable (release) surfaces; and (iii) contact-kill (non-release) surfaces.

1.2.6.1 Repellent Surfaces

Repellent surfaces are those that do not kill bacteria, but prevent the adhesion of bacteria cells. There are several methods by which this can be achieved:

Superhydrophobic Surfaces: Superhydrophobic surfaces are typically characterised as having a water contact angle of $\geq 150^\circ$.⁹⁴ In one report, paper was made superhydrophobic *via* deposition of poly(diallyldimethylammonium chloride) and silica particles and fluorination with 1H,1H,2H,2H-perfluorooctyltriethoxysilane, and it was found that only 7% of *Escherichia coli* cells adhered to the surface compared to the untreated control.⁹⁵ Another study showed that textured aluminium surface with a Teflon coating was able to reduce the number of adhered bacteria cells under flow by 99.9% for *Staphylococcus aureus* and 99.4% for *E. coli*—the superhydrophobic nanopillars minimise the contact area available for the bacteria, and weaker Van der Waals interactions both prevent adhesion.⁹⁶

Polyethylene Glycol Coating: polyethylene glycol (PEG) is a polymer with the general molecular structure $\text{H}-(\text{O}-\text{CH}_2-\text{CH}_2)_n-\text{OH}$. PEG grafted onto polyurethane surfaces could reduce adhesion by *Staphylococcus epidermidis* by about 90% compared to the untreated surface, and *E. coli* by 94%.⁹⁷ The polymer chain length plays an important role in bacterial, with number of adhering bacteria decreasing with increasing chain/brush length.⁹⁸ The mechanism of action for PEG to repel bacteria is believed to be due to the polymer chains resisting compression or penetration, which is a result of elastic forces and osmotic pressure.^{98, 99} Small Van der Waals' interactions may also account for the low adhesion.⁹⁸

One of the main drawbacks of this method is that the surfaces are not bactericidal, and bacteria can be released to infect other targets.¹⁰⁰

1.2.6.2 Leachable Surfaces

Leachable (release-based) surfaces contain an antimicrobial agent embedded in the surface which is released into the surrounding environment in order to kill bacteria.

Silver: The beneficial antibacterial effects of silver have been known for thousands of years.¹⁰¹ The antibacterial mechanism of silver is reported to occur *via* multiple mechanisms, as follows: silver has a high affinity to interact with

sulphur groups (e.g. thiols) and phosphorus groups which can lead to inhibition of enzymes, peptides, proteins, and also interactions with DNA may disrupt DNA replication—both leading to bacterial cell death.^{102,103,104} In addition, silver nanoparticles can cause damage to the cell membrane, resulting in leakage of the cell contents and proton leakage.^{105, 106} Silver can also give rise to depletion of intracellular adenosine triphosphate (ATP) levels, and cause an increase in reactive oxygen species (ROS) within cells.^{107,108,109} Silver can be impregnated into surfaces/coatings, and leaching of Ag⁺ ions results in antibacterial killing, for example, silver nanoparticles embedded in polyurethane foams by overnight immersion were able to kill all *E. coli* in water filtered through the foams.¹¹⁰ Composite poly(vinylpyridine)/silver bromide coatings were found to be antibacterial against a range of Gram-negative and Gram-positive bacteria including *E. coli*, *P. aeruginosa*, *Bacillus cereus*, and *S. aureus*, with long-lasting activity that remained for at least 17 days immersion.¹¹¹ In another study, inorganic TiO₂ nanotubes formed on the surface of titanium metal (which is commonly used for implants) were impregnated with silver nanoparticles—this was shown to have long-lasting silver release, and could kill planktonic (floating) *S. aureus* and prevent bacterial colonization on the surface.¹¹² However, there exists concern about the environmental impacts of silver, including toxicity to plants and aquatic organisms (as well as a lack of knowledge concerning toxicity in humans).^{113,114} The emergence of antimicrobial resistance is another issue surrounding silver-based antibacterial materials.¹¹⁵

Copper: Similarly, copper metal surface is known to exhibit antimicrobial effects.^{116, 117} Copper can kill microorganisms *via* multiple mechanisms: membrane damage¹¹⁸, production of reactive oxygen species¹¹⁹, and displacement of iron.¹²⁰ Additionally, copper oxide also shows antimicrobial activity, for example, Cu₂O nanoparticles embedded in polypropylene showed strong killing of *E. coli*.¹²¹ Copper complexes, such as copper pyrithione and copper thiocyanate, also exhibit antimicrobial effects, and are commonly added to paints as a biocidal agent.^{122, 123}

Zinc: Zinc oxide is capable of killing bacteria *via* production of reactive oxygen species and disruption of the cell membrane.^{124, 125} Coatings can be embedded with ZnO nanoparticles to produce an antimicrobial effect.¹²⁶ Zinc metal-organic compounds, such as zinc pyrithione, are also used as biocides in

paints, or embedded in materials, to produce antimicrobial surfaces and coatings.¹²⁷

Organic Biocides: 'Metal-free' antimicrobial coatings can utilise organic compounds as the active biocide. One example is tralopyril (a.k.a. Econeal), which can be incorporated into coatings to achieve antibacterial activity.¹²⁸ Another example is triclosan, which again, can be impregnated into surface coatings to give a leachable biocide with slow-release properties and strong, broad-spectrum antibacterial activity.¹²⁹

Antibiotics: Loading coatings with antibiotic molecules offers a relatively simple and effective way of producing antibacterial surfaces. In one study, several different antibiotics (cephalothin, carbenicillin, amoxicillin, cefamandole, tobramycin, gentamicin and vancomycin) were incorporated into carbonated hydroxyapatite coatings on titanium; all tested surfaces were able to inhibit growth of *S. aureus*.¹³⁰ Gentamicin or polymyxin B antibiotics loaded into poly(methacrylic acid) hydrogel coatings demonstrated high-efficacy killing of bacteria for *S. aureus* and *E. coli* respectively.¹³¹ In another study, layer-by-layer assembly of naturally-derived tannic acid and antibiotics (tobramycin, gentamicin, and polymyxin B) to produce a coating that was effective at killing *S. epidermidis*, *S. aureus*, and *E. coli*, and could maintain its antibacterial activity for 4 weeks.¹³² The disadvantage of using antibiotics, as described in Section 1.2.1, is the emergence of antibiotic resistance.

Nitric oxide: Nitric oxide (NO) is a molecule produced by the human immune system as an antimicrobial agent to help fight bacterial infections.¹³³ NO is a strong oxidising agent, and causes damage to the bacterial cell membrane and DNA.¹³³ A sol-gel coating on stainless steel was modified to contain NO donor groups, which resulted in reduced adhesion of *P. aeruginosa*, *S. aureus* and *S. epidermidis*.¹³⁴

In addition to the other disadvantages of leachable surfaces discussed in this section, another disadvantage is that leaching means that the surface becomes depleted of the entrapped antimicrobial agent, leading to eventual loss of antibacterial activity.

1.2.6.3 Contact-Kill Surfaces

Contact-kill (non-leachable) surfaces kill bacteria when they come into direct contact with the surface. There are several ways this can be achieved:

Quaternary Ammonium Compounds: Cationic compounds, such as quaternary ammonium compounds, are able to kill cells *via* interaction with the negatively charged phospholipid cytoplasmic cell membrane, causing destabilisation, leading to leakage of cell contents and cell death.¹³⁵ Therefore, covalently immobilising quaternised polymers can be used to produce contact kill surfaces. For example, in one of the first reports on this topic, poly(4-vinyl-N-alkylpyridinium bromide) attached to glass was able to kill *S. aureus*, *S. epidermidis*, *P. aeruginosa*, and *E. coli* with killing efficiency of >99% compared to the untreated glass substrate.¹³⁶ In another study, N-alkylated polyethyleneimine covalently attached to glass was able to produce up to a 9-Log₁₀ reduction in bacteria exposed to the surface, and could consistently achieve high killing rates over multiple repeat cycles, whilst having no cytotoxic effect on mammalian cells.¹³⁷ Antibacterial quaternary ammonium coatings have been produced on a variety of different substrates, including polyurethane¹³⁸, polypropylene¹³⁹, and silicone rubber¹⁴⁰, all of which are used for biomedical purposes. Phosphorus, being the element directly below nitrogen in the periodic table, can also be quaternised to produce antibacterial cationic polymers, which can be immobilised onto surfaces to give contact-kill coatings.¹⁴¹

TiO₂: Titanium dioxide, TiO₂, is a photocatalytic material that when exposed to UV or visible light can produce reactive oxygen species on its surface, which cause degradation of the cell wall and inhibition of coenzyme A, thus killing bacteria.^{142, 143} Chemical vapour deposited TiO₂ films on stainless steel gave 6-Log₁₀ reduction of *E. coli* in 3 h.¹⁴⁴ TiO₂ coated onto steel pins *via* dip-coating was capable of >3-Log₁₀ reductions of *S. aureus* and *S. epidermidis* with UV irradiation after 90 min.¹⁴⁵

Antimicrobial Peptides: Peptides are biological compounds consisting of short chains of amino acids, linked *via* peptide (amide) bonds. Antimicrobial peptides (AMP) kill bacteria through several mechanisms, including transmembrane pore formation leading to cell lysis, inhibition of protein synthesis, cell wall synthesis, and enzymatic activity.¹⁴⁶ Layer-by-layer thin film coating containing AMP gramicidin A was shown to be effective for killing Gram-positive *Enterococcus faecalis*.¹⁴⁷ Attachment of cationic AMP melamine to surfaces *via*

azide linkers yielded reductions in the number of adhered bacteria for both *P. aeruginosa* and *S. aureus*.¹⁴⁸

Graphene: Graphene (and its derivatives, graphene oxide and reduced graphene oxide) are known to be antibacterial either by physical puncturing and penetration of bacterial cells, or by causing oxidative stress.^{149, 150} Graphene oxide covalently immobilised on silicone rubber sheets could kill 85% of *E. coli* and 72% of *S. aureus*.¹⁵⁰ Graphene grown on silicon surface was capable of complete killing of *E. coli* and *S. aureus* after 6 h exposure.¹⁵¹

One of the main disadvantages of these coatings is that as the bacteria are killed, the dead bacteria cells remain in place and pile-up on the surface, therefore blocking other alive cells from coming into direct contact with the surface. This leads to loss of antibacterial activity and biofilm formation. To overcome this problem, smart responsive switchable surfaces have been devised—these surfaces are able to kill bacteria, then react to certain stimuli (e.g. pH, temperature, dry/wet conditions, light, electric potential) to release dead bacterial cells to yield a clean surface free from fouling.¹⁵²

1.2.6.4 Methods of Coating

Numerous methods exist for the production of antibacterial coatings. This includes: dip-coating, where the substrate is immersed into a coating solution and subsequently withdrawn, leaving behind a layer of coating at the surface¹⁵³; spin-coating, in which a substrate is rotated at high speed whilst a coating solution is dropped onto the spinning substrate, thus forming an evenly-spread coating¹⁵⁴; drop-casting, where droplets of a coating solution are placed onto the surface, and solvent allowed to evaporate¹⁵⁵; spray-coating, where the coating solution is transferred to the surface *via* a pressurised spray¹⁵⁶; layer-by-layer deposition, whereby a substrate is alternately dipped into two (or more) solutions each containing a component of the coating numerous times, each time the substrate is immersed, a layer of coating is left behind, therefore a coating is built up, layer by layer¹⁴⁷; electrospinning, where an electrical field is applied to a polymer solution of melt at a needle tip, causing the solution to gain charge and be accelerated allowing for casting of the polymer onto the target substrate¹⁵⁷; curing, where a coating solution placed on a surface which is treated with ultraviolet radiation or heat, causing a reaction to occur in the coating components

(e.g. polymer crosslinking), thus forming a desired coating^{154, 158}; grafting (also called ‘immobilisation’), where an antimicrobial agent is reacted with a functionalised surface to form a covalent bond, thus immobilising it and attaching it to the surface¹³⁷; and chemical vapour deposition (CVD), in which the vapour of a volatile precursor(s) is introduced into a reaction chamber and an energy source provides the required energy to allow the precursor(s) to react and to deposit a coating on the substrates.¹⁵⁹ There are many different types of CVD, some of which include: initiated chemical vapour deposition (iCVD), where a free radical initiator species is introduced with the precursor to enable rapid polymerisation¹⁶⁰; flame assisted chemical vapour deposition (FACVD), where the precursors are passed through a flame in order to provide the energy for reaction (this is useful for inorganic materials)¹⁶¹; and plasma enhanced chemical vapour deposition (PECVD), in which a plasma is generated in the precursor vapour which generates radical species leading to coating formation (a more detailed description of plasmachemical deposition is given in section 2.1).¹⁶² Whilst this section is by no means exhaustive, it gives an overview of some of the most commonly used coating techniques.

1.2.6.5 Conclusions

Antimicrobial coatings offer a non-invasive route to prevent the spread of infections, which could potentially help reduce the reliance on antibiotics, as well as help safeguard vulnerable people (for example, patients in hospital settings, or where people have not received a vaccination, or where no vaccine currently exists).

1.3 Literature Review

In section 1.2 of this chapter, we have looked at the main different types of antibacterial surfaces, and several general examples of the most common ones found in the scientific literature. Chapters 3–5 of this thesis describe the synthesis of several novel antimicrobial coatings. Therefore, in this section, we will briefly review the different coating systems and their applications for antimicrobial coatings.

1.3.1 Cinnamaldehyde

Many naturally-occurring plant-derived essential oil compounds are known for their antimicrobial benefits.¹⁶³ Cinnamaldehyde, a major component of cinnamon bark oil^{164,165}, is reported to show antibacterial^{166, 167}, antifungal¹⁶⁸, antiparasitic¹⁶⁹, insecticidal¹⁷⁰, antiviral¹⁷¹, anticancer¹⁷², anti-diabetic¹⁷³ and pro-wound healing¹⁷⁴ properties. Cinnamaldehyde is antibacterial through multiple mechanisms which vary according to the pathogen.¹⁷⁵ The mode of action of cinnamaldehyde against *E. coli* and *S. aureus* is reported to involve interaction of cinnamaldehyde with the cell membrane, which results in an increase in the cell permeability, changes to cell morphology, and damaging of cell membrane integrity, ultimately leading to cell lysis and cytoplasmic content leakage.^{176, 177, 178} It has also been shown that cinnamaldehyde can cause oxidative damage to *E. coli* cells.¹⁷⁹ Many of the reported cinnamaldehyde-based antibacterial materials and surfaces involve the blending of cinnamaldehyde with a polymer (either as a melt or in solution) followed by casting into a film. Some of the polymers used include: polyvinyl alcohol¹⁸⁰, polypropylene¹⁸¹, polystyrene¹⁸², cellulose¹⁸³, and chitosan.¹⁸⁴ Such cinnamaldehyde-containing films are effective at stopping bacterial or mould growth on, for example, various foodstuffs—including beef¹⁸⁰, chicken and ham¹⁸⁵, vegetable (radish, broccoli, and alfalfa) sprouts¹⁸⁶, and bakery products.¹⁸⁷ However, manufacture of such essential oil impregnated polymer films requires costly organic solvents¹⁸⁸ or involves application of heat, which can be detrimental due to degradation or volatilization of the bioactive compound.¹⁸⁹ Furthermore, much of the cinnamaldehyde content within the bulk material may be inaccessible to the external environment (bacteria).

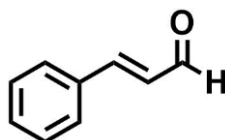


Figure 1.1: Structure of trans-cinnamaldehyde.

Cinnamaldehyde is used in chapters 3, 4, and 5 of this thesis to produce a variety of coatings with antibacterial properties.

1.3.2 Polydopamine

Polydopamine is an adhesive polymer formed via the autoxidation of dopamine (Figure 1.2) in basic solution.¹⁹⁰

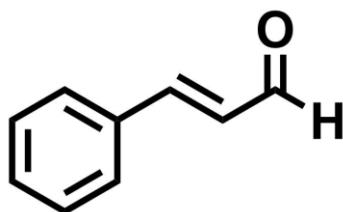


Figure 1.2: Structure of dopamine.

These coatings readily and spontaneously adhere to a variety of substrate materials, including metals, plastics, and even low surface energy polytetrafluoroethylene.¹⁹⁰ The catechol functionality of dopamine mimics the adhesive *Mytilus edulis* foot protein 5 (Mefp-5) found in mussels, which is capable of adhering to virtually any kind of surface.^{191, 192} The exact structure of polydopamine is currently not entirely well-known (in part due to polydopamine's insolubility in practically all solvents), but computer calculations and experimental evidence have been used to suggest a likely structure, Figure 1.3.

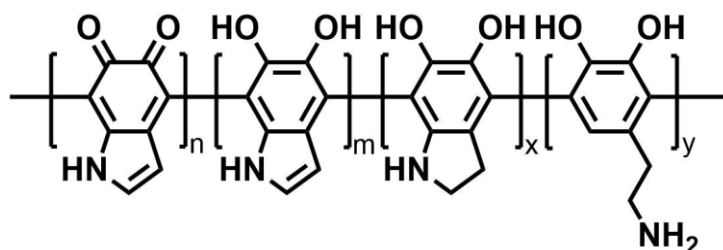


Figure 1.3: Structure of polydopamine.

Polydopamine alone does not exhibit strong antibacterial activity, and so much research has been conducted into the post-functionalization of polydopamine coatings. Examples include the attachment of silver^{193, 194, 195}, copper^{196, 197}, quaternary ammonium compounds^{198, 199}, zwitterionic compounds²⁰⁰, chlorhexidine²⁰¹, antibiotics²⁰², peptides²⁰³, or enzymes.²⁰⁴ Many of these antibacterial polydopamine-based coatings are unsuitable for industrial scale-up due to their inherent multi-step syntheses, and often prohibitively long reaction times. Also, there have been reports of combining polydopamine with an antibacterial agent for 'one-pot' (single-step) hybrid coatings; for example, polydopamine-silver and polydopamine-copper.^{205,206} However, antimicrobials such as silver and copper have inherent drawbacks, chiefly their relatively high

cost compared to organic compounds. Additionally, as described in Section 1.2.6.2, there are issues with the use of metals regarding their toxicities and antimicrobial resistance.^{113, 114, 115}

Chapter 3 of this thesis describes the fabrication of an antibacterial coating that combines polydopamine and cinnamaldehyde.

1.3.3 Tannic Acid

Tannic acid is a natural coating-forming phenolic compound—a plant polyphenol, derived from the nutgalls of *Quercus* and Sumac (*Rhus*) species, as well as the seed pods of Tara (*Caesalpinia spinosa*).²⁰⁷ The molecular structure of tannic acid is polygalloyl glucose, that is, a central glucose molecule that has formed ester bonds with multiple gallic acid molecules, Figure 1.4.

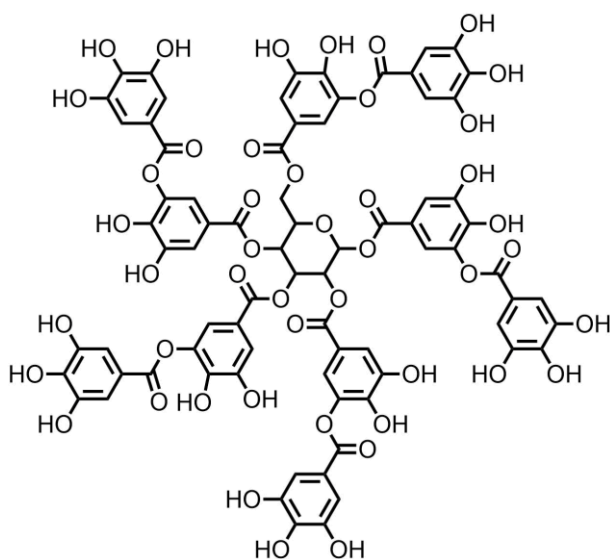


Figure 1.4: Structure of tannic acid.

Tannic acid forms an adhesive polymeric coating under oxidising basic conditions, in a similar fashion to polydopamine.²⁰⁸ One potential issue associated with the use of polydopamine coatings is the relatively high cost of the dopamine hydrochloride precursor, hence tannic acid is considered as a viable alternative for large scale applications.²⁰⁸ Antibacterial coatings made using tannic acid use similar methods to those of polydopamine, utilising additives such as silver^{209,210}, copper^{210,211}, peptides²¹², quaternary ammonium compounds^{213, 214}, zwitterionic compounds²¹³ to impart antibacterial activity. Tannic acid has also been made antibacterial *via* reaction/hydrophobisation with alkyl iodides.²¹⁵

Chapter 3 of this thesis describes how tannic acid coating can be combined with cinnamaldehyde to give an antibacterial coating.

1.3.4 Polyethyleneimine

Polyethyleneimine polymer comprises repeat units containing two methylene carbons and an amine centre. The general structure of branched polyethyleneimine is shown in Figure 1.5. The ratio of primary to secondary to tertiary amines is typically 1:1:1 in commercially available products.²¹⁶ Polyethyleneimine is not particularly antibacterial on its own, but its large number of amine functionalities can be reacted with alkyl halides to yield quaternary ammonium groups which display antibacterial activities.²¹⁷

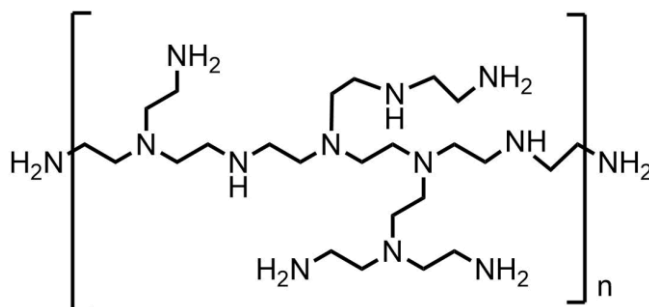


Figure 1.5: Structure of polyethyleneimine.

Chapter 3 of this thesis examines the reaction between polyethyleneimine and cinnamaldehyde, and the resulting coating that forms and its antibacterial properties.

1.3.5 Tea

Leaves from the *Camellia sinensis* plant are used to make tea, one of the most popular beverages, found worldwide. 'Tea staining' is also a well-known phenomenon, where brewed tea can leave a coating on its container.²¹⁸ Tea extracts contain a large variety of different chemical compounds, and one of the primary classes of compounds found in tea extract are polyphenols called catechins.²¹⁹ Catechins, such as epigallocatechin gallate, feature catechol and gallic acid moieties, similar to polydopamine and tannic acid, Figure 1.6. Although the composition of tea stain coatings is itself chemically complex, it is reported that oxidation of these polyphenols and their interactions with surfaces that is responsible for formation of the coating.²¹⁸ It therefore follows that tea could potentially be used as a cheaper, accessible alternative to dopamine and tannic acid for producing functional coatings. One study has shown that polymer brushes can be grafted to tea polyphenol coatings to produce functional

coatings.²²⁰ Another study has shown that silver nanoparticles can be synthesised *in situ* on green tea polyphenol coating (though this a qualitative test, and the potential antibacterial effects are not examined).²²¹

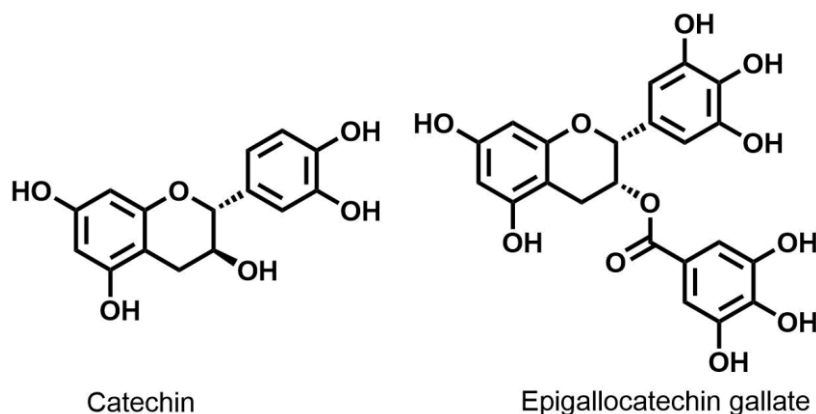


Figure 1.6: Structures of tea polyphenols—catechin and epigallocatechin gallate.

In chapter 4 of this thesis, brewed green tea solution is combined with cinnamaldehyde to produce an antibacterial coating.

1.3.6 Slippery Liquid Infused Porous Surfaces

Liquid repellent slippery liquid-infused porous surfaces (SLIPS) have been inspired by the carnivorous *Nepenthes* pitcher plant, in which a nectar film entrapped within a textured surface on the plant peristome is used to attract and capture arthropod prey.^{222, 223, 224, 225, 226} In the past, SLIPS have been fabricated by impregnating a roughened or porous surface with a lubricating liquid. The lubricant must be able to wet and adhere to the host surface in preference to the liquid which is being repelled, and the lubricant needs to be immiscible with the liquid being repelled. This can be achieved through careful matching of the solid surface and lubricant chemistries. Slippery lubricant-infused surfaces have been proposed for a wide variety of technological and societal applications including: water repellency²²⁶, antibacterial²²⁷, marine antibiofouling²²⁸, blood repellency²²⁹, icephobicity²³⁰, anti-icing²³¹, corrosion resistance²³¹, mineral fouling mitigation²³², droplet motion control²³³, water harvesting²³⁴, fog collection²³⁵, antireflectivity²³⁶, antifouling of foodstuffs²³⁷, antifouling of faecal matter²³⁸, underwater bubble transportation²³⁹, and drag reduction.²⁴⁰

In the absence of any bactericidal additives, SLIPS do not possess the ability to kill bacteria.²⁴¹ Therefore typically an antimicrobial agent (for example

drug molecules such as triclosan¹²⁹) needs to be impregnated into a pre-made SLIPS, or silver is incorporated into the substrate prior to lubricant infusion.²⁴² However, environmental concerns exist about the toxicity of triclosan towards marine life, as well as its bioaccumulation, and the risk for bacteria to develop antimicrobial resistance towards the drug.²⁴³ Furthermore, many of the reported fabrication techniques for SLIPS systems are limited in the range and geometries of materials that they can be produced on. For example, hydrothermal treatment is applicable to inorganic surfaces such as aluminium and glass^{244, 245}, whilst electroplating is restricted to metals²⁴⁶, and the use of inherently porous or micro/nanostructured materials to infiltrate lubricants cannot be extended to non-porous materials.²⁴⁷ In the case of layer-by-layer deposition techniques, typically long coating times are required to build up a sufficient coating layer thickness.²⁴⁸ Also, these methodologies require multiple steps, and often need an extra substrate hydrophobization step in order to provide sufficient surface affinity towards the lubricant impregnation.^{244, 245, 246, 247, 248}

Chapter 5 of this thesis described the pulsed plasma deposition of a variety of polymer thin film coatings, which are then combined with a range of lubricants to form liquid-infused slippery surfaces. Cinnamaldehyde is used to produce a slippery, antibacterial coating.

1.4 Scope of Thesis

Antimicrobial surfaces could be used to stop the spread of bacteria on a variety of surfaces, for example, medical equipment, medical implants, food packaging, or common touch surfaces, by killing the bacteria and preventing biofilm formation. Many different methods have been reported for the production of such coatings and surfaces. However, many of these methods involve multiple steps, and expensive reagents or equipment, making them unsuitable for mass scale-up. Many commercial antimicrobial coatings involve the use of silver and copper, for which there currently exists concerns about sustainability, toxicity, and ecological impact. Therefore, there is currently a need to create novel antimicrobial coatings that are simple to produce, using readily available and cheap reagents, that are effective at killing bacteria and viruses (and fungi) with long-lasting efficacies, and that are environmentally-friendly and sustainable.

In chapter 3, a novel antibacterial coating is described which combines adhesive polydopamine with antibacterial cinnamaldehyde. The coating is produced in a single-step, one-pot synthesis that involves the polymerisation of dopamine in basic solution, in the presence of cinnamaldehyde. The coating is also shown to work with a dopamine analogue, norepinephrine. The antibacterial activity of the polydopamine–cinnamaldehyde on non-porous substrates is tested against two bacteria species, Gram-negative *Escherichia coli* and Gram-positive *Staphylococcus aureus* (a detailed description of the antibacterial testing procedure is given in section 2.3), and shows strong bacterial killing, that lasts for multiple recycling tests. Since the amine group on dopamine/polydopamine is believed to react with cinnamaldehyde, polyethyleneimine, which contains a high concentration of amine groups, was combined with cinnamaldehyde to form another coating, and the antibacterial activity is examined. The coating method is extended to tannic acid, which is a bioderived and cheaper alternative to dopamine (dopamine hydrochloride = £268 / 100g versus tannic acid = £23.80 / 100 g, prices taken from sigmaaldrich.com, 28/08/21). (Cinnamaldehyde is also a relatively cheap chemical, £3.24 / 100 g, price taken from sigmaaldrich.com, 28/08/21). Tannic acid–cinnamaldehyde coating was also found to exhibit strong antibacterial properties. Since the mode of antibacterial action of these coatings is determined to be leaching of cinnamaldehyde, porous non-woven polypropylene cloth is either impregnated with cinnamaldehyde or coated with polydopamine–cinnamaldehyde, and both are shown to give long-lasting antibacterial activities.

In chapter 4, an antibacterial coating is described that utilises brewed tea solution and cinnamaldehyde. Tea presents an even cheaper alternative to tannic acid (Clippers Organic Green Tea (80 teabags) = £2.19 / 100 g, price taken from tesco.com, 28/08/21). The coating shows complete killing of both bacteria. The only other materials required are tap water and a container to hold the solution. This coating is further derivatised by addition of copper or silver salts, to produce three-component coatings, tea–cinnamaldehyde–copper and tea–cinnamaldehyde–silver. These coatings are testing for antiviral activities against murine coronavirus MHV-A59, which acts as a potential surrogate for SARS-CoV-2. Both coatings are shown to inactivate the virus.

In chapter 5, pulsed plasma polymer thin films are combined with liquid lubricants to produce slippery liquid-infused surfaces, that are capable of repelling

water. Several bioderived compounds are used as lubricants. The omniphobicity of a perfluorinated polymer–lubricant system is analysed. Pulsed plasma poly(vinylaniline) is used in conjunction with cinnamaldehyde lubricant to produce a multifunctional coating that can repel viscous foodstuffs (tomato ketchup and honey), and possesses strong antibacterial activities.

Chapter 6 demonstrates an alternative use of pulsed plasma polymer thin film coatings, showing their use in anti-biofouling coatings to prevent (or encourage) fouling of microalgae.

Thus, both wet chemical and plasmachemical methodologies are used for the production of thin film coatings with antibacterial, antiviral, and anti-biofouling applications.

1.5 References

- 1 Madigan M. T.; Martinko J. M.; Stahl D. A.; Clark D. P. Brock Biology of Microorganisms, 13th ed.; Pearson Education Inc., 2012.
- 2 <https://webarchive.nationalarchives.gov.uk/ukgwa/20180411170458/https://www.food.gov.uk/sites/default/files/multimedia/pdfs/campylobacterstrategy.pdf>; accessed 10/08/2021.
- 3 Campylobacter data 2008 to 2017; published January 2017., <https://www.gov.uk/government/publications/campylobacter-infection-annual-data/campylobacter-data-2008-to-2017>; access 10/08/2021.
- 4 <https://www.foodstandards.gov.scot/downloads/campylobacter-factsheet-whats-the-problem.pdf>; accessed 10/08/2021.
- 5 Annual epidemiological commentary: Gram-negative bacteraemia, MRSA bacteraemia, MSSA bacteraemia and *C. difficile* infections, up to and including financial year April 2019 to March 2020., <https://www.gov.uk/government/statistics/mrsa-mssa-and-e-coli-bacteraemia-and-c-difficile-infection-annual-epidemiological-commentary>; accessed 10/08/2021.
- 6 Naylor, N. R.; Pouwels, K. B.; Hope, R.; Green, N.; Henderson, K. L.; Knight, G. M.; Atun, R.; Robotham, J. V.; Deeny, S. R. The Health and Cost Burden of Antibiotic Resistant and Susceptible *Escherichia Coli* Bacteraemia in the English Hospital Setting: A National Retrospective Cohort Study. *PLoS One* **2019**, *14*, e0221944.
- 7 Deaths involving *E. coli* septicaemia, deaths registered in Wales between 2001 and 2015., <https://www.ons.gov.uk/peoplepopulationandcommunity/birthsdeathsandmarriages/deaths/adhocs/006005deathsinvolvingecolisepticaemiadeathsregisteredinwalesbetween2001and2015>; accessed 10/08/2021.
- 8 Laboratory surveillance of pyogenic and non-pyogenic streptococcal bacteraemia in England: 2019, <https://www.gov.uk/government/publications/pyogenic-and-non-pyogenic-streptococcal-bacteraemia-annual-data-from-voluntary-surveillance>; accessed 10/08/2021.
- 9 Lamagni, T.; Guy, R.; Chand, M.; Henderson, K. L.; Chalker, V.; Lewis, J.; Saliba, V.; Elliot, A. J.; Smith, G. E.; Rushton, S.; Sheridan, E. A.; Ramsay, M.; Johnson, A. P. Resurgence of Scarlet Fever in England, 2014–16: A Population-Based Surveillance Study. *Lancet Infect. Dis.* **2018**, *18*, 180–187.
- 10 Hughes, G. J.; Van Hoek, A. J.; Sriskandan, S.; Lamagni, T. L. The Cost of Hospital Care for Management of Invasive Group A Streptococcal Infections in England. *Epidemiol. Infect.* **2015**, *143*, 1719–1730.
- 11 Department of Health (2012) Quality and Outcomes Framework 2011/2012. Impact assessment for NHS Outcomes Framework 2011/12, No. 5014., <https://www.gov.uk/government/publications/nhs-outcomes-framework-2011-to-2012>; accessed 10/08/2021.
- 12 Deaths Involving *Clostridium difficile*, England and Wales: 2012., <https://www.ons.gov.uk/peoplepopulationandcommunity/birthsdeathsandmarriages/deaths/bulletins/deathsinvolvingclostridiumdifficileenglandandwales/2013-08-22>; accessed 10/08/2021.

- 13 Deaths involving MRSA: 2008 to 2012., <https://www.ons.gov.uk/peoplepopulationandcommunity/birthsdeathsandmarriages/deaths/bulletins/deathsinvolvingmrsa/2013-08-22>; accessed 10/08/2021.
- 14 Tuberculosis in England: 2020 report (presenting data to end of 2019), <https://www.gov.uk/government/publications/tuberculosis-in-england-annual-report>; accessed 10/08/2021.
- 15 Supply of TB drugs to patients – changes to regulations and advice on implementation., http://webarchive.nationalarchives.gov.uk/+http://www.dh.gov.uk/en/PublicHealth/CommunityCablediseases/Tuberculosis/DH_078136; access 10/08/2021.
- 16 Salmonella data 2007 to 2016., <https://www.gov.uk/government/publications/salmonella-national-laboratory-data>; accessed 10/08/2021.
- 17 Voluntary surveillance of Enterococcus spp. bacteraemia in England, Wales and Northern Ireland: 2018., <https://www.gov.uk/government/publications/enterococcus-spp-bacteraemia-voluntary-surveillance>; accessed 10/08/2021.
- 18 Pokharel, S.; Raut, S.; Adhikari, B. Tackling Antimicrobial Resistance in Low-Income and Middle-Income Countries. *BMJ Glob. Heal.* **2019**, *4*, e002104.
- 19 Nagel, T. E.; Chan, B. K.; De Vos, D.; El-Shibiny, A.; Kang'ethe, E. K.; Makumi, A.; Pirnay, J. P. The Developing World Urgently Needs Phages to Combat Pathogenic Bacteria. *Front. Microbiol.* **2016**, *7*, 882.
- 20 O'Reilly, C. E.; Jaron, P.; Ochieng, B.; Nyaguara, A.; Tate, J. E.; Parsons, M. B.; Bopp, C. A.; Williams, K. A.; Vinjé, J.; Blanton, E.; et al. Risk Factors for Death among Children Less than 5 Years Old Hospitalized with Diarrhea in Rural Western Kenya, 2005-2007: A Cohort Study. *PLoS Med.* **2012**, *9*, e1001256.
- 21 The Global View of Campylobacteriosis (2013). The Global View of Campylobacteriosis. Report of an Expert Consultation., www.who.int/iris/bitstream/10665/80751/1/9789241564601_eng.pdf; accessed 11/08/2021.
- 22 Finberg, R. W.; Moellering, R. C.; Tally, F. P.; Craig, W. A.; Pankey, G. A.; Dellinger, E. P.; West, M. A.; Joshi, M.; Linden, P. K.; Rolston, K. V.; et al. The Importance of Bactericidal Drugs: Future Directions in Infectious Disease. *Clin. Infect. Dis.* **2004**, *39*, 1314–1320.
- 23 Nicolaou, K. C.; Rigol, S. A Brief History of Antibiotics and Select Advances in Their Synthesis. *J. Antibiot.* **2017**, *71*, 153–184.
- 24 Smith, D. L.; Harris, A. D.; Johnson, J. A.; Silbergeld, E. K.; Morris, J. G. Animal Antibiotic Use Has an Early but Important Impact on the Emergence of Antibiotic Resistance in Human Commensal Bacteria. *Proc. Natl. Acad. Sci. U. S. A.* **2002**, *99*, 6434–6439.
- 25 McManus, P. S.; Stockwell, V. O.; Sundin, G. W.; Jones, A. L. Antibiotic Use in Plant Agriculture. *Annu. Rev. Phytopathol.* **2002**, *40*, 443–465.
- 26 NHS, Side Effects, Antibiotics; <https://www.nhs.uk/conditions/antibiotics/side-effects/>; accessed 06/07/2021.
- 27 Blair, J. M. A.; Webber, M. A.; Baylay, A. J.; Ogbolu, D. O.; Piddock, L. J. V. Molecular Mechanisms of Antibiotic Resistance. *Nat. Rev. Microbiol.* **2015**, *13*, 42–51.
- 28 Neu, H. C. The Crisis in Antibiotic Resistance. *Science.* **1992**, *257*, 1064–1073.

- 29 Von Wintersdorff, C. J. H.; Penders, J.; Van Niekerk, J. M.; Mills, N. D.; Majumder, S.; Van Alphen, L. B.; Savelkoul, P. H. M.; Wolffs, P. F. G. Dissemination of Antimicrobial Resistance in Microbial Ecosystems through Horizontal Gene Transfer. *Front. Microbiol.* **2016**, *7*, 173.
- 30 Ventola, C. L. The Antibiotic Resistance Crisis Part 1: Causes and Threats. *P T J.* **2015**, *40*, 277–283.
- 31 World Health Organization, Antimicrobial Resistance; <https://www.who.int/news-room/fact-sheets/detail/antimicrobial-resistance>; accessed 06/07/2021.
- 32 Sulis, G.; Daniels, B.; Kwan, A.; Gandra, S.; Daftary, A.; Das, J.; Pai, M. Antibiotic Overuse in the Primary Health Care Setting: A Secondary Data Analysis of Standardised Patient Studies from India, China and Kenya. *BMJ Glob. Heal.* **2020**, *5*, e003393.
- 33 Gross, M. Antibiotics in Crisis. *Curr. Biol.* **2013**, *23*, R1063–R1065.
- 34 Barker, A. K.; Brown, K.; Ahsan, M.; Sengupta, S.; Safdar, N. Social Determinants of Antibiotic Misuse: A Qualitative Study of Community Members in Haryana, India. *BMC Public Health* **2017**, *17*, 1–9.
- 35 Chen, J.; Sidibi, A. M.; Shen, X.; Dao, K.; Maiga, A.; Xie, Y.; Hesketh, T. Lack of Antibiotic Knowledge and Misuse of Antibiotics by Medical Students in Mali: A Cross-Sectional Study. *Expert Rev. Anti. Infect. Ther.* **2021**, *19*, 797–804.
- 36 Sulis, G.; Batomen, B.; Kotwani, A.; Pai, M.; Gandra, S. Sales of Antibiotics and Hydroxychloroquine in India during the COVID-19 Epidemic: An Interrupted Time Series Analysis. *PLOS Med.* **2021**, *18*, e1003682.
- 37 Debarshi Dasgupta, The Strait Times, published 07/06/2021; <https://www.straitstimes.com/asia/south-asia/antibiotic-overuse-on-covid-19-patients-in-india-prompts-superbug-concerns>; accessed 06/07/2021.
- 38 Larsson, D. G. J. Antibiotics in the Environment. *Ups. J. Med. Sci.* **2014**, *119*, 108–112.
- 39 Gothwal, R.; Shashidhar, T. Antibiotic Pollution in the Environment: A Review. *Clean - Soil, Air, Water* **2015**, *43*, 479–489.
- 40 Valcárcel, Y.; González Alonso, S.; Rodríguez-Gil, J. L.; Gil, A.; Catalá, M. Detection of Pharmaceutically Active Compounds in the Rivers and Tap Water of the Madrid Region (Spain) and Potential Ecotoxicological Risk. *Chemosphere* **2011**, *84*, 1336–1348.
- 41 Na, G.; Fang, X.; Cai, Y.; Ge, L.; Zong, H.; Yuan, X.; Yao, Z.; Zhang, Z. Occurrence, Distribution, and Bioaccumulation of Antibiotics in Coastal Environment of Dalian, China. *Mar. Pollut. Bull.* **2013**, *69*, 233–237.
- 42 Yiruhan; Wang, Q. J.; Mo, C. H.; Li, Y. W.; Gao, P.; Tai, Y. P.; Zhang, Y.; Ruan, Z. L.; Xu, J. W. Determination of Four Fluoroquinolone Antibiotics in Tap Water in Guangzhou and Macao. *Environ. Pollut.* **2010**, *158*, 2350–2358.
- 43 Eggen, T.; Asp, T. N.; Grave, K.; Hormazabal, V. Uptake and Translocation of Metformin, Ciprofloxacin and Narasin in Forage- and Crop Plants. *Chemosphere* **2011**, *85*, 26–33.
- 44 Hu, X.; Zhou, Q.; Luo, Y. Occurrence and Source Analysis of Typical Veterinary Antibiotics in Manure, Soil, Vegetables and Groundwater from Organic Vegetable Bases, Northern China. *Environ. Pollut.* **2010**, *158*, 2992–2998.
- 45 Gavalchin, J.; Katz, S. E. The Persistence of Fecal-Borne Antibiotics in Soil. *J. AOAC Int.* **1994**, *77*, 481–485.

- 46 Aga, D. S.; O'Connor, S.; Ensley, S.; Payero, J. O.; Snow, D.; Tarkalson, D. Determination of the Persistence of Tetracycline Antibiotics and Their Degradates in Manure-Amended Soil Using Enzyme-Linked Immunosorbent Assay and Liquid Chromatography-Mass Spectrometry. *J. Agric. Food Chem.* **2005**, *53*, 7165–7171.
- 47 Schlüsener, M. P.; Bester, K. Persistence of Antibiotics Such as Macrolides, Tiamulin and Salinomycin in Soil. *Environ. Pollut.* **2006**, *143*, 565–571.
- 48 Piddock, L. J. V. The Crisis of No New Antibiotics—What Is the Way Forward? *Lancet Infect. Dis.* **2012**, *12*, 249–253.
- 49 Lahariya, C. Vaccine Epidemiology: A Review. *J. Fam. Med. Prim. Care* **2016**, *5*, 7.
- 50 Ellenberg, S. S.; Chen, R. T. The Complicated Task of Monitoring Vaccine Safety. *Public Health Rep.* **1997**, *112*, 10–19.
- 51 Roush, S. W.; Murphy, T. V.; Basket, M. M.; Iskander, J. K.; Moran, J. S.; Seward, J. F.; Wasley, A. Historical Comparisons of Morbidity and Mortality for Vaccine-Preventable Diseases in the United States. *J. Am. Med. Assoc.* **2007**, *298*, 2155–2163.
- 52 Centers for Disease Control and Prevention (CDC). Ten Great Public Health Achievements--Worldwide, 2001-2010. *MMWR. Morb. Mortal. Wkly. Rep.* **2011**, *60*, 814–818.
- 53 Rouderfer, V.; Becker, N. G.; Hethcote, H. W. Waning Immunity and Its Effects on Vaccination Schedules. *Math. Biosci.* **1994**, *124*, 59–82.
- 54 Grubeck-Loebenstien, B. Fading Immune Protection in Old Age: Vaccination in the Elderly. *J. Comp. Pathol.* **2010**, *142*, S116–S119.
- 55 Ferdinands, J. M.; Fry, A. M.; Reynolds, S.; Petrie, J. G.; Flannery, B.; Jackson, M. L.; Belongia, E. A. Intraseason Waning of Influenza Vaccine Protection: Evidence from the US Influenza Vaccine Effectiveness Network, 2011–2012 through 2014–2015. *Clin. Infect. Dis.* **2017**, *64*, 544–550.
- 56 Maurice, J. Vaccine Shortage Threatens Spread of Meningitis in Niger. *Lancet* **2015**, *385*, 2241.
- 57 Brewer, N. T.; Hallman, W. K. Subjective and Objective Risk as Predictors of Influenza Vaccination during the Vaccine Shortage of 2004-2005. *Clin. Infect. Dis.* **2006**, *43*, 1379–1386.
- 58 Jacobson, S. H.; Sewell, E. C.; Proano, R. A. An Analysis of the Pediatric Vaccine Supply Shortage Problem. *Health Care Manag. Sci.* **2006**, *9*, 371–389.
- 59 Garland, S. M.; Stanley, M. A.; Giuliano, A. R.; Moscicki, A. B.; Kaufmann, A.; Bhatla, N.; Woo, Y. L.; Palefsky, J.; Chan, K.; Brotherton, J. IPVS Statement on “Temporary HPV Vaccine Shortage: Implications Globally to Achieve Equity.” *Papillomavirus Res.* **2020**, *9*, 100195.
- 60 Gouglas, D.; Thanh Le, T.; Henderson, K.; Kaloudis, A.; Danielsen, T.; Hammersland, N. C.; Robinson, J. M.; Heaton, P. M.; Røttingen, J. A. Estimating the Cost of Vaccine Development against Epidemic Infectious Diseases: A Cost Minimisation Study. *Lancet Glob. Heal.* **2018**, *6*, e1386–e1396.
- 61 Pronker, E. S.; Weenen, T. C.; Commandeur, H.; Claassen, E. H. J. H. M.; Osterhaus, A. D. M. E. Risk in Vaccine Research and Development Quantified. *PLoS One* **2013**, *8*, e57755.

- 62 Plotkin, S. A.; Mahmoud, A. A. F.; Farrar, J. Establishing a Global Vaccine-Development Fund. *N. Engl. J. Med.* **2015**, *373*, 297–300.
- 63 Poland, G. A.; Jacobson, R. M. Understanding Those Who Do Not Understand: A Brief Review of the Anti-Vaccine Movement. *Vaccine* **2001**, *19*, 2440–2445.
- 64 Sallam, M. Covid-19 Vaccine Hesitancy Worldwide: A Concise Systematic Review of Vaccine Acceptance Rates. *Vaccines* **2021**, *9*, 1–15.
- 65 Chen, R. T.; DeStefano, F. Vaccine Adverse Events: Causal or Coincidental? *Lancet* **1998**, *351*, 611–612.
- 66 Reid, A. M.; Oosthuizen, C. B.; Fibrich, B. D.; Twilley, D.; Lambrechts, I. A.; Canha, M. N.; Rademan, S.; Lall, N. Traditional Medicine: The Ancient Roots of Modern Practice. In *Medicinal Plants for Holistic Health and Well-Being*; Academic Press, 2018; pp 1–11.
- 67 Ekor, M. The Growing Use of Herbal Medicines: Issues Relating to Adverse Reactions and Challenges in Monitoring Safety. *Front. Pharmacol.* **2013**, *4*, 177.
- 68 World Health Organization, Report: WHO traditional medicine strategy: 2014-2023; <https://www.who.int/publications/i/item/9789241506096>; accessed 27/07/2021.
- 69 Grifo F, Newman D, Fairfield AS: The Origins of Prescription Drugs. In *Biodiversity and Human Health*. Edited by: Grifo F, Rosenthal J. 1997, Washington, DC: Island Press, 131-163.
- 70 Qiu, J. Traditional Medicine: A Culture in the Balance. *Nature* **2007**, *448*, 126–128.
- 71 World Health Organization, WHO guidelines on hand hygiene in health care, 2009; <https://www.who.int/publications/i/item/9789241597906>; accessed 29/07/2021.
- 72 Rusin, P.; Maxwell, S.; Gerba, C. Comparative Surface-to-Hand and Fingertip-to-Mouth Transfer Efficiency of Gram-Positive Bacteria, Gram-Negative Bacteria, and Phage. *J. Appl. Microbiol.* **2002**, *93*, 585–592.
- 73 Döring, G.; Jansen, S.; Noll, H.; Grupp, H.; Frank, F.; Botzenhart, K.; Magdorf, K.; Wahn, U. Distribution and Transmission of *Pseudomonas Aeruginosa* and *Burkholderia Cepacia* in a Hospital Ward. *Pediatr. Pulmonol.* **1996**, *21*, 90–100.
- 74 Kampf, G.; Löffler, H.; Gastmeier, P. Hand Hygiene for the Prevention of Nosocomial Infections. *Dtsch. Arztebl. Int.* **2009**, *106*, 649.
- 75 Doebbeling, B. N.; Stanley, G. L.; Sheetz, C. T.; Pfaller, M. A.; Houston, A. K.; Annis, L.; Li, N.; Wenzel, R. P. Comparative Efficacy of Alternative Hand-Washing Agents in Reducing Nosocomial Infections in Intensive Care Units. *N. Engl. J. Med.* **1992**, *327*, 88–93.
- 76 Green, L. R.; Selman, C. A.; Radke, V.; Ripley, D.; Mack, J. C.; Reimann, D. W.; Stigger, T.; Motsinger, M.; Bushnell, L. Food Worker Hand Washing Practices: An Observation Study. *J. Food Prot.* **2006**, *69*, 2417–2423.
- 77 Master, D.; Longe, S. H.; Dickson, H. Scheduled Hand Washing in an Elementary School Population. *Fam. Med.* **1997**, *29*, 336–339.
- 78 Ejemot-Nwadiaro, R. I.; Ehiri, J. E.; Arikpo, D.; Meremikwu, M. M.; Critchley, J. A. Hand-Washing Promotion for Preventing Diarrhoea. *Cochrane Database Syst. Rev.* **2021**, Art. No.: CD004265.

- 79 Betsch, C.; Korn, L.; Sprengholz, P.; Felgendreff, L.; Eitze, S.; Schmid, P.; Böhm, R. Social and Behavioral Consequences of Mask Policies during the COVID-19 Pandemic. *Proc. Natl. Acad. Sci. U. S. A.* **2020**, *117*, 21851–21853.
- 80 Prather, K. A.; Wang, C. C.; Schooley, R. T. Reducing Transmission of SARS-CoV-2. *Science* **2020**, *368*, 1422–1424.
- 81 Davies, A.; Thompson, K. A.; Giri, K.; Kafatos, G.; Walker, J.; Bennett, A. Testing the Efficacy of Homemade Masks: Would They Protect in an Influenza Pandemic? *Disaster Med. Public Health Prep.* **2013**, *7*, 413–418.
- 82 van der Sande, M.; Teunis, P.; Sabel, R. Professional and Home-Made Face Masks Reduce Exposure to Respiratory Infections among the General Population. *PLoS One* **2008**, *3*, e2618.
- 83 Parmet, W. E.; Sinha, M. S. Covid-19 — The Law and Limits of Quarantine. *N. Engl. J. Med.* **2020**, *382*, e28.
- 84 Howard, M. C. Gender, Face Mask Perceptions, and Face Mask Wearing: Are Men Being Dangerous during the COVID-19 Pandemic? *Pers. Individ. Dif.* **2021**, *170*, 110417.
- 85 Forsyth, D. R. Group-Level Resistance to Health Mandates during the COVID-19 Pandemic: A Groupthink Approach. *Gr. Dyn.* **2020**, *24*, 139–152.
- 86 Kramer, A.; Schwebke, I.; Kampf, G. How Long Do Nosocomial Pathogens Persist on Inanimate Surfaces? A Systematic Review. *BMC Infect. Dis.* **2006**, *6*, 130.
- 87 Donlan, R. M. Biofilm Formation: A Clinically Relevant Microbiological Process. *Clin. Infect. Dis.* **2001**, *33*, 1387–1392.
- 88 Pavithra, D.; Doble, M. Biofilm Formation, Bacterial Adhesion and Host Response on Polymeric Implants - Issues and Prevention. *Biomed. Mater.* **2008**, *3*, 034003.
- 89 Reynolds, K. A.; Watt, P. M.; Boone, S. A.; Gerba, C. P. Occurrence of Bacteria and Biochemical Markers on Public Surfaces. *Int. J. Environ. Health Res.* **2005**, *15*, 225–234.
- 90 Bright, K. R.; Boone, S. A.; Gerba, C. P. Occurrence of Bacteria and Viruses on Elementary Classroom Surfaces and the Potential Role of Classroom Hygiene in the Spread of Infectious Diseases. *J. Sch. Nurs.* **2010**, *26*, 33–41.
- 91 Møretrø, T.; Langsrud, S. Residential Bacteria on Surfaces in the Food Industry and Their Implications for Food Safety and Quality. *Compr. Rev. Food Sci. Food Saf.* **2017**, *16*, 1022–1041.
- 92 Scott, E.; Duty, S.; McCue, K. A Critical Evaluation of Methicillin-Resistant Staphylococcus Aureus and Other Bacteria of Medical Interest on Commonly Touched Household Surfaces in Relation to Household Demographics. *Am. J. Infect. Control* **2009**, *37*, 447–453.
- 93 Banerjee, I.; Pangule, R. C.; Kane, R. S. Antifouling Coatings: Recent Developments in the Design of Surfaces That Prevent Fouling by Proteins, Bacteria, and Marine Organisms. *Adv. Mater.* **2011**, *23*, 690–718.
- 94 Zhang, X.; Wang, L.; Levänen, E. Superhydrophobic Surfaces for the Reduction of Bacterial Adhesion. *RSC Adv.* **2013**, *3*, 12003–12020.
- 95 Yang, H.; Deng, Y. Preparation and Physical Properties of Superhydrophobic Papers. *J. Colloid Interface Sci.* **2008**, *325*, 588–593.

- 96 Hizal, F.; Rungraeng, N.; Lee, J.; Jun, S.; Busscher, H. J.; Van Der Mei, H. C.; Choi, C. H. Nanoengineered Superhydrophobic Surfaces of Aluminum with Extremely Low Bacterial Adhesivity. *ACS Appl. Mater. Interfaces* **2017**, *9*, 12118–12129.
- 97 Park, K. D.; Kim, Y. S.; Han, D. K.; Kim, Y. H.; Lee, E. H. B.; Suh, H.; Choi, K. S. Bacterial Adhesion on PEG Modified Polyurethane Surfaces. *Biomaterials* **1998**, *19*, 851–859.
- 98 Roosjen, A.; Van Der Mei, H. C.; Busscher, H. J.; Norde, W. Microbial Adhesion to Poly(Ethylene Oxide) Brushes: Influence of Polymer Chain Length and Temperature. *Langmuir* **2004**, *20*, 10949–10955.
- 99 Jeon, S. I.; Lee, J. H.; Andrade, J. D.; De Gennes, P. G. Protein-Surface Interactions in the Presence of Polyethylene Oxide. I. Simplified Theory. *J. Colloid Interface Sci.* **1991**, *142*, 149–158.
- 100 Kaur, R.; Liu, S. Antibacterial Surface Design – Contact Kill. *Prog. Surf. Sci.* **2016**, *91*, 136–153.
- 101 Silver, S.; Phung, L. T.; Silver, G. Silver as Biocides in Burn and Wound Dressings and Bacterial Resistance to Silver Compounds. *J. Ind. Microbiol. Biotechnol.* **2006**, *33*, 627–634.
- 102 Liao, S. Y.; Read, D. C.; Pugh, W. J.; Furr, J. R.; Russell, A. D. Interaction of Silver Nitrate with Readily Identifiable Groups: Relationship to the Antibacterial Action of Silver Ions. *Lett. Appl. Microbiol.* **1997**, *25*, 279–283.
- 103 Prabhu, S.; Poulouse, E. K. Silver Nanoparticles: Mechanism of Antimicrobial Action, Synthesis, Medical Applications, and Toxicity Effects. *Int. Nano Lett.* **2012**, *2*, 1–10.
- 104 Pal, S.; Tak, Y. K.; Song, J. M. Does the Antibacterial Activity of Silver Nanoparticles Depend on the Shape of the Nanoparticle? A Study of the Gram-Negative Bacterium *Escherichia coli*. *Appl. Environ. Microbiol.* **2007**, *73*, 1712–1720.
- 105 Li, J.; Rong, K.; Zhao, H.; Li, F.; Lu, Z.; Chen, R. Highly Selective Antibacterial Activities of Silver Nanoparticles against *Bacillus subtilis*. *J. Nanosci. Nanotechnol.* **2013**, *13*, 6806–6813.
- 106 Dibrov, P.; Dzioba, J.; Gosink, K. K.; Häse, C. C. Chemiosmotic Mechanism of Antimicrobial Activity of Ag⁺ in *Vibrio Cholerae*. *Antimicrob. Agents Chemother.* **2002**, *46*, 2668–2670.
- 107 Lok, C. N.; Ho, C. M.; Chen, R.; He, Q. Y.; Yu, W. Y.; Sun, H.; Tam, P. K. H.; Chiu, J. F.; Che, C. M. Proteomic Analysis of the Mode of Antibacterial Action of Silver Nanoparticles. *J. Proteome Res.* **2006**, *5*, 916–924.
- 108 Hsueh, Y. H.; Lin, K. S.; Ke, W. J.; Hsieh, C. Te; Chiang, C. L.; Tzou, D. Y.; Liu, S. T. The Antimicrobial Properties of Silver Nanoparticles in *Bacillus subtilis* Are Mediated by Released Ag⁺ Ions. *PLoS One* **2015**, *10*, e0144306.
- 109 Dakal, T. C.; Kumar, A.; Majumdar, R. S.; Yadav, V. Mechanistic Basis of Antimicrobial Actions of Silver Nanoparticles. *Front. Microbiol.* **2016**, *7*, 1831.
- 110 Jain, P.; Pradeep, T. Potential of Silver Nanoparticle-Coated Polyurethane Foam as an Antibacterial Water Filter. *Biotechnol. Bioeng.* **2005**, *90*, 59–63.
- 111 Sambhy, V.; MacBride, M. M.; Peterson, B. R.; Sen, A. Silver Bromide Nanoparticle/Polymer Composites: Dual Action Tunable Antimicrobial Materials. *J. Am. Chem. Soc.* **2006**, *128*, 9798–9808.

- 112 Zhao, L.; Wang, H.; Huo, K.; Cui, L.; Zhang, W.; Ni, H.; Zhang, Y.; Wu, Z.; Chu, P. K. Antibacterial Nano-Structured Titania Coating Incorporated with Silver Nanoparticles. *Biomaterials* **2011**, *32*, 5706–5716.
- 113 Yu, S.; Yin, Y.; Liu, J. Silver Nanoparticles in the Environment. *Environ. Sci. Process. Impacts* **2013**, *15*, 78–92.
- 114 Yan, A.; Chen, Z. Impacts of Silver Nanoparticles on Plants: A Focus on the Phytotoxicity and Underlying Mechanism. *Int. J. Mol. Sci.* **2019**, *20*, 1003.
- 115 Panáček, A.; Kvítek, L.; Smékalová, M.; Večeřová, R.; Kolář, M.; Röderová, M.; Dyčka, F.; Šebela, M.; Pucek, R.; Tomanec, O.; Zbořil, R. Bacterial Resistance to Silver Nanoparticles and How to Overcome It. *Nat. Nanotechnol.* **2018**, *13*, 65–71.
- 116 Grass, G.; Rensing, C.; Solioz, M. Metallic Copper as an Antimicrobial Surface. *Appl. Environ. Microbiol.* **2011**, *77*, 1541–1547.
- 117 Vincent, M.; Duval, R. E.; Hartemann, P.; Engels-Deutsch, M. Contact Killing and Antimicrobial Properties of Copper. *J. Appl. Microbiol.* **2018**, *124*, 1032–1046.
- 118 Santo, C. E.; Quaranta, D.; Grass, G. Antimicrobial Metallic Copper Surfaces Kill *Staphylococcus haemolyticus* via Membrane Damage. *Microbiologyopen* **2012**, *1*, 46–52.
- 119 Santo, C. E.; Taudte, N.; Nies, D. H.; Grass, G. Contribution of Copper Ion Resistance to Survival of *Escherichia coli* on Metallic Copper Surfaces. *Appl. Environ. Microbiol.* **2008**, *74*, 977–986.
- 120 Macomber, L.; Imlay, J. A. The Iron-Sulfur Clusters of Dehydratases Are Primary Intracellular Targets of Copper Toxicity. *Proc. Natl. Acad. Sci. U.S.A.* **2009**, *106*, 8344–8349.
- 121 Delgado, K.; Quijada, R.; Palma, R.; Palza, H. Polypropylene with Embedded Copper Metal or Copper Oxide Nanoparticles as a Novel Plastic Antimicrobial Agent. *Lett. Appl. Microbiol.* **2011**, *53*, 50–54.
- 122 Borg, D. A.; Trombetta, L. D. Toxicity and Bioaccumulation of the Booster Biocide Copper Pyrithione, Copper 2-Pyridinethiol-1-Oxide, in Gill Tissues of *Salvelinus fontinalis* (Brook Trout). *Toxicol. Ind. Health* **2010**, *26*, 139–150.
- 123 Peppiatt, C. J.; Armstrong, E.; Pisacane, A.; Burgess, J. G. Antibacterial Activity of Resin Based Coatings Containing Marine Microbial Extracts. *Biofouling* **2000**, *16*, 225–234.
- 124 Raghupathi, K. R.; Koodali, R. T.; Manna, A. C. Size-Dependent Bacterial Growth Inhibition and Mechanism of Antibacterial Activity of Zinc Oxide Nanoparticles. *Langmuir* **2011**, *27*, 4020–4028.
- 125 Xie, Y.; He, Y.; Irwin, P. L.; Jin, T.; Shi, X. Antibacterial Activity and Mechanism of Action of Zinc Oxide Nanoparticles against *Campylobacter jejuni*. *Appl. Environ. Microbiol.* **2011**, *77*, 2325–2331.
- 126 Schwartz, V. B.; Thétiot, F.; Ritz, S.; Pütz, S.; Choritz, L.; Lappas, A.; Förch, R.; Landfester, K.; Jonas, U. Antibacterial Surface Coatings from Zinc Oxide Nanoparticles Embedded in Poly(N-Isopropylacrylamide) Hydrogel Surface Layers. *Adv. Funct. Mater.* **2012**, *22*, 2376–2386.
- 127 Schwartz, V. B.; Thétiot, F.; Ritz, S.; Pütz, S.; Choritz, L.; Lappas, A.; Förch, R.; Landfester, K.; Jonas, U. Antibacterial Surface Coatings from Zinc Oxide Nanoparticles Embedded in

- Poly(N-Isopropylacrylamide) Hydrogel Surface Layers. *Adv. Funct. Mater.* **2012**, *22*, 2376–2386.
- 128 Ferreira, O.; Rijo, P.; Gomes, J.; Santos, R.; Monteiro, S.; Guedes, R.; Serralheiro, M. L.; Gomes, M.; Gomes, L. C.; Mergulhão, F. J.; Silva, E. R. Antimicrobial Ceramic Filters for Water Bio-Decontamination. *Coatings* **2021**, *11*, 323.
- 129 Manna, U.; Raman, N.; Welsh, M. A.; Zayas-Gonzalez, Y. M.; Blackwell, H. E.; Palecek, S. P.; Lynn, D. M. Slippery Liquid-Infused Porous Surfaces That Prevent Microbial Surface Fouling and Kill Non-Adherent Pathogens in Surrounding Media: A Controlled Release Approach. *Adv. Funct. Mater.* **2016**, *26*, 3599–3611.
- 130 Stigter, M.; Bezemer, J.; De Groot, K.; Layrolle, P. Incorporation of Different Antibiotics into Carbonated Hydroxyapatite Coatings on Titanium Implants, Release and Antibiotic Efficacy. *J. Control. Release* **2004**, *99*, 127–137.
- 131 Albright, V.; Zhuk, I.; Wang, Y.; Selin, V.; van de Belt-Gritter, B.; Busscher, H. J.; van der Mei, H. C.; Sukhishvili, S. A. Self-Defensive Antibiotic-Loaded Layer-by-Layer Coatings: Imaging of Localized Bacterial Acidification and PH-Triggering of Antibiotic Release. *Acta Biomater.* **2017**, *61*, 66–74.
- 132 Zhuk, I.; Jariwala, F.; Attygalle, A. B.; Wu, Y.; Libera, M. R.; Sukhishvili, S. A. Self-Defensive Layer-by-Layer Films with Bacteria-Triggered Antibiotic Release. *ACS Nano* **2014**, *8*, 7733–7745.
- 133 Fang, F. C. Perspectives series: host/pathogen interactions. Mechanisms of Nitric Oxide-Related Antimicrobial Activity. *J. Clin. Invest.* **1997**, *99*, 2818–2825.
- 134 Nablo, B. J.; Rothrock, A. R.; Schoenfisch, M. H. Nitric Oxide-Releasing Sol-Gels as Antibacterial Coatings for Orthopedic Implants. *Biomaterials* **2005**, *26*, 917–924.
- 135 Ferreira, C.; Pereira, A. M.; Pereira, M. C.; Melo, L. F.; Simões, M. Physiological Changes Induced by the Quaternary Ammonium Compound Benzyltrimethylammonium Chloride on *Pseudomonas Fluorescens*. *J. Antimicrob. Chemother.* **2011**, *66*, 1036–1043.
- 136 Tiller, J. C.; Liao, C. J.; Lewis, K.; Klivanov, A. M. Designing Surfaces That Kill Bacteria on Contact. *Proc. Natl. Acad. Sci. U. S. A.* **2001**, *98*, 5981–5985.
- 137 Milović, N. M.; Wang, J.; Lewis, K.; Klivanov, A. M. Immobilized N-Alkylated Polyethylenimine Avidly Kills Bacteria by Rupturing Cell Membranes with No Resistance Developed. *Biotechnol. Bioeng.* **2005**, *90*, 715–722.
- 138 Zanini, S.; Polissi, A.; Maccagni, E. A.; Dell’Orto, E. C.; Liberatore, C.; Riccardi, C. Development of Antibacterial Quaternary Ammonium Silane Coatings on Polyurethane Catheters. *J. Colloid Interface Sci.* **2015**, *451*, 78–84.
- 139 Pérez-Köhler, B.; Fernández-Gutiérrez, M.; Pascual, G.; García-Moreno, F.; San Román, J.; Bellón, J. M. In Vitro Assessment of an Antibacterial Quaternary Ammonium-Based Polymer Loaded with Chlorhexidine for the Coating of Polypropylene Prosthetic Meshes. *Hernia* **2016**, *20*, 869–878.
- 140 Gottenbos, B.; Van Der Mei, H. C.; Klatter, F.; Nieuwenhuis, P.; Busscher, H. J. In Vitro and in Vivo Antimicrobial Activity of Covalently Coupled Quaternary Ammonium Silane Coatings on Silicone Rubber. *Biomaterials* **2002**, *23*, 1417–1423.

- 141 Xue, Y.; Xiao, H.; Zhang, Y. Antimicrobial Polymeric Materials with Quaternary Ammonium and Phosphonium Salts. *Int. J. Mol. Sci.* **2015**, *16*, 3626–3655.
- 142 Matsunaga, T.; Tomoda, R.; Nakajima, T.; Wake, H. Photoelectrochemical Sterilization of Microbial Cells by Semiconductor Powders. *FEMS Microbiol. Lett.* **1985**, *29*, 211–214.
- 143 Krishna, V.; Pumprueg, S.; Lee, S. H.; Zhao, J.; Sigmund, W.; Koopman, B.; Moudgil, B. M. Photocatalytic Disinfection with Titanium Dioxide Coated Multi-Wall Carbon Nanotubes. *Process Saf. Environ. Prot.* **2005**, *83*, 393–397.
- 144 Evans, P.; Sheel, D. W. Photoactive and Antibacterial TiO₂ Thin Films on Stainless Steel. *Surf. Coatings Technol.* **2007**, *201*, 9319–9324.
- 145 Villatte, G.; Massard, C.; Descamps, S.; Sibaud, Y.; Forestier, C.; Awitor, K. O. Photoactive TiO₂ Antibacterial Coating on Surgical External Fixation Pins for Clinical Application. *Int. J. Nanomedicine* **2015**, *10*, 3367–3375.
- 146 Brogden, K. A. Antimicrobial Peptides: Pore Formers or Metabolic Inhibitors in Bacteria? *Nat. Rev. Microbiol.* **2005**, *3*, 238–250.
- 147 Guyomard, A.; Dé, E.; Jouenne, T.; Malandain, J.-J.; Muller, G.; Glinel, K. Incorporation of a Hydrophobic Antibacterial Peptide into Amphiphilic Polyelectrolyte Multilayers: A Bioinspired Approach to Prepare Biocidal Thin Coatings. *Adv. Funct. Mater.* **2008**, *18*, 758–765.
- 148 Chen, R.; Cole, N.; Willcox, M. D. P.; Park, J.; Rasul, R.; Carter, E.; Kumar, N. Synthesis, Characterisation and in Vitro Activity of a Surface-Attached Antimicrobial Cationic Peptide. *Biofouling* **2009**, *25*, 517–524.
- 149 Li, Y.; Yuan, H.; Von Dem Bussche, A.; Creighton, M.; Hurt, R. H.; Kane, A. B.; Gao, H. Graphene Microsheets Enter Cells through Spontaneous Membrane Penetration at Edge Asperities and Corner Sites. *Proc. Natl. Acad. Sci. U. S. A.* **2013**, *110*, 12295–12300.
- 150 Liu, Y.; Wen, J.; Gao, Y.; Li, T.; Wang, H.; Yan, H.; Niu, B.; Guo, R. Antibacterial Graphene Oxide Coatings on Polymer Substrate. *Appl. Surf. Sci.* **2018**, *436*, 624–630.
- 151 Wei, W.; Li, J.; Liu, Z.; Deng, Y.; Chen, D.; Gu, P.; Wang, G.; Fan, X. Distinct Antibacterial Activity of a Vertically Aligned Graphene Coating against Gram-Positive and Gram-Negative Bacteria. *J. Mater. Chem. B* **2020**, *8*, 6069–6079.
- 152 Wei, T.; Tang, Z.; Yu, Q.; Chen, H. Smart Antibacterial Surfaces with Switchable Bacteria-Killing and Bacteria-Releasing Capabilities. *ACS Appl. Mater. Interfaces* **2017**, *9*, 37511–37523.
- 153 Yu, J. C.; Ho, W.; Lin, J.; Yip, H.; Wong, P. K. Photocatalytic Activity, Antibacterial Effect, and Photoinduced Hydrophilicity of TiO₂ Films Coated on a Stainless Steel Substrate. *Environ. Sci. Technol.* **2003**, *37*, 2296–2301.
- 154 Schwartz, V. B.; Thétiot, F.; Ritz, S.; Pütz, S.; Choritz, L.; Lappas, A.; Förch, R.; Landfester, K.; Jonas, U. Antibacterial Surface Coatings from Zinc Oxide Nanoparticles Embedded in Poly(N-Isopropylacrylamide) Hydrogel Surface Layers. *Adv. Funct. Mater.* **2012**, *22*, 2376–2386.
- 155 Kiani, F.; Astani, N. A.; Rahighi, R.; Tayyebi, A.; Tayebi, M.; Khezri, J.; Hashemi, E.; Rothlisberger, U.; Simchi, A. Effect of Graphene Oxide Nanosheets on Visible Light-Assisted Antibacterial Activity of Vertically-Aligned Copper Oxide Nanowire Arrays. *J. Colloid Interface Sci.* **2018**, *521*, 119–131.

- 156 Schlaich, C.; Li, M.; Cheng, C.; Donskyi, I. S.; Yu, L.; Song, G.; Osorio, E.; Wei, Q.; Haag, R. Mussel-Inspired Polymer-Based Universal Spray Coating for Surface Modification: Fast Fabrication of Antibacterial and Superhydrophobic Surface Coatings. *Adv. Mater. Interfaces* **2018**, *5*, 1701254.
- 157 Ignatova, M.; Manolova, N.; Rashkov, I. Electrospun Antibacterial Chitosan-Based Fibers. *Macromol. Biosci.* **2013**, *13*, 860–872.
- 158 Yagci, M. B.; Bolca, S.; Heuts, J. P. A.; Ming, W.; De With, G. Antimicrobial Polyurethane Coatings Based on Ionic Liquid Quaternary Ammonium Compounds. *Prog. Org. Coatings* **2011**, *72*, 343–347.
- 159 Sun, L.; Yuan, G.; Gao, L.; Yang, J.; Chhowalla, M.; Gharahcheshmeh, M. H.; Gleason, K. K.; Choi, Y. S.; Hong, B. H.; Liu, Z. Chemical Vapour Deposition. *Nat. Rev. Methods Prim.* **2021**, *1*, 1–20.
- 160 Martin, T. P.; Kooi, S. E.; Chang, S. H.; Sedransk, K. L.; Gleason, K. K. Initiated Chemical Vapor Deposition of Antimicrobial Polymer Coatings. *Biomaterials* **2007**, *28*, 909–915.
- 161 Varghese, S.; Elfakhri, S.; Sheel, D. W.; Sheel, P.; Bolton, F. J.; Foster, H. A. Novel Antibacterial Silver-Silica Surface Coatings Prepared by Chemical Vapour Deposition for Infection Control. *J. Appl. Microbiol.* **2013**, *115*, 1107–1116.
- 162 Schofield, W. C. E.; Badyal, J. P. S. A Substrate-Independent Approach for Bactericidal Surfaces. *ACS Appl. Mater. Interfaces* **2009**, *1*, 2763–2767.
- 163 Dorman, H. J. D.; Deans, S. G. Antimicrobial Agents from Plants: Antibacterial Activity of Plant Volatile Oils. *J. Appl. Microbiol.* **2000**, *88*, 308–316.
- 164 Wijesekera, R. O. B.; Jayewardene, A. L.; Rajapakse, L. S. Volatile Constituents of Leaf, Stem and Root Oils of Cinnamon (*Cinnamomum Zeylanicum*). *J. Sci. Food Agric.* **1974**, *25*, 1211–1220.
- 165 Singh, G.; Maurya, S.; deLampasona, M. P.; Catalan, C. A. N. A Comparison of Chemical, Antioxidant and Antimicrobial Studies of Cinnamon Leaf and Bark Volatile Oils, Oleoresins and Their Constituents. *Food Chem. Toxicol.* **2007**, *45*, 1650–1661.
- 166 Deans, S. G.; Ritchie, G. Antibacterial Properties of Plant Essential Oils. *Int. J. Food Microbiol.* **1987**, *5*, 165–180.
- 167 Burt, S. Essential Oils: Their Antibacterial Properties and Potential Applications in Foods - A Review. *Int. J. Food Microbiol.* **2004**, *94*, 223–253.
- 168 Shreaz, S.; Wani, W. A.; Behbehani, J. M.; Raja, V.; Irshad, M.; Karched, M.; Ali, I.; Siddiqi, W. A.; Hun, L. T. Cinnamaldehyde and Its Derivatives, a Novel Class of Antifungal Agents. *Fitoterapia* **2016**, *112*, 116–131.
- 169 Ling, F.; Jiang, C.; Liu, G.; Li, M.; Wang, G. Anthelmintic Efficacy of Cinnamaldehyde and Cinnamic Acid from Cortex Cinnamon Essential Oil against *Dactylogyrus Intermedius*. *Parasitology* **2015**, *142*, 1744–1750.
- 170 Liu, X. C.; Cheng, J.; Zhao, N. N.; Liu, Z. L. Insecticidal Activity of Essential Oil of Cinnamomum Cassia and Its Main Constituent, Trans-Cinnamaldehyde, against the Booklice, *Liposcelis Bostrychophila*. *Trop. J. Pharm. Res.* **2014**, *13*, 1697–1702.

- 171 Hayashi, K.; Imanishi, N.; Kashiwayama, Y.; Kawano, A.; Terasawa, K.; Shimada, Y.; Ochiai, H. Inhibitory Effect of Cinnamaldehyde, Derived from Cinnamomi Cortex, on the Growth of Influenza A/PR/8 Virus in Vitro and in Vivo. *Antiviral Res.* **2007**, *74*, 1–8.
- 172 Ka, H.; Park, H. J.; Jung, H. J.; Choi, J. W.; Cho, K. S.; Ha, J.; Lee, K. T. Cinnamaldehyde Induces Apoptosis by ROS-Mediated Mitochondrial Permeability Transition in Human Promyelocytic Leukemia HL-60 Cells. *Cancer Lett.* **2003**, *196*, 143–152.
- 173 Zhang, W.; Xu, Y. C.; Guo, F. J.; Meng, Y.; Li, M. L. Anti-Diabetic Effects of Cinnamaldehyde and Berberine and Their Impacts on Retinol-Binding Protein 4 Expression in Rats with Type 2 Diabetes Mellitus. *Chin. Med. J. (Engl.)*. **2008**, *121*, 2124–2128.
- 174 Yuan, X.; Han, L.; Fu, P.; Zeng, H.; Lv, C.; Chang, W.; Runyon, R. S.; Ishii, M.; Han, L.; Liu, K.; Fan, T.; Zhang, W.; Liu, R. Cinnamaldehyde Accelerates Wound Healing by Promoting Angiogenesis via Up-Regulation of PI3K and MAPK Signalling Pathways. *Lab. Investig.* **2018**, *98*, 783–793.
- 175 Friedman, M. Chemistry, Antimicrobial Mechanisms, and Antibiotic Activities of Cinnamaldehyde against Pathogenic Bacteria in Animal Feeds and Human Foods. *J. Agric. Food Chem.* **2017**, *65*, 10406–10423.
- 176 Shen, S.; Zhang, T.; Yuan, Y.; Lin, S.; Xu, J.; Ye, H. Effects of Cinnamaldehyde on *Escherichia Coli* and *Staphylococcus Aureus* Membrane. *Food Control* **2015**, *47*, 196–202.
- 177 Moghimi, R.; Aliahmadi, A.; Rafati, H. Ultrasonic Nanoemulsification of Food Grade *Trans*-Cinnamaldehyde: 1,8-Cineol and Investigation of the Mechanism of Antibacterial Activity. *Ultrason. Sonochem.* **2017**, *35*, 415–421.
- 178 Nowotarska, S. W.; Nowotarski, K.; Grant, I. R.; Elliott, C. T.; Friedman, M.; Situ, C. Mechanisms of Antimicrobial Action of Cinnamon and Oregano Oils, Cinnamaldehyde, Carvacrol, 2,5-Dihydroxybenzaldehyde, and 2-Hydroxy-5-Methoxybenzaldehyde against *Mycobacterium avium* subsp. *paratuberculosis* (Map). *Foods*. **2017**, *6*, 72.
- 179 He, T. F.; Wang, L. H.; Niu, D. bao; Wen, Q. hui; Zeng, X. A. Cinnamaldehyde Inhibit *Escherichia Coli* Associated with Membrane Disruption and Oxidative Damage. *Arch. Microbiol.* **2019**, *201*, 451–458.
- 180 Han, C.; Wang, J.; Li, Y.; Lu, F.; Cui, Y. Antimicrobial-Coated Polypropylene Films with Polyvinyl Alcohol in Packaging of Fresh Beef. *Meat Sci.* **2014**, *96*, 901–907.
- 181 Ramos, M.; Jiménez, A.; Peltzer, M.; Garrigós, M. C. Characterisation and Antimicrobial Activity Studies of Polypropylene Films with Carvacrol and Thymol for Active Packaging. *J. Food Eng.* **2012**, *109*, 513–519.
- 182 Nayanathara, U.; Kottegoda, N.; Perera, I. C.; Mudiyansele, T. K. Synthesis, Photodegradable and Antibacterial Properties of Polystyrene-Cinnamaldehyde Copolymer Film. *Polym. Degrad. Stab.* **2018**, *155*, 195–207.
- 183 Sanla-Ead, N.; Jangchud, A.; Chonhenchob, V.; Suppakul, P. Antimicrobial Activity of Cinnamaldehyde and Eugenol and Their Activity after Incorporation into Cellulose-Based Packaging Films. *Packag. Technol. Sci.* **2012**, *25*, 7–17.
- 184 Hosseini, M. H.; Razavi, S. H.; Mousavi, M. A. Antimicrobial, Physical and Mechanical Properties of Chitosan-Based Films Incorporated with Thyme, Clove and Cinnamon Essential Oils. *J. Food Process. Preserv.* **2009**, *33*, 727–743.

- 185 Ravishankar, S.; Zhu, L.; Olsen, C. W.; McHugh, T. H.; Friedman, M. Edible Apple Film Wraps Containing Plant Antimicrobials Inactivate Foodborne Pathogens on Meat and Poultry Products. *J. Food Sci.* **2009**, *74*, M440–M445.
- 186 Gamage, G. R.; Park, H. J.; Kim, K. M. Effectiveness of Antimicrobial Coated Oriented Polypropylene/Polyethylene Films in Sprout Packaging. *Food Res. Int.* **2009**, *42*, 832–839.
- 187 Lopes, F. A.; De Fátima Ferreira Soares, N.; De Cássia Pires Lopes, C.; Da Silva, W. A.; Júnior, J. C. B.; Medeiros, E. A. A. Conservation of Bakery Products through Cinnamaldehyde Antimicrobial Films. *Packag. Technol. Sci.* **2014**, *27*, 293–302.
- 188 Huang, H. J.; Yuan, X. Z. Recent Progress in the Direct Liquefaction of Typical Biomass. *Prog. Energy Combust. Sci.* **2015**, *49*, 59–80.
- 189 Torres, A.; Romero, J.; Macan, A.; Guarda, A.; Galotto, M. J. Near Critical and Supercritical Impregnation and Kinetic Release of Thymol in LLDPE Films Used for Food Packaging. *J. Supercrit. Fluids* **2014**, *85*, 41–48.
- 190 Lee, H.; Dellatore, S. M.; Miller, W. M.; Messersmith, P. B. Mussel-Inspired Surface Chemistry for Multifunctional Coatings. *Science* **2007**, *318*, 426–430.
- 191 Waite, J. H.; Tanzer, M. L. Polyphenolic Substance of *Mytilus Edulis*: Novel Adhesive Containing L-Dopa and Hydroxyproline. *Science* **1981**, *212*, 1038–1040.
- 192 Lee, H.; Scherer, N. F.; Messersmith, P. B. Single-Molecule Mechanics of Mussel Adhesion. *Proc. Natl. Acad. Sci. U.S.A.* **2006**, *103*, 12999–13003.
- 193 Lu, Z.; Xiao, J.; Wang, Y.; Meng, M. *In Situ* Synthesis of Silver Nanoparticles Uniformly Distributed on Polydopamine-Coated Silk Fibers for Antibacterial Application. *J. Colloid Interface Sci.* **2015**, *452*, 8–14.
- 194 Sureshkumar, M.; Siswanto, D. Y.; Lee, C. K. Magnetic Antimicrobial Nanocomposite Based on Bacterial Cellulose and Silver Nanoparticles. *J. Mater. Chem.* **2010**, *20*, 6948–6955.
- 195 Sileika, T. S.; Kim, H. Do; Maniak, P.; Messersmith, P. B. Antibacterial Performance of Polydopamine-Modified Polymer Surfaces Containing Passive and Active Components. *ACS Appl. Mater. Interfaces* **2011**, *3*, 4602–4610.
- 196 He, T.; Zhu, W.; Wang, X.; Yu, P.; Wang, S.; Tan, G.; Ning, C. Polydopamine Assisted Immobilisation of Copper(II) on Titanium for Antibacterial Applications. *Mater. Technol.* **2015**, *30*, B68–B72.
- 197 Zhu, J.; Uliana, A.; Wang, J.; Yuan, S.; Li, J.; Tian, M.; Simoens, K.; Volodin, A.; Lin, J.; Bernaerts, K.; Zhang, Y.; Van Der Bruggen, B. Elevated Salt Transport of Antimicrobial Loose Nanofiltration Membranes Enabled by Copper Nanoparticles *Via* Fast Bioinspired Deposition. *J. Mater. Chem. A* **2016**, *4*, 13211–13222.
- 198 Shalev, T.; Gopin, A.; Bauer, M.; Stark, R. W.; Rahimipour, S. Non-Leaching Antimicrobial Surfaces through Polydopamine Bio-Inspired Coating of Quaternary Ammonium Salts or an Ultrashort Antimicrobial Lipopeptide. *J. Mater. Chem.* **2012**, *22*, 2026–2032.
- 199 Shi, H.; Xue, L.; Gao, A.; Fu, Y.; Zhou, Q.; Zhu, L. Fouling-Resistant and Adhesion-Resistant Surface Modification of Dual Layer PVDF Hollow Fiber Membrane by Dopamine and Quaternary Polyethyleneimine. *J. Memb. Sci.* **2016**, *498*, 39–47.
- 200 Liu, C. Y.; Huang, C. J. Functionalization of Polydopamine via the Aza-Michael Reaction for Antimicrobial Interfaces. *Langmuir* **2016**, *32*, 5019–5028.

- 201 Mohd Daud, N.; Saeful Bahri, I. F.; Nik Malek, N. A. N.; Hermawan, H.; Saidin, S. Immobilization of Antibacterial Chlorhexidine on Stainless Steel Using Crosslinking Polydopamine Film: Towards Infection Resistant Medical Devices. *Colloids Surfaces B* **2016**, *145*, 130–139.
- 202 He, S.; Zhou, P.; Wang, L.; Xiong, X.; Zhang, Y.; Deng, Y.; Wei, S. Antibiotic-Decorated Titanium with Enhanced Antibacterial Activity through Adhesive Polydopamine for Dental/Bone Implant. *J. R. Soc. Interface* **2014**, *11*, 20140169.
- 203 Lim, K.; Chua, R. R. Y.; Ho, B.; Tambyah, P. A.; Hadinoto, K.; Leong, S. S. J. Development of a Catheter Functionalized by a Polydopamine Peptide Coating with Antimicrobial and Antibiofilm Properties. *Acta Biomater.* **2015**, *15*, 127–138.
- 204 Lee, H.; Rho, J.; Messersmith, P. B. Facile Conjugation of Biomolecules onto Surfaces via Mussel Adhesive Protein Inspired Coatings. *Adv. Mater.* **2009**, *21*, 431–434.
- 205 Yin, Y.; Li, Y.; Cai, W.; Sui, J. One-Step Deposition of Antibacterial Ag@Pdop Hybrid Films on an NiTi Alloy. *RSC Adv.* **2019**, *9*, 29263–29272.
- 206 Liu, Z.; Hu, Y.; Liu, C.; Zhou, Z. Surface-Independent One-Pot Chelation of Copper Ions onto Filtration Membranes to Provide Antibacterial Properties. *Chem. Commun.* **2016**, *52*, 12245–12248.
- 207 Online Edition: "Combined Compendium of Food Additive Specifications" <http://www.fao.org/food/food-safety-quality/scientific-advice/jecfa/jecfa-additives/detail/en/c/249/>; accessed 18/06/2021.
- 208 Sileika, T. S.; Barrett, D. G.; Zhang, R.; Lau, K. H. A.; Messersmith, P. B. Colorless Multifunctional Coatings Inspired by Polyphenols Found in Tea, Chocolate, and Wine. *Angew. Chemie - Int. Ed.* **2013**, *52*, 10766–10770.
- 209 Guo, J.; Sun, W.; Kim, J. P.; Lu, X.; Li, Q.; Lin, M.; Mrowczynski, O.; Rizk, E. B.; Cheng, J.; Qian, G.; Yang, J. Development of Tannin-Inspired Antimicrobial Bioadhesives. *Acta Biomater.* **2018**, *72*, 35–44.
- 210 Sagbas, S.; Aktas, N.; Sahiner, N. Modified Biofunctional p(Tannic Acid) Microgels and Their Antimicrobial Activity. *Appl. Surf. Sci.* **2015**, *354*, 306–313.
- 211 Li, X.; Gao, P.; Tan, J.; Xiong, K.; Maitz, M. F.; Pan, C.; Wu, H.; Chen, Y.; Yang, Z.; Huang, N. Assembly of Metal-Phenolic/Catecholamine Networks for Synergistically Anti-Inflammatory, Antimicrobial, and Anticoagulant Coatings. *ACS Appl. Mater. Interfaces* **2018**, *10*, 40844–40853.
- 212 Xu, G.; Pranantyo, D.; Zhang, B.; Xu, L.; Neoh, K. G.; Kang, E. T. Tannic Acid Anchored Layer-by-Layer Covalent Deposition of Parasin i Peptide for Antifouling and Antimicrobial Coatings. *RSC Adv.* **2016**, *6*, 14809–14818.
- 213 Pranantyo, D.; Xu, L. Q.; Neoh, K. G.; Kang, E. T.; Ng, Y. X.; Teo, S. L. M. Tea Stains-Inspired Initiator Primer for Surface Grafting of Antifouling and Antimicrobial Polymer Brush Coatings. *Biomacromolecules* **2015**, *16*, 723–732.
- 214 Sagbas, S.; Aktas, N.; Sahiner, N. Modified Biofunctional p(Tannic Acid) Microgels and Their Antimicrobial Activity. *Appl. Surf. Sci.* **2015**, *354*, 306–313.

- 215 Payra, D.; Naito, M.; Fujii, Y.; Nagao, Y. Hydrophobized Plant Polyphenols: Self-Assembly and Promising Antibacterial, Adhesive, and Anticorrosion Coatings. *Chem. Commun.* **2016**, *52*, 312–315.
- 216 Von Harpe, A.; Petersen, H.; Li, Y.; Kissel, T. Characterisation of Commercially Available and Synthesized Polyethylenimines for Gene Delivery. *J. Control. Release* **2000**, *69*, 309–322.
- 217 Lin, J.; Qiu, S.; Lewis, K.; Klibanov, A. M. Bactericidal Properties of Flat Surfaces and Nanoparticles Derivatized with Alkylated Polyethylenimines. *Biotechnol. Prog.* **2002**, *18*, 1082–1086.
- 218 Tanizawa, Y.; Abe, T.; Yamada, K. Black Tea Stain Formed on the Surface of Teacups and Pots. Part 1 - Study on the Chemical Composition and Structure. *Food Chem.* **2007**, *103*, 1–7.
- 219 Yashin, A. Y.; Nemzer, B. V.; Combet, E.; Yashin, Y. I. Determination of the Chemical Composition of Tea by Chromatographic Methods: A Review. *J. Food Res.* **2015**, *4*, 56.
- 220 Bai, G.; Ma, S.; Qie, R.; Liu, Z.; Shi, Y.; Li, C.; Wang, R.; Guo, X.; Zhou, F.; Jia, X. UV-Triggered Surface-Initiated Polymerization from Colorless Green Tea Polyphenol-Coated Surfaces. *Macromol. Rapid Commun.* **2016**, *37*, 1256–1261.
- 221 Sileika, T. S.; Barrett, D. G.; Zhang, R.; Lau, K. H. A.; Messersmith, P. B. Colorless Multifunctional Coatings Inspired by Polyphenols Found in Tea, Chocolate, and Wine. *Angew. Chemie - Int. Ed.* **2013**, *52*, 10766–10770.
- 222 Bauer, U.; Federle, W. The Insect-Trapping Rim of Nepenthes Pitchers: Surface Structure and Function. *Plant Signal. Behav.* **2009**, *4*, 1019–1023.
- 223 Bohn, H. F.; Federle, W. Insect Aquaplaning: Nepenthes Pitcher Plants Capture Prey with the Peristome, a Fully Wettable Water-Lubricated Anisotropic Surface. *Proc. Natl. Acad. Sci. U. S. A.* **2004**, *101*, 14138–14143.
- 224 Wright, V. B.; Poulson, W. K.; Mackintosh, W. M. An Improved Manufacture of Compounds for Water-Proofing Textile and Other Fabrics, String, Ropes, and the Like, and Apparatus Therefor. Patent GB190325000A, 17th November 1904.
- 225 Vielle J. A. Improved Process for Rendering Materials Waterproof. Patent GB209138A, 7th January 1924.
- 226 Wong, T. S.; Kang, S. H.; Tang, S. K. Y.; Smythe, E. J.; Hatton, B. D.; Grinthal, A.; Aizenberg, J. Bioinspired Self-Repairing Slippery Surfaces with Pressure-Stable Omniphobicity. *Nature* **2011**, *477*, 443–447.
- 227 Epstein, A. K.; Wong, T. S.; Belisle, R. A.; Boggs, E. M.; Aizenberg, J. Liquid-Infused Structured Surfaces with Exceptional Anti-Biofouling Performance. *Proc. Natl. Acad. Sci. U. S. A.* **2012**, *109* (33), 13182–13187.
- 228 Xiao, L.; Li, J.; Mieszkin, S.; Di Fino, A.; Clare, A. S.; Callow, M. E.; Callow, J. A.; Grunze, M.; Rosenhahn, A.; Levkin, P. A. Slippery Liquid-Infused Porous Surfaces Showing Marine Antibiofouling Properties. *ACS Appl. Mater. Interfaces* **2013**, *5* (20), 10074–10080.
- 229 Leslie, D. C.; Waterhouse, A.; Berthet, J. B.; Valentin, T. M.; Watters, A. L.; Jain, A.; Kim, P.; Hatton, B. D.; Nedder, A.; Donovan, K.; Super, E. H.; Howell, C.; Johnson, C. P.; Vu, T. L.; Bolgen, D. E.; Rifai, S.; Hansen, A. R.; Aizenberg, M.; Super, M.; Aizenberg, J.; Ingber, D.

- E.. A Bioinspired Omniphobic Surface Coating on Medical Devices Prevents Thrombosis and Biofouling. *Nat. Biotechnol.* **2014**, *32*, 1134–1140.
- 230 Ozbay, S.; Yuceel, C.; Erbil, H. Y. Improved Icephobic Properties on Surfaces with a Hydrophilic Lubricating Liquid. *ACS Appl. Mater. Interfaces* **2015**, *7*, 22067–22077.
- 231 Zhang, J.; Gu, C.; Tu, J. Robust Slippery Coating with Superior Corrosion Resistance and Anti-Icing Performance for AZ31B Mg Alloy Protection. *ACS Appl. Mater. Interfaces* **2017**, *9*, 11247–11257.
- 232 Charpentier, T. V. J.; Neville, A.; Baudin, S.; Smith, M. J.; Euvrard, M.; Bell, A.; Wang, C.; Barker, R. Liquid Infused Porous Surfaces for Mineral Fouling Mitigation. *J. Colloid Interface Sci.* **2015**, *444*, 81–86.
- 233 Wang, B. L.; Heng, L.; Jiang, L. Temperature-Responsive Anisotropic Slippery Surface for Smart Control of the Droplet Motion. *ACS Appl. Mater. Interfaces* **2018**, *10*, 7442–7450.
- 234 Luo, H.; Lu, Y.; Yin, S.; Huang, S.; Song, J.; Chen, F.; Chen, F.; Carmalt, C. J.; Parkin, I. P. Robust Platform for Water Harvesting and Directional Transport. *J. Mater. Chem. A* **2018**, *6*, 5635–5643.
- 235 Dai, X.; Sun, N.; Nielsen, S. O.; Stogin, B. B.; Wang, J.; Yang, S.; Wong, T. S. Hydrophilic Directional Slippery Rough Surfaces for Water Harvesting. *Sci. Adv.* **2018**, *4*, eaaq0919.
- 236 Li, Q.; Guo, Z. Lubricant-Infused Slippery Surfaces: Facile Fabrication, Unique Liquid Repellence and Antireflective Properties. *J. Colloid Interface Sci.* **2019**, *536*, 507–515.
- 237 Mukherjee, R.; Habibi, M.; Rashed, Z. T.; Berbert, O.; Shi, X.; Boreyko, J. B. Oil-Impregnated Hydrocarbon-Based Polymer Films. *Sci. Rep.* **2018**, *8*, 1–13.
- 238 Wang, J.; Wang, L.; Sun, N.; Tierney, R.; Li, H.; Corsetti, M.; Williams, L.; Wong, P. K.; Wong, T. S. Viscoelastic Solid-Repellent Coatings for Extreme Water Saving and Global Sanitation. *Nat. Sustain.* **2019**, *2*, 1097–1105.
- 239 Zhang, J.; Liu, P.; Yi, B.; Wang, Z.; Huang, X.; Jiang, L.; Yao, X. Bio-Inspired Elastic Liquid-Infused Material for On-Demand Underwater Manipulation of Air Bubbles. *ACS Nano* **2019**, *13*, 10596–10602.
- 240 Wang, Y.; Zhang, H.; Liu, X.; Zhou, Z. Slippery Liquid-Infused Substrates: A Versatile Preparation, Unique Anti-Wetting and Drag-Reduction Effect on Water. *J. Mater. Chem. A* **2016**, *4*, 2524–2529.
- 241 Yuan, S.; Li, Z.; Song, L.; Shi, H.; Luan, S.; Yin, J. Liquid-Infused Poly(Styrene-*b*-Isobutylene-*b*-Styrene) Microfiber Coating Prevents Bacterial Attachment and Thrombosis. *ACS Appl. Mater. Interfaces* **2016**, *8*, 21214–21220.
- 242 Lee, J.; Yoo, J.; Kim, J.; Jang, Y.; Shin, K.; Ha, E.; Ryu, S.; Kim, B. G.; Wooh, S.; Char, K. Development of Multimodal Antibacterial Surfaces Using Porous Amine-Reactive Films Incorporating Lubricant and Silver Nanoparticles. *ACS Appl. Mater. Interfaces* **2019**, *11*, 6550–6560.
- 243 Tatarazako, N.; Ishibashi, H.; Teshima, K.; Kishi, K.; Arizono, K. Effects of Triclosan on Various Aquatic Organisms. *Environ. Sci.* **2004**, *11*, 133–140.
- 244 Tuo, Y.; Zhang, H.; Chen, W.; Liu, X. Corrosion Protection Application of Slippery Liquid-Infused Porous Surface Based on Aluminum Foil. *Appl. Surf. Sci.* **2017**, *423*, 365–374

- 245 Wang, P.; Zhang, D.; Sun, S.; Li, T.; Sun, Y. Fabrication of Slippery Lubricant-Infused Porous Surface with High Underwater Transparency for the Control of Marine Biofouling. *ACS Appl. Mater. Interfaces* **2017**, *9*, 972–982
- 246 Xiang, T.; Zhang, M.; Sadig, H. R.; Li, Z.; Zhang, M.; Dong, C.; Yang, L.; Chan, W.; Li, C. Slippery Liquid-Infused Porous Surface for Corrosion Protection with Self-Healing Property. *Chem. Eng. J.* **2018**, *345*, 147–155
- 247 Niemelä-Anttonen, H.; Koivuluoto, H.; Tuominen, M.; Teisala, H.; Juuti, P.; Haapanen, J.; Harra, J.; Stenroos, C.; Lahti, J.; Kuusipalo, J.; et al. Icephobicity of Slippery Liquid Infused Porous Surfaces under Multiple Freeze–Thaw and Ice Accretion–Detachment Cycles. *Adv. Mater. Interfaces* **2018**, *5*, 1800828
- 248 He, X.; Tian, F.; Bai, X.; Yuan, C. Role of Trapped Air and Lubricant in the Interactions between Fouling and SiO₂ Nanoparticle Surfaces. *Colloids Surf. B: Biointerfaces* **2019**, *184*, 110502

CHAPTER 2

2 Experimental Methods

2.1 Plasma Deposition

A plasma is made up of a partially ionised gas, containing electrons, ions (both positively and negatively charged), and non-ionised gaseous species. Despite the presence of charge carriers, plasmas are overall neutral due to the charges being balanced.¹ Plasmas are commonly referred to as the fourth state of matter, owing to their differences to conventional gases.²

Plasmas can be induced in gases by application of an electrical field at a suitable frequency. This results in the acceleration of the free electrons in the system. Collisions between the electrons and neutral gas atoms results in the freeing of electrons and ionisation. These freed electrons are also then accelerated and undergo further collisions, resulting in the formation of the plasma. The processes may occur upon collisions, such as excitation and dissociation. Excitation refers to where a ground state electron in an atom moves to a higher energy level; this is followed by relaxation where the electron moves back down to the ground state, and simultaneous emission of light takes place. Dissociation occurs when a molecule is split, resulting in the formation of radical species.

Plasmachemical deposition (or polymerisation) is a process where a plasma is induced in a monomer precursor vapour or gas. The ionised species react with each other, resulting on the formation of polymeric species. Continuous wave plasma results in harsh conditions which leads to significant fragmentation of the polymers, shorter polymer chain lengths, and loss of functionality.³ It may also result in etching of substrate surface. Therefore, a solution is to use pulsed plasma—the duty cycle comprises of a short on time (t_{on}), where the plasma is induced in the monomer and ions are being formed, and a longer off time (t_{off}) where the plasma is extinguished and the reactive species can undergo conventional polymerisation reactions.⁴ The average plasma power is defined as:

$$\langle P \rangle = P_P \left(\frac{t_{on}}{t_{on} + t_{off}} \right) \quad (2.1)$$

where $\langle P \rangle$ is the average power, and P_P is the peak power.

Polymer coatings can form on the surfaces of substrates owing to the formation of radicals on the surface during the early stages of the plasma

deposition process. Pulsing the plasma results in better retention of structure and functionality, allows longer polymer chains to form, and gives control over the amount of cross-linking between polymer chains.⁵ Pulsed plasma deposition also has several advantages over conventional polymerisation techniques: it does not require the use of solvent or the addition of an initiator, reaction times are typically much faster, it is low temperature (i.e. 20 °C), and coatings are conformal and substrate independent.

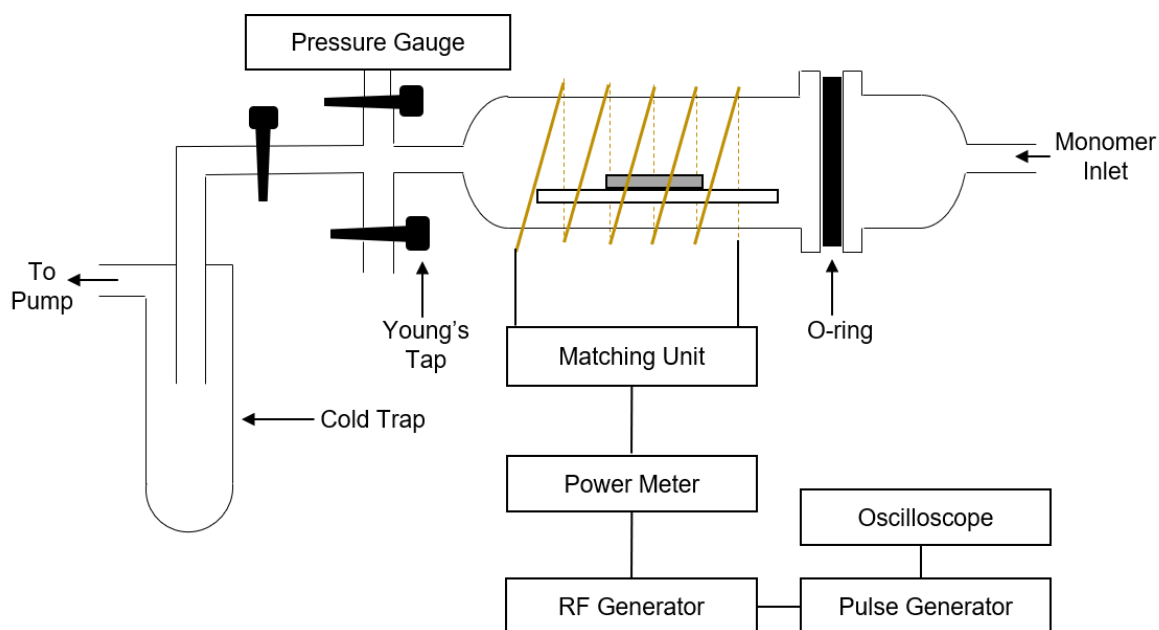


Figure 2.1: Pulsed plasma deposition apparatus. (Not to scale).

Typical pulsed plasma depositions in this thesis were carried out in a cylindrical glass reactor (5.5 cm diameter, 475 cm³ volume) housed within a Faraday cage was used for plasmachemical deposition. This was connected to a 30 L min⁻¹ rotary pump (model E2M2, Edwards Vacuum Ltd.) via a liquid nitrogen cold trap (base pressure less than 2×10^{-3} mbar and air leak rate better than 6×10^{-9} mol s⁻¹). A copper coil wound around the reactor (4 mm diameter, 10 turns, located 10 cm downstream from the gas inlet) was connected to a 13.56 MHz radio frequency (RF) power supply via an L–C matching network. A pulse signal generator was used to trigger the RF power supply. Prior to film deposition, the whole apparatus was thoroughly scrubbed using detergent and hot water, rinsed with propan-2-ol (+99.5 wt.%, Fisher Scientific UK Ltd.), oven dried at 150 °C, and further cleaned using a 50 W continuous wave air plasma at 0.2 mbar for 30 min. Silicon wafer (Silicon Valley Microelectronics Inc.,

orientation: <100>, resistivity: 5-20 $\Omega\cdot\text{cm}$, thickness: $525 \pm 25 \mu\text{m}$, front surface: polished, back surface: etched) cleaning comprised sonication in a 50:50 100 ml mixture of propan-2-ol and cyclohexane (+99.7 wt.%, Sigma–Aldrich Ltd.) for 15 min prior to air drying and placement into the centre of the chamber. Further cleaning entailed running a 50 W continuous wave air plasma at 0.2 mbar for 30 min. The monomer precursor was loaded into a sealable glass tube, degassed via several freeze–pump–thaw cycles, and then attached to the reactor. Monomer vapour was then allowed to purge the apparatus at a pressure of typically 0.15–0.20 mbar (except benzyl acrylate, which had a vapour pressure of 0.08 mbar) for 15 min prior to electrical discharge ignition. An initial continuous wave plasma was run for 30 s to ensure good adhesion to the substrate before switching to pulsed mode required for well-defined plasmachemical deposition over a period lasting 30 min. Upon electrical discharge extinction, the precursor vapour was allowed to continue to pass through the system for a further 15 min, and then the chamber was evacuated to base pressure followed by venting to atmosphere.

Atomised Spray Plasma Deposition (ASPD) is a variant of plasmachemical deposition in which a liquid is delivered to an atomising nozzle which is then atomised at its atomising surface by transferring “vibrational” energy generated by piezoelectric transducers.⁶ The atomised spray enters the reaction chamber and a continuous wave plasma is induced. This method results in greatly superior deposition times compared to pulsed plasma deposition, and allows the plasmachemical deposition of non-volatile liquids, or of solutions or suspensions of non-volatile solids that would otherwise be impossible with vapour-phase pulsed plasma techniques.^{6,7}

Atomized-spray-plasma deposition was carried out in an electrodeless, cylindrical, T-shape, glass reactor (volume 820 cm^3 , base pressure of 3×10^{-3} mbar, and with a leak rate better than $2 \times 10^{-9} \text{ mol s}^{-1}$), enclosed in a Faraday cage.⁸ The atomizer nozzle (Model No. 8700-120, 120 kHz, Sono Tek Corp.) inlet was surrounded by a copper coil (4 mm diameter, 7.5 turns). Substrates for coating were placed downstream in-line-of-sight relative to the atomizer nozzle. The chamber was pumped down using a 30 L min^{-1} rotary pump (E2M2, Edwards Vacuum Inc.) attached to a liquid nitrogen cold trap; a Pirani gauge was used to monitor system pressure. The output impedance of a 13.56 MHz radio frequency (RF) power supply was matched to the partially ionized gas load via an L–C matching unit connected to the copper coil. Prior to each deposition, the reactor

was scrubbed using detergent, rinsed in propan-2-ol, and dried in an oven. A continuous-wave air plasma was then run at 0.2 mbar pressure and 50 W power for 30 min in order to remove any remaining trace contaminants from the chamber walls. The precursor mixture was loaded into a sealable glass tube and degassed using several freeze-pump-thaw cycles. Precursor mixture was introduced into the reactor at a flow rate of 0.02 ml s^{-1} . Deposition entailed running a continuous wave plasma at a power of 40 W for 6 min. Upon plasma extinction, the system was evacuated to base pressure before venting to atmosphere.

2.2 Infrared Spectroscopy

Molecules can absorb infrared light, leading to molecular vibrations, and the frequencies that can be absorbed will depend upon the nature of the functional groups present. Therefore, by measuring the absorbance of infrared radiation by a chemical compound across the spectrum, it is possible to examine structural features of the molecule. Absorption of infrared light causes a change in the vibrational energy level of the molecule ($\nu = \pm 1$, transitions greater than 1 are formally forbidden). The absorption must also result in a change in the dipole moment, μ , of the molecule. If both these conditions are met, the absorbance is infrared-active, and can be detected via infrared spectroscopy.⁹

Scanning through a range of wavenumbers individually would lead to long analysis times, so instead Fourier Transform infrared spectroscopy (FTIR) is utilised—Fourier transform is a mathematical tool which, when performed on a wave, can be used to calculate the frequencies (i.e. wavenumbers) present in that wave, as well as their relative intensities. In an FTIR spectrometer, the infrared beam from the light source is directed onto a beam splitter, which divides the beam into two, and directs one onto a mirror with fixed position, and the other onto a moveable mirror. This introduces a path difference between the two beams, and when they recombine, they will interfere constructively or destructively. The resulting signal (known as an interferogram), once it has passed through the sample, is collected by the detector. Fourier transform is then used to convert the interferogram into the sample's infrared spectrum.

FTIR spectra of powders, liquids, or thick coatings can be acquired using attenuated total reflectance (ATR) technique. The ATR sample stage comprises a diamond crystal on top of which the sample is placed. The infrared beam is directed *via* mirrors into the crystal at such an angle that the beam undergoes

total internal reflection. An evanescent (rapidly-decaying) wave is formed at the surface of the crystal, which can penetrate a couple of micrometres into the sample.

For thin film nanocoatings (<1 μm thickness), reflection-absorption infrared spectroscopy (RAIRS) is used. The coating is deposited onto a reflective substrate (in this case, silicon wafer). The infrared beam is directed *via* mirrors at a grazing angle onto the coated substrate surface, the beam then penetrates the thin film coating, and is reflected off of the substrate surface. The beam is then passed through a polarizer which removes the s-polarized component of the beam (light that is polarized perpendicular to the plane of incidence).

The detector employed is a mercury cadmium telluride (MCT) detector— infrared photons that hit the detector promote electrons from the valence band up into the conduction band. The increase in the number of charge carriers (i.e. the conductivity) is directly proportional to the intensity of the infrared radiation.

Infrared spectra in this thesis were acquired using a FTIR spectrometer equipped with a liquid nitrogen cooled MCT detector (model Spectrum One, PerkinElmer Inc.). Spectra were collected at 4 cm^{-1} resolution across the 400–4000 cm^{-1} range and averaged over 100 scans. Attenuated total reflectance (ATR) infrared spectra were obtained using a diamond ATR accessory (model Golden Gate, Graseby Specac Ltd.). Reflection-absorption (RAIRS) measurements utilized a variable angle accessory (Graseby Specac Ltd.) fitted with a KRS-5 polarizer (to remove the s-polarized component) set at either 55° or 66° with respect to the surface normal.

2.3 Antibacterial Testing

Quantitative analysis of the ability of a surface to kill bacteria is important when producing antimicrobial coatings. Antibacterial testing is carried out against both a Gram-positive bacteria species (*S. aureus*) and a Gram-negative bacteria species (*E. coli*) in order to demonstrate broad-spectrum antibacterial activity. Reusability of coatings (i.e. performing multiple consecutive antibacterial tests using the same sample)) is important in order to gain an understanding of how the antibacterial activity of a coating/surface decreases with contact time.

Antibacterial testing in this thesis was performed as follows: Gram-negative *Escherichia coli* BW25113 (CGSC 7636; *rrnB3* Δ *lacZ4787* *hsdR514* Δ (*araBAD*)567 Δ (*rhaBAD*)568 *rph-1*) and Gram-positive *Staphylococcus aureus*

(FDA209P, an MSSA strain; ATCC 6538P) bacterial cultures were prepared using autoclaved (Autoclave Vario 1528, Dixons Ltd.) Luria-Bertani broth media (LB; L3022, Sigma-Aldrich Ltd., 2% w/v in Milli-Q[®] grade water). A 5 ml bacterial culture was grown from a single colony for 16 h at 37 °C, and then 50 µL used to inoculate a sterile polystyrene cuvette (Catalogue No. 67.742, Sarstedt AG) containing 1 ml of LB Broth. The cuvette was covered with Parafilm (Cole-Parmer Ltd.) and then placed inside a shaking incubator (model Stuart Orbital Incubator S1500, Cole-Parmer Ltd.) set at 37 °C and 120 rpm. An optical density OD_{600nm} = 0.4 was verified using a UV-Vis spectrophotometer (model Jenway 6300, Cole-Parmer Ltd.) to obtain bacteria at the mid-log phase of growth.

Both uncoated and coated samples were cut into 15 x 15 mm squares before use. Uncoated control samples were washed in absolute ethanol for 15 min and then dried under vacuum in order to make sure they were sterile and clean. Sterile microtubes (1.5 ml, Sarstedt AG) were loaded with the untreated or coated substrates. Next, 100 µL of the prepared bacterial culture was pipetted onto each substrate placed aseptically inside a microtube so that the microorganisms could interact with one side of the surface. In practice, the liquid spread over the whole area of the sample. The microtube lid was closed, to prevent the sample drying out, and the tube placed horizontally on a sample tray and incubated (model Bacterial Incubator 250, LMS Ltd.) without shaking for 4 h at 30 °C. Next, 900 µL of autoclaved Luria-Bertani broth media was pipetted into each microtube and mixed using a vortex mixer (model Vortex-Genie 2, Scientific Industries Inc.) in order to recover the bacteria as a 10-fold dilution (10^{-1}). Further ten-fold serial dilutions were undertaken to provide 10^{-2} , 10^{-3} , 10^{-4} , 10^{-5} and 10^{-6} samples. Colony-forming unit (CFU) plate counting was performed by placing 10 µL drops from each diluted sample (10^{-1} to 10^{-6} dilutions) onto autoclaved Luria-Bertani Agar solid plates (EZMix[™] powder, dust free, fast dissolving fermentation medium, L7533, Sigma-Aldrich Ltd.) and incubating (model Bacterial Incubator 250, LMS Ltd.) for 16 h at 30 °C. The number of colonies visible at each dilution was then counted. All tests were performed in triplicate. The Log₁₀ Reduction value for a treated sample was calculated relative to a control untreated sample. For each experiment, treated and untreated substrates were exposed to bacteria in parallel and incubated under identical conditions for the same time period before recovery and viability measurement. The high numbers of bacteria recovered from untreated substrates provides good evidence that the method is

effective. Furthermore, the vortex mixer agitates the samples at 2000–3000 rpm and is fully capable of removing bacteria from surfaces.¹⁰

For antibacterial recycling tests the same procedure as described above was followed, with the variation that, following 4 h incubation, the substrates were taken out from the 10^{-1} dilution solution microtubes, rinsed with ultrapure water (approximately 50 ml) for 1 min at 20 °C and then completely air-dried overnight before the next use. Consecutive repeat tests were performed using the same samples, with the bacterial culture being placed on the same side of the substrate each time. All tests were performed in triplicate.

2.4 Film Thickness Measurements

Spectrophotometry is a non-destructive technique used to measure the thickness of thin films (typically $<5\ \mu\text{m}$). A monochromated UV-visible light source beam is directed onto a thin film, and when the light reaches the air–film interface, some light will be reflected off the incident surface (specular reflectance), and some will transmit to the film (some may also be absorbed). Light that passes through the film is reflected off the substrate back through the film into air, Figure 2.2.

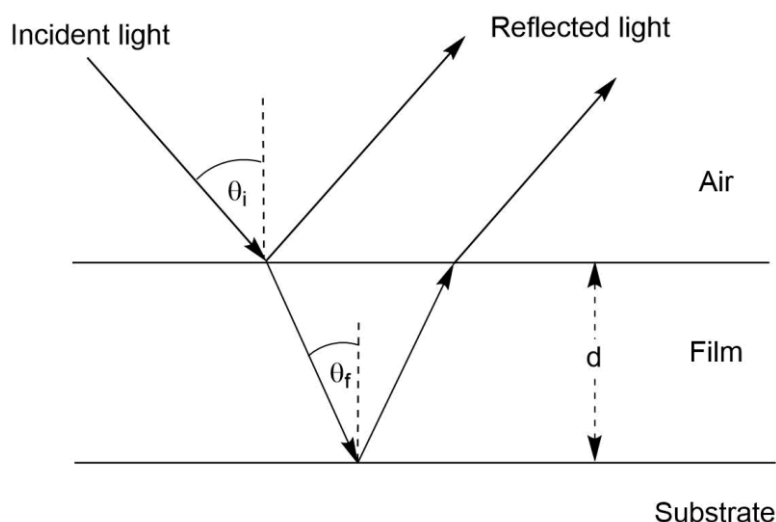


Figure 2.2: Schematic showing pathways of incident light on a thin film coating on a substrate.

Light reflected from both interfaces will recombine before reaching the detector. Since the beam that has passed through the film has travelled further than the beam reflected at the air–film interface, there will now be a phase difference between the two beams. The path difference between the two beams

depends on the film thickness, d ; the wavelength of light, λ ; the angle of incidence within the film, θ_f , and the film refractive index, n .

$$\text{Path difference} = 2dn_{\text{film}}\cos(\theta_f) \quad (2.2)$$

For a system where a polymer thin film is coated on a silicon wafer, and therefore $n_{\text{air}} < n_{\text{film}} < n_{\text{silicon}}$, constructive interference will happen when the path difference is a whole integer multiple of the wavelength:

$$2dn_{\text{film}}\cos(\theta_f) = m\lambda \quad (2.3)$$

and destructive interference when the path difference is a half integer multiple of the wavelength:

$$2dn_{\text{film}}\cos(\theta_f) = (m + \frac{1}{2})\lambda \quad (2.4)$$

where m is an integer, 0, 1, 2... etc.

The intensity of reflected light therefore will oscillate over the range of wavelengths used. Successive reflectance measurements are made incrementally over a range of wavelengths (350 nm–1000 nm). The resulting reflectance spectrum can be fitted using a Cauchy model to calculate the film thickness.

Coating thicknesses of samples on silicon wafer were measured using a spectrophotometer (model nkd-6000, Aquila Instruments Ltd.). Transmittance–reflectance curves (350–1000 nm wavelength range) were acquired for each sample and fitted to a Cauchy model for dielectric materials¹¹ using a modified Levenberg–Marquardt algorithm.¹²

2.5 Contact Angle Measurements

2.5.1 Contact Angle

When a droplet of a liquid is placed on a surface, a contact angle will form between the droplet and the surface. The contact angle can be related to the surface tensions of the solid-liquid, solid-gas, and liquid-gas interfaces (γ_{SL} , γ_{SG} , and γ_{LG} respectively) by the Young's equation¹³, Equation (2.5 and Figure 2.3:

$$\gamma_{\text{SG}} = \gamma_{\text{SL}} + \gamma_{\text{LG}}\cos\theta \quad (2.5)$$

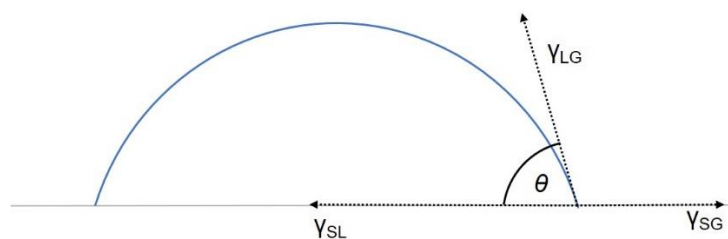


Figure 2.3: Schematic demonstrating surface tensions and contact angle for a droplet on a flat surface.

In goniometry, a small sessile droplet is placed on the surface of interest, and a camera looks at the droplet from the side. Contact angles can then be measured from the acquired images.

2.5.2 Contact Angle Hysteresis

While it may appear on the macroscale that surfaces look flat and smooth, on the microscale and nanoscale however there may be roughness which can take the form of peaks and troughs or other such features, all of which provide an energy barrier to movement of the liquid droplet. When a droplet is expanded (i.e. the volume is increased outwards from the centre), the droplet will swell and the contact angle will increase until such a point where the droplet has sufficient energy to overcome the barrier to movement, at which time, the ‘triple point’ (the point where the solid, liquid and gas phases all meet) will move outwards—the contact angle at the instance when the triple point starts to move outwards is called the ‘advancing angle’. Similarly, if the droplet volume is decreased inwards from the centre, the droplet will flatten and the contact angle will decrease until there is sufficient energy for the droplet to move and the triple point will move inwards—the contact angle at the instance when the triple point starts to move inwards is called the ‘receding angle’. The difference between the advancing angle and the receding angle is known as the ‘contact angle hysteresis’. This is used to examine the wettability and liquid repellency of the surface.

Sessile drop static contact angle measurements were carried out at 20 °C using a video capture apparatus in combination with a motorised syringe (model VCA 2500XE, A.S.T. Products Inc.). 2.0 µl droplets of ultrapure water were employed to assess hydrophobicity. Advancing and receding contact angle values were determined by respectively increasing the dispensed 2.0 µl liquid drop volume by a further 2.0 µl at a rate of 0.1 µl s⁻¹, and then decreasing the

liquid drop volume at a rate of $0.1 \mu\text{l s}^{-1}$.¹⁴ Measurements were repeated at least 3 times, at 3 randomly chosen points on the substrate surface.

2.5.3 Sliding Angle

Sliding angle (also known as ‘tilt angle’ or ‘roll-off angle’) is a simple technique used to examine the liquid repellency of a surface. The sample is placed on a stage of which the tilt angle can be adjusted. The initial angle is set to 0° , and a droplet of the liquid is placed on the surface of the sample. The tilt angle is then slowly increased until the droplet shows motion across the surface. The smallest angle at which the droplet initially starts to move is the sliding angle.

Sliding angle measurements were carried out at 20°C using a V-block adjustable angle gauge (model Adjustable Angle Gauge/Tilting Vee Blocks small, Arc Euro Trade Ltd.). Samples were placed onto the stage with an initial angle of 0° . A $50 \mu\text{l}$ droplet of deionised water was dispensed onto the sample, and the tilt angle was slowly increased at a rate of 1° every 5 s until movement of the water droplet was observed.^{15,16} Measurements were repeated at least 3 times.

2.6 UV-Vis Spectroscopy

When light is passed through a sample, light that is of the correct wavelength to cause excitations of the molecules to higher energy states are absorbed. This will cause a drop in the relative intensity for the wavelengths that are absorbed. The absorbance of a sample, A , is defined as the logarithm of the ratio of the original intensity of the beam of light, I_0 , to the intensity after it has passed through a sample, I :

$$A = \log \left(\frac{I_0}{I} \right) \quad (2.6)$$

The Beer-Lambert law states that the absorbance of light through a sample is directly proportional to the concentration, c , the path length, l , and the molar extinction coefficient, ϵ :

$$A = \epsilon cl \quad (2.7)$$

The molar extinction coefficient is an intrinsic property of a chemical which is a measurement of how much light a compound can absorb at a given wavelength.

Ultraviolet-visible (UV-Vis) spectra were collected on a UV-Vis-NIR spectrophotometer (model Cary 5000, Agilent Technologies Inc.). Reference

solution samples were analysed in quartz cuvettes with 1 cm path length. Coated samples were prepared by direct application onto quartz substrates (fused quartz plate, thickness = 1 mm, UQG Ltd.).

2.7 X-Ray Photoelectron Spectroscopy

X-ray photoelectron spectroscopy (XPS) is a useful technique used to examine the elemental composition of a surface. The sample surface is irradiated with a beam of soft X-rays, usually Mg K_{α} (1253.6 eV) or Al K_{α} (1486.6 eV). The X-rays excite atoms at the surface, which causes the ejection of a photoelectron from the core level, Figure 2.4.

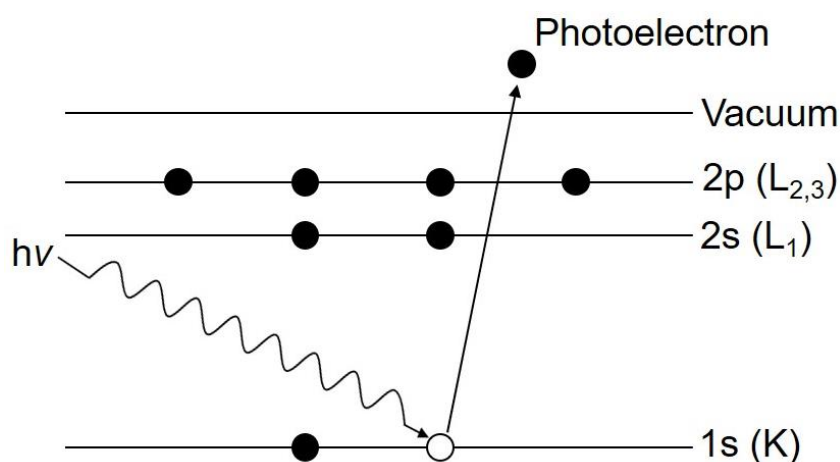


Figure 2.4: XPS emission of a photoelectron from core energy level into vacuum.

The kinetic energy of the photoelectrons is given by:

$$E_k = h\nu - E_B - \phi \quad (2.8)$$

where E_k is the kinetic energy of the photoelectron; h is the Planck's constant and ν is the frequency of the photon (and therefore $h\nu$ is the energy of the photon); E_B is the binding energy of the electron; and ϕ is the work function which is a constant, whose value is equal to the work done on an electron to move it from the sample surface to be absorbed by the detector. Since the energy levels of electrons in atoms are quantized and have discrete values, and these energies (i.e. the binding energy) is different and characteristic for each element, the kinetic energies of the detected photoelectrons can be used to determine what individual elements are present at the surface of the sample. Analysis of the relative peak areas in the produced spectra using empirically derived relative sensitivity factors can yield relative atomic compositions. Although the X-rays can penetrate several micrometres into the surface, only photoelectrons within the top

5 nm of the surface will be able to escape, meaning that XPS is very surface sensitive. XPS must be performed under ultra-high vacuum (approximately 10^{-9} – 10^{-10} mbar), otherwise the surface will have an adsorbed gas layer on the surface from the atmosphere, or it may become contaminated, for example, from dust or oxidation. Ultra-high vacuum is achieved by using diffusion pumps.

Surface elemental compositions of coatings were measured using an electron spectrometer (model VG ESCALAB II) equipped with a non-monochromated Mg $K_{\alpha 1,2}$ X-ray source (1253.6 eV) and a concentric hemispherical analyser. Photoemitted electrons were collected at a take-off angle of 20° from the substrate normal, with electron detection in the constant analyser energy mode (CAE, pass energies of 20 eV and 50 eV for high resolution and survey spectra respectively). The core level binding energy envelopes were fitted using Gaussian peak shapes with fixed full-width-half-maxima (fwhm) and linear backgrounds.^{17, 18} All binding energies were referenced to the C(1s) $-C_xH_y$ hydrocarbon peak at 285.0 eV.

2.8 Scanning Electron Microscopy

Scanning electron microscopy (SEM) is a technique used to examine the topography of an object at high magnifications that would not be possible with conventional light microscopes. A beam of high-energy electrons is focused onto the sample, and these electrons excite atoms at the surface to higher energy levels, which causes emission of low-energy secondary electrons. The secondary electrons are then collected by the detector. The number of secondary electrons is related to the sample topography, and so, by scanning across the surface of the sample, an image can be formed as the electron beam scans across the sample surface. Build-up of surface charge means that samples have to be coated with a thin coating of a conductive material—this is typically achieved by sputter-coating a gold layer onto the sample.

SEM images in this thesis were acquired as follows: substrates were mounted onto carbon disks supported on aluminium stubs, and then coated with a thin gold layer (5–10 nm, Polaron SEM Coating Unit, Quorum Technologies Ltd.). Images were acquired using a scanning electron microscope (model Vega 3LMU, Tescan Orsay Holdings a.s.) operating in secondary electron detection mode, in conjunction with an 8 kV accelerating voltage, and a working distance of 8–11 mm.

2.9 Transmission Electron Microscopy

Transmission electron microscopy (TEM) is a technique used to examine the structure of very thin samples. A beam of electrons is focused onto a sample, and passes through it, and subsequently is collected on a detector to form an image. As the electrons pass through the sample, they can be absorbed or back-scattered, depending on the thickness and transparency, leaving those areas that more strongly block the transmission of electrons darker than those areas that electrons can more easily pass through. TEM has greater resolution than SEM, but requires that the sample be very thin (<100 nm) to allow transmission of electrons. Samples must be mounted on support grids prior to TEM.

Transmission electron microscope (TEM) images were taken using a working voltage of 100 kV (Hitachi HT7800 120 kV TEM, Hitachi Ltd.).

2.10 X-Ray Diffraction

Crystalline solids contain atoms arranged in periodic three-dimensional structures. When a crystalline solid is irradiated with a beam of electromagnetic radiation that has a wavelength similar to that of the separation distance of crystal planes in the solid (i.e. of the order of 1 Å), the radiation will be diffracted. Therefore, X-rays are used to examine the crystal structures of solids. As the radiation is scattered by the crystal planes, the radiation will recombine leading to constructive and destructive interference. Constructive interference occurs at angles where the path difference of the beams is equal to a multiple of the wavelength of the radiation. Bragg's law states that:

$$n\lambda = 2d\sin(\theta) \quad (2.9)$$

where n is an integer describing the diffraction order, λ is the wavelength of radiation, d is the crystal plane separation distance, and θ is the diffraction angle. Destructive interference will occur at all other angles, leading to the appearance of diffraction peaks.

X-ray diffraction was performed using copper $K_{\alpha 1}/K_{\alpha 2}$ radiation (model Bruker AXS D8 Advance, Bruker UK Ltd.) equipped with a PSD detector (brand Lynx-Eye) and with a nickel filter, and variable slits to give a 6 mm beam on the sample. The diffractometer was operated in Bragg–Brentano mode at room temperature. Each diffraction pattern was recorded over a 2θ range of 20–80°

with a step size of 0.02° , for a total scan time of 30 min. Coated glass slides were analysed.

2.11 Raman Spectroscopy

Raman spectroscopy is used to examine the vibrational modes of molecules, and thus give insight into the molecular structure. A beam from a monochromatic laser source is directed onto the sample which causes excitation of the molecule to a 'virtual' energy state. The molecule rapidly relaxes to the ground electronic state, releasing photons, and the energy of the scattered light is measured.¹⁹ When the molecule relaxes, three different transitions can occur: (i) Rayleigh scattering, where the molecule relaxes to the original vibrational level, (ii) Stokes Raman scattering, where the molecule relaxes to a vibrational level higher than the original ground level, and (iii) anti-Stokes Raman scattering, where the molecule relaxes to a vibrational level lower than the original. Rayleigh scattering is the most intense, and is removed using a filter as it does not provide any information about vibrational modes in the molecule. Stokes and anti-Stokes Raman scattering are relatively much weaker in intensity, and it is these two that are used to examine the vibrational modes present.

Raman spectroscopy was performed on a Raman micro-scope equipped with a 300 line mm^{-1} diffraction grating (Dilor LabRam, Horiba UK Ltd.). A helium-neon laser (632.8 nm line operating at 11 mW power) was used as the excitation source, and spectra were collected over the $100\text{--}4000 \text{ cm}^{-1}$ region as an average of 10 scans each lasting 10 s.

2.12 Mass Spectrometry

In mass spectrometry, a sample is ionized and the mass-to-charge (m/z) ratio of the resulting ions is detected and recorded in a mass spectrum. From this, information such as empirical formula, possible structures of a molecule from its fragmentation ions, and analysis of components in a mixture can all be inferred. There are numerous techniques employed to ionize a sample—here, atmospheric solids analysis probe (ASAP) is utilised. The sample (either a solid, a liquid, or a solution) is applied to a capillary tube. The sample is thermally desorbed from the surface of the tube *via* heating under nitrogen flow. A corona discharge then ionizes the sample, which is then sent to a time-of-flight detector.

In a time-of-flight detector, ions are accelerated by an electric field of known strength. If the distance that the ions travel in the detector is kept constant, then the time-of-flight will be proportional to the mass-charge ratio (m/z) of the ion. Thus, by measuring the time it takes ions to move through the detector, the m/z values can be determined. This technique has the advantages that it can be used with low-volatile compounds and does not require any sample preparation.

Atmospheric pressure solids analysis probe ionisation (ASAP) mass spectrometry was performed in positive ion mode (model Xevo QToF mass spectrometer, Waters Ltd., UK).

2.13 Inductively Coupled Plasma Optical Emission Spectroscopy

Inductively coupled plasma optical emission spectroscopy (ICP-OES) is a technique used for the quantitative detection of elements. A plasma is ignited in the instrument, and a nebuliser delivers an aqueous solution containing an unknown concentration of the element of interest into the plasma. The plasma excites the atoms to higher energy states, causing them to emit light at certain wavelengths which are then detected. These spectral lines are unique to each element, so by comparing the intensities of light at these wavelengths to standard solutions of known concentrations, the concentration of the element in the unknown solution can be deduced.

ICP-OES was performed on resultant acidic solutions using a vertical torch, cyclonic spray chamber, and concentric nebulizer (model iCAP, Thermo Fisher Scientific UK Ltd.). Measurements were taken in the axial mode at the following wavelengths: Cu = 219.958 nm, 224.700 nm, 324.754 nm, 327.396 nm; and Ag = 224.641 nm, 243.779 nm, 328.068 nm, 338.288 nm.

2.14 Atomic Force Microscopy

Atomic force microscopy (AFM) is a type of scanning probe microscopy technique. The probe consists of a sharp tip attached to a cantilever—when the tip is brought into close contact with a surface, the atoms on the tip will interact with atoms at the surface of the sample *via* intermolecular forces, which causes a change in the height of the cantilever, and this change is measured to give an image of the surface topography. In tapping mode AFM, the probe is vibrated at near the resonant frequency of the cantilever—this means that the tip is only in

contact with the sample surface intermittently, which minimises damage to the surface caused by the tip. Interactions with the surface cause a change in the amplitude of vibrations, which can be measured and from which the surface topography can be calculated.

Atomic force microscopy (AFM) images were acquired using a Bruker MM8 Multimode AFM scanning probe microscope. Scans were made with at least 256-line resolution in Peakforce QNM mode at 1 kHz in the vertical direction, and Nunano Scout 150 probes with a nominal force constant of 18 N m^{-1} . Images were analysed using Gwyddion v2.53 software. Root-mean-square roughness values ($Roughness_{\text{RMS}}$) were calculated over $1 \mu\text{m} \times 1 \mu\text{m}$ scan areas.

2.15 References

- 1 Langmuir, I. Oscillations in Ionized Gases. *Proc. Natl. Acad. Sci.* **1928**, *14*, 627–637.
- 2 Langmuir, I. The Interaction of Electron and Positive Ion Space Charges in Cathode Sheaths. *Phys. Rev.* **1929**, *33*, 954–989.
- 3 Yasuda, H. Plasma Polymerization; Academic Press: New York, 1985
- 4 Yasuda, H.; Hsu, T. Some Aspects of Plasma Polymerization Investigated By Pulsed R. F. Discharge. *J Polym Sci Polym Chem Ed* **1977**, *15*, 81–97.
- 5 Tarducci, C.; Kinmond, E. J.; Badyal, J. P. S.; Brewer, S. A.; Willis, C. Epoxide-Functionalized Solid Surfaces. *Chem. Mater.* **2000**, *12*, 1884–1889.
- 6 Wood, T. J.; Badyal, J. P. S. Atomized Spray Plasma Deposition (ASPD) of Structurally Well-Defined Alkyl Functionalized Layers. *Surf. Coatings Technol.* **2013**, *227*, 28–31.
- 7 Castaneda-Montes, I.; Ritchie, A. W.; Badyal, J. P. S. Atomised Spray Plasma Deposition of Hierarchical Superhydrophobic Nanocomposite Surfaces. *Colloids Surfaces A Physicochem. Eng. Asp.* **2018**, *558*, 192–199.
- 8 Wood, T. J.; Brown, P. S.; Badyal, J. P. S. Atomized Spray Plasma Deposition of Structurally Well-Defined Bioactive Coatings. *Plasma Chem Plasma Process* **2014**, *34*, 1019–1031.
- 9 Atkins, P.; De Paula, J. Atkins' Physical Chemistry, ninth ed; Oxford University Press: Oxford, 2010; pp 447.
- 10 Cox, H. J.; Li, J.; Saini, P.; Paterson, J. R.; Sharples, G. J.; Badyal, J. P. S. Bioinspired and Eco-Friendly High Efficacy Cinnamaldehyde Antibacterial Surfaces. *J. Mater. Chem. B* **2021**, *9*, 2918–2930.
- 11 Diebold, A. C., Chism, W. W. Characterisation and metrology of medium dielectric constant gate dielectric films. In *High Dielectric Constant Materials: VSLI MOSFET Applications*; H.R. Huff, D.C. Gilmer (Eds.), Springer-Verlag, Berlin Heidelberg, 2005, pp. 486
- 12 Lovering D (1999) INKD-6000 technical manual. Aquila Instruments, Cambridge, UK.
- 13 Young, T. III. An Essay on the Cohesion of Fluids. *Phil. Trans. R. Soc.* **1805**, *95*, 65–87.
- 14 Johnson, R. E., Jr.; Dettre, R. H. Wetting of low-energy surfaces. In *Wettability*; Berg, J. C., Ed.; Marcel Dekker, Inc.: New York, **1993**; Chapter 1, p 13.
- 15 Pierce, E.; Carmona, F. J.; Amirfazli, A. Understanding of Sliding and Contact Angle Results in Tilted Plate Experiments. *Colloids Surfaces A Physicochem. Eng. Asp.* **2008**, *323*, 73–82.
- 16 Chang, C.-C.; Wu, C.-J.; Sheng, Y.-J.; Tsao, H.-K. Anti-Smudge Behavior of Facilely Fabricated Liquid-Infused Surfaces with Extremely Low Contact Angle Hysteresis Property. *RSC Advances* **2016**, *6*, 19214–19222.
- 17 Evans, J. F.; Gibson, J. H.; Moulder, J. F.; Hammond, J. S.; Goretzki, H. Angle Resolved ESCA Analysis of Plasma Modified Polyesterene. *Fresen. Z. Anal. Chem.* **1984**, *319*, 841–844.
- 18 Friedman, R. M.; Hudis, J.; Perlman, M. L. Chemical Effects on Linewidths Observed in Photoelectron Spectroscopy. *Phys. Rev. Lett.* **1972**, *29*, 692–695.
- 19 Lin-Vien, D.; Colthrup, N. B.; Fateley, W. G.; Grasselli, J. G. The Handbook of Infrared and Raman Characteristic Frequencies of Organic Molecules; Academic Press: Boston, 1991.

Chapter 3

3 Cinnamaldehyde Antibacterial Surfaces

3.1 Introduction

In this chapter, single-step dip-coating deposition of cinnamaldehyde-containing antibacterial surface layers is described. Dopamine is polymerized in the presence of an aqueous solution containing tris(hydroxymethyl)aminomethane and cinnamaldehyde, Figure 3.1. Analogous antibacterial coatings are prepared by combining polyethyleneimine or tannic acid with cinnamaldehyde. Additionally, cinnamaldehyde is impregnated into a range of porous materials, including non-woven polypropylene cloth, polytetrafluoroethylene membrane, and knitted cotton, via simple dip-coating, to achieve high levels of antibacterial activity over extended recycling. Each of these approaches is inspired by the presence of bioactive compounds often found in plant epicuticular wax layers and essential oil glands located at the surfaces of leaves and citrus peel.^{1,2,3}

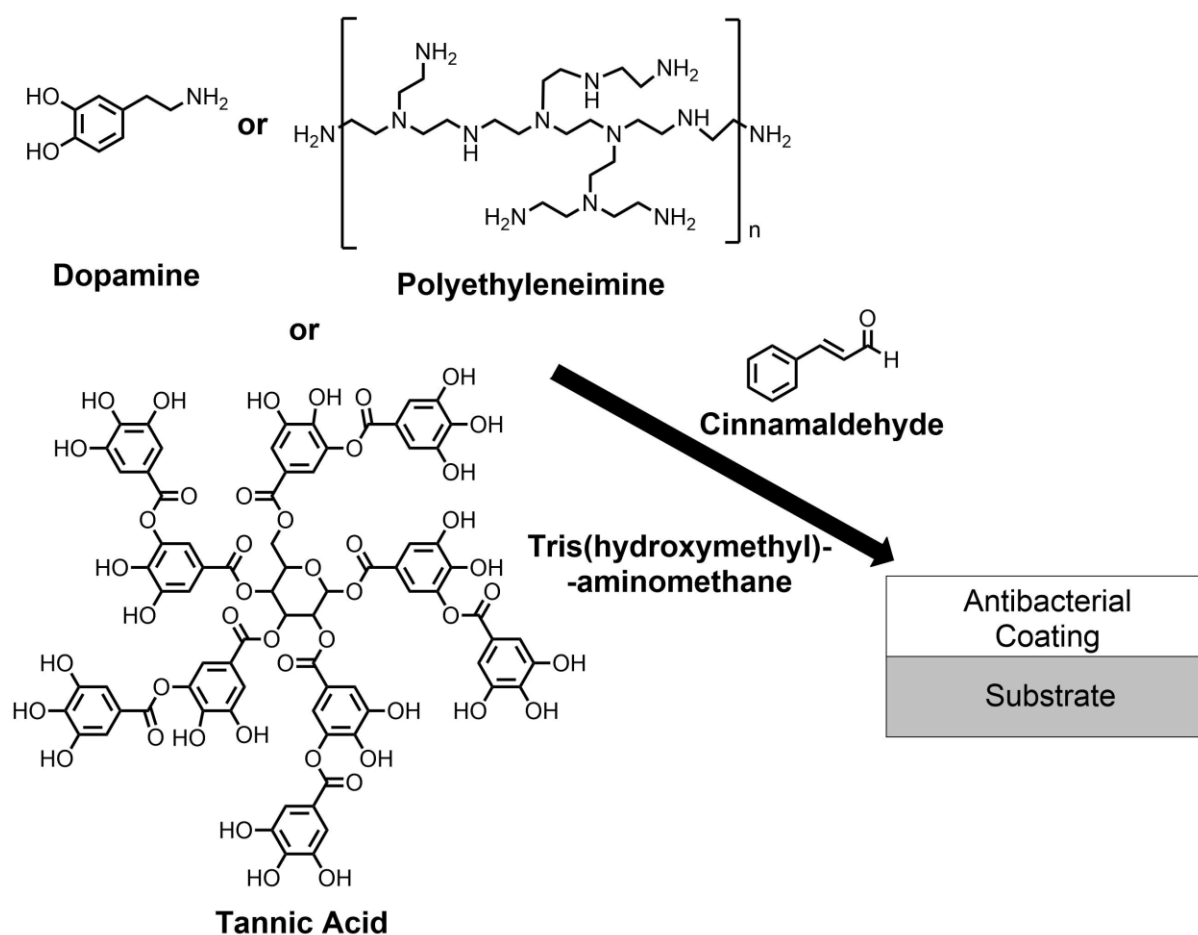


Figure 3.1: Deposition of polydopamine–cinnamaldehyde, polyethyleneimine–cinnamaldehyde, and tannic acid–cinnamaldehyde antibacterial coatings.

3.2 Experimental

3.2.1 Coating Preparation

Polyethylene terephthalate film (PET, capacitor grade, 0.10 mm thickness, Lawson Mardon Ltd.), non-woven polypropylene cloth (0.41 mm thick, 22.7 ± 4.4 μm fibre diameter, with dimpled structure 0.68 ± 0.16 mm separation, spunbond, 70 g m^{-2} , Avoca Technical Ltd.), polytetrafluoroethylene microporous membrane (PTFE, Type 3V, surface area 5.6 m^2 , Mupor Ltd.), and knitted cotton fabric (WarwickEquest Ltd.) were cut into 15 mm x 15 mm pieces and used as substrates for coating.

For the following coatings, a stock basic aqueous buffer solution was prepared by dissolving tris(hydroxymethyl)aminomethane (303 mg, 99.8%, Acros Organics brand, Fisher Scientific UK Ltd.) in 100 ml high purity water to yield a 25 mM solution. Hydrochloric acid (1 M, Fisher Scientific UK Ltd.) was then added dropwise until pH 8.5 was obtained (Pocket Checker pH Tester, Hanna Instruments Ltd.).

Polydopamine-only reference coating solutions were prepared using dopamine hydrochloride (30 mg, 99%, Alfa Aesar brand, Fisher Scientific UK Ltd.) dissolved in aqueous solution of tris(hydroxymethyl)aminomethane buffer (10 ml, 25 mM, pH 8.5) in a glass vial.¹⁹⁰ Poly(norepinephrine)-only coatings were synthesised using the same procedure as for polydopamine, but with DL-norepinephrine hydrochloride (30 mg, $\geq 97\%$, Sigma-Aldrich Ltd.) instead of dopamine hydrochloride.

Cinnamaldehyde-only reference solutions were prepared by adding trans-cinnamaldehyde (150 mg equivalent to 15 mg ml^{-1} in final solution; 99%, Acros Organics brand, Fisher Scientific UK Ltd.) into a glass vial followed by 10 ml of aqueous tris(hydroxymethyl)aminomethane buffer (25 mM, pH 8.5).

Polydopamine–cinnamaldehyde coating solutions were prepared by mixing dopamine hydrochloride (30 mg) and cinnamaldehyde (150 mg) in a glass vial. Aqueous tris(hydroxymethyl)aminomethane buffer (10 ml, 25 mM, pH 8.5) was then added to the vial (i.e. equivalent to 3 mg ml^{-1} of dopamine hydrochloride, cinnamaldehyde at 15 mg ml^{-1} solution, equivalent to a 1:5 mass ratio of dopamine hydrochloride to cinnamaldehyde and a 1:4.5 molar ratio of tris(hydroxymethyl)aminomethane to cinnamaldehyde). Poly(norepinephrine)–cinnamaldehyde coatings were synthesised using the same procedure as for

polydopamine–cinnamaldehyde, but with DL-norepinephrine hydrochloride ($\geq 97\%$, Sigma-Aldrich Inc.) instead of dopamine hydrochloride.

For polyethyleneimine–cinnamaldehyde coating, polyethyleneimine solution (2.0 g, 50 wt% aqueous, MW 750,000 Da, branched, Sigma-Aldrich Ltd.) was diluted in 50 ml of water to give a 20 mg ml⁻¹ aqueous solution of polyethyleneimine. Cinnamaldehyde (200 mg) and 10 ml of the 20 mg ml⁻¹ polyethyleneimine solution were then added to a vial. Control polyethyleneimine-only treated substrates were immersed in the 20 mg ml⁻¹ aqueous solution of polyethyleneimine.

Preparation of tannic acid–cinnamaldehyde coating solutions comprised mixing tannic acid (30 mg, Sigma-Aldrich Ltd.) with cinnamaldehyde (30 mg) in a glass vial. Aqueous tris(hydroxymethyl)aminomethane buffer (10 ml, 25 mM, pH 8.5) was added to the vial (equivalent to both tannic acid and cinnamaldehyde at 3 mg ml⁻¹ solution, and a 1:1 weight ratio of tannic acid to cinnamaldehyde)—absence of tris(hydroxymethyl)aminomethane did not lead to complete coating formation. Tannic acid-only coating solutions were similarly prepared by excluding cinnamaldehyde in the procedure.

For each of the aforementioned coating solutions, substrates were immediately placed into the vial, the lid closed, and the vials shaken for 24 h at 20 °C using an orbital shaker (model Vibrax VXR, IKA Ltd.). Subsequently the substrates were removed and washed with ultrapure water for 5 min whilst shaking, and then placed on a glass slide to dry in air for at least 3 h at 20 °C.

Phenethylamine–cinnamaldehyde product was prepared by dissolving phenethylamine (0.10 ml, 0.794 mmol, 99%, Sigma-Aldrich Ltd.) and cinnamaldehyde (0.10 ml, 0.794 mmol) in methanol (10 ml, >95%, Fisher Scientific UK Ltd.) and allowing to react in a glass vial with the lid closed for 24 h at 20 °C. The lid was then removed, and the methanol evaporated off at 20 °C. The formed product was dried under vacuum and analysed.

For cinnamaldehyde-only porous substrates: porous non-woven polypropylene cloth pieces were immersed into 10 ml aqueous suspension of cinnamaldehyde (15 mg ml⁻¹) and shaken for 24 h at 20 °C; then removed, washed in ultrapure water for 5 min, before finally drying in air for at least 3 h at 20 °C. Polytetrafluoroethylene (PTFE) membrane and knitted cotton pieces were immersed into 10 ml aqueous cinnamaldehyde suspension (3 mg ml⁻¹) and shaken for 24 h at 20 °C, then removed, rinsed in ultrapure water for 5 min, and

placed on a glass slide to dry in air for a minimum of 3 h at 20 °C. For all three porous materials, tris(hydroxymethyl)aminomethane was not included in the solutions.

3.2.2 Coating Characterisation

Infrared spectra were acquired as described in section 2.2. The infrared spectrum of dried polyethyleneimine was obtained from the supplied polyethyleneimine aqueous solution (following water removal *in vacuo*).

Ultraviolet–visible (UV-Vis) spectra were acquired as described in section 2.6. For measuring cinnamaldehyde release into aqueous medium, each coated substrate was immersed into a glass jar containing 100 ml of ultrapure water at 20 °C, with the sample fully submerged below the water surface. 1 ml aliquots were removed for UV-Vis analysis at various times. Each aliquot was further diluted with 9 ml of water. These diluted aliquots were placed into 1 cm path length quartz cuvettes and analysed using UV-Vis spectroscopy.

Mass spectrometry was carried out as described in section 2.12.

3.2.3 Antibacterial Testing

Antibacterial testing was carried out as described in section 2.3. For SEM microscopy, samples treated with bacteria were first immersed into glutaraldehyde (TAAB Laboratories Equipment Ltd.) (2% in Sorenson Phosphate Buffer) overnight, then removed and rinsed with Milli-Q[®] grade water to remove any excess glutaraldehyde. SEM images were acquired as described in section 2.8.

3.3 Results

3.3.1 Polydopamine–Cinnamaldehyde Coating

For the cinnamaldehyde-only control treatment, the cinnamaldehyde oil sunk to the bottom of the aqueous tris(hydroxymethyl)aminomethane solution in the vial. However, vigorous shaking of the vial for a few seconds turned the solution milky in appearance (due to the suspension of cinnamaldehyde in water). A slight colour change to yellow was seen in the solution. No solid formation was

observed over a period of time, until eventually the cinnamaldehyde constituent slowly coalesced to separate out from the aqueous phase.

Immersion of PET film substrate into the polydopamine-only coating solution gave rise to the appearance of a dark grey-black polydopamine surface layer, Figure 3.2. Over the course of the reaction, the polydopamine precursor solution simultaneously turned from colourless to black within the vial due to polydopamine precipitate formation.

For the combined polydopamine–cinnamaldehyde system, addition of the aqueous tris(hydroxymethyl)aminomethane solution to the dopamine hydrochloride and cinnamaldehyde solid-liquid mixture led to the dopamine hydrochloride dissolving, and the cinnamaldehyde settling at the bottom of the vial. After vigorous shaking of the vial for a few seconds, the solution turned milky in appearance (due to the suspension of cinnamaldehyde oil in the aqueous medium—as described above), Figure 3.2. Over time, the white cloudiness faded away. However, no black colouration indicative of polydopamine was observed at any point during the reaction—neither on the substrates, nor in the solution. Instead, the white cloudiness disappeared to give a clear solution with a slight yellow colour. This was accompanied by the formation of a red coating on the substrates (as well as on the vial bottoms), Figure 3.2. The mass increase of PET film following polydopamine–cinnamaldehyde coating was measured to be $4.4 \pm 0.9 \text{ mg cm}^{-2}$ (assuming both sides are coated), Table 3.1. A range of different substrates could be coated by this method, including PET, polypropylene, silicon wafer, and glass.

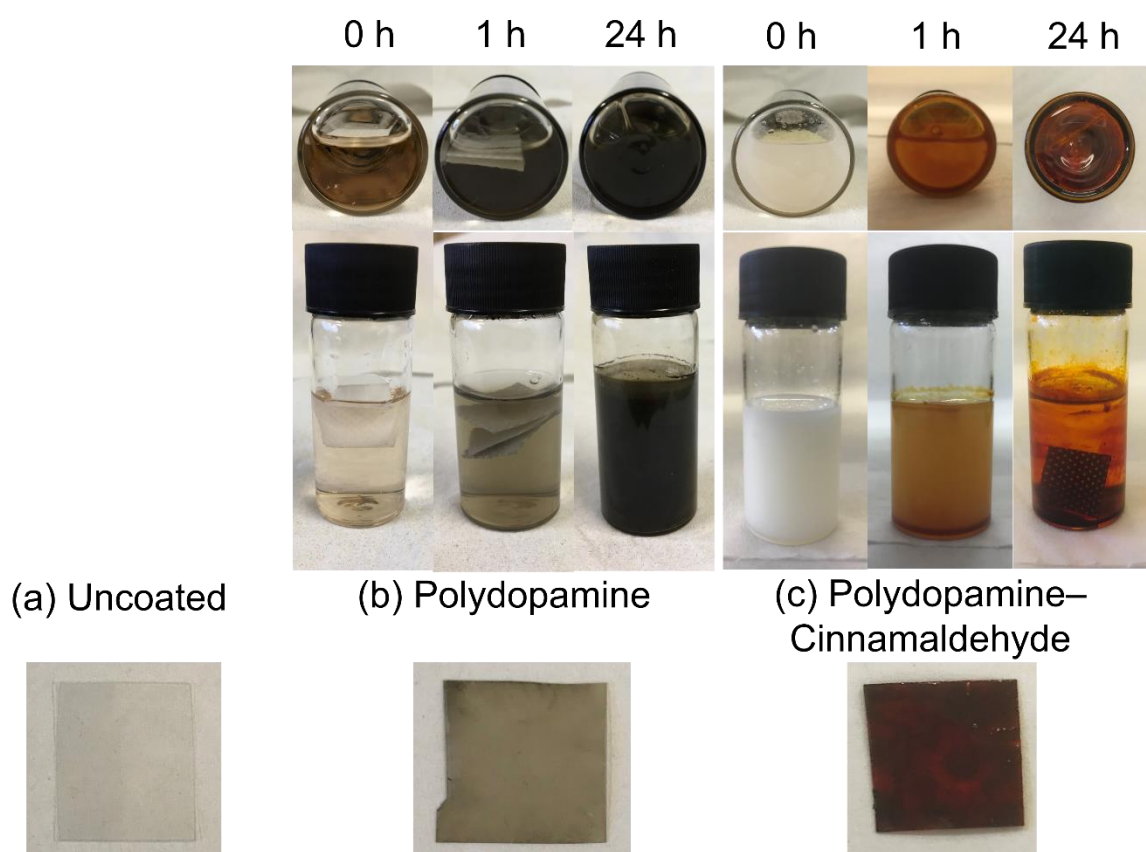


Figure 3.2: Photographs of coating solutions and 15 x 15 mm PET film substrate: (a) uncoated; (b) polydopamine-only; and (c) polydopamine-cinnamaldehyde.

Table 3.1: Mass increase for polydopamine-cinnamaldehyde, polyethyleneimine-cinnamaldehyde, and tannic acid-cinnamaldehyde coated non-porous PET film substrates, and cinnamaldehyde treated non-woven polypropylene cloth. 15 mm x 15 mm sample size. † Assuming both sides are coated.

Coating	Mass Increase / mg cm ⁻²
Polydopamine-Cinnamaldehyde / PET Film	4.4 ± 0.9 †
Polyethyleneimine-Cinnamaldehyde / PET Film	0.7 ± 0.3 †
Tannic Acid-Cinnamaldehyde / PET Film	1.0 ± 0.2 †
Cinnamaldehyde / Non-Woven Polypropylene Cloth	45 ± 4

Cinnamaldehyde oil and the polydopamine-cinnamaldehyde coatings were characterised by infrared spectroscopy, Figure 3.3. Liquid cinnamaldehyde absorption bands include aromatic and alkene C-H stretching (around 3060 cm⁻¹), aldehyde C-H stretching (2814 cm⁻¹ and 2742 cm⁻¹), C=O stretching (1668 cm⁻¹), as well as aromatic C=C stretching (1625 cm⁻¹).⁴ Polydopamine-

only coated silicon wafer displayed broad absorbances around 3220 cm^{-1} corresponding to O–H groups, and 1605 cm^{-1} and 1509 cm^{-1} from C=C stretching.⁵ For the case of polydopamine–cinnamaldehyde coated silicon wafer, the characteristic cinnamaldehyde absorbances were still visible, as well as a broad polydopamine O–H group absorption around 3220 cm^{-1} , together with a small polydopamine aromatic C=C stretching peak at 1509 cm^{-1} (both of these latter features are absent for pure cinnamaldehyde⁴).

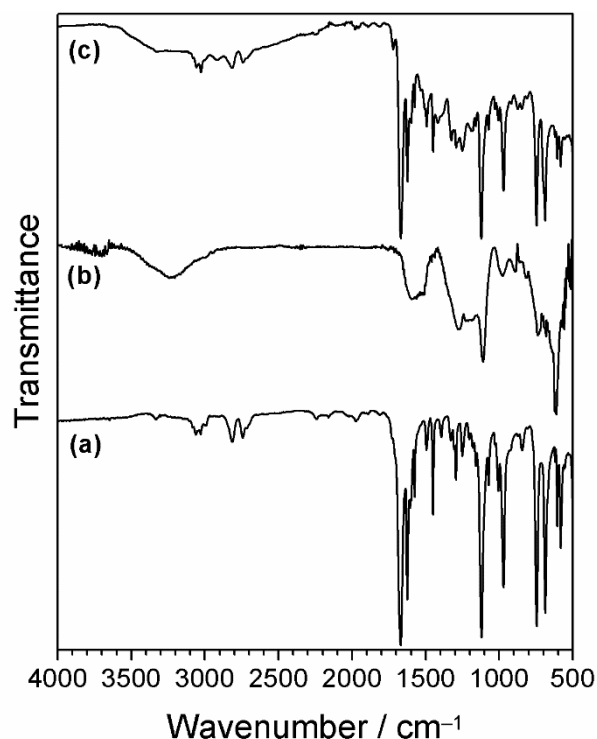


Figure 3.3: Infrared spectra of: (a) cinnamaldehyde; (b) polydopamine-only coating; and (c) polydopamine–cinnamaldehyde coating. Schiff base imine absorbance should appear around 1640 cm^{-1} —this absorbance is not distinguishable due to overlap with strong cinnamaldehyde peaks.⁶

Cinnamaldehyde displays an intense UV-Vis absorbance peak at $\lambda = 290\text{ nm}$, but no other features, Figure 3.4.^{7,8} Polydopamine coated quartz showed a weaker UV-Vis absorbance peak at $\lambda = 290\text{ nm}$, as well as broad absorption across the 200–800 nm wavelength range, Figure 3.4.⁹ Polydopamine–cinnamaldehyde coated quartz exhibited a strong absorbance at $\lambda = 288\text{ nm}$, which can be attributed to either or both of the cinnamaldehyde and dopamine coating constituents. In addition, a new absorbance peak at $\lambda = 438\text{ nm}$ is apparent (which was absent in both the aforementioned cinnamaldehyde and polydopamine UV-Vis spectra)—this accounts for the observed red coating

colour and is indicative of chemical bond formation (reaction) between polydopamine and cinnamaldehyde causing a change in electron density within the host polydopamine structure.

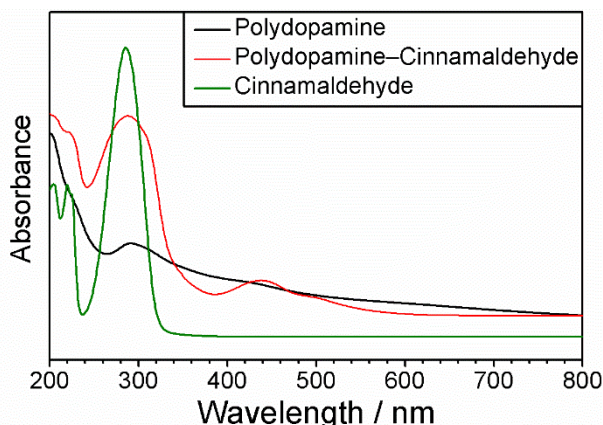


Figure 3.4: UV-Vis spectra of cinnamaldehyde solution; polydopamine coated quartz; and polydopamine–cinnamaldehyde coated quartz.

Previously it has been reported that polydopamine can undergo an Aza–Michael reaction with acrylate groups, where the polydopamine amine group nitrogen lone pair attacks the carbon–carbon double bond of the acrylate group to form a new bond.¹⁰ Given that cinnamaldehyde contains an alkene bond adjacent to a carbonyl group, an analogous Michael or Aza-Michael type reaction may be anticipated. However, other studies have shown that an amine group nitrogen lone pair can react via nucleophilic attack at the cinnamaldehyde carbonyl group to form a Schiff base imine product.^{11,12} Therefore, in order to elucidate the reaction mechanism for exactly how cinnamaldehyde reacts with dopamine/polydopamine, a mass spectrometric investigation was undertaken: cinnamaldehyde was reacted with an equimolar amount of phenethylamine—a compound analogous to dopamine but lacking the catechol OH groups (thereby unable to undergo polymerisation as observed for dopamine), Figure 3.5. The obtained product was a viscous orange oil. Mass spectrometry of the product gave mass m/z 236.1 (which is consistent with the empirical formula $C_{17}H_{17}N$ and the Schiff base imine product molecular ion $[M + H]^+$), Figure 3.6. No mass fragment was measured for the alternative Michael addition product ion expected at m/z 253 ($C_{17}H_{19}NO$). Hence, cinnamaldehyde reacts with dopamine (or polydopamine in a similar fashion) to form a Schiff base imine product. Tris(hydroxymethyl)aminomethane was not included in this reaction in order that

only the reaction between phenethylamine and cinnamaldehyde could be investigated. Although tris(hydroxymethyl)aminomethane has been reported to react with polydopamine during coating deposition, this does not occur via the Schiff base reaction.^{13,14} There also is in addition the possibility of tris(hydroxymethyl)aminomethane undergoing the Schiff base reaction with cinnamaldehyde to form imine linkages.

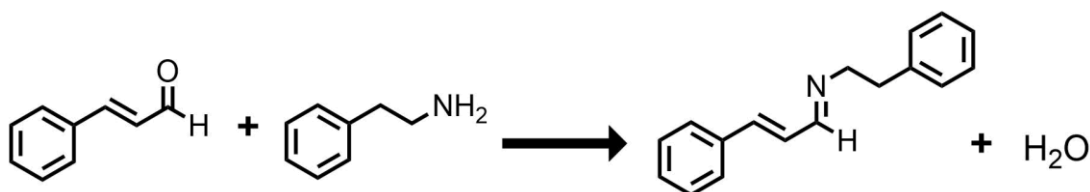


Figure 3.5: Reaction of cinnamaldehyde with phenethylamine to form a Schiff base imine product.

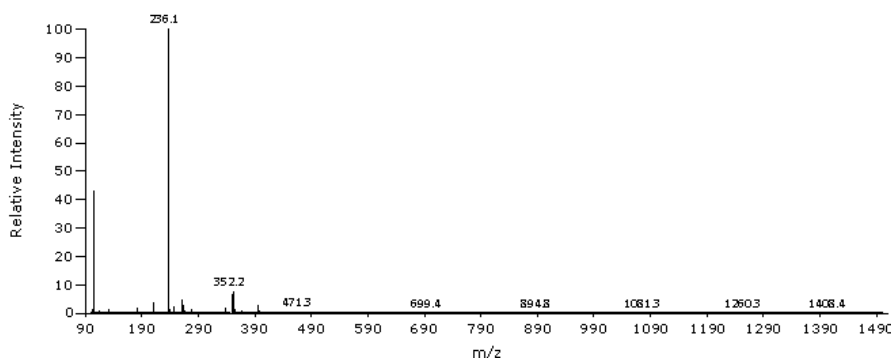


Figure 3.6: Atmospheric solids analysis probe (ASAP) mass spectrum of product of phenethylamine and cinnamaldehyde reaction.

Control cinnamaldehyde treated PET samples had a very small antibacterial effect against both Gram-negative *E. coli* and Gram-positive *S. aureus* (this could be due to a low amount of residual cinnamaldehyde remaining on the PET film surface after final washing step), Table 3.2. Polydopamine-coated PET film showed no antibacterial activity against *E. coli* and a very minor effect for *S. aureus* (less than Log₁₀ Reduction = 1). Polydopamine–cinnamaldehyde coated PET film displayed complete killing of both types of bacteria (exceeding Log₁₀ Reduction = 7), which easily exceeds the minimal (Log₁₀ Reduction > 3, in 1 h) set by the US Environmental Protection Agency Office (EPA).¹⁵ The measured antibacterial activity was retained during recycling tests against *E. coli* for the first two tests, followed by a gradual loss of efficacy during further recycling, Figure 3.7.

The cells were unaffected by vortexing (or ultrasonication (model U50, manufacturer Ultrawave Ltd.) and fully removed from the sample surface, Figure 3.8 and Figure 3.9. Following pipetting of 900 μl of autoclaved Luria-Bertani broth media into each microtube containing sample and vortexing, the polydopamine–cinnamaldehyde coated PET film was removed, and viability testing experiments were performed on the retained cultures in the 1 ml solution, in order to show that all bacteria were killed. Firstly, 100 μl from the 1 ml bacteria solution sample was spread onto Luria-Bertani Agar plates. After incubation, nothing grew, Figure 3.10. Then the remaining 900 μl of bacteria solution was centrifuged and any pelleted bacteria resuspended in 100 μl of phosphate-buffered saline followed by spreading onto fresh Luria-Bertani Agar plates—again, nothing grew, Figure 3.11. The viability of *E. coli* on untreated PET film control samples gave an average of 3.6×10^9 CFU ml^{-1} (or 3.6×10^8 CFU per 100 μl of bacteria solution), Figure 3.8. When 100 μl from the 1 ml bacteria solution from untreated PET film control samples was spread onto Luria-Bertani Agar plates, after incubation, considerable bacteria growth was observed, Figure 3.10. The observed lack of bacterial growth for the coated samples confirms that exposure of *E. coli* to the polydopamine–cinnamaldehyde coated PET film does indeed kill all the bacteria present in the exposed bacteria-containing solution, and that none remain attached to the substrate surface.

Table 3.2: Antibacterial activities for PET film coated with: polydopamine; polydopamine–cinnamaldehyde; polyethyleneimine–cinnamaldehyde; tannic acid; or tannic acid–cinnamaldehyde. Log_{10} Reduction values are calculated relative to the untreated substrate (mean \pm standard deviation). † Control samples comprised immersion of PET film in 15 mg ml^{-1} cinnamaldehyde aqueous solution, or 20 mg ml^{-1} polyethyleneimine aqueous solution, or 3 mg ml^{-1} tannic acid aqueous solution followed by rinsing in water.

Dipping Solution	Bacteria Loss / Log_{10} Reduction	
	<i>E. coli</i> (Gram-negative)	<i>S. aureus</i> (Gram-positive)
Cinnamaldehyde †	0.12 \pm 0.07	0.29 \pm 0.07
Polydopamine †	0.00	0.34 \pm 0.06
Polydopamine–Cinnamaldehyde	8.15 \pm 0.03	7.68 \pm 0.05
Polyethyleneimine †	0.00	0.00
Polyethyleneimine–Cinnamaldehyde	3.87 \pm 0.56	7.44 \pm 0.03
Tannic Acid †	0.00	0.13 \pm 0.07
Tannic acid–Cinnamaldehyde	8.33 \pm 0.03	7.56 \pm 0.06

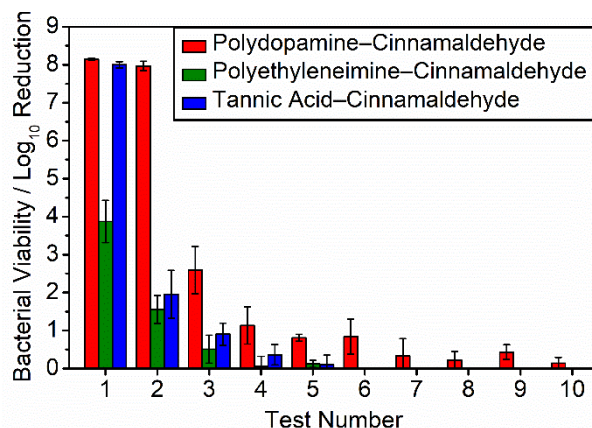


Figure 3.7: Recycle antibacterial activity against *E. coli* for coated PET films: polydopamine–cinnamaldehyde; polyethyleneimine–cinnamaldehyde; and tannic acid–cinnamaldehyde. Log₁₀ Reduction values are calculated relative to the untreated PET substrate (mean ± standard deviation). Following each antibacterial test, samples were rinsed with water for 1 min at 20 °C and completely air-dried prior to the next re-use.

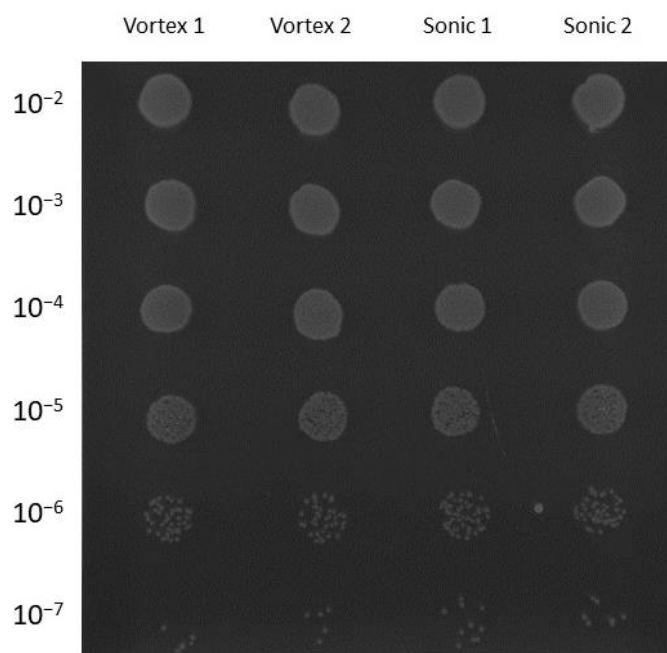


Figure 3.8: Uncoated PET samples were used to create a 1:10 dilution series in LB broth from 10^{-2} to 10^{-7} . 10 μ l of each *E. coli* bacteria solution at each dilution was then plated onto a Luria-Bertani Agar plate which was incubated overnight at 30 °C. Cell counts at 10^{-6} : V1 = 32 (= 3.2×10^9 ml⁻¹), V2 = 37 (= 3.7×10^9 ml⁻¹), S1 = 40 (= 4.0×10^9 ml⁻¹), and S2 = 35 (= 3.5×10^9 ml⁻¹). Images taken by Joy Paterson.

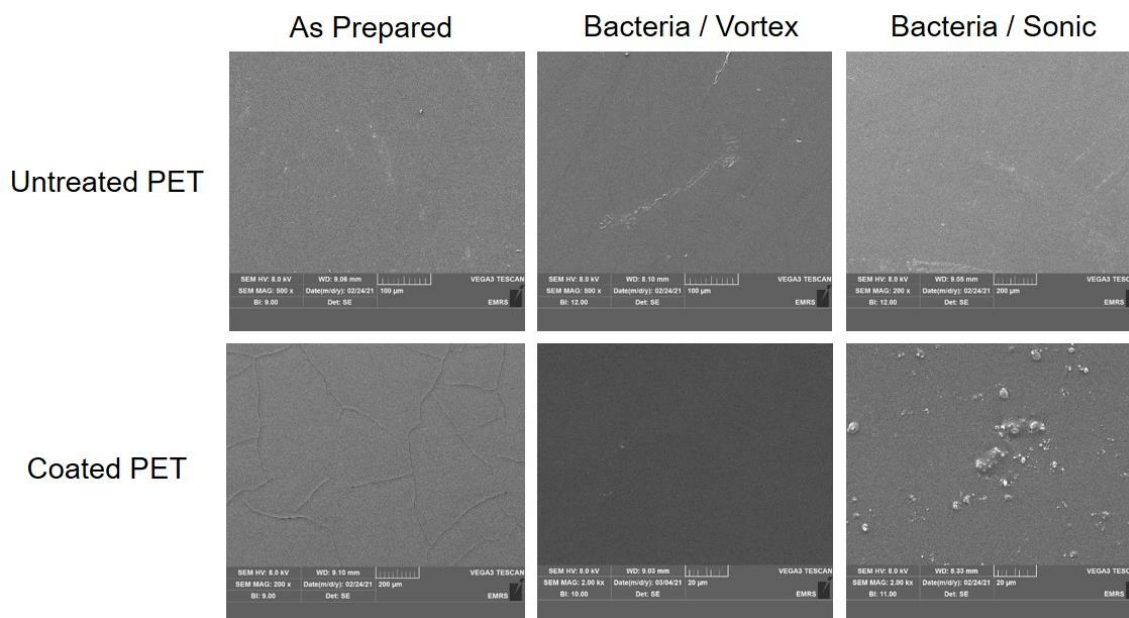


Figure 3.9: Scanning electron microscopy (SEM) images of uncoated and polydopamine–cinnamaldehyde coated PET film surfaces: as prepared, or after exposure of *E. coli* bacteria solution and vortexing or sonication to remove any surface bound bacterial cells. Images taken by Tracey Davey.

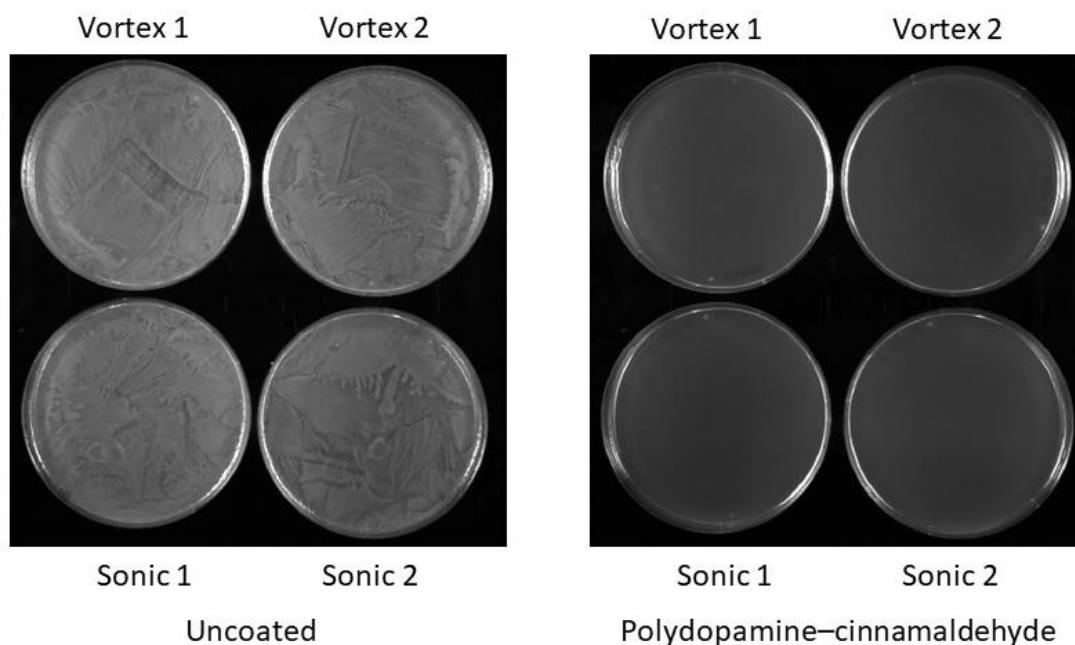


Figure 3.10: After 4 h exposure of *E. coli* bacteria solution to uncoated PET film or polydopamine–cinnamaldehyde coated PET film, then pipetting 900 μ L of autoclaved Luria-Bertani broth media into each microtube containing a sample, then either vortexing or sonication, the PET film was removed and 100 μ L of each bacteria solution was spread onto a Luria-Bertani Agar plate and incubated overnight at 30 °C. Images taken by Joy Paterson.

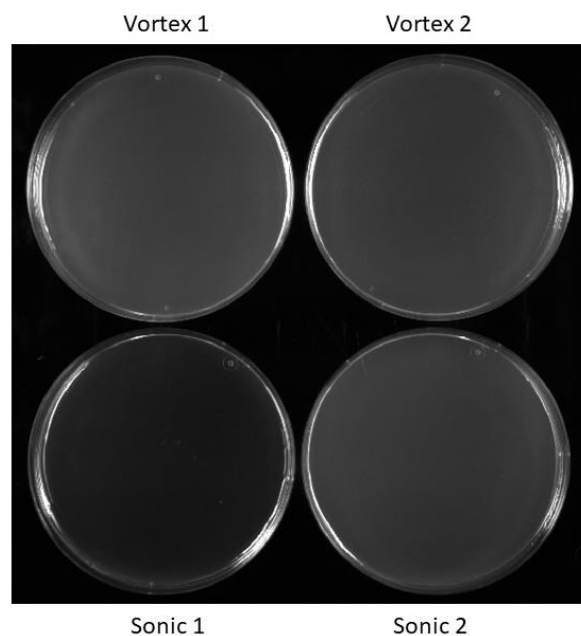


Figure 3.11: After exposure of polydopamine–cinnamaldehyde coated PET film to *E. coli* solution, then pipetting 900 μL of autoclaved Luria-Bertani broth media into each microtube containing a sample, then either vortexing or sonication, the polydopamine–cinnamaldehyde coated PET film was removed, and 900 μL of *E. coli* bacteria solution was centrifuged at 13,000 rpm for 2 min. The supernatant was discarded, and 100 μL of PBS was used to resuspend any remaining cells. 100 μL of each resuspension was then spread onto an LB agar plate, and incubated overnight at 30 $^{\circ}\text{C}$. No living colonies were seen. Images taken by Joy Paterson.

In order to further examine the mechanism of antibacterial activity, time-resolved UV-Vis spectroscopy studies were performed using the polydopamine–cinnamaldehyde coated PET film, Figure 3.12. Release of cinnamaldehyde into water from the host coating showed a rapid increase followed by levelling off after 24 h. This is consistent with the antibacterial recycle testing, which showed a gradual drop-off in efficacy, Figure 3.7.

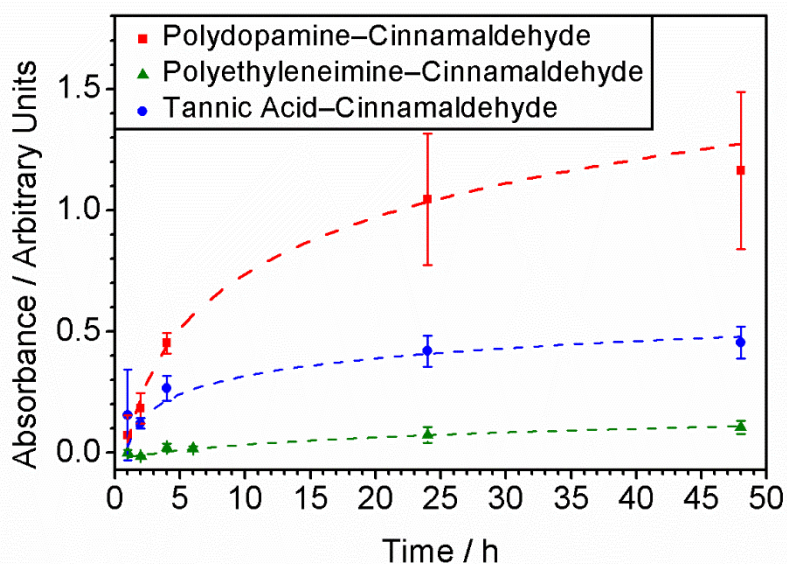


Figure 3.12: Release of cinnamaldehyde from antibacterial coatings into water at 20 °C monitored by UV-Vis spectroscopy ($\lambda = 290$ nm): polydopamine–cinnamaldehyde; polyethyleneimine–cinnamaldehyde; and tannic acid–cinnamaldehyde.

3.3.2 Poly(norepinephrine)–Cinnamaldehyde Coating

A brief investigation was performed in order to determine whether the formation of an adhesive polymer–cinnamaldehyde coating was limited to polydopamine or whether the coating technique could be extended to similar compounds. Norepinephrine is structurally very similar to dopamine, but contains an extra hydroxyl group, Figure 3.13.

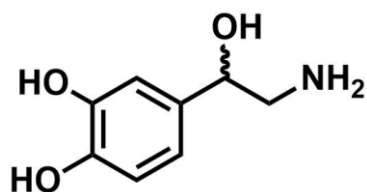


Figure 3.13: Structure of norepinephrine.

Poly(norepinephrine) coated PET showed a faint, transparent brown coating, Figure 3.14. Poly(norepinephrine)–cinnamaldehyde (30 mg) coating gave a solid red coating, as did poly(norepinephrine)–cinnamaldehyde (60 mg) coating. Poly(norepinephrine)–cinnamaldehyde (100 mg) coating and poly(norepinephrine)–cinnamaldehyde (150 mg) coating both gave sticky, oily, non-uniform, red coloured coatings.

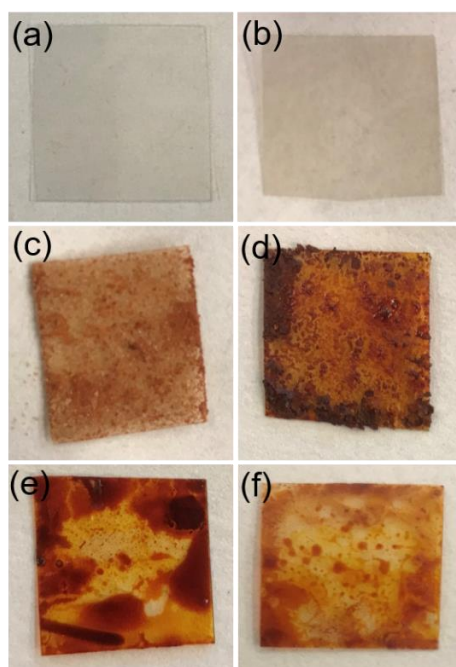


Figure 3.14: Photographs of PET: (a) untreated; (b) polynorepinephrine coating; (c) polynorepinephrine–cinnamaldehyde (30 mg) coating; (d) polynorepinephrine–cinnamaldehyde (60 mg) coating; (e) polynorepinephrine–cinnamaldehyde (100 mg) coating; and (f) polynorepinephrine–cinnamaldehyde (150 mg) coating.

Infrared spectrum of norepinephrine hydrochloride showed the following characteristic absorption bands: N–H and O–H stretches (3266 cm^{-1} , br), C–H stretch (3056 cm^{-1} and 2960 cm^{-1}), C=C stretch (1630 cm^{-1}), NH_2 scissoring (1602 cm^{-1}), and O–H in-plane bend (1240 cm^{-1}), Figure 3.15.¹⁶ Poly(norepinephrine) coating showed O–H stretch (3300 cm^{-1} , br), and aromatic C=C stretches (1619 cm^{-1} and 1510 cm^{-1}).¹⁷ Poly(norepinephrine)–cinnamaldehyde (60 mg) coating showed cinnamaldehyde aldehyde C–H stretching peaks at 2814 cm^{-1} and 2742 cm^{-1} , and cinnamaldehyde C=O stretch peak at 1668 cm^{-1} , which are not present in norepinephrine FTIR spectrum, therefore confirming the presence of cinnamaldehyde in the coating. Interestingly, the broad O–H stretching peak (3300 cm^{-1}) was not present in the poly(norepinephrine)–cinnamaldehyde (60 mg) coating FTIR spectrum, and two new peaks are visible at 3538 cm^{-1} and 3436 cm^{-1} (these peaks are not present in the infrared spectra of norepinephrine hydrochloride powder, poly(norepinephrine) coating, or cinnamaldehyde). This seems to indicate that the cinnamaldehyde has an effect on all of the –OH groups of the poly(norepinephrine) component of the coating. It is possible that reaction of the amine group with cinnamaldehyde causes steric hindrance that stops the alkyl –OH group from forming intermolecular hydrogen bonds, and thus the peak at 3538 cm^{-1} is due to ‘free’ (i.e. non-hydrogen bonded) hydroxyl groups, and the

peak at 3436 cm^{-1} is due to intramolecular hydrogen bonds.¹⁸ Alternatively, the norepinephrine–cinnamaldehyde Schiff base imine product could undergo cyclisation *via* nucleophilic attack of the alkyl –OH oxygen on the imine carbon atom to yield an oxazoline type product. Whatever the case, the reason for the absence of the broad O–H stretch is likely complex and difficult to determine, owing to the wide variety of reactions that are taking place.

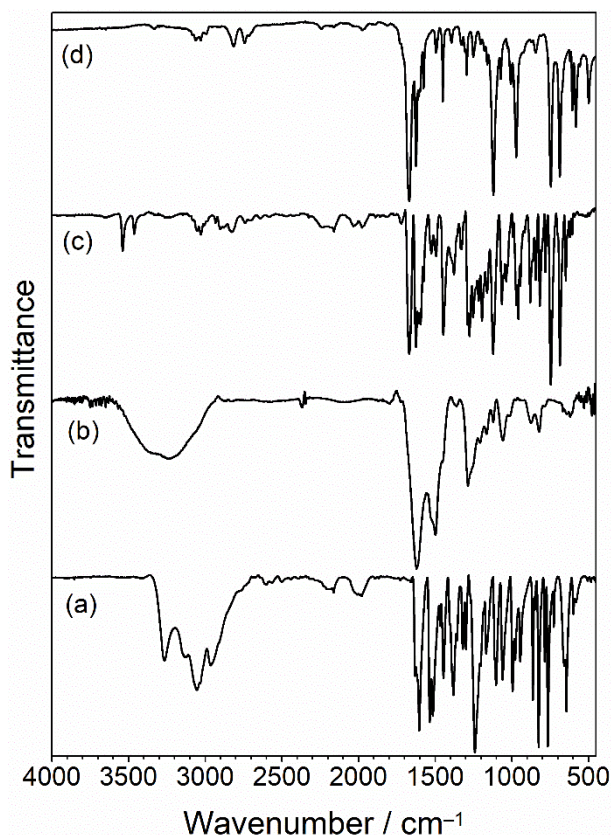


Figure 3.15: Infrared spectra of: (a) norepinephrine hydrochloride powder (ATR); (b) polynorepinephrine coating on Si wafer (RAIRS, 66°); (c) polynorepinephrine–cinnamaldehyde (60 mg) coating (ATR); and (d) cinnamaldehyde (ATR).

3.3.3 Polyethyleneimine–Cinnamaldehyde Coating

Polyethyleneimine was utilised to develop further understanding, given that it contains amine groups like polydopamine, and therefore polyethyleneimine should undergo the Schiff base reaction with cinnamaldehyde to form an antibacterial coating, Figure 3.1. Solution mixtures utilising varying ratios of polyethyleneimine to cinnamaldehyde were screened in order to determine optimal quantities of both components for the production of a high efficacy antibacterial coating. Mixing of polyethyleneimine solution with cinnamaldehyde led to the formation of an off-white precipitate which was found to uniformly adhere onto the test substrates (as well as onto the bottom of the glass vials),

and remained unchanged in appearance following washing with water. For formulations where a higher weight proportion of polyethyleneimine relative to cinnamaldehyde was used, much less precipitate was found to form, whereas excess cinnamaldehyde compared to polyethyleneimine led to a yellow solution, and practically no adhesive precipitate formed on the substrate. Equal masses of polyethyleneimine and cinnamaldehyde yielded good performance coatings (20 mg ml⁻¹ polyethyleneimine and 20 mg ml⁻¹ cinnamaldehyde mixture solutions were chosen for further studies). The mass increase following coating of PET substrates was measured to equal 0.71 mg cm⁻² (assuming both sides are coated), Table 3.1.

Infrared absorption peaks for polyethyleneimine include N–H stretching (3275 cm⁻¹), aliphatic C–H stretching (2930–2810 cm⁻¹), primary amine group NH₂ bending (1580 cm⁻¹), and CH₂ symmetric bending vibration (1460 cm⁻¹), Figure 3.16.^{19,20} The polyethyleneimine–cinnamaldehyde coating showed a broad absorption peak around 3300 cm⁻¹, corresponding to N–H stretching. A new feature at 1634 cm⁻¹ is present, consistent with imine bond formation following the Schiff base reaction between amine groups from polyethyleneimine and cinnamaldehyde (akin to the reactions between phenethylamine/polydopamine and cinnamaldehyde), Figure 3.5. Otherwise, many of the infrared fingerprint region absorption bands of cinnamaldehyde and polyethyleneimine overlap with the polyethyleneimine–cinnamaldehyde spectrum.

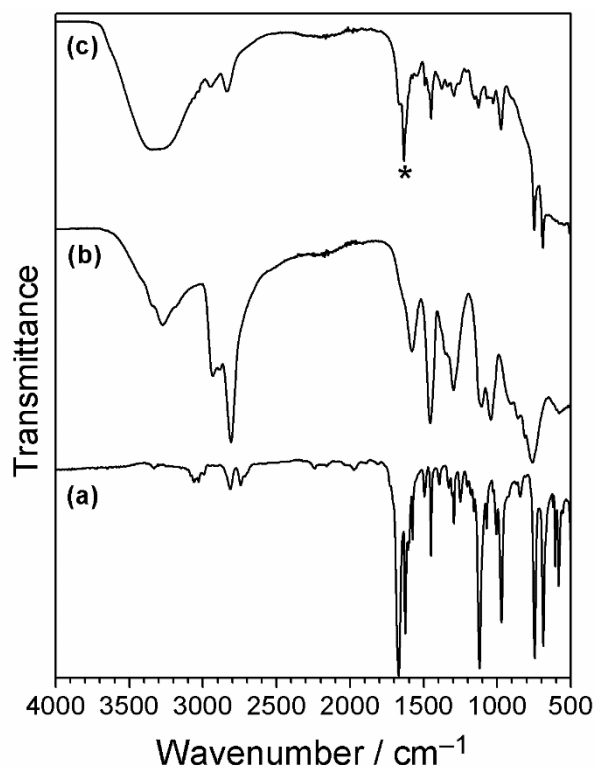


Figure 3.16: Infrared spectra of: (a) cinnamaldehyde; (b) polyethyleneimine; and (c) polyethyleneimine–cinnamaldehyde coating. * New imine feature at 1634 cm⁻¹.⁶

PET films immersed in polyethyleneimine-only 20 mg ml⁻¹ aqueous solution followed by washing in ultrapure water and drying for at least 3 h at 20 °C were tested as a control and found to possess no antibacterial activity, Table 3.2. The polyethyleneimine–cinnamaldehyde coated PET films showed at least Log₁₀ Reduction = 3 or 4 against *E. coli*, and complete killing (exceeding Log₁₀ Reduction = 7) for *S. aureus*. Antibacterial recycling tests were carried out against *E. coli*, and there was a drop in bacterial killing following the second test with practically all biocidal activity lost after the fourth test, Figure 3.7.

The release behaviour of the polyethyleneimine–cinnamaldehyde coating in water was further investigated by immersion of coated PET substrates into water for 24 h at 20 °C whilst shaking. 0.5 ± 0.4 mg cm⁻² of material was released after 24 h, and 0.22 ± 0.14 mg cm⁻² of the coating remained. Visually, there did not seem to be any alteration to the appearance of the coatings. This would suggest that the observed mass loss following immersion in water for 24 h is due to the release of trapped or loosely bound cinnamaldehyde and/or polyethyleneimine.

Time-resolved UV-Vis spectroscopy studies were performed using the polyethyleneimine–cinnamaldehyde coated PET films in order to determine the

release profile of cinnamaldehyde into aqueous solution from the coating, Figure 3.12. A much lower cinnamaldehyde absorbance was measured compared to the polydopamine–cinnamaldehyde system, which is consistent with the polyethyleneimine–cinnamaldehyde coating being a lot thinner and thereby losing its recycling antibacterial activity faster compared to the polydopamine–cinnamaldehyde coating, Table 3.1 and Figure 3.7.

3.3.4 Tannic Acid–Cinnamaldehyde Coating

Tannic acid-only coatings were found to be very thin; whilst tannic acid–cinnamaldehyde coatings appeared to be much thicker. Variation in tannic acid–cinnamaldehyde solution composition was explored in order to provide the optimum coating: 3.0, 4.5, 6.0, and 15 mg ml⁻¹ cinnamaldehyde combined with fixed 3 mg ml⁻¹ tannic acid (corresponding to a tannic acid:cinnamaldehyde mass ratio of 1:1, 1:1.5, 1:2, and 1:5 respectively). The solid coating obtained using a 1:1 mass ratio was yellow in appearance and evenly covered the PET film, whereas all of the other solution compositions yielded oily (non-solid), non-uniform coatings on the PET film surfaces, Figure 3.17. Hence, 3 mg ml⁻¹ cinnamaldehyde–3 mg ml⁻¹ tannic acid mixture coating solution was chosen for further investigation. The mass increase for this tannic acid–cinnamaldehyde coating was 1.0 ± 0.2 mg cm⁻² (assuming both sides of each substrate are coated), Table 3.1.

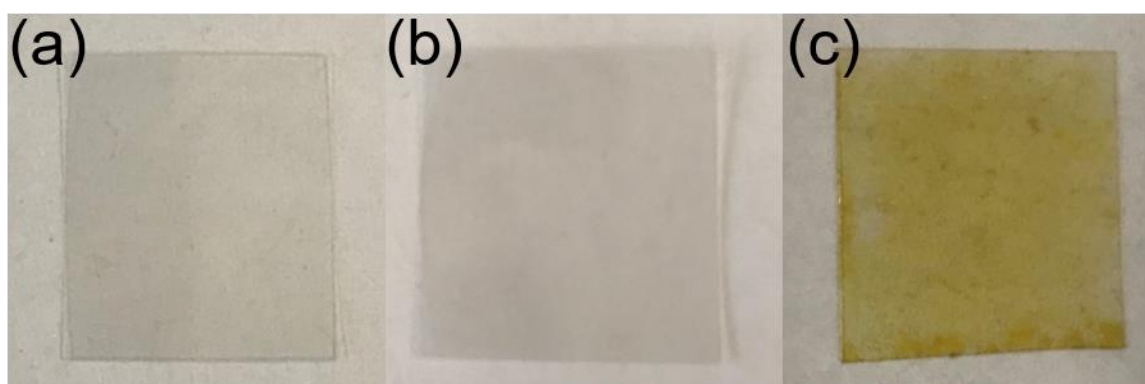


Figure 3.17: Photographs of PET film: (a) uncoated; (b) tannic acid-only coating; and (c) tannic acid-cinnamaldehyde coating.

The infrared spectrum of tannic acid displays absorbances for O–H groups (3300 cm⁻¹), C=O stretching (1700 cm⁻¹), and three peaks at 1605 cm⁻¹, 1530 cm⁻¹ and 1444 cm⁻¹ associated with aromatic ring stretching, Figure 3.18.²¹ For

the tannic acid–cinnamaldehyde coating, the infrared spectrum resembles the tannic acid spectrum. In addition, there is a new absorbance at 1649 cm^{-1} , characteristic of imine group C=N stretching (which appears at a lower wavenumber compared to the cinnamaldehyde C=O stretching vibration (1670 cm^{-1})). An explanation for this new peak could be the Schiff base reaction product between tris(hydroxymethyl)aminomethane and cinnamaldehyde (this may also explain the formation of yellow colour in the cinnamaldehyde control solution mentioned previously—the cinnamaldehyde and tris(hydroxymethyl)aminomethane react to form a yellow Schiff base imine product). It has been reported that tris(hydroxymethyl)aminomethane can undergo Schiff base reaction with carbonyl-containing compounds, yielding C=N infrared stretching frequencies in the region of $1640\text{--}1630\text{ cm}^{-1}$.^{22,23} Tris(hydroxymethyl)aminomethane and cinnamaldehyde are present in almost equimolar amounts in the tannic acid–cinnamaldehyde coating solution (whereas in the polydopamine–cinnamaldehyde coating solution there is a significant excess of cinnamaldehyde relative to tris(hydroxymethyl)aminomethane, which masks the imine bond region of the infrared absorption). Another likely explanation could be that the tannic acid ester groups react with the amine to form an amide. Oxidised tannic acid, which will likely contain quinone-type carbonyl groups, may also be capable of reacting with amines via the Schiff base reaction to form an imine—however, the wavenumber for such imine group stretching should be much lower (1585 cm^{-1}), thus making it unlikely that this new peak is due to the reaction of tannic acid with tris(hydroxymethyl)aminomethane to form an imine.²⁴

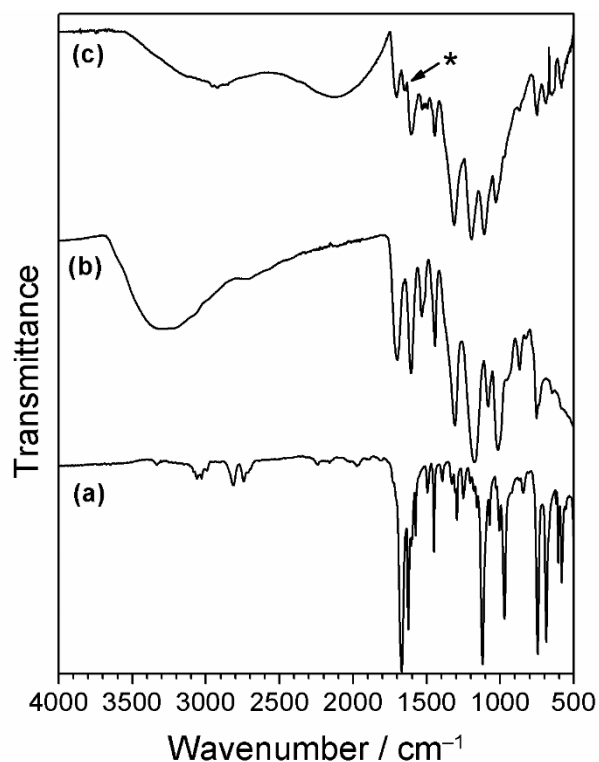


Figure 3.18: Infrared spectra of: (a) cinnamaldehyde; (b) tannic acid; and (c) tannic acid–cinnamaldehyde coating. * New imine feature at 1649 cm^{-1} .

Tannic acid-only coated PET film displayed no antibacterial activity against *E. coli* and only a modest reduction in viability against *S. aureus*, Table 3.2. The tannic acid–cinnamaldehyde coating was found to give rise to complete killing of both types of bacteria (exceeding Log_{10} Reduction = 7). Antibacterial recycling tests performed with *E. coli* for the tannic acid–cinnamaldehyde coated PET film showed a decrease in antibacterial activity after the first test, and negligible activity was found by the fifth test, Figure 3.7. A possible reason for why the tannic acid–cinnamaldehyde coating does not display as long-lasting antibacterial activity as the polydopamine–cinnamaldehyde coating could be as a consequence of the smaller amount of cinnamaldehyde used to prepare the coatings (3 mg ml^{-1} versus 15 mg ml^{-1} solutions respectively), or due to the coating being thinner, Table 3.1.

Time-resolved UV-Vis spectroscopy studies were performed using tannic acid–cinnamaldehyde coated PET film in order to follow the release of cinnamaldehyde from the coating into the aqueous phase, Figure 3.12. The amount of cinnamaldehyde release measured for the tannic acid–cinnamaldehyde coatings was lower compared to the polydopamine–cinnamaldehyde coatings, and can be attributed to the smaller concentration of

cinnamaldehyde employed to prepare the former (3 mg ml⁻¹ versus 15 mg ml⁻¹ solutions respectively), or because the coating is thinner, Table 3.1. This correlates with the antibacterial recycling tests, where the tannic acid–cinnamaldehyde coated PET film showed a faster decline in antibacterial activity relative to the polydopamine–cinnamaldehyde coated PET film, Figure 3.7.

3.3.5 Cinnamaldehyde–Porous Substrates

Given that cinnamaldehyde loading in the coating has been shown to be a key factor governing antibacterial longevity (Figure 3.7 and Figure 3.12), non-woven polypropylene host substrate containing a larger open pore structure (micron scale) was impregnated with cinnamaldehyde, Table 3.1.²⁵ The cloth pieces were weighed before and after impregnation of cinnamaldehyde, and the average mass increase was measured to be 45 ± 4 mg cm⁻², Table 3.1.

Testing against *E. coli* and *S. aureus* showed complete killing of the bacteria (Log₁₀ Reduction = 8.31 ± 0.12 and 7.76 ± 0.07 respectively). Seventeen consecutive antibacterial recycling tests against *E. coli*. (equivalent to continuous contact with bacteria in liquid for 68 h), showed that the cloths killed all bacteria in every test (Log₁₀ Reduction = ~8), Figure 3.19. The dip in antibacterial activity on tests 18 and 19 may be due to depletion of the cinnamaldehyde from the material. The observed high antibacterial activity over such a prolonged period of recycling rules out the possibility of live bacteria cells just sticking to the cloth surface—which is consistent with the previously reported biocidal activity of cinnamaldehyde.^{176,177,178}

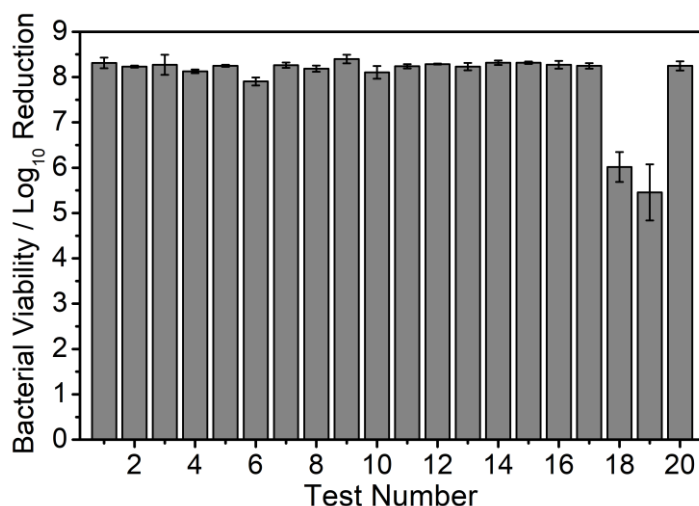


Figure 3.19: *E. coli* antibacterial recycling of cinnamaldehyde impregnated non-woven polypropylene cloth. Values are reported as the average Log₁₀ Reduction relative to untreated non-woven polypropylene cloth (average ± standard deviation).

Polydopamine–cinnamaldehyde coating on polypropylene cloth was also tested for antibacterial efficacy against *E. coli* and *S. aureus* showed complete killing of the bacteria (Log_{10} Reduction = 8.31 ± 0.12 and 7.76 ± 0.07 respectively). Twenty consecutive antibacterial recycling tests against *E. coli* (equivalent to continuous contact with bacteria in liquid for 80 h), showed that the cloths killed all bacteria in every test (Log_{10} Reduction = ~ 8), Figure 3.20.

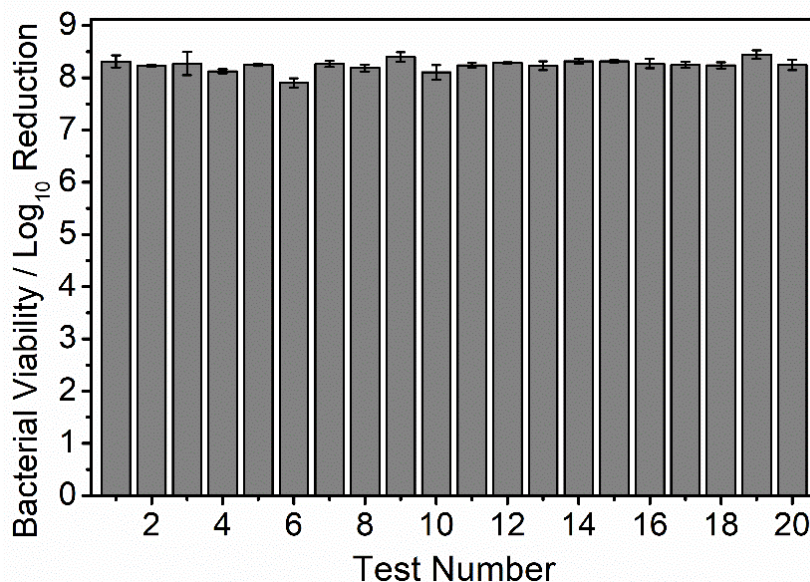


Figure 3.20: *E. coli* antibacterial recycling of polydopamine–cinnamaldehyde coated non-woven polypropylene cloth. Values are reported as the average Log_{10} Reduction relative to untreated non-woven polypropylene cloth (average \pm standard deviation).

Since cinnamaldehyde was found to impregnate into porous non-woven polypropylene cloth without the need for any extra reagents (e.g. aforementioned polydopamine, polyethyleneimine, tannic acid or tris(hydroxymethyl)aminomethane), alternative porous material substrates were also evaluated in order to assess the broader applicability of this approach. Porous polytetrafluoroethylene (PTFE) membrane was chosen as a more hydrophobic type of material. Untreated PTFE membrane exhibited no antibacterial activity, whereas the cinnamaldehyde impregnated PTFE membrane gave rise to complete killing of *E. coli* (Log_{10} Reduction = 8.27 ± 0.04).

Considering that the aforementioned polypropylene and PTFE porous substrates are both hydrophobic and therefore unlikely to absorb water in preference to cinnamaldehyde whilst immersed in aqueous solution, cotton fabric was selected as a hydrophilic porous material for comparison. Untreated cotton displayed no antibacterial effect, while the cinnamaldehyde-impregnated cotton

pieces killed all *E. coli* (Log_{10} Reduction = 8.29 ± 0.06), thereby confirming that the hydrophilic cotton was capable of sufficient cinnamaldehyde uptake to subsequently provide a strong antibacterial efficacy.

3.4 Discussion

Polydopamine, tannic acid, and cinnamaldehyde are all biodegradable and not harmful to human health.^{26, 27, 28, 29, 30} The polydopamine–cinnamaldehyde, polyethyleneimine–cinnamaldehyde, and tannic acid–cinnamaldehyde coatings exhibit strong antibacterial activity against both Gram-negative and Gram-positive bacteria. They retained their red, off-white, and yellow colours respectively following antibacterial test recycling. This indicates that the coatings are well adhered to the underlying substrates, and the solid host polymer coating alone cannot be responsible for the observed antibacterial activity. Cinnamaldehyde interacts with the polydopamine, polyethyleneimine, or tannic acid during coating formation, either reacting, binding via non-covalent interactions, or becoming trapped within the polymer coating. Cinnamaldehyde reaction within the host polymers provides compatibilization for excess cinnamaldehyde oil—the surface energies of the solid and fluid become better matched, leading to highly stable entrapped cinnamaldehyde liquid. Cinnamaldehyde is then able to leach out (release) during the antibacterial testing studies (Figure 3.7 and Figure 3.12). Once the cinnamaldehyde becomes depleted, there is no longer any antibacterial activity. Amongst these coatings, the polydopamine–cinnamaldehyde system displays the best recycling properties, and this correlates to its extended release of cinnamaldehyde over a longer period of time, Figure 3.7 and Figure 3.12. On the other hand, the solution for polyethyleneimine–cinnamaldehyde coated PET film after 48 h immersion in water displayed a lower final UV-Vis absorbance compared to polydopamine–cinnamaldehyde or tannic acid–cinnamaldehyde coated PET films, Figure 3.12. This correlates with its lower overall antibacterial efficacy against *E. coli*, as well as quicker loss of activity during antibacterial recycling, and with its smaller mass increase (thickness), Table 3.1, Table 3.2, and Figure 3.7.

Unlike dopamine/polydopamine and polyethyleneimine, tannic acid does not contain amine functional groups, meaning that it cannot undergo the Schiff base reaction with cinnamaldehyde as occurs for dopamine/polydopamine and

polyethyleneimine. Rather, tris(hydroxymethyl)aminomethane plays a dual role both initiating oxidative polymerisation of tannic acid, and reacting with cinnamaldehyde, which in turn may help to entrap cinnamaldehyde through compatibilisation. The trapped tris(hydroxymethyl)aminomethane–cinnamaldehyde Schiff base product may also be antibacterial. Another possibility is that tannic acid and cinnamaldehyde interact with each other via non-covalent bonding such as π - π interactions, hydrogen bonding or hydrophobic interactions to form an insoluble coating, with excess less strongly bound cinnamaldehyde able to release into water. Alternative conceivable mechanisms could include an oxa-Michael type reaction (whereby tannic acid OH groups are deprotonated by base to form an oxyanion which then performs a nucleophilic attack on the cinnamaldehyde alkene group leading to bond formation between the tannic acid and cinnamaldehyde).

Antibacterial activities have been reported previously for cinnamaldehyde impregnated into porous substrates including microporous polyurethane⁴, polypropylene foot sweat pads³¹, and wet wipes made from cellulose and polyester.³² However, no recycle/reuse testing was performed. Impregnation of cinnamaldehyde into porous hydrophobic (non-woven polypropylene cloth and polytetrafluoroethylene membrane) as well as into hydrophilic cotton through cinnamaldehyde entrapment is an effective means for incorporating large amounts of the essential oil into a substrate for multiple use antibacterial applications, Figure 3.19. The inherent larger pore volumes (micron scale) and thicker materials provide greater cinnamaldehyde loading capacity leading to longer lasting antibacterial efficacies compared to the much thinner polydopamine–cinnamaldehyde, polyethyleneimine–cinnamaldehyde, and tannic acid–cinnamaldehyde coatings which contain essential oil dispersed on the nanoscale. The fact that the cinnamaldehyde impregnated non-woven polypropylene cloth shows no drop-off in antibacterial activity after 17 cycles of washing (equivalent to continuous contact with bacteria in liquid for 68 h) indicates robustness, and this is entirely suitable for potential applications where reusability is desirable, Figure 3.19. Alternative long-lasting antibacterial coatings include the use of silver nanoparticles and quaternary ammonium polymers.^{33,34} Both of these antimicrobial agents involve multiple synthesis steps and are potentially damaging towards the environment.^{35,36} Conversely, the present eco-

friendly approach is a simple one-step process and can use natural biodegradable compounds such as dopamine, tannic acid, and cinnamaldehyde.

The present study opens up scope for the large scale, low-cost fabrication of antibacterial coatings using plant-derived essential oil compounds (as alternatives to environmentally harmful metal-based systems). Naturally occurring and synthetic antimicrobial compounds could also be incorporated (including those with antiviral, antifouling, antifungal, or antiparasitic properties). These coating methods could also be extended to other natural and synthetic phenolic and polyphenol compound coatings besides polydopamine and tannic acid—such as derivatives of dihydroxyphenol (catechol) and pyrogallol (including gallic acid, epigallocatechin gallate, and epicatechin gallate), which are found in tea. Such coatings are explored in chapter 4. Potential applications include healthcare, prevention of the spread of pathogens and diseases, building materials, transportation, clothing, footwear, marine coatings, and active food packaging.

3.5 Conclusions

Coatings comprising cinnamaldehyde hosted within a compatible matrix on the nanoscale can be applied to a variety of substrates without the requirement for organic solvents or any further surface derivatization. Polydopamine–cinnamaldehyde coatings display high antibacterial efficacy towards both Gram-positive (*S. aureus*) and Gram-negative (*E. coli*) bacteria. Polyethyleneimine–cinnamaldehyde and tannic acid–cinnamaldehyde coatings also show good antibacterial activity against both *E. coli* and *S. aureus*. Cinnamaldehyde impregnated into a variety of porous substrates (non-woven polypropylene cloth, polytetrafluoroethylene membrane, and knitted cotton), exhibits strong antibacterial performance; with non-woven polypropylene cloth containing cinnamaldehyde providing long-lasting and recyclable antibacterial activity.

3.6 References

- 1 Mathekgga, A. D. M.; Meyer, J. J. M. Antibacterial Activity of South African Helichrysum Species. *S. Afr. J. Bot.* **1998**, *64*, 293–295.
- 2 Gersbach, P. V. The Essential Oil Secretory Structures of *Prostanthera ovalifolia* (Lamiaceae). *Ann Bot.* **2002**, *89*, 255–260.
- 3 Voo, S. S.; Grimes, H. D.; Lange, B. M. Assessing the Biosynthetic Capabilities of Secretory Glands in Citrus Peel. *Plant Physiol.* **2012**, *159*, 81–94.
- 4 Kucinska-Lipka, J.; Gubanska, I.; Lewandowska, A.; Terebieniec, A.; Przybytek, A.; Cieśliński, H. Antibacterial Polyurethanes, Modified with Cinnamaldehyde, as Potential Materials for Fabrication of Wound Dressings. *Polym. Bull.* **2019**, *76*, 2725–2742.
- 5 Dreyer, D. R.; Miller, D. J.; Freeman, B. D.; Paul, D. R.; Bielawski, C. W. Elucidating the Structure of Poly(Dopamine). *Langmuir* **2012**, *28*, 6428–6435.
- 6 A. Mohammed, A.; H. Taher, N. Synthesis and Characterisation of Some Cinnamaldehyde Schiff Base Complexes. *Raf. J. Sci.* **2008**, *19*, 45–51.
- 7 Konar, S.; Samanta, D.; Mandal, S.; Das, S.; Mahto, M. K.; Shaw, M.; Mandal, M.; Pathak, A. Selective and Sensitive Detection of Cinnamaldehyde by Nitrogen and Sulphur Co-Doped Carbon Dots: A Detailed Systematic Study. *RSC Adv.* **2018**, *8*, 42361–42373.
- 8 Guo, K.; Chen, Y. Simple and Rapid Detection of Aromatic Amines Using a Thin Layer Chromatography Plate. *Anal. Methods* **2010**, *2*, 1156–1159.
- 9 Lin, J. H.; Yu, C. J.; Yang, Y. C.; Tseng, W. L. Formation of Fluorescent Polydopamine Dots from Hydroxyl Radical-Induced Degradation of Polydopamine Nanoparticles. *Phys. Chem. Chem. Phys.* **2015**, *17*, 15124–15130.
- 10 Liu, C. Y.; Huang, C. J. Functionalization of Polydopamine via the Aza-Michael Reaction for Antimicrobial Interfaces. *Langmuir* **2016**, *32*, 5019–5028.
- 11 Singh, K. K.; Mathela, C. S. Synthesis, Characterisation and in Vitro Antibacterial Activity of Cinnamyl Amine Derivatives. *Indian J. Chem.* **2014**, *53*, 907–912.
- 12 Badawy, M. E. I.; Rabea, E. I. Synthesis and Structure-Activity Relationship of N-(Cinnamyl) Chitosan Analogs as Antimicrobial Agents. *Int. J. Biol. Macromol.* **2013**, *57*, 185–192.
- 13 Della Vecchia, N. F.; Avolio, R.; Alfè, M.; Errico, M. E.; Napolitano, A.; D'Ischia, M. Building-Block Diversity in Polydopamine Underpins a Multifunctional Eumelanin-Type Platform Tunable through a Quinone Control Point. *Adv. Funct. Mater.* **2013**, *23*, 1331–1340.
- 14 Della Vecchia, N. F.; Luchini, A.; Napolitano, A.; Derrico, G.; Vitiello, G.; Szekeley, N.; Dischia, M.; Paduano, L. Tris Buffer Modulates Polydopamine Growth, Aggregation, and Paramagnetic Properties. *Langmuir* **2014**, *30*, 9811–9818.
- 15 Protocol for the Evaluation of Bactericidal Activity of Hard, Non-porous Copper/Copper-Alloy Surfaces. US Environmental Protection Agency Office. 3rd February 2015.
- 16 Yadav, T.; Mukherjee, V. Structural Confirmation and Spectroscopic Study of a Biomolecule: Norepinephrine. *Spectrochim. Acta - Part A Mol. Biomol. Spectrosc.* **2018**, *202*, 222–237.
- 17 Tan, X.; Gao, P.; Li, Y.; Qi, P.; Liu, J.; Shen, R.; Wang, L.; Huang, N.; Xiong, K.; Tian, W.; et al. Poly-Dopamine, Poly-Levodopa, and Poly-Norepinephrine Coatings: Comparison of

- Physico-Chemical and Biological Properties with Focus on the Application for Blood-Contacting Devices. *Bioact. Mater.* **2021**, *6*, 285–296.
- 18 Kondo, T. The Assignment of IR Absorption Bands Due to Free Hydroxyl Groups in Cellulose. *Cellulose* **1997**, *4*, 281–292.
 - 19 Kasprzak, A.; Popławska, M.; Bystrzejewski, M.; Łabędź, O.; Grudziński, I. P. Conjugation of Polyethyleneimine and Its Derivatives to Carbon-Encapsulated Iron Nanoparticles. *RSC Adv.* **2015**, *5*, 85556–85567.
 - 20 Yoshitake, H.; Koiso, E.; Horie, H.; Yoshimura, H. Polyamine-Functionalized Mesoporous Silicas: Preparation, Structural Analysis and Oxyanion Adsorption. *Microporous Mesoporous Mater.* **2005**, *85*, 183–194.
 - 21 Sagbas, S.; Aktas, N.; Sahiner, N. Modified Biofunctional p(Tannic Acid) Microgels and Their Antimicrobial Activity. *Appl. Surf. Sci.* **2015**, *354*, 306–313.
 - 22 Lee, S. M.; Sim, K. S.; Lo, K. M. Synthesis, Characterisation and Biological Studies of Diorganotin(IV) Complexes with Tris[(Hydroxymethyl)Aminomethane] Schiff Bases. *Inorganica Chim. Acta* **2015**, *429*, 195–208.
 - 23 Martínez, R. F.; Úvalos, M.; Babiano, R.; Cintas, P.; Jiménez, J. L.; Light, M. E.; Palacios, J. C. Schiff Bases from TRIS and Ortho-Hydroxyarene-carbaldehydes: Structures and Tautomeric Equilibria in the Solid State and in Solution. *European J. Org. Chem.* **2011**, *2011*, 3137–3145.
 - 24 Lim, M. Y.; Choi, Y. S.; Kim, J.; Kim, K.; Shin, H.; Kim, J. J.; Shin, D. M.; Lee, J. C. Cross-Linked Graphene Oxide Membrane Having High Ion Selectivity and Antibacterial Activity Prepared Using Tannic Acid-Functionalized Graphene Oxide and Polyethyleneimine. *J. Memb. Sci.* **2017**, *521*, 1–9.
 - 25 Gürsoy, M.; Harris, M.T.; Downing, J.O.; Barrientos-Palomo, S.N.; Carletto, A.; Yaprak, A.E.; Karaman, M.; Badyal, J.P.S. Bioinspired Fog Capture and Channel Mechanism Based on the Arid Climate Plant *Salsola crassa*. *Colloids Surfaces A* **2017**, *529*, 195–202.
 - 26 Lee, H.; Dellatore, S. M.; Miller, W. M.; Messersmith, P. B. Mussel-Inspired Surface Chemistry for Multifunctional Coatings. *Science*. **2007**, *318*, 426–430.
 - 27 Sun, T.; Li, Z. J.; Wang, H. G.; Bao, D.; Meng, F. L.; Zhang, X. B. A Biodegradable Polydopamine-Derived Electrode Material for High-Capacity and Long-Life Lithium-Ion and Sodium-Ion Batteries. *Angew. Chemie - Int. Ed.* **2016**, *55*, 10662–10666.
 - 28 Chung, K. T.; Wong, T. Y.; Wei, C. I.; Huang, Y. W.; Lin, Y. Tannins and Human Health: A Review. *Crit. Rev. Food Sci. Nutr.* **1998**, *38*, 421–464.
 - 29 Shin, M.; Ryu, J. H.; Park, J. P.; Kim, K.; Yang, J. W.; Lee, H. DNA/Tannic Acid Hybrid Gel Exhibiting Biodegradability, Extensibility, Tissue Adhesiveness, and Hemostatic Ability. *Adv. Funct. Mater.* **2015**, *25*, 1270–1278.
 - 30 Adams, T. B.; Cohen, S. M.; Doull, J.; Feron, V. J.; Goodman, J. I.; Marnett, L. J.; Munro, I. C.; Portoghese, P. S.; Smith, R. L.; Waddell, W. J.; Wagner, B. M. The FEMA GRAS Assessment of Cinnamyl Derivatives Used as Flavor Ingredients. *Food Chem. Toxicol.* **2004**, *42*, 157–185.
 - 31 Aksoy, A.; Kaplan, S. Production and Performance Analysis of an Antibacterial Foot Sweat Pad. *Fibers Polym.* **2013**, *14*, 316–323.

- 32 Kaplan, S.; Pulan, S.; Ulusoy, S. Objective and Subjective Performance Evaluations of Wet Wipes Including Herbal Components. *J. Ind. Text.* **2018**, *47*, 1959–1978.
- 33 Ho, C. H.; Odermatt, E. K.; Berndt, I.; Tiller, J. C. Long-Term Active Antimicrobial Coatings for Surgical Sutures Based on Silver Nanoparticles and Hyperbranched Polylysine. *J. Biomater. Sci. Polym. Ed.* **2013**, *24*, 1589–1600.
- 34 Fik, C. P.; Konieczny, S.; Pashley, D. H.; Waschinski, C. J.; Ladisch, R. S.; Salz, U.; Bock, T.; Tiller, J. C. Telechelic Poly(2-oxazoline)s with a Biocidal and a Polymerizable Terminal as Collagenase Inhibiting Additive for Long-Term Active Antimicrobial Dental Materials. *Macromol. Biosci.* **2014**, *14*, 1569–1579.
- 35 Faunce, T.; Watal, A. Nanosilver and Global Public Health: International Regulatory Issues. *Nanomedicine*, 2010, *5*, 617–632.
- 36 Hora, P. I.; Pati, S. G.; McNamara, P. J.; Arnold, W. A. Increased Use of Quaternary Ammonium Compounds During the SARS-CoV-2 Pandemic and Beyond: Consideration of Environmental Implications. *Environ. Sci. Technol. Lett.* **2020**, *7*, 622–631.

Chapter 4

4 Antimicrobial Tea Coatings

4.1 Introduction

In the year 2020, the emergence and spread of severe acute respiratory syndrome coronavirus 2 (SARS-CoV-2—which causes the COVID-19 disease) led to the World Health Organization to declare the outbreak a global pandemic.¹ As of June 2021, there have been 3.57 million documented deaths due to the disease.^{2, 3, 4} The virus is spread via close contact with infected people (for example, exhaled aerosol droplets) and touching of contaminated surfaces. It has been shown that the virus can remain infectious for several days on a variety of surfaces.^{5, 6} Therefore, developing low-cost sustainable technology solutions to help stop the spread of contagious diseases is a critical global challenge for mankind.

Copper and silver are known to display antiviral activities—for example, copper can inactivate influenza virus (H1N1)⁷, and silver nanoparticles display an anti-HIV-1 effect.⁸ Both metals are reported to be effective against coronaviruses such as SARS-CoV⁹, and Human Coronavirus 229E.¹⁰ Copper surfaces have been found to deactivate SARS-CoV-2—for example, spray-coated copper powder gives rise to 92% reduction after 2 h; and cuprous oxide (Cu₂O) coatings gave about Log₁₀ Reduction = 3 towards SARS-CoV-2 viral titre after 1 h.^{11,12} Exposure of SARS-CoV-2 to silver nanoparticles for 1 h prior to infection of cells causes the viral load to drop to negligible levels¹³; and a sputter-coated silver nanocluster/silica composite coating led to Log₁₀ Reduction = 4 loss in infectivity after 90 min.¹⁴ However, these previous examples of copper and silver antiviral coatings suffer from drawbacks including lengthy multiple-step fabrication processes, expensive reagents, specialist equipment, and dependency upon substrate material types (which restricts their rapid scale-up and widespread deployment).

In order to help fight against infectious disease transmission on the global scale, the materials and methods employed for producing antimicrobial coatings must be cheap and readily available to facilitate local manufacturing in remote locations and low-income countries, without requiring any specialist training or equipment. The utilisation of ultrathin (nano) coatings and biodegradable

substrate materials are important factors for sustainability and environmental impact.

In this chapter, a low-cost single-step hybrid coating system utilising brewed tea, cinnamaldehyde essential oil, and a metal salt (of either silver or copper) is reported—which utilises the well-known everyday ‘tea cup staining’ phenomenon to ensure good adhesion to a wide range of substrate materials. Compounds contained in tea extract, such as epigallocatechin gallate, are known to exhibit antiviral activity¹⁵, and have been used in antiviral air filters/cleaners.¹⁶ Tea polyphenols display good binding with SARS-CoV-2 main protease (MPro), making them promising compounds for the inactivation of the virus.¹⁷ In the case of cinnamaldehyde (derived from the oil of cinnamon tree bark¹⁸), it is also known to exhibit antiviral effects against a variety of viruses.^{19, 20} This includes an *in silico* study demonstrating that cinnamaldehyde exhibits favourable binding with the SARS-CoV-2 spike (S) glycoprotein (which is a key target for antiviral drugs).²¹ The tea–cinnamaldehyde–metal coatings described in the present study offer multi-mode antimicrobial activity, with tea, cinnamaldehyde, and metal constituents all potentially contributing to the observed antimicrobial effects. These tea–cinnamaldehyde–metal coatings require no additional reagents or processes apart from readily available tap water. Tea and cinnamaldehyde (or cinnamon bark oil) are widely available, relatively cheap, and sustainable organic products. Combined with utilisation of low concentrations of metal salts, these coatings can be easily produced anywhere on a large scale and at low cost (for example, remote field hospitals during humanitarian crises and in low-income countries).

4.2 Experimental

4.2.1 Materials

Silicon wafer (<100> orientation; 5-20 Ω -cm resistivity; 525 \pm 25 μ m thickness, polished front surface; Silicon Valley Microelectronics Inc.), glass slides (1 mm thickness, Academy Science Ltd.), polyethylene terephthalate film (PET, capacitor grade, 0.10 mm thickness, Lawson Mardon Ltd.), hydrophilic non-woven polypropylene cloth (spunbond, 0.32 mm thickness, 25 g m⁻², Daltex[®] Absorb, Don & Low Ltd.), and polytetrafluoroethylene sheet (Gilbert Curry

Industrial Plastics Co Ltd.) were cut into 15 mm x 15 mm pieces and used as substrates for coating. Cotton gloves (product code 1232600, Arco Ltd.), tennis balls (part number DWSQ03002, Slazenger brand, Frasers Group plc.), and personal protection 3-ply non-woven polypropylene face masks (Hygiene & Sicherheit product code 043-06/2019, Goetzloff GmbH) were used as supplied. Substrates were cleaned by immersing into a sufficient quantity so as to fully immerse in a 50:50 volume solvent mixture of propan-2-ol (+95%, Fisher Scientific UK Ltd.) and cyclohexane (+99.5%, Fisher Scientific UK Ltd.) and agitated in an ultrasonic bath for 15 min, before drying in air at 20 °C.

4.2.2 Tea Coatings Preparation

Tea-only coating was produced by brewing one teabag (containing 2 g organic Fairtrade pure green tea, Clipper Teas Ltd.) in 100 ml boiled drinking tap water for 10 min, then 10 ml was transferred immediately into a glass vial (while the tea was still hot, approximately 65 °C) and a piece of clean substrate (15 mm x 15 mm) was immersed into the brewed tea solution.

Tea–cinnamaldehyde coating was prepared by brewing one teabag in 100 ml boiled drinking tap water for 10 min, then 10 ml was transferred immediately to a glass vial (while the tea was still hot, approximately 65 °C) containing 30 mg trans-cinnamaldehyde (99%, Acros Organics brand, Fisher Scientific UK Ltd.). The closed glass vial was manually shaken vigorously for 10 s, and then a clean substrate (15 mm x 15 mm) was immersed into the solution for coating.

Tea–cinnamaldehyde–metal hybrid coatings were fabricated by adding a specified amount of cinnamaldehyde and either copper sulphate pentahydrate (+98%, Sigma-Aldrich Ltd.) or silver nitrate (+99.9%, Apollo Scientific Ltd.) to an appropriately sized container, Table 4.1. Immediately after brewing the specified number of teabags for 10 min in the specified volume of boiled drinking tap water, the specified quantity of tea solution was added to the container mixture (whilst the tea was still hot, approximately 65 °C), and the container lid was closed. The container was manually shaken vigorously for 10 s, and then a clean substrate was immersed into the solution for coating.

For all of the above coating systems, the container was placed on a shaker (model Vibrax VXR, IKA Ltd.) at 20 °C for 16 h. Next, the substrate sample was removed from solution, washed in deionised water on the shaker at 20 °C for 5

min, and then dried in air at 20 °C for at least 3 h. Control tea–metal coatings were produced using the same method, but without the addition of cinnamaldehyde.

Table 4.1: Experimental parameters for fabrication of tea–cinnamaldehyde–metal coatings.

Substrate	Substrate Dimensions	Teabags	Tap Water / ml	Brewed Tea / ml	Cinnamaldehyde / mg	Metal Salt / mg	Container
Silicon wafer	15 mm x 15 mm	1	100	10	30	10	Glass vial
Glass slides (for photos)	76 mm x 26 mm	2	500	500	1500	200	Plastic Container
Glass (for XRD)	15 mm x 15 mm	1	100	10	30	10	Glass vial
PET film	15 mm x 15 mm	1	100	10	30	10 or 50	Glass vial
Hydrophilic PP cloth (for photos)	210 mm x 150 mm	2	400	400	600	200	Plastic Container
Hydrophilic PP cloth (for antibacterial testing)	210 mm x 150 mm	2	400	400	900	300	Plastic Container
Hydrophilic PP cloth (for leaching)	90 mm x 90 mm	2	400	200	600	200	Glass jar
Polypropylene face masks	-	2	400	400	900	300	Glass jar
PTFE	15 mm x 15 mm	1	100	10	30	10	Glass vial
TEM grids	-	1	100	10	30	10	Glass vial
Cotton gloves	-	2	300	300	900	300	Glass jar
Tennis balls	-	2	350	350	788	260	Glass jar

4.2.3 Coating Characterisation

Infrared spectra were acquired as described in section 2.2. Coating thicknesses were measured as described in section 2.4. X-ray photoelectron spectroscopy was performed as described in section 2.7—instrument sensitivity (multiplication) factors were C(1s) : N(1s) : O(1s) : Cu(2p) : Ag(3d) equals 1.00 : 0.37 : 0.35 : 0.040 : 0.048 respectively. X-ray diffraction patterns were acquired as described in section 2.10. Transmission electron microscope images were acquired as described in section 2.8—tea-based coatings were deposited onto carbon film supported on 200 mesh copper grids (part number AGS160, Agar Scientific Ltd.). Raman spectroscopy was performed as described in section 2.11.

4.2.4 Metal Leaching

Coated hydrophilic non-woven polypropylene cloths were cut into 20 mm x 20 mm pieces and immersed into a glass vial filled with high-purity water (10 ml) for a predetermined time. The cloth was then removed, and nitric acid (70%, SG 1.42, Fisher Scientific UK Ltd.) was added to give a 4% v/v aqueous HNO₃ solution to aid digestion of any leached metal. Control 'blanks' were also examined using uncoated pieces of hydrophilic non-woven polypropylene cloth, but otherwise prepared in the same way. ICP-OES analysis was performed as described in section 2.13.

4.2.5 Antibacterial Testing

Tea-cinnamaldehyde, tea-cinnamaldehyde-silver nitrate and tea-cinnamaldehyde-copper sulphate coatings were deposited onto hydrophilic non-woven polypropylene cloth (as described above). Antibacterial testing was performed as described in section 2.3.

4.2.6 Antiviral Testing

The deposited coatings were tested for their antiviral potency against murine coronavirus (mouse hepatitis virus strain A59, MHV-A59). MHV-A59 is used as a potential surrogate for SARS-CoV-2 (MHV and SARS-CoV-2 belong to the same genus and are structurally similar to each other).^{22, 23, 24} Antiviral testing was performed on coatings applied to non-woven fabric face masks using a simulated splash test (modified ISO 18184): Aliquots of viral stocks were thawed on ice. Murine coronavirus (mouse hepatitis virus strain A59, MHV-A59) stock titre used was approximately 1×10^9 infectious units per ml (titred when prepared). The face mask edges were cut off, and the front face fabric of each mask was separated. 2 cm squares were cut from the front face piece, sterilised by subjecting each surface to 15 min UV irradiation in a Class II MSC, and then placed into sterile plastic Petri dishes. 5 x 4 μ L aliquots of virus were inoculated onto the surface of each of the test materials, and tested in triplicate. Test materials remained within Petri dishes (without lids) inside a Class II Microbiological Safety Cabinet (MSC) at a stable temperature and humidity for the specified contact time (2 h). Contact time began as soon as the inoculum was pipetted onto the surface of the material.

At $t = 0$ h and $t = 2$ h, the respective samples were submerged in 0.5 ml of 1.5% (w/v) beef extract in a 50 ml Greiner tube and vortexed vigorously for 10 s. The resultant viral suspensions (eluates) were aseptically collected and 25 μ L aliquots diluted by serial 10-fold dilutions in 2.5% FBS DMEM (low glucose, no glutamate). Non-inoculated samples were subject to the same elution and dilution procedures to assay for cytopathic effects associated with the uncoated fabric. 50 μ L aliquots of eluted and diluted viral suspensions were added to individual wells of 96-well culture plates containing monolayers of 17Cl-1 cells cultured in 100 μ L of the appropriate medium. Viral eluate from each sample was used to inoculate 4 wells of cells, i.e. 12 wells in total for each dilution given triplicate samples. Dilutions ranged from neat eluate through to 10^{-6} dilution. The final row of wells/cells was inoculated with sterile culture medium. Assay plates were incubated for up to 48 h at 37 °C in a 5% CO₂ atmosphere. Plates were assessed and scored by microscopy at 24 h intervals for the presence of cytopathic effects (CPE), as evidenced by the presence of gaps in cell confluence and/or detached cells. Wells in which >50% of the cells showed CPE were judged as being positive for TCID₅₀ purposes. The TCID₅₀ (median Tissue Culture Infectivity Dose) value represents the endpoint dilution where 50% of cell monolayers challenged by the eluted virus sample show observable cytopathic effects as a result of infection by the test virus. TCID₅₀ values were calculated via the Reed and Muench method.

4.3 Results

4.3.1 Tea–Cinnamaldehyde Coating

Immersion in brewed tea–only gave rise to no visible change in appearance of the clear transparent PET substrates due to the very thin nature of the deposited coating, Figure 4.1 and Table 4.2. In contrast, the tea–cinnamaldehyde (30 mg) solution produced an opaque, uniform yellow-brown coating. Higher concentrations of cinnamaldehyde were found not to be optimal—a patchy coating was obtained for tea–cinnamaldehyde (50 mg), while a tea–cinnamaldehyde (100 mg) solution produced a poorly adhered oily coating with incomplete coverage, Figure 4.2. Hence, the optimum tea–cinnamaldehyde (30 mg) solution was selected for further investigation.

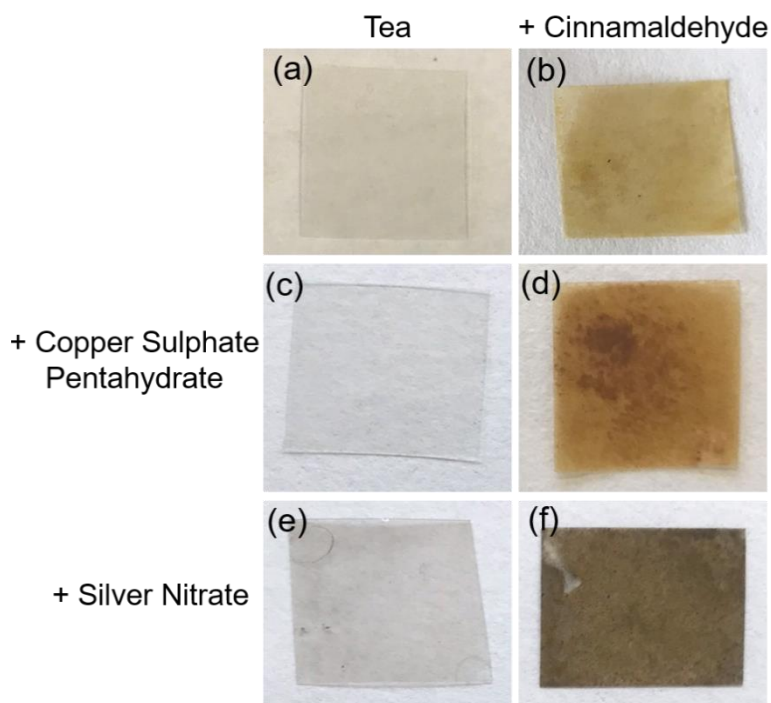


Figure 4.1: Photographs of coated PET film substrate: (a) tea-only; (b) tea-cinnamaldehyde; (c) tea-copper sulphate pentahydrate; (d) tea-cinnamaldehyde-copper sulphate pentahydrate; (e) tea-silver nitrate; and (f) tea-cinnamaldehyde-silver nitrate. 30 mg cinnamaldehyde and 10 mg metal salt added to 10 ml tea solution.

Table 4.2: Thickness values for tea-based coatings deposited onto silicon wafer. 30 mg cinnamaldehyde and / or 10 mg metal salt added to 10 ml tea solution.

Coating	Thickness / nm
Tea-Only	14 ± 12
Tea-Cinnamaldehyde	151 ± 5
Tea-Copper sulphate pentahydrate	1.3 ± 1.6
Tea-Cinnamaldehyde-Copper sulphate pentahydrate	146 ± 5
Tea-Silver nitrate	0.7 ± 0.9
Tea-Cinnamaldehyde-Silver nitrate	159 ± 16

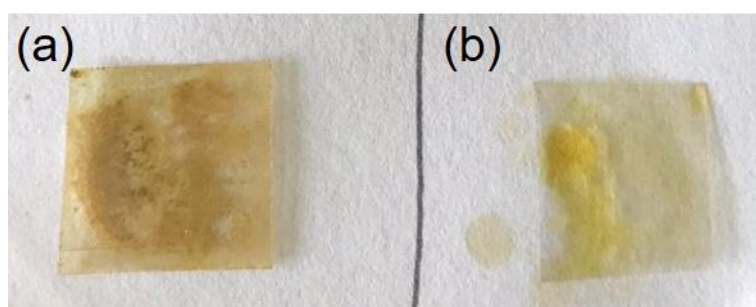


Figure 4.2: Photographs of coated PET substrate: (a) tea-50 mg cinnamaldehyde; and (b) tea-100 mg cinnamaldehyde coating. 10 ml tea solutions used for both.

The tea–cinnamaldehyde coatings were found to be at least an order of magnitude thicker than the tea-only coatings (approximately 151 nm versus 14 nm respectively, Table 4.2). The tea–cinnamaldehyde coating shows rapid formation, reaching maximum thickness in 5 min, with very little subsequent variation in thickness values, Figure 4.3. In contrast, the tea-only coating is ultrathin, and does not get appreciably thicker after 24 h.

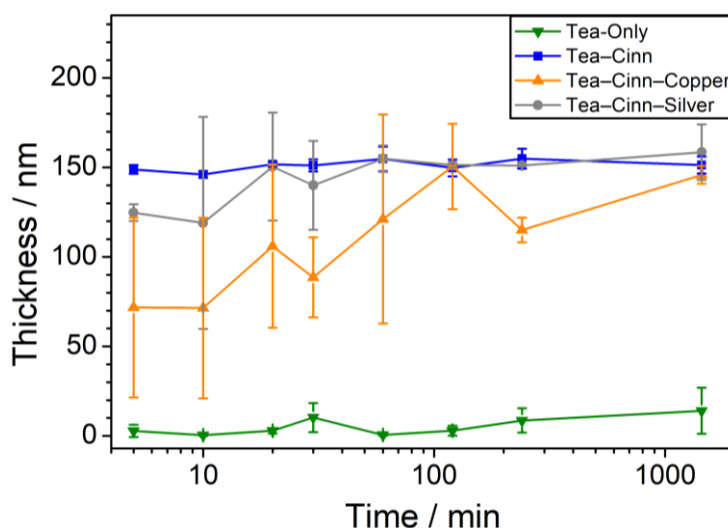


Figure 4.3: Coating thickness on silicon wafer substrate versus deposition time for tea-only, tea–cinnamaldehyde, tea–cinnamaldehyde–copper sulphate pentahydrate, and tea–cinnamaldehyde–silver nitrate coatings. 30 mg cinnamaldehyde and / or 10 mg metal salt added to 10 ml tea solution.

Infrared spectroscopy indicated that the tea-only coating displayed absorbance features similar to those previously reported for tea-staining studies²⁵ and tea extracts²⁶: O–H stretch ($3500\text{--}3300\text{ cm}^{-1}$), C–H stretch (2915 cm^{-1} and 2847 cm^{-1}), C=O stretch, C=C stretch and N–H bend ($1700\text{--}1450\text{ cm}^{-1}$), and C–O stretch ($1300\text{--}1200\text{ cm}^{-1}$), Figure 4.4. The infrared spectrum of the tea–cinnamaldehyde coating displays similar absorbances to those seen for the tea-only coating. The incorporation of cinnamaldehyde into the tea–cinnamaldehyde coating is confirmed by the presence of cinnamaldehyde aldehyde C–H stretching features (2814 cm^{-1} and 2742 cm^{-1}) and ring summation peaks ($2000\text{--}1700\text{ cm}^{-1}$)—all absent in the tea-only coating infrared spectrum. It was not possible to distinguish cinnamaldehyde C=O aldehyde (1668 cm^{-1}) and C=C (1625 cm^{-1}) absorbances from overlapping tea C=O, C=C, and N–H bond absorbances ($1700\text{--}1450\text{ cm}^{-1}$).

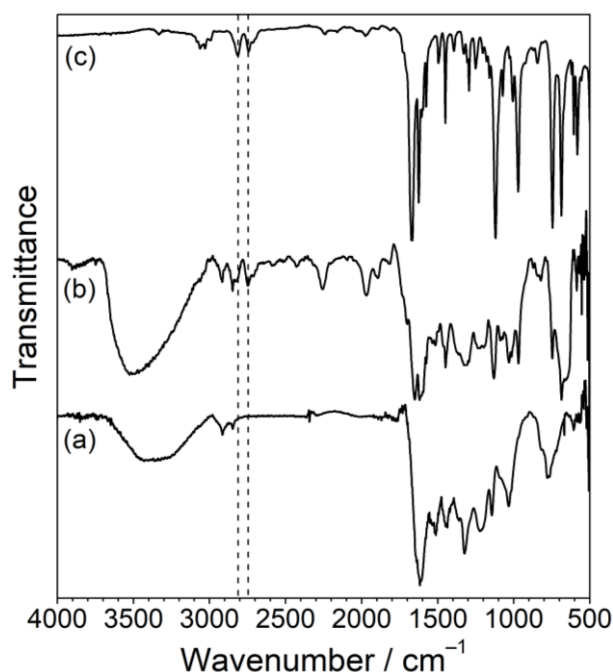


Figure 4.4: Infrared spectra of: (a) tea-only coating (RAIRS); (b) tea-cinnamaldehyde (30 mg in 10 ml tea solution) coating (RAIRS); and (c) liquid cinnamaldehyde (ATR). Cinnamaldehyde aldehyde C–H stretch (2814 and 2742 cm^{-1}) absorbances are shown as dashed lines.

4.3.2 Tea-Cinnamaldehyde-Copper Coating

Tea-copper sulphate pentahydrate (10 mg) coated PET film substrate showed no visible change in appearance, whilst the tea-cinnamaldehyde-copper sulphate pentahydrate (10 mg) coating was opaque orange-brown in colour, Figure 4.1. Higher loading tea-copper sulphate pentahydrate (50 mg) and tea-cinnamaldehyde-copper sulphate pentahydrate (50 mg) coatings were similar in appearance to their 10 mg equivalents, Figure 4.5.

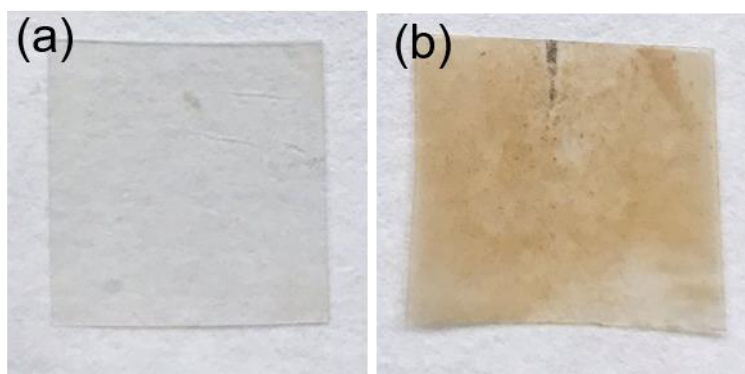


Figure 4.5: Photographs of coated PET substrate: (a) tea-copper; and (b) tea-cinnamaldehyde-copper. 30 mg cinnamaldehyde and 50 mg metal salt added to 10 ml tea solution.

The tea–cinnamaldehyde–copper sulphate pentahydrate (10 mg) coating was measured to be of comparable thickness to the tea–cinnamaldehyde coating indicating that copper incorporation does not significantly impact film thickness, Table 4.2. The coating shows slower growth than tea–cinnamaldehyde coating, only approaching the maximum thickness after 24 h, Figure 4.3.

XPS analysis of the tea–cinnamaldehyde–copper sulphate pentahydrate (10 mg) coating confirmed that copper was present in the coating and there was an absence of sulphur, Table 4.3. X-ray diffraction (XRD) analysis of uncoated and tea–cinnamaldehyde coated glass slides indicated amorphous structure with no crystalline peaks, Figure 4.6. X-ray diffraction and transmission electron microscopy (TEM) analysis of the tea–cinnamaldehyde–copper sulphate pentahydrate (10 mg) coating did not provide any evidence for the formation of large copper crystallites and is consistent with a high level of metallic species dispersion, Figure 4.6 and Figure 4.7. Features attributable to the organic component of the coating (i.e. tea–cinnamaldehyde) were visible in the TEM images.

Table 4.3: XPS atomic percentages of tea–cinnamaldehyde and tea–cinnamaldehyde–metal coatings on PET substrate. 30 mg cinnamaldehyde and 10 mg metal salt added to 10 ml tea solution. *No sulphur was detected.

Coating	XPS Atomic Composition / %				
	C	N	O	Cu	Ag
Tea–Cinnamaldehyde	80.7 ± 0.6	0.5 ± 0.1	18.8 ± 0.7	-	-
Tea– Cinnamaldehyde– Copper *	76.6 ± 0.7	0.8 ± 0.1	22.4 ± 0.7	0.20 ± 0.04	-
Tea– Cinnamaldehyde– Silver	79.5 ± 1.6	0.6 ± 0.3	19.8 ± 1.5	-	0.10 ± 0.04

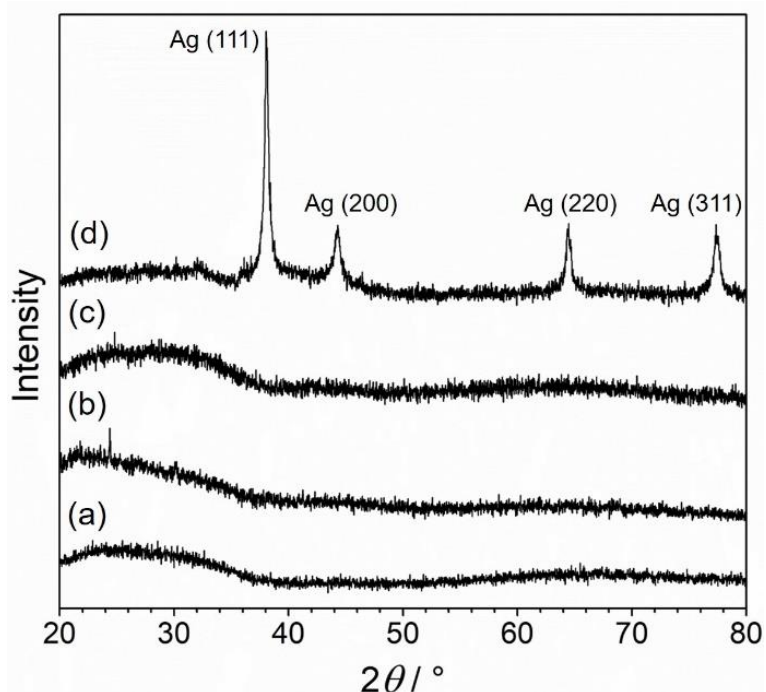


Figure 4.6: XRD patterns for glass substrate: (a) uncoated; (b) tea-cinnamaldehyde coating; (c) tea-cinnamaldehyde-copper coating, and (d) tea-cinnamaldehyde-silver coating. 30 mg cinnamaldehyde and 10 mg metal salt added to 10 ml tea solution. XRD data obtained by Gary Oswald.

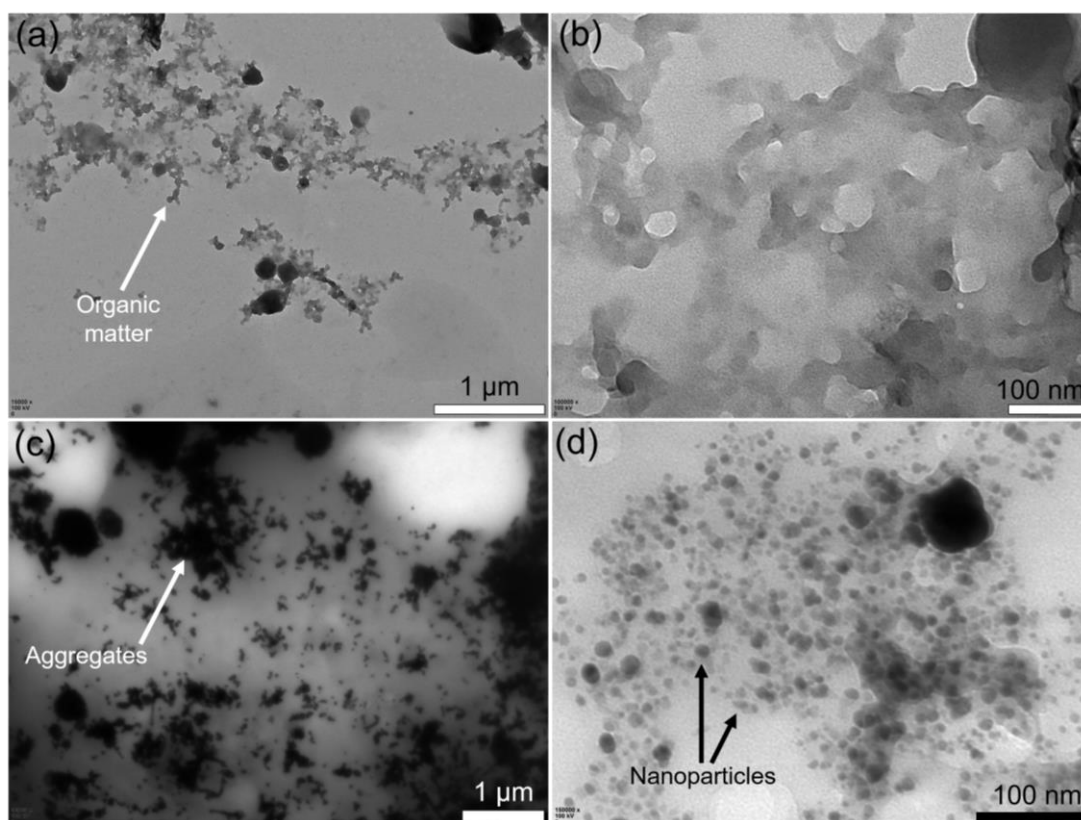


Figure 4.7: Transmission electron microscopy (TEM) images of: (a–b) tea-cinnamaldehyde-copper sulphate pentahydrate coating; and (c–d) tea-cinnamaldehyde-silver nitrate coating. 30 mg cinnamaldehyde and 10 mg metal salt added to 10 ml tea solution. Images taken by Tracey Davey.

Raman spectroscopy of non-woven polypropylene cloth displayed the following peaks: 808 cm^{-1} (CH_2 rocking and C–C stretching), 841 cm^{-1} (CH_2 rocking), 979 cm^{-1} (CH_3 rocking and C–C stretching), 998 cm^{-1} (CH_3 rocking), 1158 cm^{-1} (C–C stretching and CH bending), 1170 cm^{-1} (C–C stretching, CH_3 rocking and C–C wagging), 1220 cm^{-1} (CH_2 twisting, CH wagging, and C–C stretching), 1440 cm^{-1} (CH_2 bending), and 1464 cm^{-1} (CH_2 bending), Figure 4.8.²⁷ Green tea-only treated polypropylene cloth showed an identical spectrum to the untreated cloth (this is probably due to the ultrathin nature (14 nm) of the tea coating compared to the Raman technique sampling depth²⁸). The tea–cinnamaldehyde coating Raman spectrum shows polypropylene peaks together with a broad absorption peak centred at 1100 cm^{-1} . Copper sulphate pentahydrate shows Raman symmetric bending vibrations of SO_4^{2-} (ν_2 modes) (430 cm^{-1} and 470 cm^{-1}), antisymmetric bending (ν_4 mode) (616 cm^{-1}), symmetric stretching (ν_1 mode) (989 cm^{-1}), and antisymmetric stretching (ν_3 mode) (1149 cm^{-1}).²⁹ Tea–cinnamaldehyde–copper coated onto polypropylene cloth shows a broad, featureless Raman spectrum with very broad absorption over the whole range of wavenumbers examined. No new peaks are visible, and no peaks from copper sulphate pentahydrate are present.

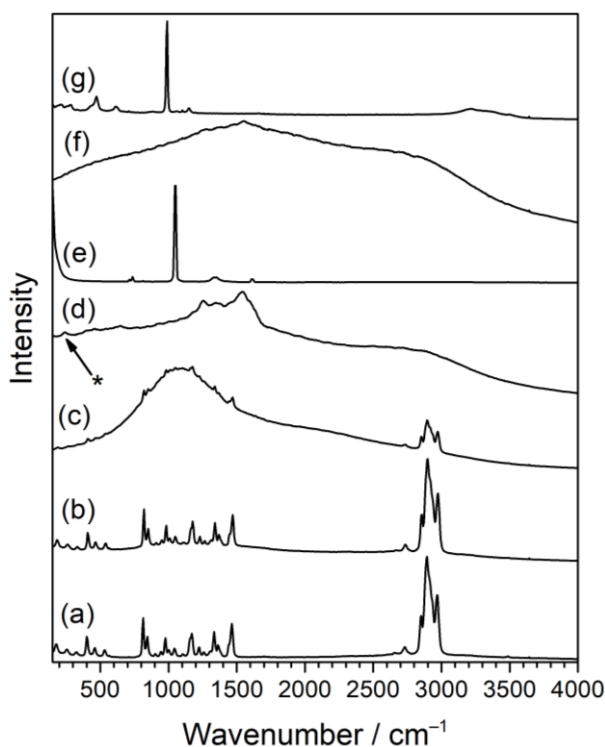


Figure 4.8: Raman spectra of: (a) untreated polypropylene cloth; (b) green tea-only coated polypropylene cloth; (c) tea–cinnamaldehyde coated polypropylene cloth; (d) tea–cinnamaldehyde–silver nitrate (10 mg) coated polypropylene cloth; (e) silver nitrate

powder; (f) tea–cinnamaldehyde–copper sulphate pentahydrate (10 mg) coated polypropylene cloth; and (g) copper sulphate pentahydrate powder. * New peak at 235 cm^{-1} corresponding to Ag–O bond.

Potential metal leaching of the tea–cinnamaldehyde–copper coating deposited onto hydrophilic polypropylene cloth upon immersion into water was examined using ICP-OES over a range of immersion times (30 s–24 h), Figure 4.9. A control ‘blank’ was also run, where an uncoated piece of hydrophilic non-woven polypropylene cloth substrate was immersed into water for 24 h, in order to check that there were not any significant amounts of copper in the water, glass vial, cloth, or nitric acid. No increase or trend was observed in the quantities of copper detected in solution after 24 h immersion, and the copper concentrations remained very low (<4 ppm, i.e. <4 $\mu\text{g ml}^{-1}$). Visually the coated cloths looked completely unchanged after 24 h immersion. Therefore, the tea–cinnamaldehyde–copper coating is stable, and the copper component is not prone to rapid leaching out into aqueous media.

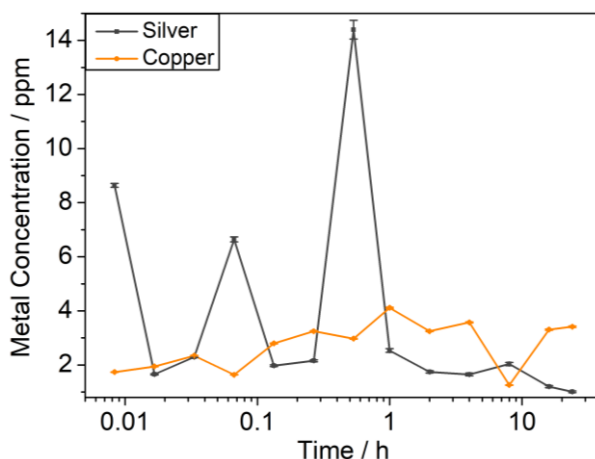


Figure 4.9: ICP-OES metal concentrations in solution vs. immersion time, after immersion of tea–cinnamaldehyde–silver or tea–cinnamaldehyde–copper coated hydrophilic non-woven polypropylene cloth (2 cm x 2 cm) into high-purity water. 600 mg cinnamaldehyde and 200 mg metal salt added to 200 ml tea solution. Control blank hydrophilic non-woven polypropylene cloth (2 cm x 2 cm) tested for copper showed a concentration of 0.3 ppm, and for silver showed a concentration of 0.1 ppm. Instrument detection limit is 0.01 ppm for both copper and silver. ICP-OES data obtained by Emily Unsworth.

4.3.3 Tea–Cinnamaldehyde–Silver Coating

Tea–silver nitrate (10 mg) coating displayed a faint grey colouration, whereas the tea–cinnamaldehyde–silver nitrate (10 mg) coating was opaque dark greyish-brown in appearance, Figure 4.1. The corresponding higher loading tea–silver

nitrate (50 mg) and tea–cinnamaldehyde–silver nitrate (50 mg) coatings were found to be a darker grey colouration and non-uniform dark grey with a brown tint respectively, Figure 4.10.

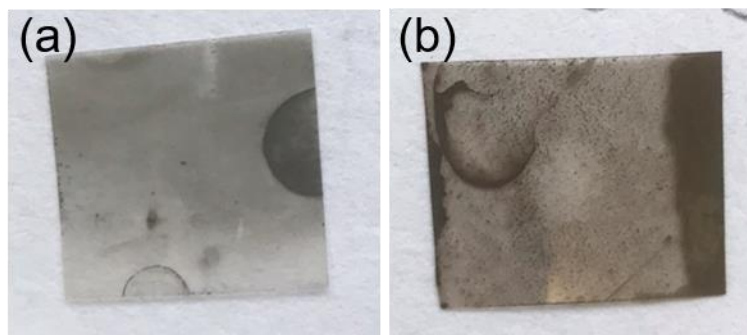


Figure 4.10: Photographs of coated PET substrate: (a) tea–silver; and (b) tea–cinnamaldehyde–silver. 30 mg cinnamaldehyde and 50 mg metal salt added to 10 ml tea solution.

As noted for the copper-containing coatings, the thickness of the tea–cinnamaldehyde–silver nitrate (10 mg) coating was comparable to the tea–cinnamaldehyde coating, thereby indicating that the incorporation of silver does not have a significant effect upon coating thickness, Table 4.2. Tea–cinnamaldehyde–silver coating thickness increased at a slower rate compared to the tea–cinnamaldehyde coating, approaching the maximum coating thickness after 20–30 min, Figure 4.3.

XPS characterisation of the tea–cinnamaldehyde–silver nitrate (10 mg) coating surface confirmed the incorporation of silver into the coating, Table 4.3. The carbon, oxygen, and nitrogen elemental compositions were similar to the control tea–cinnamaldehyde coating, indicating that silver incorporation does not significantly affect formation of the coating (which is consistent with the aforementioned thickness measurements, Table 4.2).

X-ray diffraction analysis of the tea–cinnamaldehyde–silver nitrate (10 mg) coating gave rise to the appearance of new peaks which confirm the reduction of silver nitrate to metallic silver crystallites taking place ($2\theta = 38.0^\circ, 44.3^\circ, 64.5^\circ,$ and 77.5° corresponding to silver (111), (200), (220), and (311) crystal planes respectively), Figure 4.6.³⁰

Transmission electron microscopy analysis of the tea–cinnamaldehyde–silver nitrate (10 mg) coating showed nanostructured metal aggregates at lower magnifications, and individual silver nanoparticles at higher magnifications, Figure 4.7.

Tea–cinnamaldehyde–silver nitrate (10 mg) coated polypropylene cloth produced a Raman spectrum with very broad absorption spanning the whole range of wavenumbers examined, Figure 4.8. Peaks are observed at 1250 cm^{-1} and 1530 cm^{-1} that are absent in the tea–cinnamaldehyde coating, or the silver nitrate powder Raman spectra. It is likely that the silver nanoparticles are creating a surface enhanced Raman spectroscopic (SERS) effect, enhancing the signal of certain bands.³¹ The Ag–O feature at 235 cm^{-1} is consistent with the presence of silver nanoparticles.³²

Leaching tests for silver from the tea–cinnamaldehyde–silver nitrate coating on hydrophilic non-woven polypropylene cloth yielded similar results to the tea–cinnamaldehyde–copper sulphate pentahydrate coating—no increase or trend was observed, and the silver content remained low (less than 2 ppm) after 24 h, thus indicating that the silver does not readily leach into aqueous medium from the coating, Figure 4.9. It was attempted to determine the metal contents of both the tea–cinnamaldehyde–copper and tea–cinnamaldehyde–silver coatings via ICP-OES by depositing them first onto glass, then scraping off the coatings, and digesting them in nitric acid. However, it was found that the coatings were completely resistant to digestion; even after reflux at $200\text{ }^{\circ}\text{C}$ for 24 h in 5%v/v nitric acid, the solid coatings were visibly not digested/dissolved. Therefore, the coatings appear to be robust.

Tea–cinnamaldehyde–metal coatings could be deposited onto a wide range of substrate materials, for example, glass, PTFE, cotton gloves, hydrophilic non-woven polypropylene cloth, and tennis balls; Figure 4.11, Figure 4.12, Figure 4.13, Figure 4.14, and Figure 4.15 respectively.

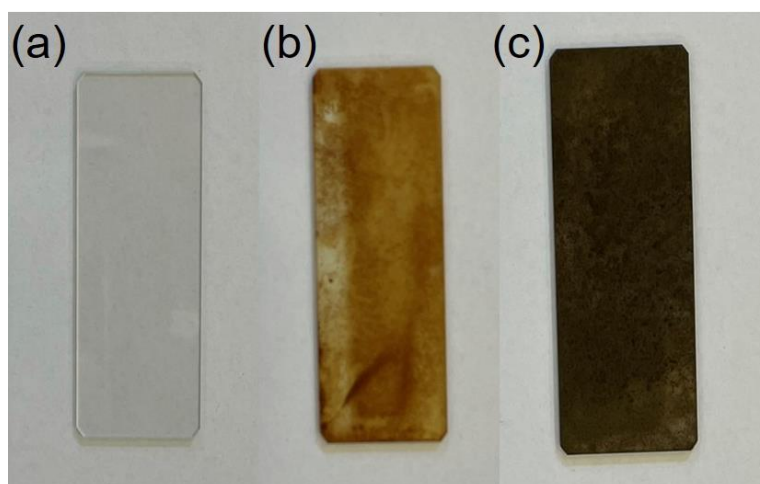


Figure 4.11: Photographs of glass slides: (a) untreated; (b) tea-cinnamaldehyde-copper coated; and (c) tea-cinnamaldehyde-silver coated. 1500 mg cinnamaldehyde and 200 mg metal salt added to 500 ml tea solution.

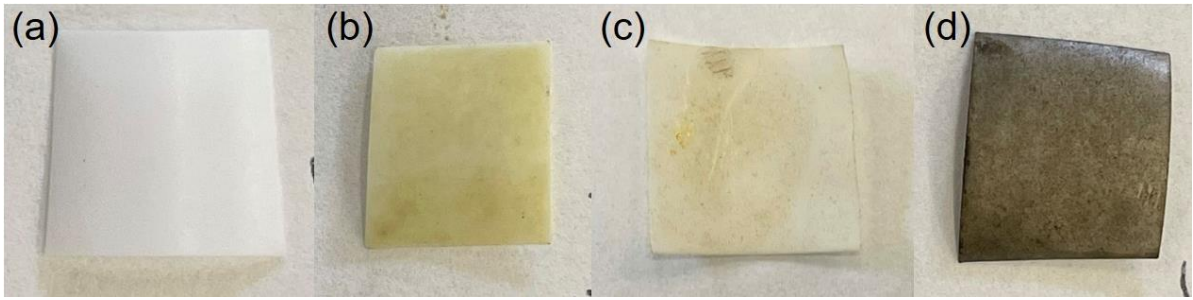


Figure 4.12: Photographs of PTFE: (a) untreated; (b) tea-cinnamaldehyde coated; (c) tea-cinnamaldehyde-copper coated; and (d) tea-cinnamaldehyde-silver coated. 30 mg cinnamaldehyde and 10 mg metal salt added to 10 ml tea solution.

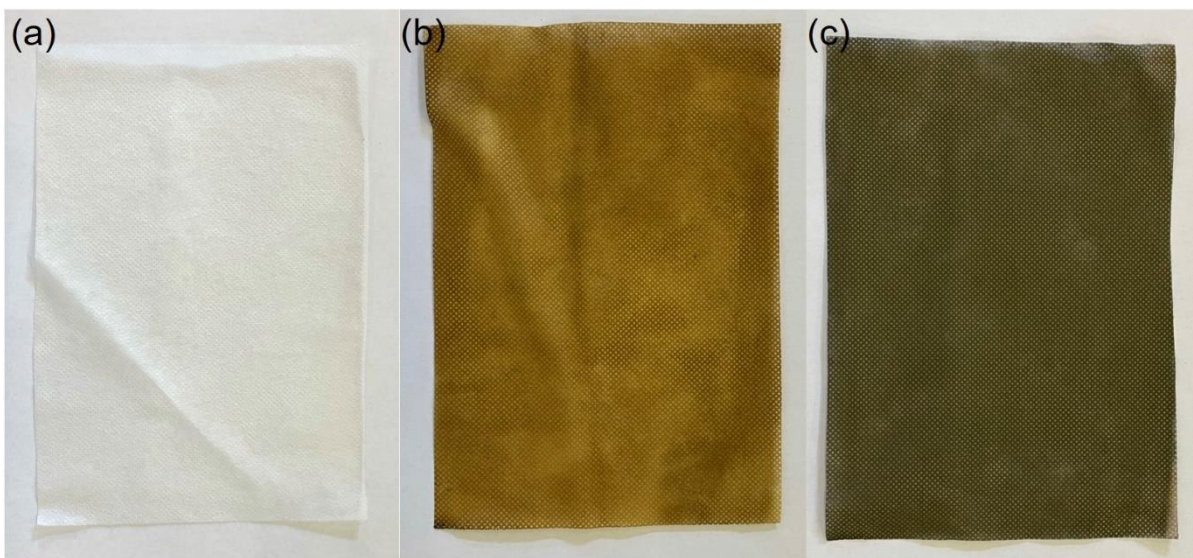


Figure 4.13: Photographs of hydrophilic non-woven polypropylene cloth: (a) untreated; (b) tea-cinnamaldehyde-copper coated; and (c) tea-cinnamaldehyde-silver coated. 600 mg cinnamaldehyde and 200 mg metal salt added to 400 ml tea solution.



Figure 4.14: Photographs of cotton gloves: (a) uncoated; (b) tea-cinnamaldehyde-silver coated; and (c) tea-cinnamaldehyde-copper coated. 900 mg cinnamaldehyde and 300 mg metal salt added to 300 ml tea solution.

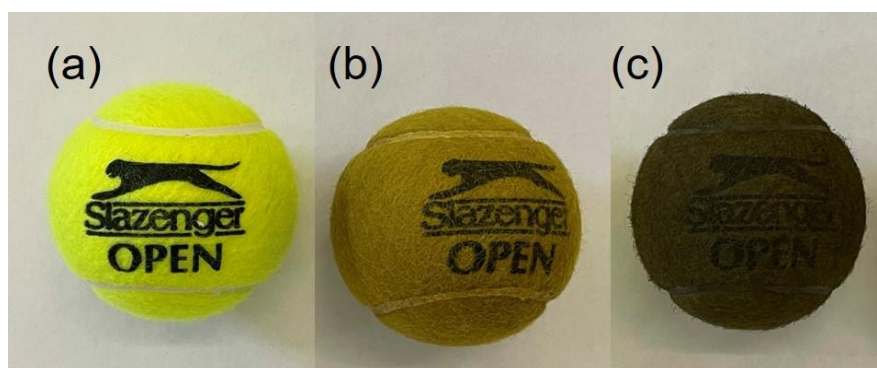


Figure 4.15: Photographs of tennis balls: (a) untreated; (b) tea-cinnamaldehyde-copper coated; and (c) tea-cinnamaldehyde-silver coated. 788 mg cinnamaldehyde and 260 mg metal salt added to 350 ml tea solution.

4.3.4 Antibacterial Testing

Tea-cinnamaldehyde coating on hydrophilic non-woven polypropylene cloth showed complete killing of *E. coli* and *S. aureus*, giving Log₁₀ Reduction values of 8.44 ± 0.07 and 7.90 ± 0.09 respectively, Table 4.4. The tea-cinnamaldehyde-copper and tea-cinnamaldehyde-silver coatings also gave complete killing of both bacteria (thus yielding identical Log₁₀ Reduction values towards respective bacteria, since all three coatings were tested concurrently alongside the same controls), Table 4.4.

Table 4.4: Antibacterial tests for tea-cinnamaldehyde, tea-cinnamaldehyde-copper, and tea-cinnamaldehyde-silver coatings on hydrophilic non-woven polypropylene cloth. 900 mg cinnamaldehyde and 300 mg metal salt added to 400 ml tea solution. Values are given as mean \pm standard deviation.

Coating	Bacterial Log ₁₀ Reduction	
	<i>E. coli</i>	<i>S. aureus</i>
Tea-Cinnamaldehyde	8.44 ± 0.07	7.90 ± 0.09
Tea-Cinnamaldehyde-Copper	8.44 ± 0.07	7.90 ± 0.09
Tea-Cinnamaldehyde-Silver	8.44 ± 0.07	7.90 ± 0.09

4.3.5 Antiviral Testing

Non-woven polypropylene face masks were coated with tea-cinnamaldehyde-copper and tea-cinnamaldehyde-silver, Figure 4.16. The front sheet of the mask was removed and tested against murine coronavirus (MHV-A59), Table 4.5.

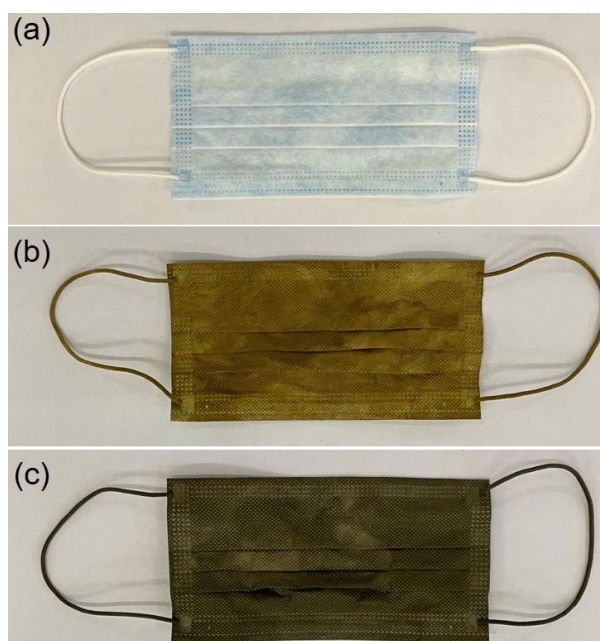


Figure 4.16: Non-woven polypropylene personal protection face masks used for antiviral testing against murine coronavirus (MHV-A59): (a) untreated control; (b) tea-cinnamaldehyde-copper coated; and (c) tea-cinnamaldehyde-silver coated. 900 mg cinnamaldehyde and 300 mg metal salt added to 400 ml tea solution.

Tea-cinnamaldehyde-copper coating produced a 98.6% reduction in the viral titre after 2 h contact time, while the tea-cinnamaldehyde-silver coating gave a 99.8% reduction. In contrast, there was no decrease in MHV-A59 titre recovered from the control untreated mask material corresponding to the same contact time.

Table 4.5: Median Tissue Culture Infectious Dose (TCID₅₀) values (expressed as Log₁₀ values); and percentage (%) reduction of viral titre values after 2 h contact time for murine coronavirus (MHV-A59) on face mask fabric. Error associated with the test technique employed is approximately 0.5 Log₁₀, hence these data are indicative of virucidal activity associated with the coatings. 900 mg cinnamaldehyde and 300 mg metal salt added to 400 ml tea solution. Antiviral testing performed by Graham Christie.

Sample	TCID ₅₀ (Log ₁₀ values)		% Reduction
	0 h	2 h	
Control	-7.28	-7.37	0
Tea-Cinnamaldehyde-Copper	-7.63	-5.78	98.6
Tea-Cinnamaldehyde-Silver	-7.56	-4.93	99.8

4.4 Discussion

In contrast to previous multiple-step fabrication approaches for antimicrobial coatings, the outlined single-step methodology is simple and cheap. Tea-only

coatings form as a result of oxidation and polymerisation of the natural plant constituent polyphenols.³³ In the absence of any other reagents, these types of polyphenol coatings typically require long reaction times (~24 h) to produce a coating and tend to be ultrathin (14 nm), Table 4.2 and Figure 4.3.³⁴ In contrast, the tea–cinnamaldehyde coating reported in the present study shows rapid deposition, producing a 150 nm coating in as little as 5 min without any requirement for additional chemicals, Table 4.2 and Figure 4.3. It is therefore unlikely that the tea–cinnamaldehyde coating forms solely as a result of oxidation reactions. One possible explanation for the rapid aggregation and precipitation of a coating which can spontaneously adhere to substrate surfaces in solution is that the tea–cinnamaldehyde coating forms due to various intermolecular interactions between the constituent tea compounds and cinnamaldehyde—such as hydrophobic interactions, π - π aromatic interactions, hydrogen bonding, and van der Waals' forces. Addition of silver nitrate or copper sulphate pentahydrate salts to the tea–cinnamaldehyde coating solution results in a slowing down of the deposition rate, but does not attenuate the final thickness, Table 4.2 and Figure 4.3. This may be due to the metal ions interacting or coordinating with the tea compounds and / or cinnamaldehyde, thereby slowing the interactions between the tea compounds and cinnamaldehyde responsible for coating formation.

Previous reports on tannic acid–copper products describe the copper as being coordinated to the tannic acid in the form of Cu(II) coordinated with phenol oxygens.^{35,36} This may be applicable here with the copper centres coordinated to the structurally-similar tea polyphenol compounds within the coating (e.g. epigallocatechin gallate). The silver nanoparticles detected in the tea–cinnamaldehyde–silver coating are consistent with previous reports which have employed tea extract to reduce silver salts to generate nanoparticles, Figure 4.7.³⁰

A rough estimate of the metal loading weight percent (wt%) can be made using the XPS atomic percentages: Cu = 0.99 wt% for the tea–cinnamaldehyde–copper coating and Ag = 0.84 wt% for the tea–cinnamaldehyde–silver coating, Table 4.3. It is possible that the metal content in the bulk may differ to that of the surface detected by XPS (sampling depth 2–5 nm)³⁷; and that some of the metal at the surface may be encapsulated by the tea and cinnamaldehyde coating components—these values therefore represent a lower bound estimate. This strategy of using tea and essential oils in conjunction with metals enables much

lower quantities of bioactive metals to be used, thereby alleviating any potential environmental and toxicological health concerns. The rates of metal leaching have been found to be very low (less than 5 ppm over 24 h), Figure 4.9.

The tea–cinnamaldehyde and tea–cinnamaldehyde–metal coatings readily adhere to a wide array of substrate material surfaces, including silicon, glass, polyester, polypropylene cloth, polytetrafluorethylene, and cotton. Adhesion is likely to occur via a similar mechanism to that reported for polydopamine coatings—the catechol and gallic acid moieties in the tea compounds provide strong types of interaction with the surface, allowing the coatings to stick.³⁸

Complete killing of both *E. coli* and *S. aureus* bacteria (Log_{10} Reduction = 8.44 ± 0.07 and 7.90 ± 0.09 respectively) is found for the tea–cinnamaldehyde coating. This is comparable to previously reported polydopamine–cinnamaldehyde and tannic acid–cinnamaldehyde coatings (chapter 3)³⁹; and is many orders of magnitude better than the minimum Log_{10} Reduction = 3 recommended by the United States Environmental Protection Agency.⁴⁰ Tea–cinnamaldehyde coatings containing silver or copper also showed complete killing of bacteria, indicating that addition of the metals does not negatively affect the antibacterial efficacy of the coatings, Table 4.4. The antibacterial activity of copper could be occurring via several modes of action: copper causes cell membrane damage⁴¹, production of reactive oxygen species (ROS),⁴² and DNA fragmentation and disintegration.⁴³ Similarly, silver is reported to be antibacterial *via* multiple mechanisms: silver has a high affinity to interact with sulphur groups (e.g. thiols) and phosphorus groups which can lead to inhibition of enzymes and also interactions with DNA may disrupt DNA replication—both leading to bacterial cell death.^{44,45,46} In addition, silver nanoparticles can cause damage to the cell membrane, resulting in leakage of the cell contents.⁴⁷ They can also give rise to depletion of intracellular adenosine triphosphate (ATP) levels, and cause an increase in reactive oxygen species (ROS) within cells.^{48,49,50}

The infectivity of murine coronavirus MHV-A59 after a 2 h contact time with tea–cinnamaldehyde–copper and tea–cinnamaldehyde–silver coated face mask fabrics was attenuated by 98.6% and 99.8% respectively, Table 4.5. Copper is understood to inactivate viruses via production of hydroxyl free radicals which damage the virus^{51, 52}, or via binding to cysteine residues on virus proteases.⁵³ Inhibition of viruses with silver can occur via a number of different potential

pathways depending on the virus type, including interfering with viral attachment mechanisms⁵⁴, breakage of sulphur–sulphur disulphide bonds in enzymes⁵⁵, or interacting with viral DNA.⁵⁶ These metal-containing coatings display antiviral activities against murine coronavirus MHV-A59 which are comparable to those reported in the literature for copper and silver towards SARS-CoV-2—although accurate and direct comparisons are very difficult to make due to differing test procedures, type of virus, and metal loadings, etc.^{11,12,13,14} Regardless, the sheer simplicity and scalability make the present coatings highly suitable for widespread societal applications.

Alternative variations of these tea-cinnamaldehyde-metal coatings could combine together different elements (for example alloy formation), and the use of other natural compounds or essential oils to produce coatings with even more potent antimicrobial efficacies. Sustainability is also an important factor when considering societal applications of antimicrobial coatings. The utilisation of low amounts of bioactive metals whilst retaining high biocidal activities is beneficial to the environment.⁵⁷

4.5 Conclusions

Tea–cinnamaldehyde and tea–cinnamaldehyde–metal coatings spontaneously adhere to substrates (including silicon, glass, polyester, polypropylene, polytetrafluoroethylene, and cotton) and give rise to complete killing of both *E. coli* and *S. aureus* bacteria after 4 h exposure (Log_{10} Reduction = 8.44 ± 0.07 and 7.90 ± 0.09 respectively). Tea–cinnamaldehyde–copper and tea–cinnamaldehyde–silver coatings gave 98.6% and 99.8% reduction respectively against murine coronavirus, MHV-A59 after 2 h exposure. These single-step fabrication coatings utilise cheap and readily available everyday reagents which do not require any specialized technical expertise or equipment.

4.6 References

- 1 WHO Director-General's opening remarks at the media briefing on COVID-19 - 11 March 2020 <https://www.who.int/director-general/speeches/detail/who-director-general-s-opening-remarks-at-the-media-briefing-on-covid-19---11-march-2020>; accessed 22/02/2021.
- 2 Ioannidis, J. P. A. Global Perspective of COVID-19 Epidemiology for a Full-Cycle Pandemic. *European Journal of Clinical Investigation*. Blackwell Publishing Ltd December 1, 2020, p e13423.
- 3 Meyerowitz-Katz, G.; Merone, L. A Systematic Review and Meta-Analysis of Published Research Data on COVID-19 Infection Fatality Rates. *Int. J. Infect. Dis.* **2020**, *101*, 138–148.
- 4 COVID-19 Dashboard by the Center for Systems Science and Engineering (CSSE) at Johns Hopkins University (JHU), <https://gisanddata.maps.arcgis.com/apps/dashboards/bda7594740fd40299423467b48e9ecf6>; accessed 02/06/2021.
- 5 Pastorino, B.; Touret, F.; Gilles, M.; de Lamballerie, X.; Charrel, R. N. Prolonged Infectivity of SARS-CoV-2 in Fomites. *Emerg. Infect. Dis.* **2020**, *26*, 2256.
- 6 van Doremalen, N.; Bushmaker, T.; Morris, D. H.; Holbrook, M. G.; Gamble, A.; Williamson, B. N.; Tamin, A.; Harcourt, J. L.; Thornburg, N. J.; Gerber, S. I.; Lloyd-Smith, J. O.; de Wit, E.; Munster, V. J.; Aerosol and Surface Stability of SARS-CoV-2 as Compared with SARS-CoV-1. *N. Engl. J. Med.* **2020**, *382*, 1564–1567.
- 7 Noyce, J. O.; Michels, H.; Keevil, C. W. Inactivation of Influenza A Virus on Copper versus Stainless Steel Surfaces. *Appl. Environ. Microbiol.* **2007**, *73*, 2748–2750.
- 8 Sun, R. W. Y.; Chen, R.; Chung, N. P. Y.; Ho, C. M.; Lin, C. L. S.; Che, C. M. Silver Nanoparticles Fabricated in Hepes Buffer Exhibit Cytoprotective Activities toward HIV-1 Infected Cells. *Chem. Commun.* **2005**, No. 40, 5059–5061.
- 9 Han, J.; Chen, L.; Duan, S. M.; Yang, Q. X.; Yang, M.; Gao, C.; Zhang, B. Y.; He, H.; Dong, X. P. Efficient and Quick Inactivation of SARS Coronavirus and Other Microbes Exposed to the Surfaces of Some Metal Catalysts. *Biomed. Environ. Sci.* **2005**, *18*, 176–180.
- 10 Warnes, S. L.; Little, Z. R.; Keevil, C. W. Human Coronavirus 229E Remains Infectious on Common Touch Surface Materials. *MBio* **2015**, *6*, e01697-15.
- 11 Hutasoit, N.; Kennedy, B.; Hamilton, S.; Luttick, A.; Rahman Rashid, R. A.; Palanisamy, S. Sars-CoV-2 (COVID-19) Inactivation Capability of Copper-Coated Touch Surface Fabricated by Cold-Spray Technology. *Manuf. Lett.* **2020**, *25*, 93–97.
- 12 Behzadinasab, S.; Chin, A.; Hosseini, M.; Poon, L.; Ducker, W. A. A Surface Coating That Rapidly Inactivates SARS-CoV-2. *ACS Appl. Mater. Interfaces* **2020**, *12*, 34723–34727.
- 13 Jeremiah, S. S.; Miyakawa, K.; Morita, T.; Yamaoka, Y.; Ryo, A. Potent Antiviral Effect of Silver Nanoparticles on SARS-CoV-2. *Biochem. Biophys. Res. Commun.* **2020**, *533*, 195–200.
- 14 Balagna, C.; Perero, S.; Percivalle, E.; Nepita, E. V.; Ferraris, M. Virucidal Effect against Coronavirus SARS-CoV-2 of a Silver Nanocluster/Silica Composite Sputtered Coating. *Open Ceram.* **2020**, *1*, 100006.

- 15 Mhatre, S.; Srivastava, T.; Naik, S.; Patravale, V. Antiviral Activity of Green Tea and Black Tea Polyphenols in Prophylaxis and Treatment of COVID-19: A Review. *Phytomedicine* **2021**, *85*, 153286.
- 16 Nashimoto, K.; Tashiro, Y.; Kosaka, Y.; Hara, Y. Antiviral filter air cleaner impregnated with tea extract. U.S. Patent US5747053A, 5th May 1998.
- 17 Ghosh, R.; Chakraborty, A.; Biswas, A.; Chowdhuri, S. Evaluation of Green Tea Polyphenols as Novel Corona Virus (SARS CoV-2) Main Protease (Mpro) Inhibitors—an *in Silico* Docking and Molecular Dynamics Simulation Study. *J. Biomol. Struct. Dyn.* **2020**, 1–13.
- 18 Wijesekera, R. O. B.; Jayewardene, A. L.; Rajapakse, L. S. Volatile Constituents of Leaf, Stem and Root Oils of Cinnamon (*Cinnamomum Zeylanicum*). *J. Sci. Food Agric.* **1974**, *25*, 1211–1220.
- 19 Fabra, M. J.; Castro-Mayorga, J. L.; Randazzo, W.; Lagarón, J. M.; López-Rubio, A.; Aznar, R.; Sánchez, G. Efficacy of Cinnamaldehyde Against Enteric Viruses and Its Activity After Incorporation Into Biodegradable Multilayer Systems of Interest in Food Packaging. *Food Environ. Virol.* **2016**, *8*, 125–132.
- 20 Hayashi, K.; Imanishi, N.; Kashiwayama, Y.; Kawano, A.; Terasawa, K.; Shimada, Y.; Ochiai, H. Inhibitory Effect of Cinnamaldehyde, Derived from Cinnamomi Cortex, on the Growth of Influenza A/PR/8 Virus in Vitro and in Vivo. *Antiviral Res.* **2007**, *74*, 1–8.
- 21 Kulkarni, S. A.; Nagarajan, S. K.; Ramesh, V.; Palaniyandi, V.; Selvam, S. P.; Madhavan, T. Computational Evaluation of Major Components from Plant Essential Oils as Potent Inhibitors of SARS-CoV-2 Spike Protein. *J. Mol. Struct.* **2020**, *1221*, 128823.
- 22 Ahmed, W.; Bertsch, P. M.; Bibby, K.; Haramoto, E.; Hewitt, J.; Huygens, F.; Gyawali, P.; Korajkic, A.; Riddell, S.; Sherchan, S. P.; Simpson, S. L.; Sirikanchana, K.; Symonds, E. M.; Verhagen, R.; Vasani, S. S.; Kitajima, M.; Bivins, A. Decay of SARS-CoV-2 and Surrogate Murine Hepatitis Virus RNA in Untreated Wastewater to Inform Application in Wastewater-Based Epidemiology. *Environ. Res.* **2020**, *191*, 110092.
- 23 Körner, R. W.; Majjouti, M.; Alejandro Alcazar, M. A.; Mahabir, E. Of Mice and Men: The Coronavirus MHV and Mouse Models as a Translational Approach to Understand SARS-CoV-2. *Viruses* **2020**, *12*, 880.
- 24 Gorbalenya, A. E.; Baker, S. C.; Baric, R. S.; de Groot, R. J.; Drosten, C.; Gulyaeva, A. A.; Haagmans, B. L.; Lauber, C.; Leontovich, A. M.; Neuman, B. W.; Penzar, D.; Perlman, S.; Poon, L. L. M.; Samborskiy, D. V.; Sidorov, I. A.; Sola, I.; Ziebuhr, J. The Species Severe Acute Respiratory Syndrome-Related Coronavirus: Classifying 2019-NCoV and Naming It SARS-CoV-2. *Nat. Microbiol.* **2020**, *5*, 536–544.
- 25 Yamada, K.; Abe, T.; Tanizawa, Y. Black Tea Stain Formed on the Surface of Teacups and Pots. Part 2 - Study of the Structure Change Caused by Aging and Calcium Addition. *Food Chem.* **2007**, *103*, 8–14.
- 26 Baldemir, A.; Köse, N. B.; İldiz, N.; İlgün, S.; Yusufbeyoğlu, S.; Yilmaz, V.; Ocsoy, I. Synthesis and Characterisation of Green Tea (*Camellia sinensis* (L.) Kuntze) Extract and Its Major Components-Based Nanoflowers: A New Strategy to Enhance Antimicrobial Activity. *RSC Adv.* **2017**, *7*, 44303–44308.

- 27 Nielsen, A. S.; Batchelder, D. N.; Pyrz, R. Estimation of Crystallinity of Isotactic Polypropylene Using Raman Spectroscopy. *Polymer (Guildf)*. **2002**, *43*, 2671–2676.
- 28 Presser, V.; Keuper, M.; Berthold, C.; Nickel, K. G. Experimental Determination of the Raman Sampling Depth in Zirconia Ceramics. *Appl. Spectrosc.* **2009**, *63*, 1288–1292.
- 29 Fu, X.; Yang, G.; Sun, J.; Zhou, J. Vibrational Spectra of Copper Sulfate Hydrates Investigated with Low-Temperature Raman Spectroscopy and Terahertz Time Domain Spectroscopy. *J. Phys. Chem. A* **2012**, *116*, 7314–7318.
- 30 Rolim, W. R.; Pelegrino, M. T.; de Araújo Lima, B.; Ferraz, L. S.; Costa, F. N.; Bernardes, J. S.; Rodrigues, T.; Brocchi, M.; Seabra, A. B. Green Tea Extract Mediated Biogenic Synthesis of Silver Nanoparticles: Characterisation, Cytotoxicity Evaluation and Antibacterial Activity. *Appl. Surf. Sci.* **2019**, *463*, 66–74.
- 31 Willets, K. A.; Van Duyne, R. P. Localized Surface Plasmon Resonance Spectroscopy and Sensing. *Annu. Rev. Phys. Chem.* **2007**, *58*, 267–297.
- 32 Dhafer, C. E. B.; Dhahri, M.; Mezni, A.; Smiri, L. S. Surface-Enhanced Raman Scattering Study of PP/Ag Nanocomposite Developed to Prevent Postsurgery Infection. *J. Raman Spectrosc.* **2018**, *49*, 1445–1451.
- 33 Tanizawa, Y.; Abe, T.; Yamada, K. Black Tea Stain Formed on the Surface of Teacups and Pots. Part 1 - Study on the Chemical Composition and Structure. *Food Chem.* **2007**, *103*, 1–7.
- 34 Sileika, T. S.; Barrett, D. G.; Zhang, R.; Lau, K. H. A.; Messersmith, P. B. Colorless Multifunctional Coatings Inspired by Polyphenols Found in Tea, Chocolate, and Wine. *Angew. Chemie - Int. Ed.* **2013**, *52*, 10766–10770.
- 35 Li, X.; Gao, P.; Tan, J.; Xiong, K.; Maitz, M. F.; Pan, C.; Wu, H.; Chen, Y.; Yang, Z.; Huang, N. Assembly of Metal-Phenolic/Catecholamine Networks for Synergistically Anti-Inflammatory, Antimicrobial, and Anticoagulant Coatings. *ACS Appl. Mater. Interfaces* **2018**, *10*, 40844–40853.
- 36 Chakrabarty, T.; Pérez-Manríquez, L.; Neelakanda, P.; Peinemann, K. V. Bioinspired Tannic Acid-Copper Complexes as Selective Coating for Nanofiltration Membranes. *Sep. Purif. Technol.* **2017**, *184*, 188–194.
- 37 D. Briggs, M.P. Seah, Practical surface analysis, Auger and X-Ray Photoelectron Spectroscopy, vol. 1, John Wiley, Chichester, UK (1990)
- 38 Lee, H.; Dellatore, S. M.; Miller, W. M.; Messersmith, P. B. Mussel-Inspired Surface Chemistry for Multifunctional Coatings. *Science* **2007**, *318*, 426–430.
- 39 Cox, H. J.; Li, J.; Saini, P.; Paterson, J. R.; Sharples, G. J.; Badyal, J. P. S. Bioinspired and Eco-Friendly High Efficacy Cinnamaldehyde Antibacterial Surfaces. *J. Mater. Chem. B* **2021**, *9*, 2918–2930.
- 40 Updated Draft Protocol for the Evaluation of Bactericidal Activity of Hard, Non-porous Copper Containing Surface Products. US Environmental Protection Agency Office. 29th January 2016.
- 41 Santo, C. E.; Lam, E. W.; Elowsky, C. G.; Quaranta, D.; Domaille, D. W.; Chang, C. J.; Grass, G. Bacterial Killing by Dry Metallic Copper Surfaces. *Appl. Environ. Microbiol.* **2011**, *77*, 794–802.

- 42 Li, M.; Ma, Z.; Zhu, Y.; Xia, H.; Yao, M.; Chu, X.; Wang, X.; Yang, K.; Yang, M.; Zhang, Y.; Mao, C. Toward a Molecular Understanding of the Antibacterial Mechanism of Copper-Bearing Titanium Alloys against *Staphylococcus aureus*. *Adv. Healthc. Mater.* **2016**, *5*, 557–566.
- 43 Warnes, S. L.; Green, S. M.; Michels, H. T.; Keevil, C. W. Biocidal Efficacy of Copper Alloys against Pathogenic Enterococci Involves Degradation of Genomic and Plasmid DNAs. *Appl. Environ. Microbiol.* **2010**, *76*, 5390–5401.
- 44 Liao, S. Y.; Read, D. C.; Pugh, W. J.; Furr, J. R.; Russell, A. D. Interaction of Silver Nitrate with Readily Identifiable Groups: Relationship to the Antibacterial Action of Silver Ions. *Lett. Appl. Microbiol.* **1997**, *25*, 279–283.
- 45 Prabhu, S.; Poulouse, E. K. Silver Nanoparticles: Mechanism of Antimicrobial Action, Synthesis, Medical Applications, and Toxicity Effects. *Int. Nano Lett.* **2012**, *2*, 1–10.
- 46 Pal, S.; Tak, Y. K.; Song, J. M. Does the Antibacterial Activity of Silver Nanoparticles Depend on the Shape of the Nanoparticle? A Study of the Gram-Negative Bacterium *Escherichia coli*. *Appl. Environ. Microbiol.* **2007**, *73*, 1712–1720.
- 47 Li, J.; Rong, K.; Zhao, H.; Li, F.; Lu, Z.; Chen, R. Highly Selective Antibacterial Activities of Silver Nanoparticles against *Bacillus subtilis*. *J. Nanosci. Nanotechnol.* **2013**, *13*, 6806–6813.
- 48 Lok, C. N.; Ho, C. M.; Chen, R.; He, Q. Y.; Yu, W. Y.; Sun, H.; Tam, P. K. H.; Chiu, J. F.; Che, C. M. Proteomic Analysis of the Mode of Antibacterial Action of Silver Nanoparticles. *J. Proteome Res.* **2006**, *5*, 916–924.
- 49 Hsueh, Y. H.; Lin, K. S.; Ke, W. J.; Hsieh, C. Te; Chiang, C. L.; Tzou, D. Y.; Liu, S. T. The Antimicrobial Properties of Silver Nanoparticles in *Bacillus subtilis* Are Mediated by Released Ag⁺ Ions. *PLoS One* **2015**, *10*, e0144306.
- 50 Dakal, T. C.; Kumar, A.; Majumdar, R. S.; Yadav, V. Mechanistic Basis of Antimicrobial Actions of Silver Nanoparticles. *Front. Microbiol.* **2016**, *7*, 1831.
- 51 Carubelli, R.; Schneider, J. E.; Pye, Q. N.; Floyd, R. A. Cytotoxic Effects of Autoxidative Glycation. *Free Radic. Biol. Med.* **1995**, *18*, 265–269.
- 52 Fujimori, Y.; Sato, T.; Hayata, T.; Nagao, T.; Nakayam, M.; Nakayam, T.; Sugamat, R.; Suzuki, K. Novel Antiviral Characteristics of Nanosized Copper(i) Iodide Particles Showing Inactivation Activity against 2009 Pandemic H1N1 Influenza Virus. *Appl. Environ. Microbiol.* **2012**, *78*, 951–955.
- 53 Karlstrom, A. R.; Shames, B. D.; Levine, R. L. Reactivity of Cysteine Residues in the Protease from Human Immunodeficiency Virus: Identification of a Surface-Exposed Region Which Affects Enzyme Function. *Arch. Biochem. Biophys.* **1993**, *304*, 163–169.
- 54 Lara, H. H.; Ayala-Nuñez, N. V.; Ixtapan-Turrent, L.; Rodriguez-Padilla, C. Mode of Antiviral Action of Silver Nanoparticles against HIV-1. *J. Nanobiotechnology* **2010**, *8*, 1.
- 55 Minoshima, M.; Lu, Y.; Kimura, T.; Nakano, R.; Ishiguro, H.; Kubota, Y.; Hashimoto, K.; Sunada, K. Comparison of the Antiviral Effect of Solid-State Copper and Silver Compounds. *J. Hazard. Mater.* **2016**, *312*, 1–7.
- 56 Lu, L.; Sun, R. W. Y.; Chen, R.; Hui, C. K.; Ho, C. M.; Luk, J. M.; Lau, G. K. K.; Che, C. M. Silver Nanoparticles Inhibit Hepatitis B Virus Replication. *Antivir. Ther.* **2008**, *13*, 252–262.

- 57 García, M.; Stupak, M.; Pérez, M.; Blustein, G. Transitioning to Nontoxic Antifouling Paints. *Pigment Resin Technol.* **2015**, *44*, 116–121.

Chapter 5

5 Slippery Lubricant Infused Surfaces

Prevention of bacterial biofilm formation and surface fouling are of considerable societal importance, particularly in the healthcare and medical settings (for example, the vast majority of catheter-associated urinary tract infections are caused by biofilms formed on the catheters¹). In the marine environment on the hulls of ships, bacterial biofilm formation and fouling results in increased frictional drag, which leads to more fuel consumption and greater greenhouse gas emissions.² Bacterial biofilms are also of concern in the food industry, given their role in food spoilage and risks to public health.³ Therefore, eco-friendly lubricant-infused slippery surfaces are potential candidates for tackling a wide range of societal and environmental issues.

In this chapter, a simple and quick two-step coating method is described, comprising conformal pulsed plasma polymerisation of a variety of functional monomers onto solid substrates, followed by lubricant impregnation into the deposited functional nanolayer to produce slippery lubricant-infused surfaces, Figure 5.1. Pulsed plasmachemical deposition entails two distinct reaction regimes: the short period on-time (t_{on} —typically microseconds, where electrical discharge ignition leads to the formation of initiator radical species from the monomer) and then the longer period off-time (t_{off} —typically milliseconds, where conventional stepwise addition chain-growth monomer polymerisation proceeds).^{4,5} This culminates in excellent structural retention of the monomer functional groups to yield well-defined functional polymer nanocoatings.⁴ Key advantages of pulsed plasmachemical surface functionalisation include a simple and quick single-step process, ambient temperature, conformal 3-dimensional coating, independent of substrate material, excellent adhesion, solventless, minimal waste, and low energy consumption. Such dry coating processes are scalable and capable of reaching roll-to-roll line speeds of several hundred metres per minute.⁶ A variety of different functional monomers have been utilised to prepare a range of pulsed plasma deposited nanolayer surface chemistries for compatibilization with appropriate functional lubricants to yield a structure–behaviour relationship for slippery surface fabrication, Figure 5.2 and Figure 5.3. Further fine tuning (molecular tailoring) of the surface compatibilization properties can be achieved by varying the pulsed plasma duty cycle parameters.

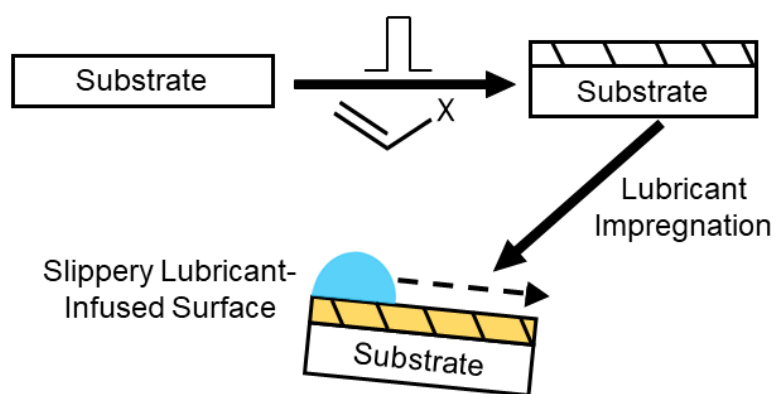


Figure 5.1: Pulsed plasma deposited slippery lubricant-infused nanocoatings.

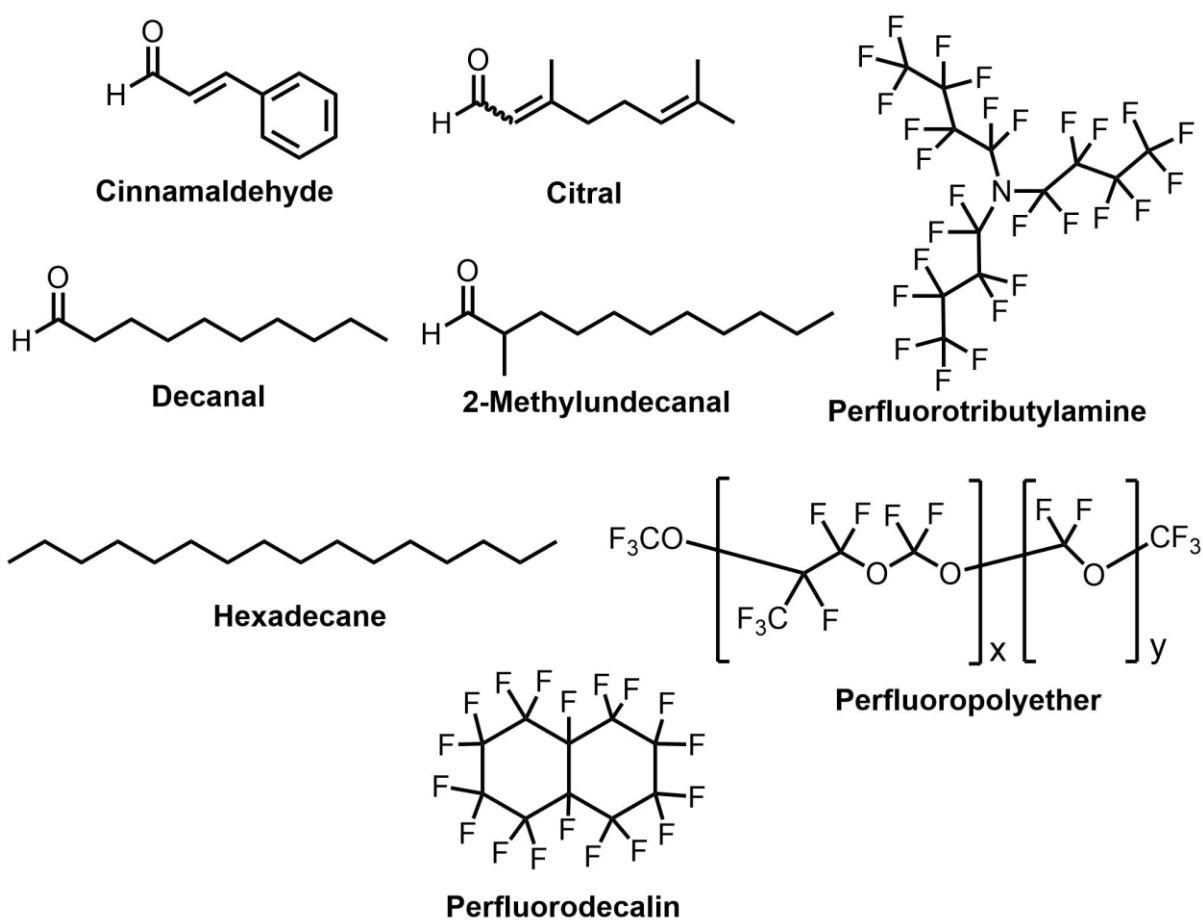


Figure 5.2: Lubricant chemical structures.

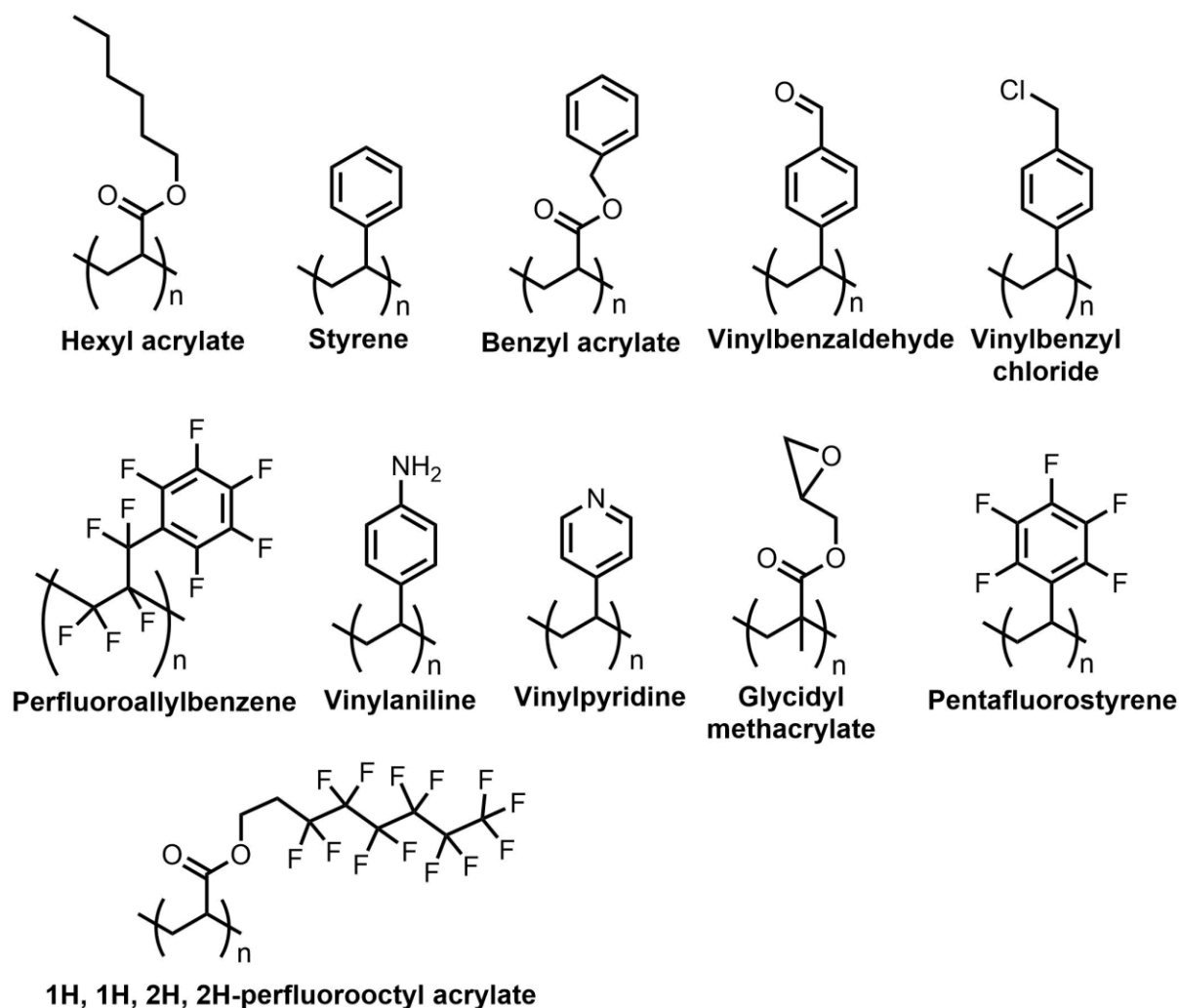


Figure 5.3: Chemical structures of pulsed plasma functional nanolayers and associated monomer names.

Lubricants employed include: environmentally-friendly cinnamaldehyde (a major component of cinnamon tree bark oil⁷—which displays potent broad-spectrum antibacterial activity⁸, as well as antiviral⁹, and antifungal¹⁰ efficacies); citral (present in the oils of lemon (*Citrus limon*), sweet orange (*Citrus sinensis*), and bergamot (*Citrus bergamia*)¹¹); decanal (contained in the oils of sweet orange (*Citrus sinensis*), and coriander leaf (*Coriandrum sativum* L.)^{12, 13}); and 2-methylundecanal (found in the essential oils extracted from members of the Rutaceae family (including *Ruta graveolens*¹⁴), Figure 5.2. Cinnamaldehyde, citral, and decanal lubricants are all classified as, ‘generally recognised as safe’ (GRAS) by the US Food and Drug Administration¹⁵, and 2-methylundecanal does not present a safety concern to human health according to the Joint FAO/WHO Expert Committee on Food Additives (JECFA).¹⁶ Other lubricants investigated include hexadecane (as a non-polar lubricant) and fluorinated lubricants

(perfluorotributylamine, perfluoropolyether and perfluorodecalin). A molecular level structure–behaviour relationship has been developed for the fabrication of slippery surfaces by comparing the liquid repellency between different combinations of functional pulsed plasma nanocoating and impregnated lubricant liquid, Figure 5.2 and Figure 5.3.

5.1 Experimental

5.1.1 Pulsed Plasmachemical Deposition

Pulsed plasma deposition was carried out as described in section 2.1. Polyethylene terephthalate film (PET, capacitor grade, 0.10 mm thickness, Lawson Mardon Ltd.) or non-woven porous polypropylene cloth (0.41 mm thick, $22.7 \pm 4.4 \mu\text{m}$ fibre diameter, with dimpled structure $0.68 \pm 0.16 \text{ mm}$ separation, spunbond, 70 g m^{-2} , Avoca Technical Ltd) was rinsed in absolute ethanol (+99.5 %, Fisher Scientific UK Ltd.) for 15 min prior to insertion into the centre of the plasma chamber.

Monomers utilised for pulsed plasmachemical deposition were: hexyl acrylate (98%, Sigma-Aldrich Inc.), styrene (>99%, Sigma-Aldrich Inc.), benzyl acrylate (97%, Alfa Aesar, Fisher Scientific UK Ltd.), 3-vinylbenzaldehyde (97%, Sigma-Aldrich Inc.), vinylbenzyl chloride (97%, mixture of 2-, 3- and 4- isomers, Sigma-Aldrich Inc.), perfluoroallylbenzene (Fluorochem Ltd.), 4-vinylaniline (aka 4-aminostyrene, 97%, Alfa Aesar, Fisher Scientific UK Ltd.), 4-vinylpyridine (95%, Sigma-Aldrich Inc.), glycidyl methacrylate (97%, Sigma Aldrich), pentafluorostyrene (Apollo Scientific Ltd.), and 1H, 1H, 2H, 2H-perfluorooctyl acrylate (Fluorochem Ltd.). The pulsed plasma deposition duty cycle parameters for each precursor are given in Table 5.1. Less than 0.1 ml of monomer was consumed during a typical pulsed plasma deposition experiment, which meant that there was negligible chemical waste.

Table 5.1: Pulsed plasma deposition parameters for deposited polymer coatings, film thicknesses values and deposition rates.

Monomer	Peak Power / W	t_{on} / μ s	t_{off} / ms	Deposition Temperature / °C	Film Thickness / nm	Deposition Rate / nm min ⁻¹
Hexyl acrylate	40	20	20	20	373	12.4
Butyl acrylate	40	20	20	20	314	10.5
Isooctyl acrylate	40	20	20	20	1541	51
Styrene	30	100	4	20	200	6.7
Benzyl acrylate	40	20	20	20	168	5.6
3-Vinylbenzaldehyde	30	100	4	20	1242	41.4
Vinylbenzyl chloride	30	100	4	20	1774	59.1
Perfluoroallylbenzene	40	100	4	20	1363	45.4
4-Vinylaniline	40	100	4	40	238	7.9
4-Vinylpyridine	40	100	4	20	341	11.4
Glycidyl methacrylate	40	20	20	20	304	10.1
Pentafluorostyrene	30	100	4	20	1558	51.9
1H, 1H, 2H, 2H-Perfluorooctyl acrylate	40	20	20	20	1214	40.5

5.1.2 Polystyrene Surfaces

Polystyrene (pellets, average M_w 280,000) was dissolved in chloroform (99.8+%, Fisher Scientific UK Ltd.) to give a 5% w/v solution. Glass slides (15 mm x 15 mm) were cleaned ultrasonically in 100 ml of a 50:50 mixture of propan-2-ol and cyclohexane for 15 min and then dried. Several drops of the polystyrene solution were placed onto the glass slide so that the entire surface was covered. The solvent was allowed to evaporate under ambient conditions at 20 °C. In addition, polystyrene petri dishes (Fisherbrand™ polystyrene Petri dishes, Fisher Scientific UK Ltd.) were cut into small pieces (15 mm x 15 mm).

5.1.3 Formation of Slippery Lubricant-Infused Surfaces

The lubricants used were: cinnamaldehyde (99%, Acros Organics brand, Fisher Scientific UK Ltd.), citral (95%, mixture of isomers, Acros Organics brand, Fisher Scientific UK Ltd.), decanal (>98%, Mystic Moments Madar Corporation Ltd.), 2-methylundecanal (>98%, Mystic Moments Madar Corporation Ltd.), hexadecane (99%, Sigma-Aldrich Inc.), perfluorodecalin (90%, mixture of cis and trans isomers, Acros Organics brand, Fisher Scientific UK Ltd.), perfluorotributylamine

(Fluorinert FC-43, 3M Inc.), and perfluoropolyether (Fomblin® Y LVAC 06/6, Ausimont Ltd.).

Lubricant infused surfaces were prepared by immersing the coated substrate into several millilitres of the neat lubricant liquid at 20 °C for 15 min. Afterwards, the substrates were removed from solution, placed in deionised water and shaken for 5 min, followed by removal and drying in air for at least 3 h at 20 °C, with the samples stood upright to allow any excess lubricant to run off directly onto tissue paper—the quantities of lubricant were very small, and the tissue paper was subsequently placed into the appropriate laboratory chemical waste category, for safe disposal in a controlled manner.

Control substrates were prepared by immersing untreated PET film substrates into the lubricant and removing any excess lubricant as described above.

5.1.4 Coating Characterisation

Infrared spectra were acquired as described in section 2.2. Coating thicknesses were measured as described in section 2.4. Atomic force microscopy (AFM) images were acquired as described in section 2.14.

5.1.5 Contact Angle Analysis

Sessile drop static contact angle measurements were carried out as described in section 2.5.

5.1.6 Sliding Angle Analysis

Sliding angle measurements were carried out as described in section 2.5. Heptane (99%, Sigma-Aldrich Inc.), motor engine oil (GTX Magnatec 15W-40, Castrol Ltd.), and vacuum pump oil (Ultragrade Performance 19 Vacuum Oil, Edwards Vacuum Ltd.) were tested for the poly(perfluoroallylbenzene)-perfluoropolyether coating in the same way.

For longevity and regeneration testing, slippery lubricant-infused surfaces were prepared on PET film pieces as previously described. Samples were subsequently left to sit under ambient conditions for a period of 4–5 months. Samples were then qualitatively assessed for slippery behaviour by placing drops

of deionised water onto the samples—if the droplets were found to easily slide off at low tilt angles, the sample was considered to be still slippery, whereas if the droplets were seen not to move, to only slide at high tilt angles, or to wet the sample, then the sample was considered to have lost its slippery behaviour. Samples which had lost their slippery behaviour during storage were regenerated by immersion in a few millilitres of the relevant neat lubricant liquid for 5 min, washing in deionised water with shaking for 5 min, followed by removal and drying in air for at least 3 h at 20 °C. Samples were then tested for slippery behaviour as described earlier.

5.1.7 Foodstuffs Repellency

Pulsed plasma poly(vinylaniline) was deposited onto the insides of glass vials. Slippery lubricant-infused surfaces were produced by filling these vials with either cinnamaldehyde, citral, decanal, or 2-methylundecanal. The vials were left to stand with the lids closed for 15 min. Next, the aldehyde liquid was discarded from the vials and the vials were upturned to dry with lids off for 15 min so that any excess unbound lubricant could run off. The vials were then rinsed twice with deionised water to help remove any remaining unbound lubricant, and subsequently upturned to dry for 15 min. Finally, the vials were turned upright and dried for a further 15 min before use. Uncoated glass vials were treated with aldehyde liquids in the same way to serve as controls.

Tomato ketchup and clear honey (Sainsbury's Supermarkets Ltd.) were used for repellency testing. Approximately a few millilitres of the foodstuff was dispensed into the glass vials. The vials were then upturned, and the behaviour of the foodstuffs recorded using a video camera.

5.1.8 Antibacterial Testing

Antibacterial testing was performed as described in section 2.3.

5.2 Results

5.2.1 Control Studies

Water contact angle hysteresis and sliding angle values for uncoated PET film substrate and following treatment with each of the lubricants were all measured to be relatively large in magnitude, Table 5.2.

Table 5.2: Water droplet static, advancing, receding, and hysteresis contact angle values and water droplet sliding angle values following lubricant treatment of uncoated PET film substrates. Values are reported as mean \pm standard deviation.

Surface	Contact Angle / °		Sliding Angle / °
	Static	Hysteresis	
PET	66.8 \pm 1.6	52 \pm 4	48 \pm 2
PET–Cinnamaldehyde	71 \pm 4	40 \pm 4	27.3 \pm 0.5
PET–Citral	64 \pm 3	46 \pm 4	29 \pm 1
PET–Decanal	71.9 \pm 1.6	29 \pm 6	10.3 \pm 0.5
PET– 2-Methylundecanal	65 \pm 3	20 \pm 1.5	10.0 \pm 0.0
PET–Hexadecane	67 \pm 4	20 \pm 4	24.7 \pm 1.7
PET–Perfluorotributylamine	114 \pm 2	53 \pm 3	29 \pm 2
PET–Perfluoropolyether	82 \pm 6	58 \pm 8	41.0 \pm 1.6
PET–Perfluorodecalin	100 \pm 5	81 \pm 5	57 \pm 2

Pulsed plasma deposition covering a range of functional monomers was undertaken to provide a variety of well-adhered conformal host layers for lubricant impregnation, Figure 5.3, Table 5.1 and Table 5.3.

Table 5.3: Water droplet static, advancing, receding, and hysteresis contact angle values, and water droplet sliding angle values, for coated PET film substrates. Values are reported as mean \pm standard deviation. * Water droplet showed no movement at 90° inclination of substrate from the horizontal. † Cinnamaldehyde dissolves poly(styrene), and so it is not possible to prepare slippery surfaces for this combination.

Surface	Contact Angle / °		Sliding Angle / °
	Static	Hysteresis	
PET Untreated	66.8 \pm 1.6	52 \pm 4	48 \pm 2
Pulsed Plasma Poly(hexyl acrylate)	82.2 \pm 0.8	8.5 \pm 1.1	10.7 \pm 0.5
Pulsed Plasma Poly(butyl acrylate)	67.8 \pm 1.9	76 \pm 3	32 \pm 3
Pulsed Plasma Poly(iso-octyl acrylate)	98.7 \pm 0.4	101.7 \pm 1.2	70 \pm 4
Pulsed Plasma Poly(styrene) (ppPS)	79 \pm 2	29 \pm 10	37 \pm 1
ppPS–Decanal	82.5 \pm 0.7	9 \pm 7	1.3 \pm 0.2
ppPS–Hexadecane	98.6 \pm 0.4	0.8 \pm 0.5	1.0 \pm 0.0
ppPS–2-Methylundecanal	68.8 \pm 1.6	3 \pm 3	1.7 \pm 0.2
ppPS–Cinnamaldehyde	89 \pm 4	37 \pm 11	39 \pm 1
Drop-Cast Poly(styrene) (dcPS)	90.3 \pm 1.0	20 \pm 3	14 \pm 1
dcPS–Hexadecane	87.9 \pm 1.0	5 \pm 3	3 \pm 1
Petri Dish Poly(styrene) (pdPS)	88.8 \pm 1.1	30 \pm 2	25 \pm 1
pdPS–Hexadecane	94.7 \pm 0.5	6 \pm 3	6.7 \pm 0.5
pdPS–Cinnamaldehyde †	-	-	-
Pulsed Plasma Poly(benzyl acrylate) (ppBA)	72.4 \pm 0.6	30 \pm 2	37.7 \pm 0.5
ppBA–Decanal	56.1 \pm 0.5	2 \pm 4	2.7 \pm 0.5
ppBA–Hexadecane	85 \pm 2	21 \pm 2	14 \pm 0
ppBA–2-Methylundecanal	66 \pm 1	0.5 \pm 0.4	2 \pm 0
ppBA–Cinnamaldehyde	60 \pm 2	4 \pm 4	3.3 \pm 0.5
Pulsed Plasma Poly(vinylbenzaldehyde) (ppVBA)	70.2 \pm 1.5	38 \pm 8	44 \pm 1
ppVBA–Decanal	35.3 \pm 0.7	5.9 \pm 1.2	4 \pm 1
ppVBA–Hexadecane	74 \pm 2	1 \pm 2	17 \pm 1
ppVBA–2-Methylundecanal	67.6 \pm 0.1	2.6 \pm 1.6	1.7 \pm 0.2
ppVBA–Cinnamaldehyde	58 \pm 3	2.3 \pm 1.2	13 \pm 1
Pulsed Plasma Poly(vinylbenzyl chloride) (ppVBC)	84.4 \pm 0.5	18 \pm 2	14 \pm 1
ppVBC–Decanal	54 \pm 3	3 \pm 4	6.8 \pm 0.2
ppVBC–Hexadecane	81 \pm 3	2 \pm 3	15 \pm 1
ppVBC–2-Methylundecanal	67 \pm 2	1 \pm 4	1 \pm 0
ppVBC–Cinnamaldehyde	67 \pm 3	9 \pm 3	27 \pm 1
Pulsed Plasma Poly(perfluoroallylbenzene) (ppPFAB)	97 \pm 2	23 \pm 4	30 \pm 1
ppPFAB–Perfluorotributylamine	118.4 \pm 0.4	2.6 \pm 0.9	2.7 \pm 0.5
ppPFAB–Perfluoropolyether	109 \pm 3	3.8 \pm 3.8	1.7 \pm 0.2
ppPFAB–Perfluorodecalin	119.1 \pm 0.5	18 \pm 5	9 \pm 1
Pulsed Plasma Poly(vinylaniline) (ppVA)	75 \pm 6	66 \pm 3	90 (*)
ppVA–Decanal	72.6 \pm 0.9	4.6 \pm 1.6	13 \pm 1
ppVA–Hexadecane	75.4 \pm 0.3	5.3 \pm 1.6	17 \pm 1
ppVA–2-Methylundecanal	80.0 \pm 1.4	8.8 \pm 1.3	14 \pm 2
ppVA–Cinnamaldehyde	56.6 \pm 0.1	2.8 \pm 1.0	10 \pm 1
ppVA–Citral	67.3 \pm 0.6	1.7 \pm 0.3	12 \pm 2

In the case of pulsed plasma deposited poly(vinylpyridine), poly(glycidyl methacrylate), poly(pentafluorostyrene), and poly(1H, 1H, 2H, 2H, perfluorooctyl acrylate), all were found to produce non-slippery surfaces when treated with the selection of test lubricants, Sections 5.2.9–5.2.12.

5.2.2 Pulsed Plasma Poly(Hexyl Acrylate)

Hexyl acrylate monomer displays the following characteristic infrared absorption bands: C–H stretching ($3000\text{--}2830\text{ cm}^{-1}$), acrylate carbonyl C=O stretching (1724 cm^{-1}), acrylate C=C stretching (1638 cm^{-1} and 1631 cm^{-1}), and the C–O ester stretch (1182 cm^{-1}), Figure 5.4.¹⁷ Pulsed plasma deposited poly(hexyl acrylate) shows loss of the acrylate carbon–carbon double bond infrared absorbance features, thereby confirming that polymerisation had taken place.⁴

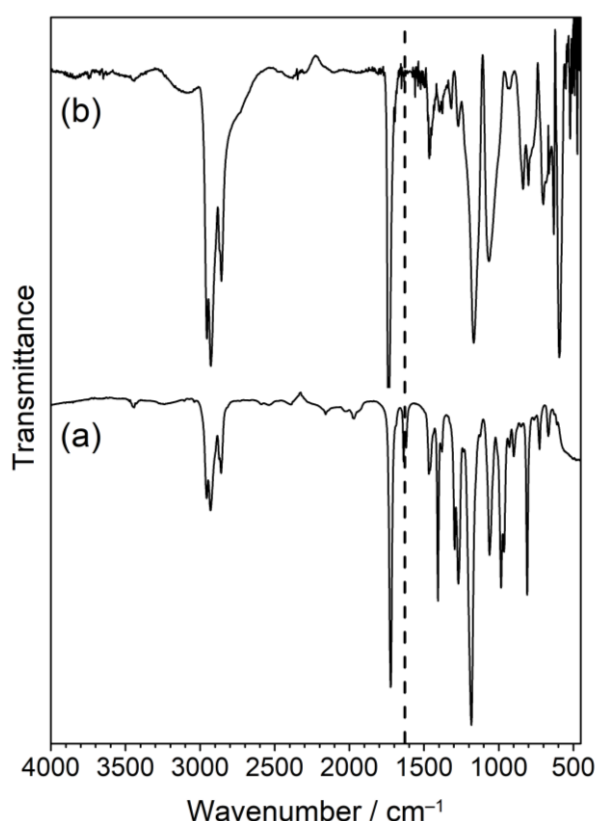


Figure 5.4: Infrared spectra of: (a) hexyl acrylate monomer (ATR); and (b) pulsed plasma poly(hexyl acrylate) deposited onto silicon wafer (RAIRS, 55°). The dashed line corresponds to acrylate carbon–carbon double bond absorbance (1638 cm^{-1}).

Pulsed plasma polymerised hexyl acrylate coatings displayed relatively small water contact angle hysteresis ($<10^\circ$) and sliding angle ($\sim 10^\circ$) values, Table

5.3. None of the lubricant liquids tested significantly lowered the water contact angle hysteresis value, Table 5.4.

Table 5.4: Water droplet static, advancing, receding, and hysteresis contact angle values following lubricant impregnation of pulsed plasma poly(hexyl acrylate) (ppHA) coated PET film substrates. Values are reported as mean \pm standard deviation.

Surface	Contact Angle / °	
	Static	Hysteresis
ppHA–Decanal	83 \pm 5	8 \pm 5
ppHA–Hexadecane	91.6 \pm 1.0	11.4 \pm 1.5
ppHA–2-Methylundecanal	73.8 \pm 0.5	5.9 \pm 1.5
ppHA–Cinnamaldehyde	71 \pm 5	17 \pm 9
ppHA–Perfluorotributylamine	83 \pm 3	13 \pm 6

AFM roughness measurements showed that the pulsed plasma poly(hexyl acrylate) coating surface is not significantly more rough compared to uncoated silicon wafer substrate ($Roughness_{SRMS} = 1.99$ nm versus 0.68 nm respectively for 10 μ m scan size)—which is typical of low duty cycle pulsed plasma deposited polymer nanocoatings, Figure 5.5.^{18,19}

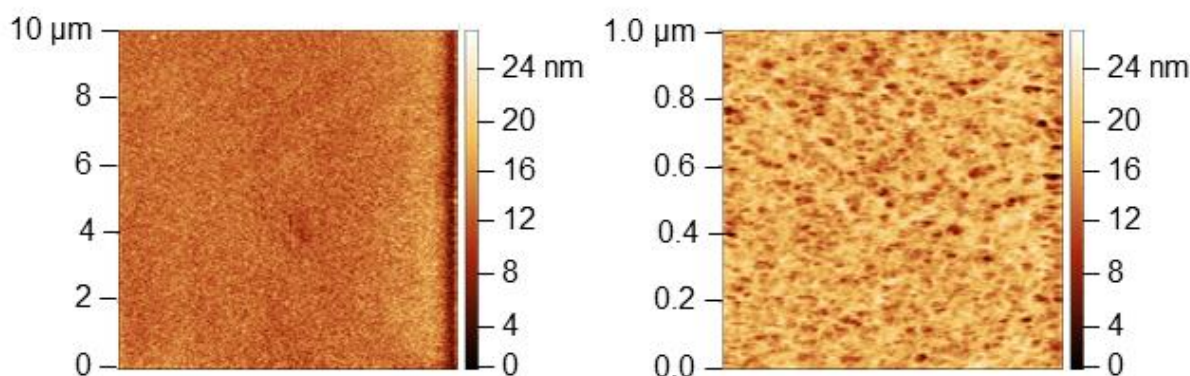


Figure 5.5: Atomic force microscopy (AFM) images of pulsed plasma poly(hexyl acrylate) coated silicon wafer. Images taken by Colin Gibson.

For the same electrical discharge parameters employed, pulsed plasma deposited poly(butyl acrylate) and poly(iso-octyl acrylate) nanolayers were not found to be slippery (i.e. exhibited high water contact angle hysteresis and sliding angles).

5.2.3 Pulsed Plasma Poly(Styrene)

Liquid styrene monomer exhibits the following characteristic infrared absorption bands: C–H stretching ($3100\text{--}2965\text{ cm}^{-1}$), aromatic ring summations ($2000\text{--}1700\text{ cm}^{-1}$), vinyl C=C stretch (1629 cm^{-1}), aromatic C=C stretching (1600 cm^{-1} , 1574 cm^{-1} , 1494 cm^{-1} , and 1448 cm^{-1}), CH₂ deformations (1412 cm^{-1}), HC=CH trans wag (994 cm^{-1}), and =CH₂ wag (906 cm^{-1}), Figure 5.6.²⁰ The vinyl group bands were absent in the deposited pulsed plasma poly(styrene) infrared spectrum, indicating that polymerisation has taken place. Whilst aromatic ring features are still present, thereby confirming structural retention of the phenyl rings.

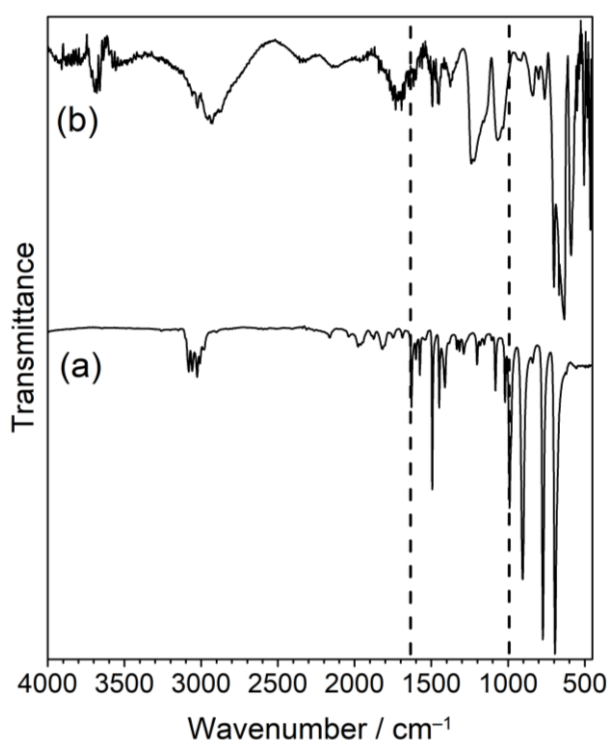


Figure 5.6: Infrared spectra of: (a) styrene monomer (ATR); and (b) pulsed plasma poly(styrene) deposited onto silicon wafer (RAIRS, 66°). The dashed lines correspond to vinyl group absorptions (1629 cm^{-1} and 994 cm^{-1}).

Pulsed plasma deposited poly(styrene) on PET substrate displays a large water contact angle hysteresis, Table 5.3. Whereas a slippery surface was obtained following decanal, 2-methylundecanal, or hexadecane impregnation into the pulsed plasma poly(styrene) coating. Hexadecane lubricant in particular gave excellent water-repellent properties, with both contact angle hysteresis and sliding angle values measured to be $\leq 1^\circ$. Cinnamaldehyde and perfluorotributylamine lubricants did not form a slippery surface when combined with the poly(styrene) coating.

In order to determine whether this approach for making slippery lubricant-infused surfaces could be extended beyond pulsed plasma deposited poly(styrene) coatings, conventional poly(styrene) coatings were drop-cast onto glass slides and treated with hexadecane lubricant. This led to a significant reduction of both the water contact angle hysteresis and the sliding angle values ($\leq 5^\circ$), thereby demonstrating that the drop-cast poly(styrene) films also form slippery lubricant-infused surfaces, Table 5.3. Pre-formed poly(styrene) pieces cut from Petri dishes and then treated with hexadecane behaved in a similar fashion. Henceforth, a range of aromatic ring containing pulsed plasma polymer coatings were investigated and also shown to provide slippery surfaces following impregnation with lubricants—these included pulsed plasma deposited poly(benzyl acrylate), poly(vinylbenzaldehyde), poly(vinylbenzyl chloride), poly(perfluoroallylbenzene), and poly(vinylaniline), Figure 5.3, Table 5.3.

5.2.4 Pulsed Plasma Poly(Benzyl Acrylate)

Benzyl acrylate monomer displays the following characteristic infrared absorption bands: C–H stretching ($3100\text{--}2850\text{ cm}^{-1}$), aromatic ring summations ($2000\text{--}1800\text{ cm}^{-1}$), acrylate carbonyl C=O stretching (1720 cm^{-1}), acrylate C=C stretching (1633 cm^{-1} and 1621 cm^{-1}), and the C–O ester stretch (1171 cm^{-1}), Figure 5.7. Similar to the alkyl acrylates, pulsed plasma deposited poly(benzyl acrylate) showed absence of the acrylate carbon–carbon double bond band, indicating that polymerisation had taken place, whereas the phenyl rings remain intact.

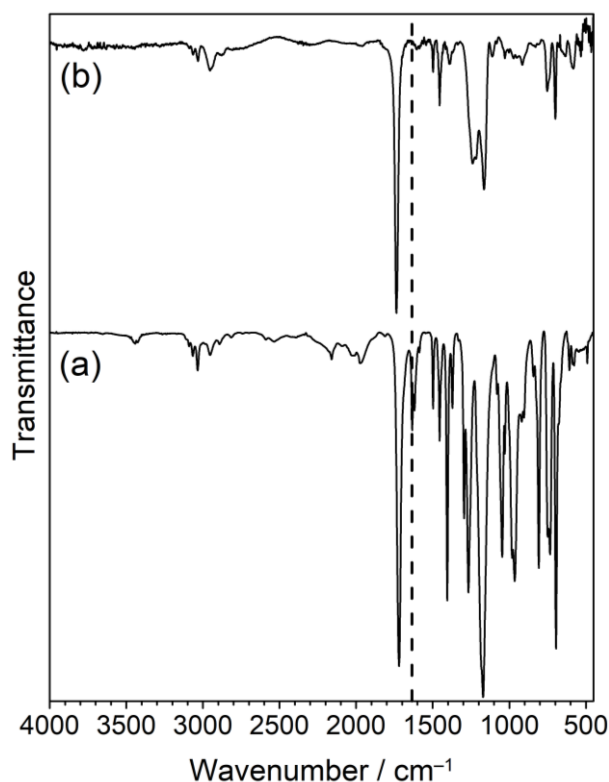


Figure 5.7: Infrared spectra of: (a) benzyl acrylate monomer (ATR); and (b) pulsed plasma poly(benzyl acrylate) deposited onto silicon wafer (RAIRS, 66°). The dashed line corresponds to acrylate carbon-carbon double bond absorbance (1633 cm^{-1}).

Pulsed plasma polymerised poly(benzyl acrylate) showed large water contact angle hysteresis and sliding angle values, Table 5.3. Hexadecane-infused pulsed plasma poly(benzyl acrylate) coating gave rise to lower hysteresis and sliding angles, although not particularly low. Cinnamaldehyde-, decanal-, and 2-methylundecanal-infused pulsed plasma poly(benzyl acrylate) coatings all displayed water contact angle hysteresis and sliding angles $< 5^\circ$. In particular, the 2-methylundecanal-infused coating showed excellent slippery properties, with a mean hysteresis of 0.5° , and a sliding angle of 2° .

5.2.5 Pulsed Plasma Poly(Vinylbenzaldehyde)

Vinylbenzaldehyde monomer displays the following characteristic infrared bands: C-H stretches ($3090\text{--}2900\text{ cm}^{-1}$), aldehyde CHO stretches (2815 cm^{-1} and 2726 cm^{-1}), aldehyde C=O stretch (1695 cm^{-1}), vinyl C=C stretch (1630 cm^{-1}), di-substituted benzene quadrant stretch (1599 cm^{-1} and 1582 cm^{-1}), meta-substituted benzene semicircle stretch (1478 cm^{-1} and 1445 cm^{-1}), aldehyde CH

rock (1378 cm^{-1}), meta ring stretch (1143 cm^{-1}), meta in-phase CH wag (990 cm^{-1}), and meta single CH wag (908 cm^{-1}), Figure 5.8.²¹

Pulsed plasma deposited poly(vinylbenzaldehyde) shows good structural retention and minimal cross-linking, as indicated by the retention of the aldehyde CHO stretches (2815 cm^{-1} and 2726 cm^{-1}), aldehyde C=O stretch (1695 cm^{-1}), meta-substituted aromatic ring semicircle stretch (1478 cm^{-1} and 1445 cm^{-1}), and meta-substituted benzene semicircle stretch (1478 cm^{-1} and 1445 cm^{-1}). Disappearance of the vinyl C=C stretch (1630 cm^{-1}), and the appearance of aliphatic C–H stretches ($2950\text{--}2850\text{ cm}^{-1}$) confirmed that polymerisation had taken place.

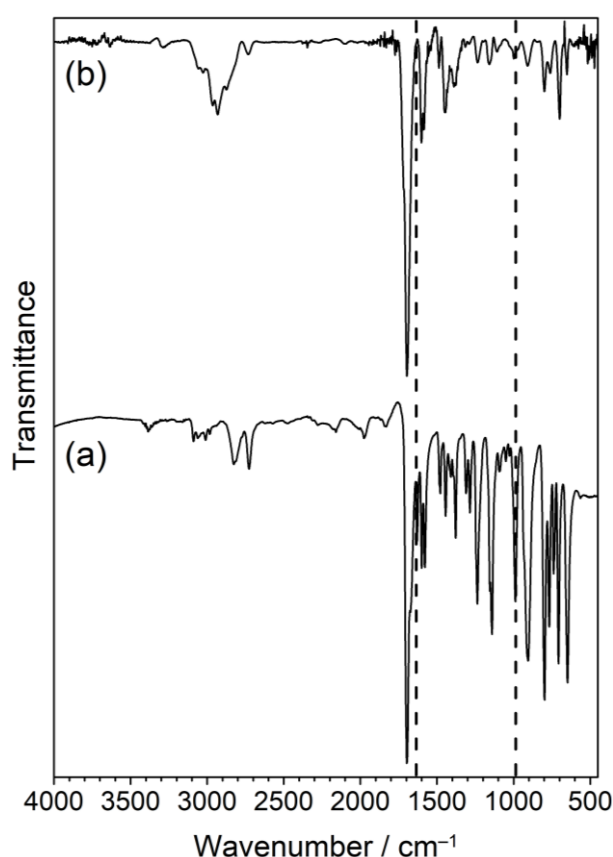


Figure 5.8. Infrared spectra of: (a) vinylbenzaldehyde monomer (ATR); and (b) pulsed plasma poly(vinylbenzaldehyde) deposited onto silicon wafer (RAIRS, 55°). The dashed lines correspond to vinyl group absorbances (1630 cm^{-1}).

Pulsed plasma poly(vinylbenzaldehyde) coating showed relatively high water contact angle hysteresis and sliding angle values, Table 5.3. Impregnation with lubricants resulted in a significant decrease in the water contact angle hysteresis. Decanal and 2-methylundecanal also gave rise to low sliding angles ($<5^\circ$). Although cinnamaldehyde and hexadecane reduced the sliding angles

compared to the pulsed plasma poly(vinylbenzaldehyde)-only coating, they did not exhibit comparably low sliding angles.

Polypropylene cloth treated with 2-methylundecanal did not exhibit a slippery surface, Table 5.5. Pulsed plasma poly(vinylbenzaldehyde) coated polypropylene cloth showed complete wetting in contact with water, which is likely due to the plasma polymer altering the surface wettability, therefore allowing the water to wick into the porous structure. Cinnamaldehyde and 2-methylundecanal impregnated pulsed plasma poly(vinylbenzaldehyde) coated polypropylene cloth both showed slippery surfaces. The water droplet sliding angles are not as low as it was for the same coatings on the flat PET substrate surface, Table 5.3, which is likely due to the dimpled, rough structure of the polypropylene cloth. Placing a 100 μ l water droplet onto the pulsed plasma poly(vinylbenzaldehyde)-cinnamaldehyde coated polypropylene cloth for 4 h, and then a further 16 h produced no change in water droplet sliding angle values. Immersion of the coated sample into water for 16 h also yielded no change to the sliding angle.

Table 5.5. Water droplet sliding angle values for pulsed plasma poly(vinylbenzaldehyde) (ppVBA) coated porous polypropylene (PP) cloth substrates. Values are reported as mean \pm standard deviation. † Samples display complete wetting / absorption of water droplets.

Surface	Sliding Angle / °
Polypropylene (PP) Cloth Untreated	36 \pm 1
2-Methylundecanal-PP Cloth	29.3 \pm 0.5
Cinnamaldehyde-PP Cloth †	-
ppVBA-PP Cloth †	-
ppVBA-2-Methylundecanal	12.3 \pm 0.5
ppVBA-Cinnamaldehyde	15.3 \pm 0.5
ppVBA-Cinnamaldehyde, 100 μ l water droplet, 4 h	14.3 \pm 0.5
ppVBA-Cinnamaldehyde, 100 μ l water droplet, 20 h	14.7 \pm 0.9
ppVBA-Cinnamaldehyde, immersion, 10 ml water, 16 h	15.3 \pm 0.5

5.2.6 Pulsed Plasma Poly(Vinylbenzyl Chloride)

Vinylbenzyl chloride monomer displays the following characteristic infrared bands: C-H stretches (3095–2830 cm^{-1}), aromatic ring summations (2000–1750 cm^{-1}), vinyl C=C stretch (1630 cm^{-1}), para-substituted aromatic ring stretches (1603 cm^{-1} and 1511 cm^{-1}), and Cl-CH₂ wag (1263 cm^{-1}), Figure 5.9.²² Pulsed

plasma deposited poly(vinylbenzyl chloride) retained the para-substituted aromatic ring stretches (1603 cm^{-1} and 1511 cm^{-1}), and Cl-CH₂ wag (1263 cm^{-1}) infrared bands, demonstrating high structural retention and minimal cross-linking. The vinyl C=C stretch (1630 cm^{-1}) disappeared indicating polymerisation had taken place.

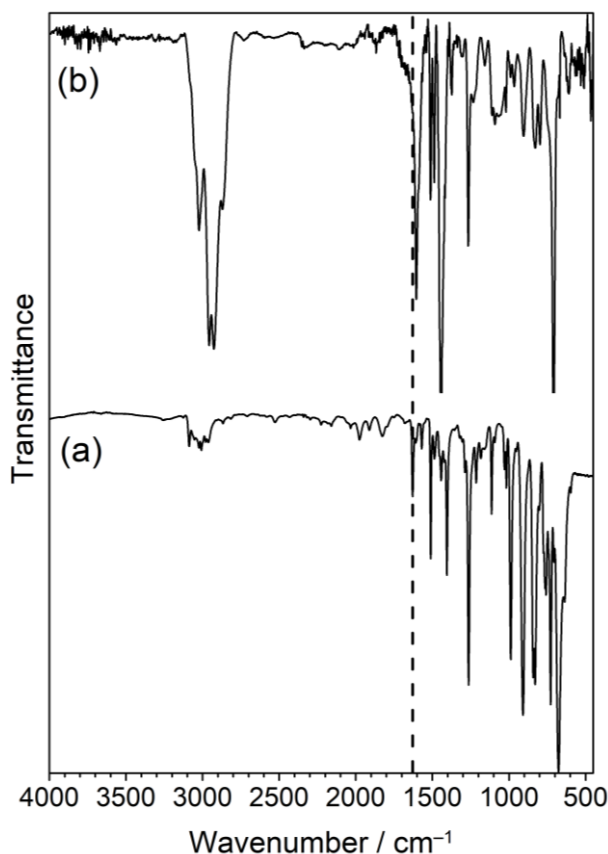


Figure 5.9. Infrared spectra of: (a) vinylbenzyl chloride monomer (ATR); and (b) pulsed plasma poly(vinylbenzyl chloride) deposited onto silicon wafer (RAIRS, 55°). The dashed line corresponds to vinyl group absorbance (1630 cm^{-1}).

Pulsed plasma poly(vinylbenzyl chloride) coated PET surface exhibited a relatively lower water contact angle hysteresis and sliding angle compared to the other styrene-type monomers investigated in this study, Table 5.3. Impregnation with lubricants gave rise to slippery coatings. In particular, 2-methylundecanal lubricant produced a coating with excellent water repellency, with mean contact angle hysteresis and sliding angle values of 1°. Cinnamaldehyde lubricant did not give rise to a slippery surface.

5.2.7 Pulsed Plasma Poly(Perfluoroallylbenzene)

Perfluoroallylbenzene monomer displays the following characteristic infrared absorption bands: allyl C=C stretch (1787 cm^{-1}), aromatic C–C stretching (1657 cm^{-1} , 1528 cm^{-1} , and 1502 cm^{-1}), Figure 5.10.²³ It is difficult to unambiguously assign features in the spectral region below 1400 cm^{-1} , but peaks in this region are typically characteristic of C–F stretching vibrational modes.²⁴ Following pulsed plasma deposition, the allyl bond diminished in intensity (which is consistent with polymerisation taking place). Retention of the aromatic stretching bands in the pulsed plasma deposited layer confirms structural retention of the perfluorinated phenyl rings in the coating.²³

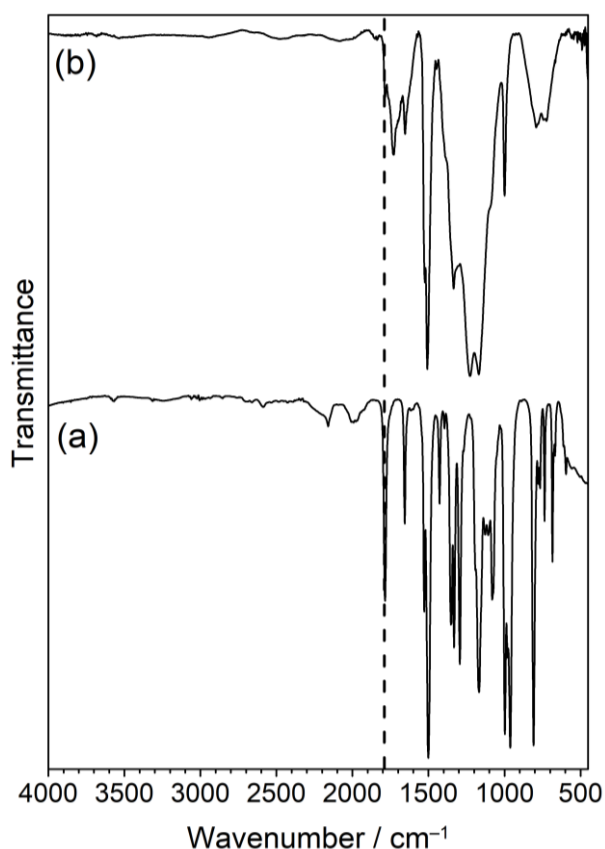


Figure 5.10: Infrared spectra of: (a) perfluoroallylbenzene monomer (ATR); and (b) pulsed plasma poly(perfluoroallylbenzene) deposited onto silicon wafer (RAIRS, 55°). The dashed line corresponds to allyl group carbon–carbon double bond stretch absorbance (1787 cm^{-1}).

Pulsed plasma poly(perfluoroallylbenzene)-only coating did not display low water contact angle hysteresis or water sliding angle values, Table 5.3. Both perfluorotributylamine and perfluoropolyether infused surfaces yielded coatings with low water contact angle hysteresis and sliding angle values ($< 5^\circ$). In order

to demonstrate omniphobicity, the perfluorotributylamine-infused surface was able to resist wetting by heptane (surface tension = 20.14 mN m^{-1}). Whilst, the perfluoropolyether-infused surface coating resisted wetting by pentane (surface tension = 15.8 mN m^{-1}), as well as heptane, vacuum pump oil, and engine oil all slide off at low angles ($< 17 \pm 1^\circ$, $2.3 \pm 0.2^\circ$, and $2.2 \pm 0.2^\circ$ respectively). For the case of perfluorodecalin infused surface, both the water contact angle hysteresis and sliding angle values were lowered.

5.2.8 Pulsed Plasma Poly(Vinylaniline)

The characteristic infrared bands of vinylaniline monomer can be assigned as follows: asymmetric amine stretch (3440 cm^{-1}), symmetric amine stretch (3370 cm^{-1}), aromatic C–H stretch ($3100\text{--}3000 \text{ cm}^{-1}$), ring summations ($2000\text{--}1750 \text{ cm}^{-1}$), vinyl C=C stretch (1622 cm^{-1}), NH_2 deformations (1610 cm^{-1}), para-substituted aromatic ring stretch (1513 cm^{-1}), $=\text{CH}_2$ deformations (1412 cm^{-1}), aromatic C–N stretch (1314 cm^{-1}), para-substituted benzene ring stretch (1177 cm^{-1}), HC=CH trans wag (994 cm^{-1}), $=\text{CH}_2$ wag (893 cm^{-1}), and $-\text{NH}_2$ wag (830 cm^{-1}), Figure 5.11.²⁵ Pulsed plasma deposited poly(vinylaniline) shows similar infrared absorption bands, apart from the disappearance of the vinyl C=C group features (1622 cm^{-1} and 994 cm^{-1}) and the appearance of an aliphatic C–H stretch (2865 cm^{-1}) confirming that polymerisation has taken place.²⁵

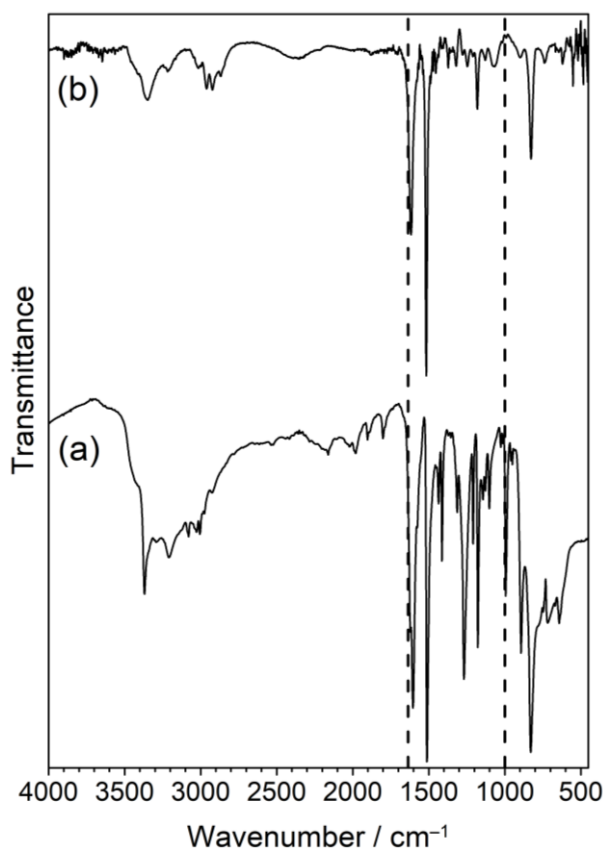


Figure 5.11: Infrared spectra of: (a) vinylaniline monomer (ATR); and (b) pulsed plasma poly(vinylaniline) deposited onto silicon wafer (RAIRS, 66°). The dashed lines correspond to vinyl group absorbances (1622 cm⁻¹ and 994 cm⁻¹).

Pulsed plasma poly(vinylaniline)-coated PET substrates display large water contact angle hysteresis and sliding angle values (water droplet showed no movement at 90° inclination of the substrate from the horizontal), Table 5.3. Following impregnation with decanal, 2-methylundecanal, hexadecane, cinnamaldehyde, or citral lubricants, low water contact angle hysteresis and sliding angle values were measured. The citral-infused surface gave rise to the lowest water contact angle hysteresis value ($1.7 \pm 0.3^\circ$), and cinnamaldehyde-infused surface produced the lowest water sliding angle ($10 \pm 1^\circ$). The slippery behaviour displayed by the hexadecane-infused surface indicates that the pulsed plasma poly(vinylaniline) coating is also compatible with non-polar lubricants. Perfluorotributylamine did not form a slippery surface when combined with the pulsed plasma poly(vinylaniline) coating.

Decanal, 2-methylundecanal, cinnamaldehyde, and citral, lubricant-infused surfaces were left to stand for 4 months under ambient open-air laboratory conditions. Decanal and 2-methylundecanal lubricant-infused surfaces continued to display slippery behaviour after this 4-month storage period. It was

found that the cinnamaldehyde and citral lubricant-infused surfaces no longer showed any slippery behaviour towards water droplets (probably due to essential oil evaporation). However, these slippery surfaces could easily be regenerated by immersion for 5 min in the corresponding essential oil. Less volatile essential oil molecules should give rise to even longer shelf-lives for these lubricant-impregnated surfaces.

The coatings' slippery performance was further tested using real-world foodstuffs. Tomato ketchup filled into an untreated glass vial showed no movement at all during gentle shaking, and when the vial was inverted, some of the ketchup fell out but much of it remained stuck to the insides of the vial, Video 5.1 (for videos, see section 5.5). Control uncoated glass vials were also rinsed with just the lubricant aldehydes (decanal, 2-methylundecanal cinnamaldehyde, and citral). For the decanal control vial, some very slow ketchup movement was observed over the course of 50 s, Video 5.2. Shaking the vial removed some ketchup, although much still remained. No ketchup movement was observed for the 2-methylundecanal control vial, and shaking the vial left much ketchup stuck to the walls of the vial, Video 5.3. Cinnamaldehyde and citral control vials showed increased ketchup movement compared to the untreated vial, with some ketchup sliding out of the vial without any need to shake it, Video 5.4 and Video 5.5. However, there remained ketchup in the vial which stopped moving after approximately 30 s.

For decanal, 2-methylundecanal, and cinnamaldehyde infused pulsed plasma poly(vinylaniline) coated glass vial surfaces, the ketchup readily slid out of the vial as soon as it was flipped over, with all the ketchup having left the vial in about 5 s, Video 5.6, Video 5.7, and Video 5.8. For citral-infused coating, the ketchup remained in place for approximately 5 s after the vial was upturned, and then started to slide out. Most of the ketchup left the vial, but some was still visible on the side, Video 5.9.

In the case of honey placed into an untreated glass vial, the honey started to run slowly down the wall of the vial over the course of a minute or so, and several drops exited the vial, Video 5.10. The rate at which the honey subsequently came out slowed down, and a relatively large amount of content was left behind attached to the bottom and sides of the vial. Similarly, for honey placed into the aldehyde lubricant rinsed control glass vials (decanal, 2-methylundecanal cinnamaldehyde, and citral), the honey flowed slowly with a

significant amount remaining behind, Video 5.11, Video 5.12, Video 5.13, and Video 5.14. The movement of honey in the vials coated with lubricant-infused pulsed plasma poly(vinylaniline) surfaces (decanal, 2-methylundecanal, cinnamaldehyde, and citral) was significant, leading to the majority of the honey leaving the vials (with the exception of a few small droplets) over the same timeframe as the controls, Video 5.15, Video 5.16, Video 5.17, and Video 5.18.

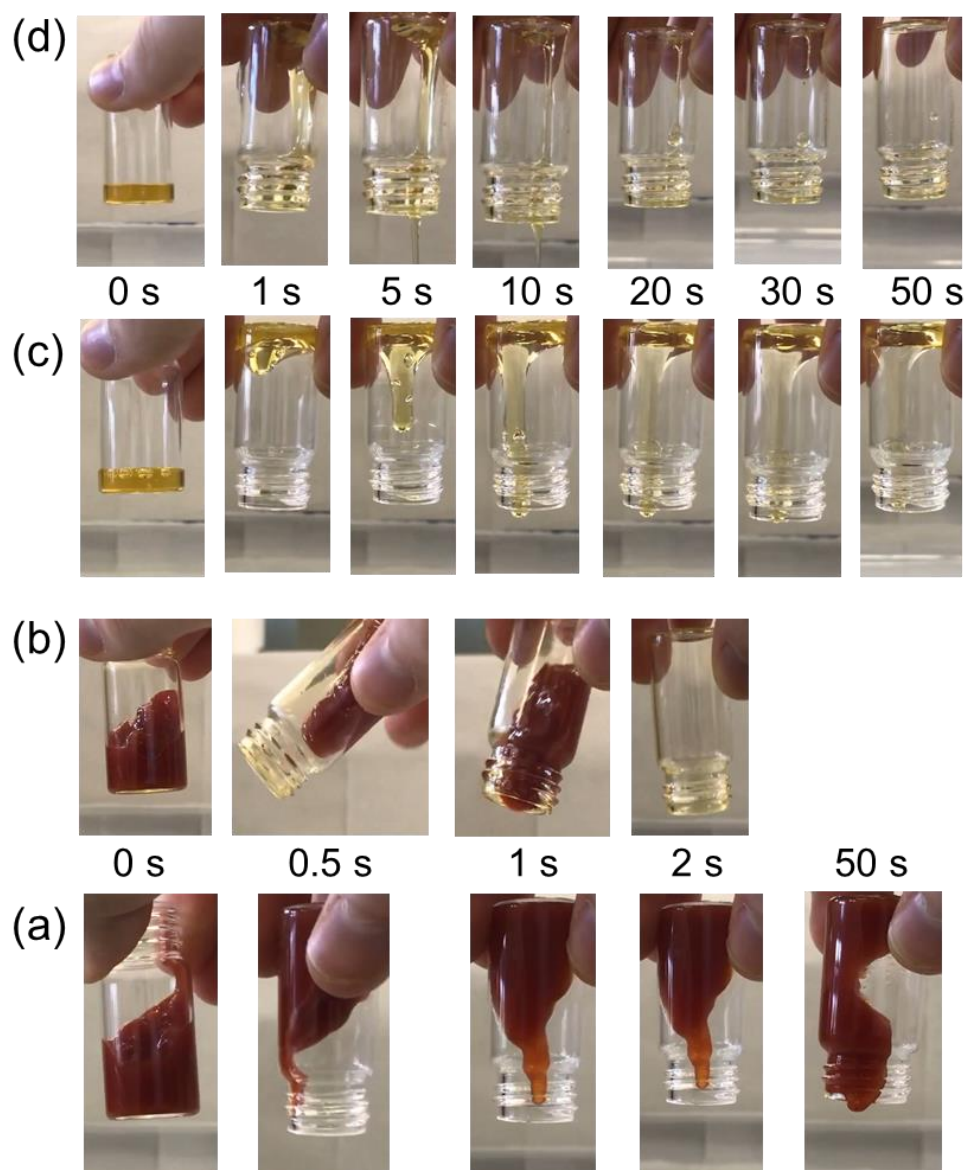


Figure 5.12: Time lapse photographs of: (a) ketchup applied to glass vial rinsed with decanal (control), Video 5.2; (b) ketchup applied to pulsed plasma poly(vinylaniline) coated glass vial impregnated with decanal lubricant, Video 5.6; (c) honey applied to glass vial rinsed with 2-methylundecanal (control), Video 5.12; and (d) honey applied to pulsed plasma poly(vinylaniline) coated glass vial impregnated with 2-methylundecanal lubricant, Video 5.16. (For videos, see section 5.5)

Cinnamaldehyde-infused pulsed plasma poly(vinylaniline) coated PET film surfaces were tested for antibacterial activities against Gram-negative *E. coli* and

Gram-positive *S. aureus*, Figure 5.13 and Table 5.6. PET substrates rinsed in cinnamaldehyde-only or coated with pulsed plasma poly(vinylaniline) showed a very small effect against *E. coli* and *S. aureus* bacteria (Log_{10} Reduction < 1). This could be due to a small residual amount of cinnamaldehyde remaining on the surface after washing and drying. In contrast, the pulsed plasma poly(vinylaniline)–cinnamaldehyde coated PET substrates displayed strong antibacterial activity, giving rise to complete killing of both bacterial species (Log_{10} Reduction > 7).

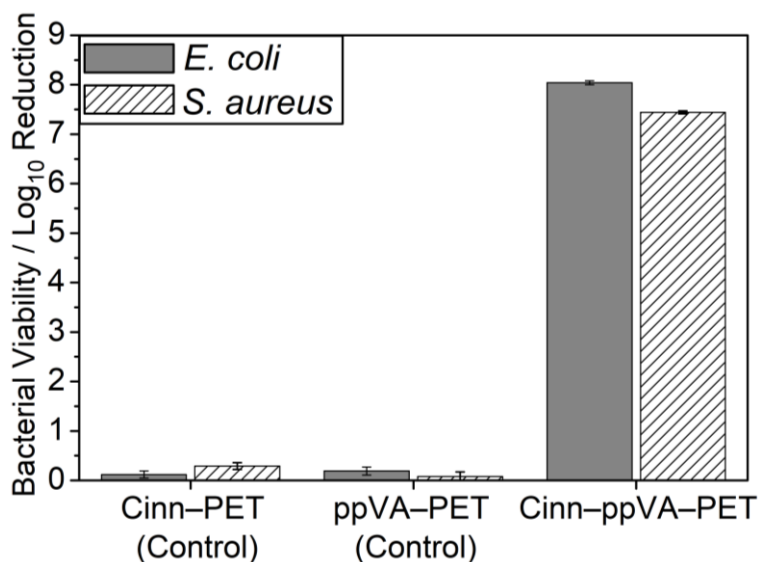


Figure 5.13: *E. coli* and *S. aureus* antibacterial tests for cinnamaldehyde-only treated PET (Cinn–PET, control); pulsed plasma poly(vinylaniline) coated PET (ppVA–PET, control); and pulsed plasma poly(vinylaniline)–cinnamaldehyde lubricant infused coating on PET substrate (Cinn–ppVBA–PET). Mean Log_{10} Reduction values are relative to untreated PET substrates. Error bars represent \pm standard deviation.

Table 5.6: Antibacterial tests for pulsed plasma poly(vinylaniline)–cinnamaldehyde coated PET film. Log_{10} Reduction values are relative to the untreated substrate (average \pm standard deviation).

Coating	Log_{10} Reduction	
	<i>E. coli</i>	<i>S. aureus</i>
Cinnamaldehyde-Only (control)	0.12 ± 0.07	0.29 ± 0.07
Pulsed Plasma Poly(vinylaniline)-Only (Control)	0.19 ± 0.08	0.08 ± 0.09
Pulsed Plasma Poly(vinylaniline)–Cinnamaldehyde	8.04 ± 0.04	7.44 ± 0.03

Recycle testing of pulsed plasma poly(vinylaniline)–cinnamaldehyde lubricant infused surfaces against *E. coli* showed complete loss of activity on the second test (Log_{10} Reduction (*E. coli*) = 0 ± 0), confirming that the antibacterial mechanism corresponds to cinnamaldehyde release from the surface.

Recharging the samples by repeating immersion into cinnamaldehyde again led to the complete killing of the *E. coli* (Log_{10} Reduction (*E. coli*) = 8.06 ± 0.03), thereby demonstrating that the coating could be easily regenerated and reused multiple times.

Pulsed plasma poly(vinylaniline) was coated onto non-woven porous polypropylene cloth, impregnated with cinnamaldehyde, and the water sliding angle values were measured. Due to the dimpled surface structure of the cloth, accurate static contact angle and contact angle hysteresis values could not be measured. Therefore, only water sliding angle values are reported here, Table 5.7. The untreated polypropylene cloth does not show a slippery surface. After impregnation with cinnamaldehyde lubricant, the polypropylene cloth showed complete absorption/wetting by water droplets—this is likely due to the cinnamaldehyde displacing the trapped air layer in the cloth, allowing water to wick through the porous structure, but not forming a thin lubricant layer at the surface, meaning the substrate does not repel water. The pulsed plasma poly(vinylaniline) coated polypropylene cloth exhibited a very large water sliding angle, consistent with the same coating on non-porous PET. After impregnation with cinnamaldehyde lubricant, the coating formed a slippery surface, with the water sliding angle comparable to the pulsed plasma poly(vinylaniline)–cinnamaldehyde coated PET, Table 5.3.

A 100 μl droplet of high-purity water was placed onto 1.5 cm x 1.5 cm piece of pulsed plasma poly(vinylaniline)–cinnamaldehyde coated polypropylene cloth and stored in a sealed tube for 4 h. The water droplet was removed and the water sliding angle measured again—the surface remained slippery and no change was measured for the sliding angle (within error), Table 5.7. Another 100 μl water droplet was dispensed onto the same sample surface and left to stand for a further 16 h (i.e. for a total water contact time of 20 h), once again, there was no change to the water droplet sliding angle. In a separate experiment, pulsed plasma poly(vinylaniline)–cinnamaldehyde coated polypropylene cloth was fully immersed into 10 ml of high purity water for 16 h, removed, and the water droplet sliding angles were measured—this also did not affect the slipperiness of the coating, and no increase to the water droplet sliding angle was observed, Table 5.7.

Table 5.7: Water droplet sliding angle values for porous polypropylene (PP) cloth substrates coated with pulsed plasma poly(vinylaniline) (ppVA) and / or cinnamaldehyde. Values are reported as mean \pm standard deviation. † Sample displays complete wetting / absorption of water droplets.

Surface	Sliding Angle / °
PP Cloth Untreated	36 \pm 1
Cinnamaldehyde–PP Cloth †	-
ppVA–PP Cloth	75.3 \pm 0.5
ppVA–Cinnamaldehyde	14.0 \pm 0.8
ppVA–Cinnamaldehyde, 100 μ l water droplet, 4 h	13.7 \pm 0.5
ppVA–Cinnamaldehyde, 100 μ l water droplet, 20 h	14.0 \pm 0.8
ppVA–Cinnamaldehyde, immersion, 10 ml water, 16 h	14.7 \pm 0.5

5.2.9 Pulsed Plasma Poly(Vinylpyridine)

Infrared spectroscopy of vinylpyridine monomer showed the following characteristic bands: C–H stretches (3100–2885 cm^{-1}), ring summations (2000–1700 cm^{-1}), vinyl C=C stretching (1633 cm^{-1}), aromatic quadrant C=C stretching (1595 cm^{-1} and 1547 cm^{-1}), aromatic semicircle C=C and C=N stretching (1494 cm^{-1} and 1408 cm^{-1} respectively), and vinyl =CH₂ wag (922 cm^{-1}), Figure 5.14.²⁶ Pulsed plasma deposited poly(vinylpyridine) showed good structural retention, with the disappearance of the vinyl group bands indicating that polymerisation had taken place.

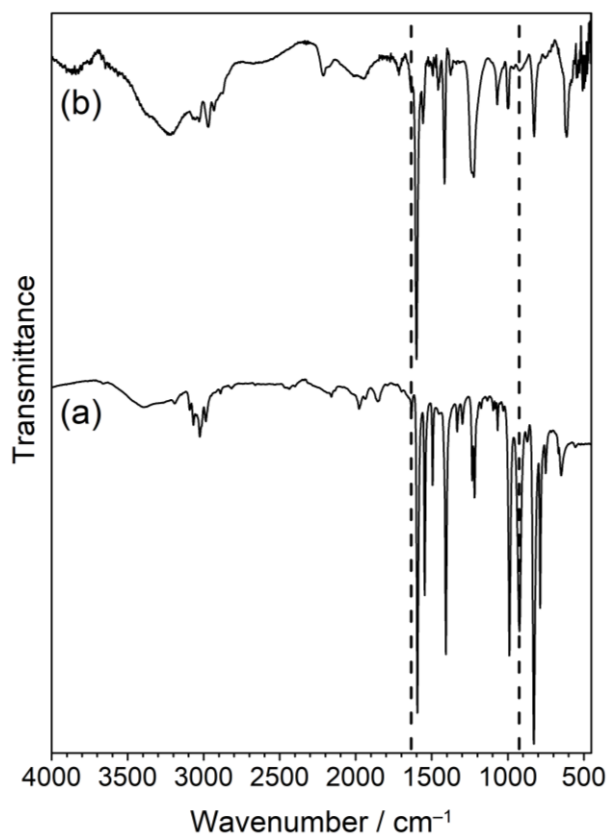


Figure 5.14: Infrared spectra of: (a) vinylpyridine monomer (ATR); and (b) pulsed plasma poly(vinylpyridine) deposited onto silicon wafer (RAIRS, 55°). The dashed lines correspond to vinyl group absorbances (1633 cm⁻¹ and 922 cm⁻¹).

Pulsed plasma poly(vinylpyridine)-only coatings were hydrophilic and showed water droplet pinning on the receding angles. Contact angle hysteresis for pulsed plasma poly(vinylpyridine) demonstrated that all the tested lubricants (cinnamaldehyde, decanal, 2-methylundecanal, and hexadecane) failed to infuse into the poly(vinylpyridine) plasma polymer and produce slippery coatings, and also demonstrated that the poly(vinylpyridine) coating showed preferential wetting with water, Table 5.8. Cinnamaldehyde caused at least partial washing off or dissolving of the coating, as determined by the loss of the brown colour of the coating (hence the lack of pinning on receding angles). Perfluorotributylamine failed to make the coating slippery, as seen from qualitative assessment of the sliding angle (quantitative analysis of contact angle hysteresis and sliding angle was not measured with this lubricant).

Table 5.8: Water droplet static, advancing, receding, hysteresis contact angle values following lubricant impregnation of pulsed plasma poly(vinylpyridine)-coated PET film substrates. Values are reported as mean \pm standard deviation.

Surface	Contact Angle / °	
	Static	Hysteresis
PET	67 \pm 2	52 \pm 4
Pulsed Plasma Poly(vinylpyridine) (ppVP)	38 \pm 5	57.4 \pm 0.5
ppVP–Cinnamaldehyde	65 \pm 9	38 \pm 13
ppVP–Decanal	53 \pm 5	69 \pm 6
ppVP–2-Methylundecanal	49 \pm 3	60 \pm 3
ppVP–Hexadecane	43 \pm 7	55 \pm 10

5.2.10 Pulsed Plasma Poly(Glycidyl Methacrylate)

For glycidyl methacrylate monomer, the following characteristic infrared band assignments were as follows: epoxide ring C–H stretching (3062 cm^{-1}), C–H stretching (3000–2880 cm^{-1}), acrylate carbonyl C=O stretching (1714 cm^{-1}), acrylate C=C stretching (1638 cm^{-1}), epoxide ring breathing (1253 cm^{-1}), antisymmetric epoxide ring deformation (908 cm^{-1}), and symmetric epoxide ring deformation (842 cm^{-1}), Figure 5.15.²⁷ Loss of the acrylate carbon–carbon double bond after pulsed plasma deposition showed that polymerisation had successfully taken place. The epoxide bands are still visible, indicating good structural retention.

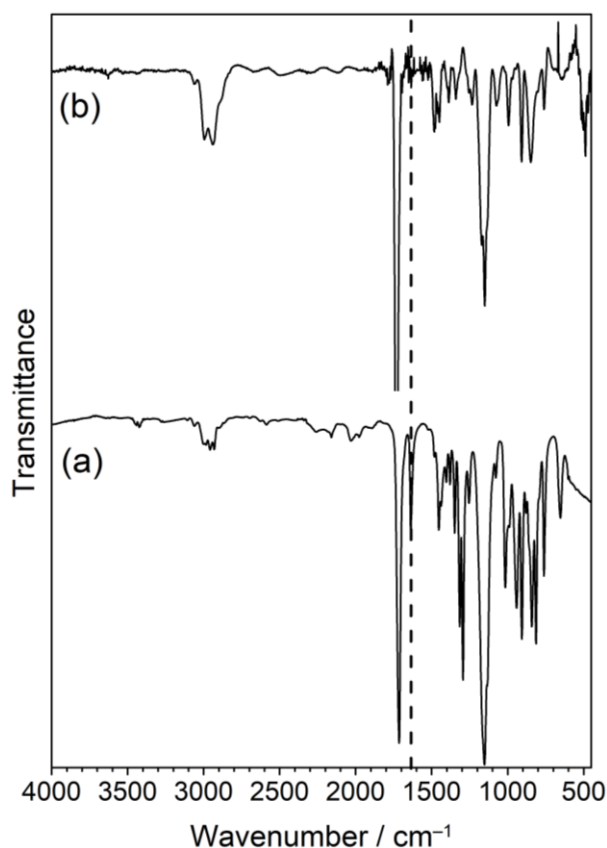


Figure 5.15: Infrared spectra of: (a) glycidyl methacrylate monomer (ATR); and (b) pulsed plasma poly(glycidyl methacrylate) deposited onto silicon wafer (RAIRS, 55°). The dashed line corresponds to acrylate carbon-carbon double bond absorbance (1638 cm^{-1}).

None of the tested lubricants produced slippery surfaces with the pulsed plasma poly(glycidyl methacrylate) coating, Table 5.9. In fact, they all resulted in an increase to the water contact angle hysteresis compared to the pulsed plasma poly(glycidyl methacrylate)-only coating. Since the coatings were not slippery, sliding angles were not measured.

Table 5.9: Water droplet static, advancing, receding, and hysteresis contact angle values following lubricant impregnation of pulsed plasma poly(glycidyl methacrylate)-coated PET film substrates. Values are reported as mean \pm standard deviation.

Surface	Contact Angle / °	
	Static	Hysteresis
PET	66.8 \pm 1.6	52 \pm 4
Pulsed Plasma Poly(GMA) (ppGMA)	56 \pm 2	21.6 \pm 0.8
ppGMA-Cinnamaldehyde	68 \pm 2	35 \pm 3
ppGMA-Decanal	68.1 \pm 0.4	38 \pm 4
ppGMA-2-Methylundecanal	57.0 \pm 1.7	23 \pm 4
ppGMA-Hexadecane	75.1 \pm 0.7	42 \pm 5

5.2.11 Pulsed Plasma Poly(Pentafluorostyrene)

Pentafluorostyrene monomer infrared spectra showed the following characteristic bands: vinyl C=C stretch (1625 cm^{-1}), fluorinated aromatic ring vibrations (1519 cm^{-1} and 1492 cm^{-1}), C-F (aromatic) stretching (973 cm^{-1}), and vinyl =CH₂ wag (927 cm^{-1}), Figure 5.16.²⁸ Disappearance of the vinyl group bands in the pulsed plasma deposited poly(pentafluorostyrene) showed that polymerisation had successfully taken place.

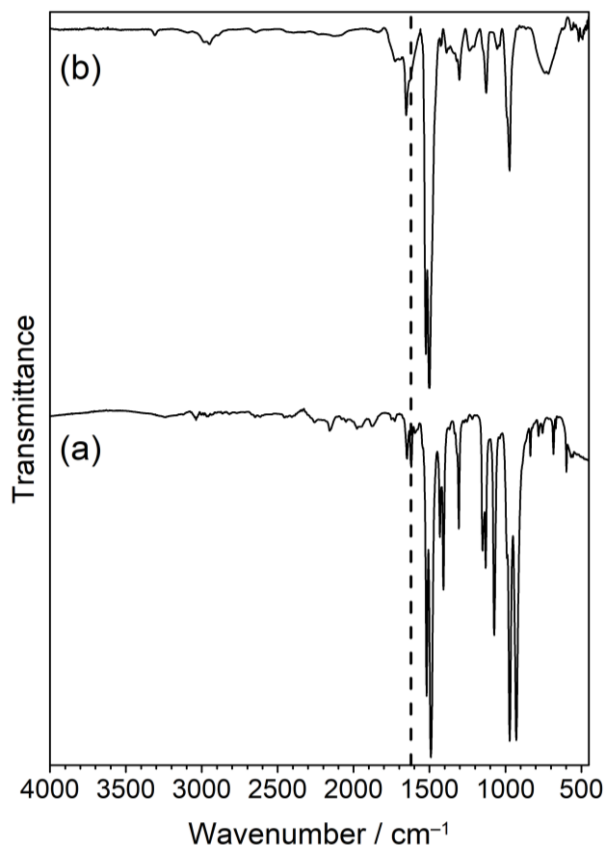


Figure 5.16: Infrared spectra of: (a) pentafluorostyrene monomer (ATR); and (b) pulsed plasma poly(pentafluorostyrene) deposited onto silicon wafer (RAIRS, 55°). The dashed line corresponds to vinyl carbon-carbon double bond absorbance (1625 cm^{-1}).

Pulsed plasma poly(pentafluorostyrene) coated PET substrates were treated with fluorinated lubricants (perfluorotributylamine and perfluoropolyether), but it was found that they did not produce slippery surfaces, and in fact the lubricants appeared to increase the water contact angle hysteresis compared to the pulsed plasma poly(pentafluorostyrene)-only coating, Table 5.10. Since the coatings were not slippery, sliding angles were not measured.

Table 5.10: Water droplet static, advancing, receding, and hysteresis contact angle values following lubricant impregnation of pulsed plasma poly(pentafluorostyrene)-coated PET film substrates. Values are reported as mean \pm standard deviation.

Surface	Contact Angle / °	
	Static	Hysteresis
PET	66.8 \pm 1.6	52 \pm 4
Pulsed Plasma Poly(pentafluorostyrene) (ppPFS)	96 \pm 3	29.1 \pm 1.4
ppPFS–Perfluorotributylamine	116.7 \pm 0.5	43 \pm 7
ppPFS–Perfluoropolyether	113.8 \pm 1.3	30 \pm 2

5.2.12 Pulsed Plasma Poly(1H, 1H, 2H, 2H-Perfluorooctyl Acrylate)

1H, 1H, 2H, 2H-perfluorooctyl acrylate monomer infrared characteristic peaks were observed as follows: C–H stretching (2975 cm^{-1}), acrylate carbonyl C=O stretch (1732 cm^{-1}), C=C stretching (1638 cm^{-1}), and C-F stretching ($1260\text{--}1100\text{ cm}^{-1}$), Figure 5.17.²⁹ The carbon–carbon double bond bands disappeared upon plasma polymerisation, indicating that polymerisation was successful.

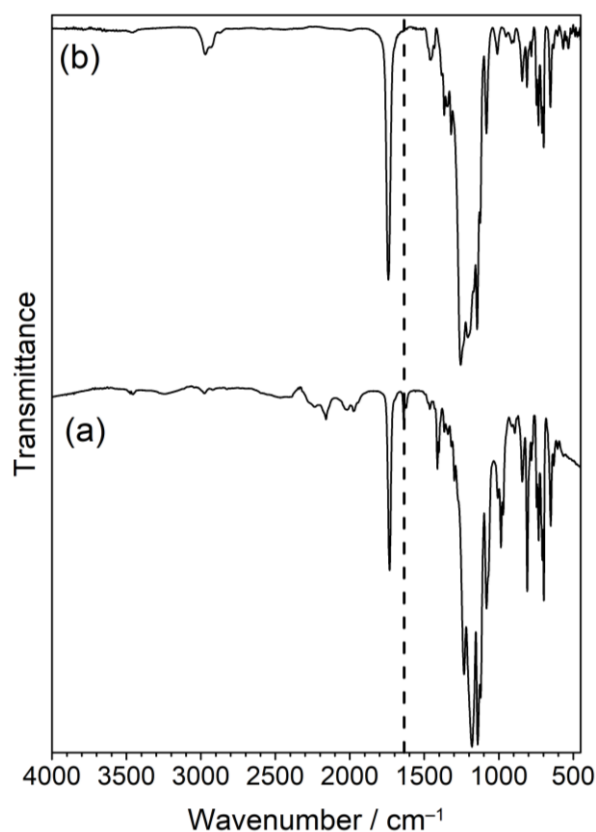


Figure 5.17: Infrared spectra of: (a) 1H, 1H, 2H, 2H-perfluorooctyl acrylate monomer (ATR); and (b) pulsed plasma poly(1H, 1H, 2H, 2H-perfluorooctyl acrylate) deposited onto silicon wafer (RAIRS, 55°). The dashed line corresponds to acrylate carbon–carbon double bond absorbance (1638 cm^{-1}).

None of the pulsed plasma poly(1H, 1H, 2H, 2H-perfluorooctyl acrylate) coated samples produced slippery surfaces when immersed into either of the fluorinated lubricants, Table 5.11. Perfluoropolyether did reduce the water contact angle hysteresis somewhat compared to the poly(1H, 1H, 2H, 2H-perfluorooctyl acrylate)-only coated surface, but the hysteresis was still relatively high. Since the coatings were not slippery, sliding angles were not measured.

Table 5.11: Water droplet static, advancing, receding, and hysteresis contact angle values following lubricant impregnation of pulsed plasma poly(1H, 1H, 2H, 2H-perfluorooctyl acrylate)-coated PET film substrates. Values are reported as mean \pm standard deviation.

Surface	Contact Angle / °	
	Static	Hysteresis
PET	66.8 \pm 1.6	52 \pm 4
Pulsed Plasma 1H, 1H, 2H, 2H-perfluorooctyl acrylate (ppPFAC6)	122 \pm 3	79 \pm 9
ppPFAC6–Perfluorotributylamine	121.7 \pm 0.3	72 \pm 3
ppPFAC6–Perfluoropolyether	117 \pm 3	33 \pm 5

5.3 Discussion

Superhydrophobic surfaces are typically characterized as having low water contact angle hysteresis values.³⁰ For example, this can be achieved by combining a hydrophobic surface and topographical micro- and/or nanostructure (roughness)—which effectively traps an air layer on the surface.³¹ However, these surfaces can fail when subjected to high pressures³², and therefore are unable to mitigate bacterial adhesion and biofouling under such conditions.³³ This is attributed to displacement of the trapped air pockets leading to exposure of the underlying rough surface towards favourable bacterial colonization.

Pulsed plasma deposited poly(hexyl acrylate) is found to display low water contact angle hysteresis ($< 10^\circ$) and sliding angle ($< 10^\circ$) values, Table 5.3. These may be attributed to either the relative flatness of the surface or weak (liquid-like) interactions between neighbouring surface alkyl chains, Figure 5.5.³⁴

It has been reported that favourable molecular level interactions of impregnated lubricants with the subsurface of non-porous flat polymer films (without any prior treatment of the polymer solid surface) can also lead to slippery surfaces (low water contact angle hysteresis).^{35,36,37} This slipperiness is not due

to excess lubricant remaining on the surface, and can be stable for prolonged periods of time (provided that the surface and lubricant polarities are well matched). In a similar way, functional pulsed plasma polymer film coatings have been shown to form slippery surfaces by infusion of lubricants into the deposited layer, with the added advantage of being independent of substrate material and geometry, Table 5.3.

In terms of a structure–behaviour relationship, nonaromatic (aliphatic) pulsed plasma polymer coatings (i.e. poly(hexyl acrylate), poly(glycidyl methacrylate), and poly(1H, 1H, 2H, 2H-perfluorooctyl acrylate)) do not show a tendency to form lubricant-infused slippery surfaces, Table 5.3. Whereas aromatic group containing pulsed plasma polymer coatings give rise to low contact angle hysteresis and sliding angle values following lubricant application (pulsed plasma poly(styrene), drop-cast poly(styrene), Petri dish poly(styrene), pulsed plasma poly(benzyl acrylate), pulsed plasma poly(vinylbenzaldehyde), pulsed plasma poly(vinylbenzyl chloride), and pulsed plasma poly(vinylaniline)). Previous studies have shown that molecular level aromatic–aliphatic interactions can be significantly stronger than aliphatic–aliphatic and aromatic–aromatic interactions.^{38,39} It is therefore likely that the aromatic group containing plasma polymer coatings interact more strongly with the lubricants compared to the aliphatic group containing plasma polymers; this leads to lubricant infusion into the subsurface to create slippery surfaces for the former but not the latter. For the case of the aromatic group containing lubricant cinnamaldehyde, aromatic–aromatic as well as aromatic–aliphatic intermolecular interactions may be contributing towards slippery surface formation, Table 5.3.

Out of the three fluorinated pulsed plasma polymer coatings investigated for omniphobicity (poly(perfluoroallylbenzene), poly(pentafluorostyrene), and poly(1H, 1H, 2H, 2H-perfluorooctyl acrylate)), only the first one yielded a slippery surface when combined with fluorinated lubricants. The latter two contain carbon-hydrogen and carbon-oxygen bonds which most likely act to hinder the compatibility of the fluorinated lubricants with the pulsed plasma polymer host matrix; whereas perfluoroallylbenzene is fully fluorinated, meaning it has good compatibility with the perfluorotributylamine and perfluoropolyether lubricants—thereby highlighting the importance of the surface chemistry/energy matching with the lubricant. Perfluorodecalin lubricant also produced a slippery surface when combined with pulsed plasma poly(perfluoroallylbenzene), Table 5.3.⁴⁰

Such omniphobic slippery surfaces could provide protection against chemical and biological warfare agents as well as offering bloodphobicity for healthcare applications.

Pulsed plasma poly(vinylpyridine) failed to form a slippery lubricant-infused surface when treated with lubricants, Table 5.8. Pyridine is a basic organic compound, with a pK_a value of 5.2, and can form hydrogen-bonds (due to the nitrogen lone-pair electrons, which are orthogonal to the aromatic π orbitals, and therefore do not donate any electron density into aromatic π orbitals).⁴¹ Indeed, pulsed plasma poly(vinylpyridine) has previously been described as 'superhydrophilic' and displays preferential wetting by water.⁴² Furthermore, it has been reported that spin-coated poly(vinylpyridine) did not form a slippery surface with silicone oil lubricant due to preferential wetting by water.⁴³ In contrast, the aromatic pulsed plasma poly(vinylaniline), which contains a relatively polar amine group, has been shown in the present study to successfully form slippery surfaces, Table 5.3. The reason is that the nitrogen lone pair in the aniline ring is able to delocalise via resonance into the aromatic π system, giving rise to lower pK_a value of only 4.6, and the amine group does not form hydrogen bonds with water as readily compared to the pulsed plasma poly(vinylpyridine) system.⁴² This manifests in the relatively higher static water contact angle for pulsed plasma poly(vinylaniline) versus pulsed plasma poly(vinylpyridine) (75° and 38° respectively, Table 5.3 and Table 5.8). Similarly, glycidyl methacrylate contains a polar epoxide group, and pulsed plasma poly(glycidyl methacrylate) exhibits a fairly low static water contact angle (i.e. it is hydrophilic), and thus does not form a slippery lubricant-infused coating, Table 5.9.

Pulsed plasma polymer slippery lubricant infused surfaces formed on porous polypropylene cloth showed improved resistance towards leaching of lubricant into water, Table 5.5 and Table 5.7. It has previously been reported that this particular cloth can absorb $45 \pm 4 \text{ mg cm}^{-2}$ of cinnamaldehyde (chapter 3, Table 3.1)⁴⁴, meaning that there is a 'reservoir' of cinnamaldehyde contained within the bulk of the cloth that can move to the surface to replenish any lost lubricant. This could have potential applications in underwater slippery surfaces, such as preventing marine biofouling or manipulation of air bubbles.^{45 46}

The successful production of slippery lubricant-infused surfaces on drop-cast polystyrene and pre-formed polystyrene plastic (from Petri dishes)

demonstrates that this approach is not only limited to plasma polymer coatings, but could potentially be applicable to a range of alternative surface functionalisation methods including: atomised spray plasma deposition, initiated chemical vapour deposition, electron/ion beam deposition, self-assembled layers, as well as other dry and wet surface coating methods. Other functional lubricants could also be employed in order to create alternative multifunctional slippery surfaces, for example non-volatile ionic liquids.⁴⁷ Furthermore, the rechargeable pulsed plasma polymer–antimicrobial lubricant slippery surfaces could find application in re-usable air filtration systems, healthcare personal protective clothing, and food packaging materials to help reduce plastic waste.

5.4 Conclusions

A range of slippery surfaces have been devised by combining different functional pulsed plasma polymer layers and lubricants to provide a molecular level structure–behaviour relationship. The fabrication process involves a simple, quick, substrate-independent, and conformal two-step methodology. Hydrophilic pulsed plasma polymer coatings are found not to produce slippery lubricant-infused coatings. Whilst the structure–behaviour relationship demonstrates that aromatic–aliphatic intermolecular interactions between coating and lubricant favours slippery surface formation. Fluorinated lubricant-infused coatings display omniphobicity and repel liquids with a range of surface tensions (including water, heptane and motor oil). Natural antimicrobial compound cinnamaldehyde-infused pulsed plasma polymer surfaces give rise to multifunctionality comprising liquid repellency (self-cleaning) and antibacterial activity against both Gram-positive *Staphylococcus aureus* and Gram-negative *Escherichia coli*. In addition, these antimicrobial natural compound lubricant-infused pulsed plasma polymer surfaces repel a range of everyday liquid foodstuffs (such as tomato ketchup and honey).

5.5 Videos

Video 5.1: Ketchup applied to untreated glass vial (control).

Video 5.2: Ketchup applied to glass vial rinsed with decanal (control).

Video 5.3: Ketchup applied to glass vial rinsed with 2-methylundecanal (control).

Video 5.4: Ketchup applied to glass vial rinsed with cinnamaldehyde (control).

Video 5.5: Ketchup applied to glass vial rinsed with citral (control).

Video 5.6: Ketchup applied to pulsed plasma poly(vinylaniline) coated glass vial impregnated with decanal lubricant.

Video 5.7: Ketchup applied to pulsed plasma poly(vinylaniline) coated glass vial impregnated with 2-methylundecanal lubricant.

Video 5.8: Ketchup applied to pulsed plasma poly(vinylaniline) coated glass vial impregnated with cinnamaldehyde lubricant.

Video 5.9: Ketchup applied to pulsed plasma poly(vinylaniline) coated glass vial impregnated with citral lubricant.

Video 5.10: Honey applied to untreated glass vial (control).

Video 5.11: Honey applied to glass vial rinsed with decanal (control).

Video 5.12: Honey applied to glass vial rinsed with 2-methylundecanal (control).

Video 5.13: Honey applied to glass vial rinsed with cinnamaldehyde (control).

Video 5.14: Honey applied to glass vial rinsed with citral (control).

Video 5.15: Honey applied to pulsed plasma poly(vinylaniline) coated glass vial impregnated with decanal lubricant.

Video 5.16: Honey applied to pulsed plasma poly(vinylaniline) coated glass vial impregnated with 2-methylundecanal lubricant.

Video 5.17: Honey applied to pulsed plasma poly(vinylaniline) coated glass vial impregnated with cinnamaldehyde lubricant.

Video 5.18: Honey applied to pulsed plasma poly(vinylaniline) coated glass vial impregnated with citral lubricant.

N.B. Videos can be accessed from the data archive that accompanies this thesis. Videos are provided in .mp4 format.

5.6 References

- 1 Smith, D. R. M.; Pouwels, K. B.; Hopkins, S.; Naylor, N. R.; Smieszek, T.; Robotham, J. V. Epidemiology and Health-Economic Burden of Urinary-Catheter-Associated Infection in English NHS Hospitals: A Probabilistic Modelling Study. *J. Hosp. Infect.* **2019**, *103*, 44–54.
- 2 Schultz, M. P.; Bendick, J. A.; Holm, E. R.; Hertel, W. M. Economic Impact of Biofouling on a Naval Surface Ship. *Biofouling* **2011**, *27*, 87–98.
- 3 Araújo, E. A.; de Andrade, N. J.; da Silva, L. H. M.; de Carvalho, A. F.; de Silva, C. A. S.; Ramos, A. M. Control of Microbial Adhesion as a Strategy for Food and Bioprocess Technology. *Food Bioprocess Technol.* **2010**, *3*, 321–332.
- 4 Ryan, M. E.; Hynes, A. M.; Badyal, J. P. S. Pulsed Plasma Polymerization of Maleic Anhydride. *Chem. Mater.* **1996**, *8*, 37–42.
- 5 Carletto, A.; Badyal, J. P. S. Ultra-High Selectivity Pulsed Plasmachemical Deposition Reaction Pathways. *Phys. Chem. Chem. Phys.* **2019**, *21*, 16468–16476.
- 6 Miller, T. A.; Mikhael, M. G.; Ellwanger, R.; Boufelfel, A.; Booth, D.; Yializis, A. Polymer Multi-Layer Processing of Thin Film Materials. *MRS Proceedings* **1999**, *555*, 247–254.
- 7 Singh, G.; Maurya, S.; deLampasona, M. P.; Catalan, C. A. N. A Comparison of Chemical, Antioxidant and Antimicrobial Studies of Cinnamon Leaf and Bark Volatile Oils, Oleoresins and Their Constituents. *Food Chem. Toxicol.* **2007**, *45*, 1650–1661.
- 8 Burt, S. Essential Oils: Their Antibacterial Properties and Potential Applications in Foods - A Review. *Int. J. Food Microbiol.* **2004**, *94*, 223–253.
- 9 Hayashi, K.; Imanishi, N.; Kashiwayama, Y.; Kawano, A.; Terasawa, K.; Shimada, Y.; Ochiai, H. Inhibitory Effect of Cinnamaldehyde, Derived from Cinnamomi Cortex, on the Growth of Influenza A/PR/8 Virus *In Vitro* and *In Vivo*. *Antiviral Res.* **2007**, *74*, 1–8.
- 10 Shreaz, S.; Wani, W. A.; Behbehani, J. M.; Raja, V.; Irshad, M.; Karched, M.; Ali, I.; Siddiqi, W. A.; Hun, L. T. Cinnamaldehyde and Its Derivatives, a Novel Class of Antifungal Agents. *Fitoterapia* **2016**, *112*, 116–131.
- 11 Fisher, K.; Phillips, C. A. The Effect of Lemon, Orange and Bergamot Essential Oils and Their Components on the Survival of *Campylobacter jejuni*, *Escherichia coli* O157, *Listeria monocytogenes*, *Bacillus cereus* and *Staphylococcus aureus* *In Vitro* and in Food Systems. *J. Appl. Microbiol.* **2006**, *101*, 1232–1240.
- 12 Liu, K.; Chen, Q.; Liu, Y.; Zhou, X.; Wang, X. Isolation and Biological Activities of Decanal, Linalool, Valencene, and Octanal from Sweet Orange Oil. *J. Food Sci.* **2012**, *77*, C1156–C1161.
- 13 Kubo, I.; Fujita, K. I.; Kubo, A.; Nihei, K. I.; Ogura, T. Antibacterial Activity of Coriander Volatile Compounds against *Salmonella Choleraesuis*. *J. Agric. Food Chem.* **2004**, *52*, 3329–3332.
- 14 Al-Shuneigat, J. M.; Al-Tarawneh, I. N.; Al-Qudah, M. A.; Al-Sarayreh, S. A.; Al-Saraireh, Y. M.; Alsharafa, K. Y. The Chemical Composition and the Antibacterial Properties of *Ruta graveolens* L. Essential Oil Grown in Northern Jordan. *Jordan J. Biol. Sci.* **2015**, *8*, 139–143.

- 15 <https://www.accessdata.fda.gov/scripts/cdrh/cfdocs/cfcfr/cfrsearch.cfm?cfrpart=182&showfr=1> Title 21–Food and Drugs; Chapter I–Food and Drug Administration; Department of Health and Human Services; Subchapter B–Food for Human Consumption (Continued); Part 182 Substances Generally Recognized as Safe. Accessed 10/08/2020.
- 16 <http://www.inchem.org/documents/jecfa/jecmono/v040je11.htm> Safety Evaluation of Certain Food Additives and Contaminants; WHO Food Additives Series 40. Accessed 10/08/2020.
- 17 Schofield, W. C. E.; Badyal, J. P. S. Pulsed Plasma Polymerisation of Butylacrylate for Pressure-Sensitive Adhesion. *Plasma Chem. Plasma Process.* **2006**, *26*, 361–369.
- 18 Coulson, S. R.; Woodward, I. S.; Badyal, J. P. S.; Brewer, S. A.; Willis, C. Ultralow Surface Energy Plasma Polymer Films. *Chem. Mater.* **2000**, *12*, 2031–2038.
- 19 Morsch, S.; Schofield, W. C. E.; Badyal, J. P. S. Surface Actuation of Smart Nanoshutters. *Langmuir* **2010**, *26*, 12342–12350.
- 20 Fang, J.; Xuan, Y.; Li, Q. Preparation of Polystyrene Spheres in Different Particle Sizes and Assembly of the PS Colloidal Crystals. *Sci. China Technol. Sci.* **2010**, *53*, 3088–3093.
- 21 McGettrick, J. D.; Schofield, W. C. E.; Garrod, R. P.; Badyal, J. P. S. A Substrate-Independent Approach for the Surface Immobilization of Oligonucleotides Using Aldehyde Functionalized Surfaces. *Chem. Vap. Depos.* **2009**, *15*, 122–127.
- 22 Wilson, M.; Kore, R.; Ritchie, A. W.; Fraser, R. C.; Beaumont, S. K.; Srivastava, R.; Badyal, J. P. S. Palladium–Poly(Ionic Liquid) Membranes for Permselective Sonochemical Flow Catalysis. *Colloids Surfaces A Physicochem. Eng. Asp.* **2018**, *545*, 78–85.
- 23 Hynes, A.; Badyal, J. P. S. Selective Incorporation of Perfluorinated Phenyl Rings during Pulsed Plasma Polymerization of Perfluoroallylbenzene. *Chem. Mater.* **1998**, *10*, 2177–2182.
- 24 Chambers, R. D. *Fluorine in Organic Chemistry*; Wiley & Sons: London, 1973.
- 25 Harris, L. G.; Schofield, W. C. E.; Doores, K. J.; Davis, B. G.; Badyal, J. P. S. Rewritable Glycochips. *J. Am. Chem. Soc.* **2009**, *131*, 7755–7761.
- 26 Bradley, T. J.; Schofield, W. C. E.; Garrod, R. P.; Badyal, J. P. S. Electroless Metallization onto Pulsed Plasma Deposited Poly(4-Vinylpyridine) Surfaces. *Langmuir* **2006**, *22*, 7552–7555.
- 27 Tarducci, C.; Kinmond, E. J.; Badyal, J. P. S.; Brewer, S. A.; Willis, C. Epoxide-Functionalized Solid Surfaces. *Chem. Mater.* **2000**, *12*, 1884–1889.
- 28 Brown, P. S.; Wood, T. J.; Schofield, W. C. E.; Badyal, J. P. S. A Substrate-Independent Lift-off Approach for Patterning Functional Surfaces. *ACS Appl. Mater. Interfaces* **2011**, *3*, 1204–1209.
- 29 Teare, D. O. H.; Spanos, C. G.; Ridley, P.; Kinmond, E. J.; Roucoules, V.; Badyal, J. P. S.; Brewer, S. A.; Coulson, S.; Willis, C. Pulsed Plasma Deposition of Super-Hydrophobic Nanospheres. *Chem. Mater.* **2002**, *14*, 4566–4571.
- 30 Öner, D.; McCarthy, T. J. Ultrahydrophobic Surfaces. Effects of Topography Length Scales on Wettability. *Langmuir* **2000**, *16*, 7777–7782.

- 31 Brown, P. S.; Berson, A.; Talbot, E. L.; Wood, T. J.; Schofield, W. C. E.; Bain, C. D.; Badyal, J. P. S. Impact of Picoliter Droplets on Superhydrophobic Surfaces with Ultralow Spreading Ratios. *Langmuir* **2011**, *27*, 13897–13903.
- 32 Nhung Nguyen, T. P.; Brunet, P.; Coffinier, Y.; Boukherroub, R. Quantitative Testing of Robustness on Superomniphobic Surfaces by Drop Impact. *Langmuir* **2010**, *26*, 18369–18373.
- 33 Hwang, G. B.; Page, K.; Patir, A.; Nair, S. P.; Allan, E.; Parkin, I. P. The Anti-Biofouling Properties of Superhydrophobic Surfaces Are Short-Lived. *ACS Nano* **2018**, *12*, 6050–6058.
- 34 Wang, L.; McCarthy, T. J. Covalently Attached Liquids: Instant Omniphobic Surfaces with Unprecedented Repellency. *Angew. Chem. Int. Ed.* **2016**, *55*, 244–248.
- 35 Mukherjee, R.; Habibi, M.; Rashed, Z. T.; Berbert, O.; Shi, X.; Boreyko, J. B. Oil-Impregnated Hydrocarbon-Based Polymer Films. *Sci. Rep.* **2018**, *8*, 1–13.
- 36 Urata, C.; Dunderdale, G. J.; England, M. W.; Hozumi, A. Self-Lubricating Organogels (SLUGs) With Exceptional Syneresis-Induced Anti-Sticking Properties Against Viscous Emulsions and Ices. *Journal of Materials Chemistry A* **2015**, *3*, 12626–12630.
- 37 Howell, C.; Vu, T. L.; Lin, J. J.; Kolle, S.; Juthani, N.; Watson, E.; Weaver, J. C.; Alvarenga, J.; Aizenberg, J. Self-Replenishing Vascularized Fouling-Release Surfaces. *ACS Applied Materials & Interfaces* **2014**, *6*, 13299–13307.
- 38 Ninković, D. B.; Vojislavljević-Vasilev, D. Z.; Medaković, V. B.; Hall, M. B.; Brothers, E. N.; Zarić, S. D. Aliphatic-Aromatic Stacking Interactions in Cyclohexane-Benzene Are Stronger than Aromatic-Aromatic Interaction in the Benzene Dimer. *Phys. Chem. Chem. Phys.* **2016**, *18*, 25791–25795.
- 39 Togasawa, R.; Tenjimbayashi, M.; Matsubayashi, T.; Moriya, T.; Manabe, K.; Shiratori, S. A Fluorine-free Slippery Surface with Hot Water Repellency and Improved Stability against Boiling. *ACS Appl. Mater. Interfaces* **2018**, *10*, 4198–4205.
- 40 Leslie, D. C.; Waterhouse, A.; Berthet, J. B.; Valentin, T. M.; Watters, A. L.; Jain, A.; Kim, P.; Hatton, B. D.; Nedder, A.; Donovan, K.; Super, E. H.; Howell, C.; Johnson, C. P.; Vu, T. L.; Bolgen, D. E.; Rifai, S.; Hansen, A. R.; Aizenberg, M.; Super, M.; Aizenberg, J.; Ingber, D. E. A Bioinspired Omniphobic Surface Coating on Medical Devices Prevents Thrombosis and Biofouling. *Nat. Biotechnol.* **2014**, *32*, 1134–1140.
- 41 Krygowski, T. M.; Szatyłowicz, H.; Zachara, J. E. How H-Bonding Modifies Molecular Structure and π -Electron Delocalization in the Ring of Pyridine/Pyridinium Derivatives Involved in H-Bond Complexation. *J. Org. Chem.* **2005**, *70*, 8859–8865.
- 42 Garrod, R. P.; Harris, L. G.; Schofield, W. C. E.; McGettrick, J.; Ward, L. J.; Teare, D. O. H.; Badyal, J. P. S. Mimicking a Stenocara Beetle's Back for Microcondensation Using Plasmachemical Patterned Superhydrophobic-Superhydrophilic Surfaces. *Langmuir* **2007**, *23*, 689–693.
- 43 Ware, C. S.; Smith-Palmer, T.; Peppou-Chapman, S.; Scarratt, L. R. J.; Humphries, E. M.; Balzer, D.; Neto, C. Marine Antifouling Behavior of Lubricant-Infused Nanowrinkled Polymeric Surfaces. *ACS Appl. Mater. Interfaces* **2018**, *10*, 4173–4182.

- 44 Cox, H. J.; Li, J.; Saini, P.; Paterson, J. R.; Sharples, G. J.; Badyal, J. P. S. Bioinspired and Eco-Friendly High Efficacy Cinnamaldehyde Antibacterial Surfaces. *J. Mater. Chem. B* **2021**, *9*, 2918–2930.
- 45 Wang, P.; Zhang, D.; Sun, S.; Li, T.; Sun, Y. Fabrication of Slippery Lubricant-Infused Porous Surface with High Underwater Transparency for the Control of Marine Biofouling. *ACS Appl. Mater. Interfaces* **2017**, *9*, 972–982.
- 46 Zhang, J.; Liu, P.; Yi, B.; Wang, Z.; Huang, X.; Jiang, L.; Yao, X. Bio-Inspired Elastic Liquid-Infused Material for On-Demand Underwater Manipulation of Air Bubbles. *ACS Nano* **2019**, *13*, 10596–10602.
- 47 Charpentier, T. V. J.; Neville, A.; Baudin, S.; Smith, M. J.; Euvrard, M.; Bell, A.; Wang, C.; Barker, R. Liquid Infused Porous Surfaces for Mineral Fouling Mitigation. *J. Colloid Interface Sci.* **2015**, *444*, 81–86.

Chapter 6

6 Anti-Biofouling Coatings for Marine Aquaculture

6.1 Introduction

Historically, paints containing tributyltin have had widespread use to mitigate marine biofouling.¹ However, serious concerns about toxicological effects on marine ecosystems have arisen over the years, and many countries have now banned their use.² Some reports detail the use of antimicrobial additives contained within coatings in order to prevent biofouling. One study showed TiO₂/Ag in chitosan polymer nanocomposites are anti-algal and antifouling against *Dunaliella salina* microalgae.³ The TiO₂ mode of antimicrobial action is production of reactive oxygen species upon UV irradiation. In another case, polydopamine–Ag nanoparticle coatings inhibited attachment by *Dunaliella tertiolecta*.⁴ There are however concerns about the toxicological effects of silver upon release into the environment, in addition to the potential for antimicrobial resistance.^{5,6} Copper-doped TiSiN coatings have inhibited adhesion of *Phaeodactylum tricornutum*, *Nitzschia closterium* and *Chlorella* sp. due to the algicidal effect of leaching copper.⁷ Copper and copper oxide-based leaching coatings are applied in large volumes commercially to prevent biofouling.⁸ The use of non-leaching polymer coatings to mitigate biofouling by microalgae includes coatings based upon polystyrene-*b*-poly(ethylene glycol) methacrylate copolymer⁹, UV-cured poly(isoprene)-based¹⁰, and negatively charged poly(styrenesulfonate)/poly-(diallyldimethylammonium chloride) layer-by-layer assemblies.¹¹

Such coating methods suffer from disadvantages including being multi-step, solvent-based, and often 3-dimensional objects are difficult to coat. In this study, pulsed plasmachemical deposition has been used with advantages of it being a quick single-step, dry, independent of substrate material, excellent adhesion, solventless, low energy consumption, minimal waste, and conformal method. Mechanistically, this entails two distinct reaction regimes: the short period on-time (t_{on} —typically microseconds, where electrical discharge ignition leads to the formation of initiator radical species from the monomer) and then the longer period off-time (t_{off} —typically milliseconds, where conventional stepwise addition chain-growth monomer polymerisation proceeds).^{12,13} Excellent

structural retention of the monomer functional groups is attained to yield well-defined functional polymer nanocoatings.^{4, 14}

Chaetoceros calcitrans, *Chaetoceros mulleri*, and *Tisochrysis lutea* (T-Iso) are marine microalgae commonly grown in aquaculture as food for filter feeding marine organisms, such as mussel larvae.^{15, 16} Under certain conditions, they exude extracellular polymeric substances which are slimy and stick to bioreactor walls, leading to biofilms and deterioration of quantity and quality of the algae production.¹⁷ Photobioreactor polyethylene film used for continuous algae production is coated with a variety of functional nanocoatings prepared via pulsed plasmachemical deposition, Figure 6.1. The structure-behaviour relationship of different wetting surfaces towards biofouling by marine microalgae is investigated.

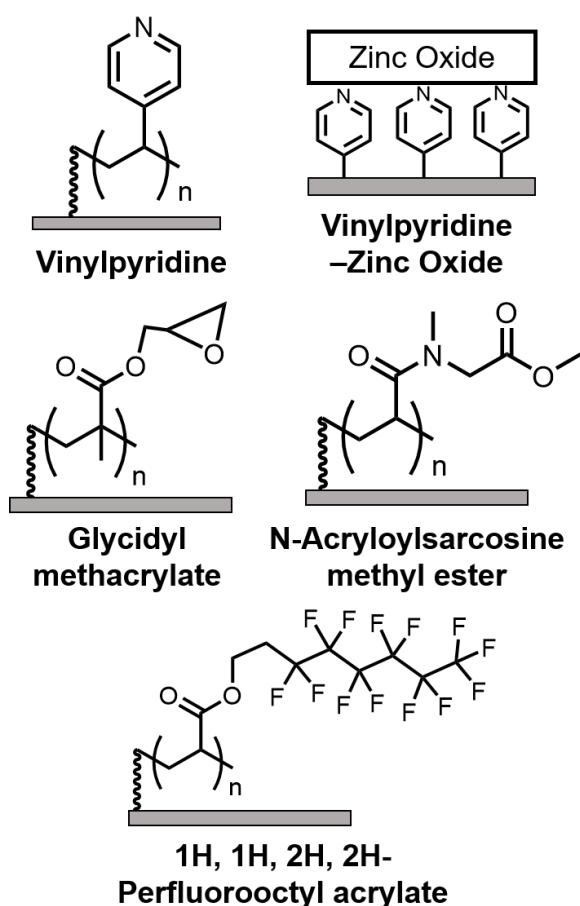


Figure 6.1: Functional nanocoatings and corresponding monomer names.

6.2 Experimental

6.2.1 Pulsed Plasma Deposition

Pulsed plasma deposition was performed as described in section 2.1. Photobioreactor polyethylene film used for continuous algae production (250 μm thick, Amcor Flexibles NZ Ltd.) was cleaned by sonication in a 50:50 volume mixture of propan-2-ol and cyclohexane (+99.7 wt.%, Sigma-Aldrich Ltd.) for 15 min followed by air drying.

Monomers utilised for pulsed plasmachemical deposition were: 4-vinylpyridine (95%, Sigma-Aldrich Inc.), *N*-acryloylsarcosine methyl ester (+97%, Lancaster Synthesis Ltd.), glycidyl methacrylate (97%, Sigma-Aldrich Inc.), and 1H, 1H, 2H, 2H-perfluorooctyl acrylate (+95%, Fluorochem Ltd.), Table 6.1.

Table 6.1: Pulsed plasma deposition parameters and nanocoating growth rates.

Monomer	Peak Power / W	t_{on} / μs	t_{off} / ms	Deposition Temperature / $^{\circ}\text{C}$	Deposition Rate / nm min^{-1}
4-Vinylpyridine	40	100	4	20	11
<i>N</i> -Acryloylsarcosine methyl ester	40	20	5	50	9
Glycidyl methacrylate	40	20	20	20	10
1H, 1H, 2H, 2H-Perfluorooctyl acrylate	40	20	20	20	41

For zinc oxide coatings, pulsed plasma poly(4-vinylpyridine) functionalized surfaces were immersed into an aqueous catalyst solution containing 2 μM palladium(II) chloride (+99.999%, Alfa Aesar, FisherScientific UK Ltd.), 3.0 M sodium chloride (+99.5%, Sigma-Aldrich Inc.), and 0.5 M sodium citrate dihydrate (+99%, Sigma-Aldrich Inc.) (which had been adjusted to pH 4.5 with citric acid monohydrate (+99%, Sigma-Aldrich Inc.)) for 12 h, and subsequently washed in deionized water.¹⁸ Next, the palladium(II) chloride immobilized surfaces were placed into an aqueous chemical bath containing 0.05 M zinc nitrate (+98%, Sigma-Aldrich Inc.) and 0.05 M dimethylaminoborane (+97%, Sigma-Aldrich Inc.) at pH 6.5 and a temperature of 323 K for 2 h. Following zinc oxide growth, the surface was rinsed with deionized water.

6.2.2 Coating Characterisation

Coating thicknesses were measured as described in section 2.4. Sessile drop static contact angle measurements were carried out as described in section 2.5. Infrared spectra were acquired as described in section 2.2.

6.2.3 Immersed Coating Stability

Pulsed plasma poly(vinylpyridine) was coated onto silicon wafers. The coated silicon wafers were then fully immersed into deionised water (100 ml) at 293 K for predetermined periods of time and then removed for air drying at 293 K, followed by coating thickness measurement (section 2.4). Afterwards, the coated silicon wafers were re-submerged into the deionised water, and the process repeated for extended time intervals.

For the uncoated and pulsed plasma poly(vinylpyridine) coated polyethylene film samples used for *Chaetoceros calcitrans*, *Chaetoceros mulleri*, and *Tisochrysis lutea* (T-Iso) microalgae toxicity testing, these were analysed following removal from the microalgae solutions, and subsequently after immersing into cyclohexane (99.5+%, Fisher Scientific UK Ltd.) solvent followed by air drying prior to surface analysis.

6.2.4 Biofouling Testing

Test samples were glued (superglue) to plastic frames that were made from food grade container lids. An untreated control substrate sample (250 µm thick photobioreactor polyethylene film, Amcor Flexibles NZ Ltd) was glued next to each coated sample using the same substrate material, Figure 6.2(a). The frames were inserted into photobioreactor bag tubing and heat-sealed to form short bags (volume of about 15 L). These short bags were hung in 2 rows with random distribution of the samples, Figure 6.2(b). *Chaetoceros calcitrans* microalgae was produced continuously in two rows of photobioreactor bags. The harvest line from each row was fed into separate harvest bins. From these bins the culture was pumped into the two rows of short bags containing the samples. Each sample bag received about 27 L fresh culture per day in short pulses at 2.5 s intervals. The bags overflowed into harvest bins. The cultures were aerated.

Production and test bags were cleaned at 1–3 days intervals. This involved turning off the air, tapping the bags, letting flocs of algae settle to the bottom of the bags for 15 min, draining the accumulated flocs, and turning the air back on. The algae concentration in all test bags was visibly higher than in the harvest bins, indicating growth and that there was no major toxic effect from the samples. After 20 days, the sample bags were drained in order to observe fouling on the samples. Care was taken to avoid contact between bag walls and samples.

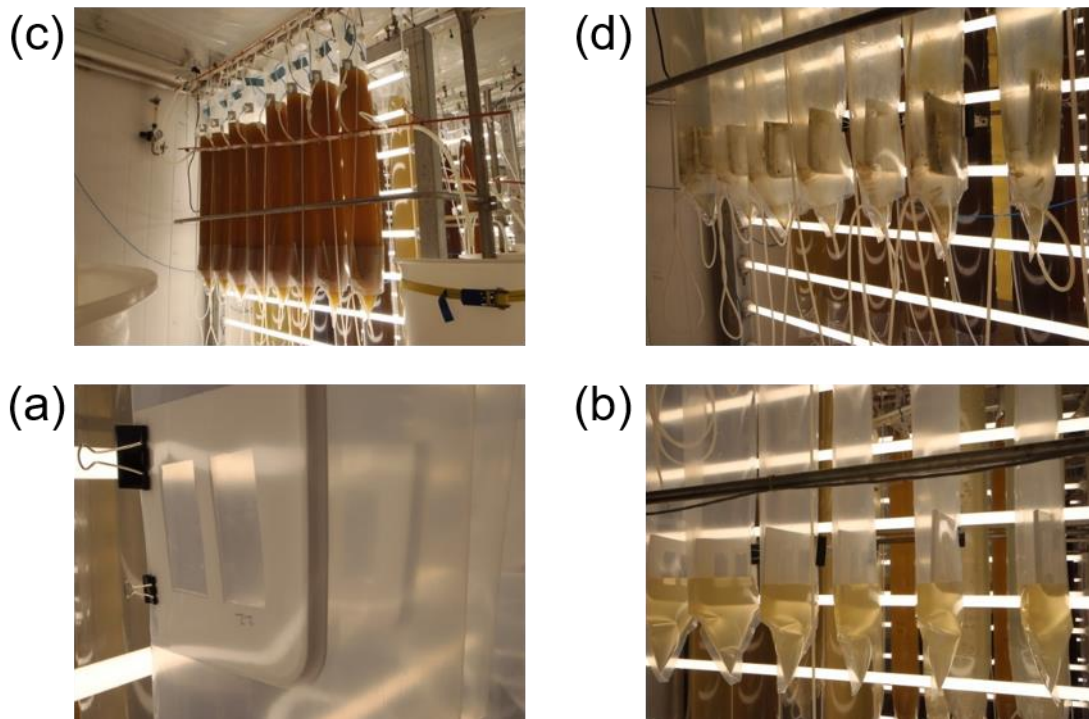


Figure 6.2: (a) Sample frame inside plastic photobioreactor bag clamped into position before filling with microalgae culture (the black temporary positioning clips pushed off when the bags became rounded during filling with microalgae culture); (b) in the foreground are the short photobioreactor bags containing samples and partially filled with fresh microalgae culture (the large photobioreactor bags producing microalgae culture which feed into the short photobioreactor bags can be seen in the background); (c) good uniform culture in all bags with the microalgae concentration visibly higher in all test bags compared to the harvest bins indicating growth and that there are no major toxicological effects from the samples; and (d) following drainage of photobioreactor bags showing fouling on the bag walls and sample holder frames. Images taken by Mike Packer.

6.2.5 Toxicity Testing

The algal species used in these experiments had been grown in a consistent environment for several months preceding experimental exposure. *Chaetoceros calcitrans* inoculum cultures were grown from the Australian National Algae Culture Collection (ANACC) as CS178, and *Tisochrysis lutea* (T-Iso) and *Chaetoceros mulleri* from stocks originally obtained from the Scottish Association

of Science (SAMS) Culture Collection of Algae and Protists (CCAP) as CCAP927/14 and CCAP1010/3 respectively. Mother stocks of algae are replaced on an annual basis. The algal species were placed in 500 ml Erlenmeyer flasks containing 0.35 μm filtered seawater (FSW) that had been previously autoclaved at a salinity of 35-36 ppt using F culture medium nutrient, supplied by Varicon Aqua Ltd, product F2P)—this was used at double strength so as to extend the life of the culture to provide a longer exposure time of the algae to the test samples (otherwise these cultures would run out of nutrients and die in about 4–5 days). For *Chaetoceros calcitrans* and *Chaetoceros mulleri*, silica was added separately to the medium in the form of sodium metasilicate at a final concentration of 105.6 μM . Stock cultures and experiments were kept at 294 K and irradiated with continuous white fluorescent light at $\sim 100 \mu\text{mol photons m}^{-2} \text{ s}^{-1}$ as described previously.¹⁷

For microalgal toxicity evaluation, triplicate 300 ml batch cultures of *Chaetoceros calcitrans*, *Chaetoceros mulleri*, and *Tisochrysis lutea* (T-Iso) in 500 ml Erlenmeyer flasks were used to test the toxicity of the coated plastic films to algae. Each of the four different batch coated films and a non-coated control of polyethylene film were fixed into a 35 mm photographic slide frame, which had a 1 mm thick length of silicone tube fixed to it so it could be suspended in the culture, Figure 6.3. Cultures were inoculated on day 0 with 40 ml of a parent stock and randomly placed on a shelf with a light frame. Experimental cultures were static but were swirled once every day during the testing period and moved to a new random location on the shelf after each sampling to control for varying distances from the light frame and therefore varying light intensities. The flasks were opened in a sterile laminar flow cabinet for sampling where a 2 ml aliquot was removed using a sterile pipette. The experiment was carried out for 14 days with 10 or 11 samplings occurring over that period.



Figure 6.3: Microalgal toxicity apparatus using triplicate 300 ml batch cultures of *Chaetoceros calcitrans*, *Chaetoceros mulleri*, and *Tisochrysis lutea* (T-Iso) in 500 ml Erlenmeyer flasks. Images taken by Mike Packer.

For photosynthetic parameter analyses stress measurements, a Pulse Amplitude Modulation (PAM) fluorescence analyser (model Aquapen AP 110-C, Photon Systems Instruments spol. s r.o.) was used to measure the dark-adapted quantum yield (F_v/F_m) as an indicator of stress in the algae.¹⁹ Algae were diluted 50% in culture media for measurement and the dark-adaption period was 10 min. Optical density (OD) of the algae was also recorded with the same instrument as the absorbance of light at 720 nm (OD720) as a proxy for cell number in the culture, and at 680 nm (OD680) as an indicator of light scattering and chlorophyll absorption, as well as fluorescence—all of which were used to compare growth rates for the different sample batches. The order of measurements on this instrument were fluorescence first, then quantum yield, then OD on the same sample, so that the measurements did not interfere with each other. The instrument was used with a 455 nm wavelength measuring light, and for F_v/F_m a 30 μs pulse of 0.0135 $\mu\text{mol m}^{-2}$ was used for the flash pulse and 1650 $\mu\text{mol photons m}^{-2} \text{s}^{-1}$ was used for the saturating pulse. The dilution, dark adaption period and intensity of both the flash and saturating pulses were optimised for these algae in separate experiments and the flash pulse was determined to not drive photosynthesis (i.e. it is not actinic, it does not drive photochemical reactions such as production of ATP used in photosynthesis) for these algae under these conditions.

6.3 Results

6.3.1 Biofouling

The best antifouling performance towards *Chaetoceros calcitrans* microalgae was observed for pulsed plasma poly(vinylpyridine); whilst pulsed plasma poly(1H,1H,2H,2H-perfluorooctylacrylate) gave rise to more biofouling compared to the control uncoated polyethylene substrate after 20 days, Figure 6.4. Pulsed plasma poly(glycidyl methacrylate), pulsed plasma poly(*N*-acryloylsarcosine methyl ester), and zinc oxide also displayed some level of biofouling hindrance, but were found not to be as consistent as pulsed plasma poly(vinylpyridine) coatings.





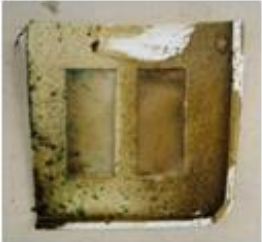
<u>Nanocoating</u>		<u>Biofouling</u>	<u>Contact Angle</u>
Pulsed plasma poly(vinylpyridine)		-2	38 ± 5°
Pulsed plasma poly(<i>N</i> -acryloylsarcosine methyl ester)		-2	52 ± 3°
Pulsed plasma poly(glycidyl methacrylate)		-1	56 ± 2°
Zinc oxide		-1	150 ± 1°
Pulsed plasma poly(1H,1H,2H,2H-perfluorooctylacrylate)		+1	122 ± 3°

Figure 6.4: Photographs following 20 days exposure to *Chaetoceros calcitrans* microalgae in photobioreactor (relative degree of biofouling scale ('in-house' method of assessment): significantly cleaner than control (-2); marginally cleaner than control (-1); equal to control (0); marginally more fouled than control (+1); significantly more fouled than control (+2)). Where the uncoated control polyethylene film substrate is mounted in the left window of each pair. Coatings (except poly(vinylpyridine)) were produced by Haley Andrews. Biofouling testing was performed by, and images taken by, Mike Packer and Henry Kasper.

The best performing pulsed plasma poly(vinylpyridine) coating was further examined for aqueous stability by measuring layer thickness on silicon wafers as a function of immersion time under water, Figure 6.5. The coatings showed a

small decrease in thickness to eventually plateau after 24 h—this is likely due to some loosely bound low molecular weight polymer chains initially washing off. No further loss of material after this time confirmed that the pulsed plasma poly(vinylpyridine) coating is stable in water.

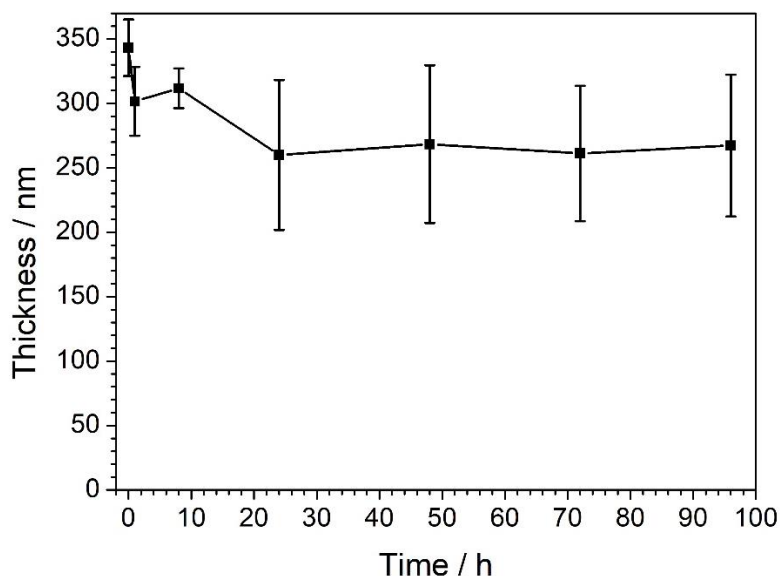


Figure 6.5: Pulsed plasma poly(vinylpyridine) coating thickness variation with time of immersion in water. (Mean values, errors bars represent standard deviation).

Following microalgae exposure, the sample surfaces were analysed using infrared spectroscopy, Figure 6.6. The as-removed surfaces all displayed very similar infrared absorbance features which can be attributed to surface settlement during removal from the microalgae solution. This settlement layer could be easily washed off using cyclohexane (as found for the control uncoated polyethylene film sample which required just 5 s of immersion into the solvent). Even after 30 min of immersion in cyclohexane, the pulsed plasma poly(vinylpyridine) coated samples which had been exposed to microalgae in solution still exhibited infrared absorbance peaks which are characteristic of pulsed plasma poly(vinylpyridine) coated polyethylene prior to immersion into the microalgae solutions at around 3300 cm^{-1} (O–H or N–H bonds from absorbed water^{20, 21}), 1650 cm^{-1} (C=C stretching), and 1090 cm^{-1} (aromatic C=C–H in-plane bends, and/or C–N stretches).^{22,23,24} Given the hydrophilic nature of poly(vinylpyridine), these absorbances are a combination of adsorbed water and the underlying pulsed plasma poly(vinylpyridine) coating.

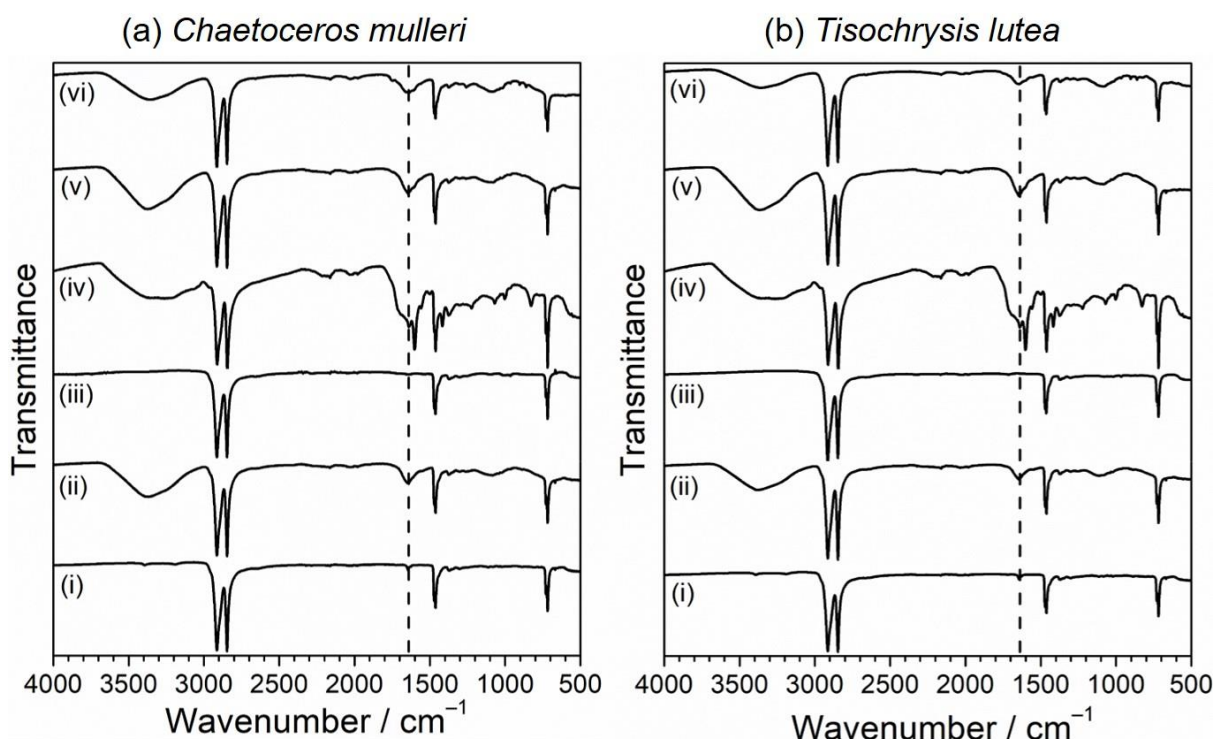


Figure 6.6: Infrared spectra for (a) *Chaetoceros mulleri*; and (b) *Tisochrysis lutea* where: (i) control uncoated polyethylene (not exposed to microalgae); (ii) control uncoated polyethylene exposed to microalgae; (iii) control uncoated polyethylene exposed to microalgae and washed with cyclohexane for 5 s; (iv) control pulsed plasma poly(vinylpyridine) coated polyethylene (not exposed to microalgae); (v) pulsed plasma poly(vinylpyridine) coated polyethylene exposed to microalgae; and (vi) pulsed plasma poly(vinylpyridine) coated polyethylene exposed to microalgae and washed with cyclohexane for 30 min.

6.3.2 Toxicity

Optical density measurements showed that cell number in the culture increased linearly over time, with no notable difference observed between the uncoated and pulsed plasma poly(vinylpyridine) coated polyethylene film samples, Figure 6.7. The drop-off observed after day 10 for *C. calcitrans* is to be expected due to nutrient deprivation in the batch culture by that stage. Similarly, no difference was seen for the photosynthetic health parameter. The photosynthetic health parameter is determined from the chlorophyll fluorescence of the algae—when the algae cells are exposed to external factors (such as a polymer coating), the stress on the cells may increase. Generally, the greater the stress, the fewer the reactive fluorescent sites are present, and thus a decrease in the quantum yield (the ratio of the minimum baseline fluorescence and the maximum fluorescence) means a decrease in the health of the algae caused by the surface coating. This

confirms that there is an absence of toxicity for the pulsed plasma poly(vinylpyridine) coatings towards the microalgae.

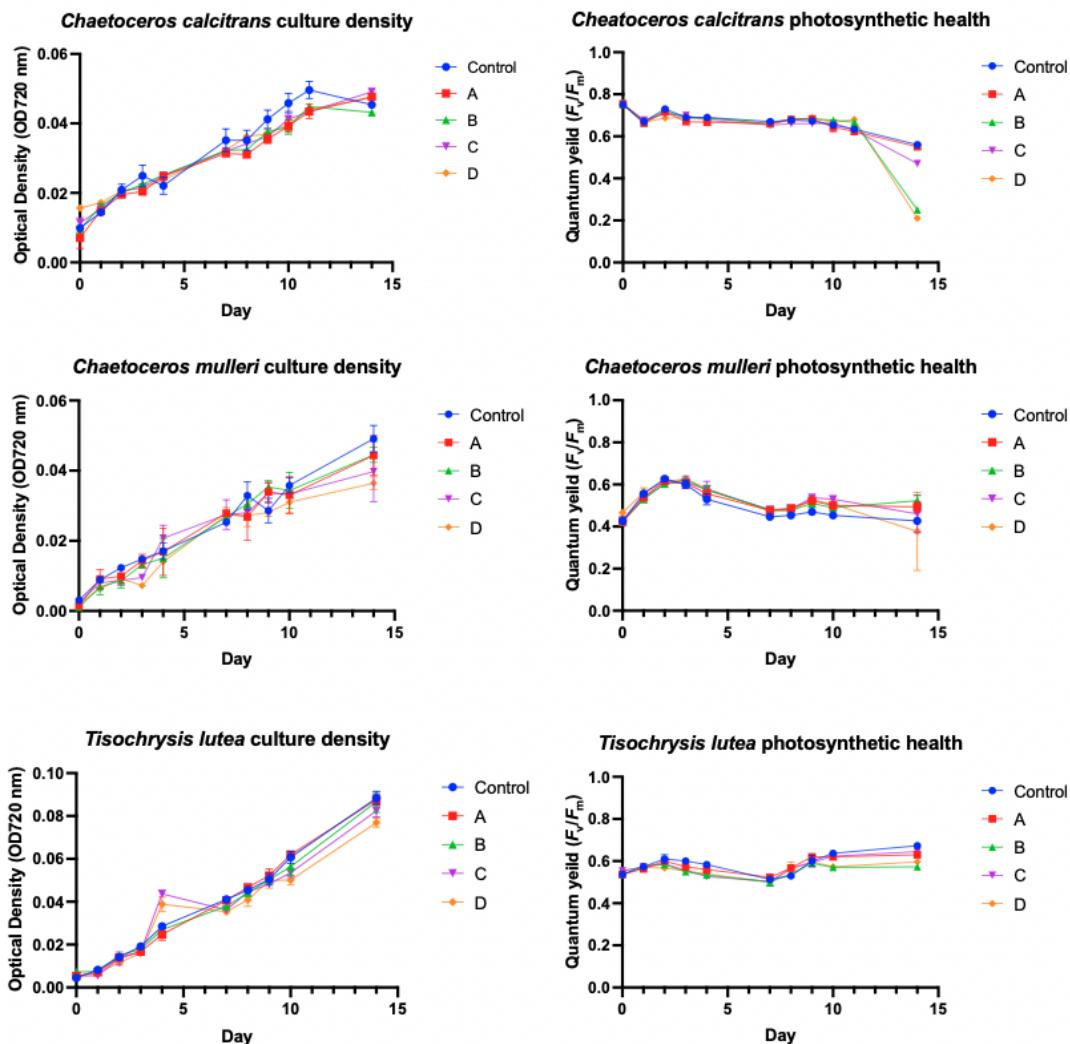


Figure 6.7: Growth and photosynthetic health of *Chaetoceros calcitrans*, *Chaetoceros mulleri*, and *Tisochrysis lutea* (T-Iso) microalgae versus time for uncoated control and pulsed plasma poly(vinylpyridine) coated polyethylene film samples using optical density (720 nm) and quantum yield respectively. Data obtained by Mike Packer and Henry Kasper.

6.4 Discussion

The plasma deposited coatings investigated in this study do not utilise any harmful antimicrobial additives, which is important for addressing environmental toxicity concerns. Given that low duty cycle pulsed plasma polymer coating surfaces tend to be smooth in nature, the water repellency of the pulsed plasma polymer layers correlates to the chemical functional groups.^{25,26} For the case of the zinc oxide layer, there is inherent hydrophobicity due to the Cassie-Baxter

effect trapped gas layer²⁷, however this air layer will collapse during prolonged immersion in aqueous media, leading to some hydrophilicity due to hydroxyl groups, which in conjunction with the antimicrobial properties of zinc oxide, provides some degree of antifouling performance.¹⁸ The most hydrophilic nanocoating surface (pulsed plasma poly(vinylpyridine)) showed the best antifouling behaviour, Figure 6.4. Whilst the good performance noted for pulsed plasma poly(*N*-acryloylsarcosine methyl ester) is consistent with its protein resistance properties.²⁸ Hydrophilic surfaces are able to resist fouling due to the formation of a tightly-bound surface water layer which creates a barrier towards biofoulant attachment.^{29,30,31} Such hydrophilic surfaces typically have the following four characteristics: (i) polar, (ii) hydrogen-bond acceptor, (iii) no hydrogen bond donor groups, and (iv) charge neutral.^{31,32} Pyridine molecule is known to form hydrogen bonds with water molecules (i.e. act as a hydrogen bond acceptor) and form a hydration sphere.^{33,34,35,36} Hence, grafted poly(4-vinylpyridine) coatings are able to resist fouling by bovine serum albumin and human fibrinogen proteins, which is attributable to the presence of the hydration layer.²³

The physical structure of coatings can also play an important role in preventing biofouling of microalgae—for example, biomimetic silicon modified acrylic resin surface moulded from shark skin has been shown to display good antibiofouling against a range of microalgae due to its V-groove riblets and imbricate boundary structure preventing adhesion.³⁷ Hence, pulsed plasma poly(vinylpyridine) nanocoatings applied to such physical structures may enhance the antifouling performance further.

While the prevention of fouling is important for many applications, the encouragement of fouling may be equally desirable, e.g. in bioreactors using surface-dwelling algae/micro-organisms, or in the collection of biomass from dilute suspensions where the usual physical methods (filtration, centrifugation etc.) are not feasible or are expensive (e.g. open ocean).^{38, 39} And so, the utilisation of hydrophobic pulsed plasma nanocoatings (for example hydrocarbon alkyl group variants) would be well suited for such applications.

6.5 Conclusions

Hydrophobic pulsed plasma poly(1H,1H,2H,2H-perfluorooctylacrylate) coating increases the level of microalgae biofouling. Whereas hydrophilic surfaces reduce the extent of biofouling, with the most hydrophilic pulsed plasma poly(vinylpyridine) coating performing the best. Furthermore, this coating was found to be non-toxic towards marine microalgae.

6.6 References

- 1 Alzieu, C. Tributyltin: Case Study of a Chronic Contaminant in the Coastal Environment. *Ocean Coast. Manag.* **1998**, *40*, 23–36.
- 2 Jellali, R.; Kromkamp, J. C.; Campistron, I.; Laguerre, A.; Lefebvre, S.; Perkins, R. G.; Pilard, J. F.; Mouget, J. L. Antifouling Action of Polyisoprene-Based Coatings by Inhibition of Photosynthesis in Microalgae. *Environ. Sci. Technol.* **2013**, *47*, 6573–6581.
- 3 Natarajan, S.; Lakshmi, D. S.; Thiagarajan, V.; Mrudula, P.; Chandrasekaran, N.; Mukherjee, A. Antifouling and Anti-Algal Effects of Chitosan Nanocomposite (TiO₂/Ag) and Pristine (TiO₂ and Ag) Films on Marine Microalgae *Dunaliella Salina*. *J. Environ. Chem. Eng.* **2018**, *6*, 6870–6880.
- 4 Ren, J.; Han, P.; Wei, H.; Jia, L. Fouling-Resistant Behavior of Silver Nanoparticle-Modified Surfaces against the Bioadhesion of Microalgae. *ACS Appl. Mater. Interfaces* **2014**, *6*, 3829–3838.
- 5 S. Yu, Y. Yin and J. Liu, Silver Nanoparticles in the Environment. *Environ. Sci.: Processes Impacts*, **2013**, *15*, 78–92.
- 6 Panáček, A.; Kvítek, L.; Smékalová, M.; Večeřová, R.; Kolář, M.; Röderová, M.; Dyčka, F.; Šebela, M.; Pucek, R.; Tomanec, O.; Zbořil, R. Bacterial Resistance to Silver Nanoparticles and How to Overcome It. *Nat. Nanotechnol.* **2018**, *13*, 65–71.
- 7 Bai, X.; Li, J.; Zhu, L.; Wang, L. Effect of Cu Content on Microstructure, Mechanical and Anti-Fouling Properties of TiSiN-Cu Coating Deposited by Multi-Arc Ion Plating. *Appl. Surf. Sci.* **2018**, *427*, 444–451.
- 8 Thomas, K. V.; Brooks, S. The Environmental Fate and Effects of Antifouling Paint Biocides. *Biofouling* **2010**, *26*, 73–88.
- 9 Venault, A.; Ballad, M. R. B.; Huang, Y. T.; Liu, Y. H.; Kao, C. H.; Chang, Y. Antifouling PVDF Membrane Prepared by VIPS for Microalgae Harvesting. *Chem. Eng. Sci.* **2016**, *142*, 97–111.
- 10 Jellali, R.; Kromkamp, J. C.; Campistron, I.; Laguerre, A.; Lefebvre, S.; Perkins, R. G.; Pilard, J. F.; Mouget, J. L. Antifouling Action of Polyisoprene-Based Coatings by Inhibition of Photosynthesis in Microalgae. *Environ. Sci. Technol.* **2013**, *47*, 6573–6581.
- 11 Huang, R.; Liu, Z.; Yan, B.; Li, Y.; Li, H.; Liu, D.; Wang, P.; Cui, F.; Shi, W. Layer-by-Layer Assembly of High Negatively Charged Polycarbonate Membranes with Robust Antifouling Property for Microalgae Harvesting. *J. Memb. Sci.* **2020**, *595*, 117488.
- 12 Ryan, M. E.; Hynes, A. M.; Badyal, J. P. S. Pulsed Plasma Polymerization of Maleic Anhydride. *Chem. Mater.* **1996**, *8*, 37–42.
- 13 Carletto, A.; Badyal, J. P. S. Ultra-High Selectivity Pulsed Plasmachemical Deposition Reaction Pathways. *Phys. Chem. Chem. Phys.* **2019**, *21*, 16468–16476.
- 14 Miller, T. A.; Mikhael, M. G.; Ellwanger, R.; Boufelfel, A.; Booth, D.; Yializis, A. Polymer Multi-Layer Processing of Thin Film Materials. *MRS Proceedings* **1999**, *555*, 247–254
- 15 Tredici, M. R.; Biondi, N.; Ponis, E.; Rodolfi, L.; Chini Zittelli, G. Advances in Microalgal Culture for Aquaculture Feed and Other Uses. In *New Technologies in Aquaculture*:

- Improving Production Efficiency, Quality and Environmental Management; G. Burnell, G. Allan (Eds.), CRC Press, Boca Raton 2009; pp 610–676.
- 16 Ragg, N. L. C.; King, N.; Watts, E.; Morrish, J. Optimising the Delivery of the Key Dietary Diatom *Chaetoceros calcitrans* to Intensively Cultured Greenshell™ Mussel Larvae, *Perna Canaliculus*. *Aquaculture* **2010**, *306*, 270–280.
 - 17 Kaspar, H. F.; Keys, E. F.; King, N.; Smith, K. F.; Kesarcodi-Watson, A.; Miller, M. R. Continuous Production of *Chaetoceros calcitrans* in a System Suitable for Commercial Hatcheries. *Aquaculture* **2014**, *420–421*, 1–9.
 - 18 Wood, T. J.; Hurst, G. A.; Schofield, W. C. E.; Thompson, R. L.; Oswald, G.; Evans, J. S. O.; Sharples, G. J.; Pearson, C.; Petty, M. C.; Badyal, J. P. S. Electroless Deposition of Multi-Functional Zinc Oxide Surfaces Displaying Photoconductive, Superhydrophobic, Photowetting, and Antibacterial Properties. *J. Mater. Chem.* **2012**, *22*, 3859–3867.
 - 19 Rolton, A.; McCullough, A.; Tuckey, N. P. L.; Finnie, B.; Cooper, I.; Packer, M. A.; Vignier, J. Early Biomarker Indicators of Health in Two Commercially Produced Microalgal Species Important for Aquaculture. *Aquaculture* **2020**, *521*, 735053.
 - 20 Freda, M.; Piluso, A.; Santucci, A.; Sassi, P. Transmittance Fourier Transform Infrared Spectra of Liquid Water in the Whole Mid-Infrared Region: Temperature Dependence and Structural Analysis. *Appl. Spectrosc.* **2005**, *59*, 1155–1159.
 - 21 Madikizela, L. M.; Mdluli, P. S.; Chimuka, L. Experimental and Theoretical Study of Molecular Interactions between 2-Vinyl Pyridine and Acidic Pharmaceuticals Used as Multi-Template Molecules in Molecularly Imprinted Polymer. *React. Funct. Polym.* **2016**, *103*, 33–43.
 - 22 Bradley, T. J.; Schofield, W. C. E.; Garrod, R. P.; Badyal, J. P. S. Electroless Metallization onto Pulsed Plasma Deposited Poly(4-Vinylpyridine) Surfaces. *Langmuir* **2006**, *22*, 7552–7555.
 - 23 Raczowska, J.; Stetsyshyn, Y.; Awsiuk, K.; Zemła, J.; Kostruba, A.; Harhay, K.; Marzec, M.; Bernasik, A.; Lishchynskiy, O.; Ohar, H.; Budkowski, A. Temperature-Responsive Properties of Poly(4-Vinylpyridine) Coatings: Influence of Temperature on the Wettability, Morphology, and Protein Adsorption. *RSC Adv.* **2016**, *6*, 87469–87477.
 - 24 Ibrahim, I. M.; Yunus, S.; Hashim, M. A. Relative Performance of Isoproopylamine, Pyrrole and Pyridine as Corrosion Inhibitors for Carbon Steels in Saline Water at Mildly Elevated Temperatures. *Int. J. Sci. Eng. Res.* **2013**, *4*.
 - 25 Coulson, S. R.; Woodward, I. S.; Badyal, J. P. S.; Brewer, S. A.; Willis, C. Ultralow Surface Energy Plasma Polymer Films. *Chem. Mater.* **2000**, *12*, 2031–2038.
 - 26 Morsch, S.; Schofield, W. C. E.; Badyal, J. P. S. Surface Actuation of Smart Nanoshutters. *Langmuir* **2010**, *26*, 12342–12350.
 - 27 Cassie, A. B. D.; Baxter, S. Wettability of Porous Surfaces. *Trans. Faraday Soc.* **1944**, *40*, 546–551.
 - 28 Teare, D. O. H.; Schofield, W. C. E.; Garrod, R. P.; Badyal, J. P. S. Poly(N-acryloylsarcosine methyl ester) Protein-Resistant Surfaces. *J. Phys. Chem. B* **2005**, *109*, 20923–20928.
 - 29 Chen, S.; Li, L.; Zhao, C.; Zheng, J. Surface Hydration: Principles and Applications Toward Low-Fouling/Nonfouling Biomaterials. *Polymer (Guildf)*. **2010**, *51*, 5283–5293.

- 30 Harder, P.; Grunze, M.; Dahint, R.; Whitesides, G. M.; Laibinis, P. E. Molecular Conformation in Oligo(Ethylene Glycol)-Terminated Self-Assembled Monolayers on Gold and Silver Surfaces Determines Their Ability to Resist Protein Adsorption. *J. Phys. Chem. B* **1998**, *102*, 426–436.
- 31 Ostuni, E.; Chapman, R. G.; Holmlin, R. E.; Takayama, S.; Whitesides, G. M. A Survey of Structure-Property Relationships of Surfaces That Resist the Adsorption of Protein. *Langmuir* **2001**, *17*, 5605–5620.
- 32 Chapman, R. G.; Ostuni, E.; Takayama, S.; Holmlin, R. E.; Yan, L.; Whitesides, G. M. Surveying for Surfaces That Resist the Adsorption of Proteins. *J. Am. Chem. Soc.* **2000**, *122*, 8303–8304.
- 33 Johnson, J. R.; Kilpatrick, P. J.; Christian, S. D.; Afsprung, H. E. The Hydration of Pyridine in Organic Solvents. *J. Phys. Chem.* **1968**, *72*, 3223–3229.
- 34 Choudhary, A.; Chandra, A. Spatially Resolved Structure and Dynamics of the Hydration Shell of Pyridine in Sub- and Supercritical Water. *J. Mol. Liq.* **2019**, *287*, 110881.
- 35 Schlücker, S.; Singh, R. K.; Asthana, B. P.; Popp, J.; Kiefer, W. Hydrogen-Bonded Pyridine-Water Complexes Studied by Density Functional Theory and Raman Spectroscopy. *J. Phys. Chem. A* **2001**, *105*, 9983–9989.
- 36 Sicilia, M. C.; Niño, A.; Muñoz-Caro, C. Mechanism of Pyridine Protonation in Water Clusters of Increasing Size. *J. Phys. Chem. A* **2005**, *109*, 8341–8347.
- 37 Zhang, Y.; Zhao, W.; Chen, Z.; Liu, Z.; Cao, H.; Zhou, C.; Cui, P. Influence of Biomimetic Boundary Structure on the Antifouling Performances of Siloxane Modified Resin Coatings. *Colloids Surfaces A Physicochem. Eng. Asp.* **2017**, *528*, 57–64.
- 38 Milledge, J. J.; Heaven, S. A Review of the Harvesting of Micro-Algae for Biofuel Production. *Rev. Environ. Sci. Biotechnol.* **2013**, *12*, 165–178.
- 39 Singh, G.; Patidar, S. K. Microalgae Harvesting Techniques: A Review. *J. Environ. Manage.* **2018**, *217*, 499–508.

Chapter 7

7 Conclusions and Further Work

7.1 Conclusions

Antimicrobial surfaces offer a potential route to stop the spread of pathogens where other methods (such as those reviewed in chapter 2) are not appropriate or available. In chapter 3, adhesive polymer polydopamine is combined with antibacterial bioderived cinnamaldehyde to produce an antibacterial coating. The cinnamaldehyde is believed to react with the dopamine as it polymerises, leading to incorporation of cinnamaldehyde in the coating. The coating's antibacterial activity was tested using Gram-negative *Escherichia coli* and Gram-positive *Staphylococcus aureus*, in order to demonstrate broad-spectrum antibacterial activity, and was found to produce a strong antibacterial effect against both bacteria, giving complete killing ($\sim 8\text{-Log}_{10}$ Reduction compared to the untreated substrates). The longevity of the coatings antibacterial activity was examined by recycling the same samples for multiple tests, and it was found that the polydopamine–cinnamaldehyde coating could last for 10 tests before complete loss of activity, with the activity dropping off after the first two tests. Tannic acid, a compound derived from plants, which also forms adhesive coatings, was combined with cinnamaldehyde. The tannic acid–cinnamaldehyde coating was also found to produce strong antibacterial effects against both bacteria ($\sim 8\text{-Log}_{10}$ Reduction). The antibacterial reusability of this coating lasted for 5 cycles, due to it being thinner than the polydopamine–cinnamaldehyde coating. Tannic acid represents a cheaper, bioderived alternative to polydopamine. Both coatings use simple, one-pot, single-step methods. Since the cinnamaldehyde is believed to have reacted with the amine group on the dopamine molecule (as demonstrated *via* reaction of cinnamaldehyde with phenethylamine), cinnamaldehyde was combined with polyethyleneimine, a polymer containing numerous amine groups, to produce another antibacterial coating. Polyethyleneimine–cinnamaldehyde coating showed the weakest antibacterial activities of the three coatings, but nonetheless demonstrates further how cinnamaldehyde may be combined with polymers. Finally, porous non-woven polypropylene cloth was either impregnated with cinnamaldehyde, or coated with polydopamine–cinnamaldehyde. Antibacterial recycling tests showed that both systems had long-lasting, strong antibacterial activities.

In chapter 4, the tannic acid–cinnamaldehyde coating method is further extended to utilise tea in combination with cinnamaldehyde. The tea–cinnamaldehyde coating was characterised, and shown to exhibit complete killing of *E. coli* and *S. aureus*. The coating is further derivatised *via* addition of copper or silver metals. The resulting tea–cinnamaldehyde–copper and tea–cinnamaldehyde–silver coatings were tested for antiviral activities against murine coronavirus MHV-A59, a potential surrogate for SARS-CoV-2. Both were found to give a reduction in the viral titre, with the silver coating having a slightly stronger effect (98.6% and 99.8% respectively). The tea–cinnamaldehyde coatings utilise a single-step, one-pot, simple coating method, that uses cheap readily-available materials.

In chapter 5, pulsed plasma polymer thin films are deposited onto substrates, and subsequently treated with lubricant liquids to produce stable slippery liquid-infused surfaces. A variety of plasma polymers are examined and a structure-behaviour relationship is established. The liquid-infused coatings show good water repellency. A perfluorinated pulsed plasma polymer and lubricants system showed omniphobic slippery behaviour against water and a selection of oils. Lubricant infused pulsed plasma poly(vinylaniline) could repel viscous foodstuffs, tomato ketchup and honey. Use of cinnamaldehyde as a lubricant led to slippery surfaces with strong antibacterial activities against both *E. coli* and *S. aureus*.

Chapter 6 demonstrates how pulsed plasma polymer thin film coatings can be used to reduce (or potentially encourage) biofouling by microalgae. Hydrophilic coatings, such as pulsed plasma poly(vinylpyridine) can prevent biofouling due to the presence of an associated hydration layer that stops microalgae from attaching to the surface, whereas hydrophobic coatings (such as pulsed plasma poly(1H,1H,2H,2H-perfluorooctylacrylate) were found to increase biofouling compared to the untreated substrate.

Overall, wet chemical methods that combine adhesive polymers or (bioderived) compounds and bioderived cinnamaldehyde offer a simple, cheap, accessible, and effective route for the production of antibacterial coatings. Pulsed plasma polymers provide effective means of fabrication of multifunctional antibacterial coatings, as well as antibiofouling coatings.

7.2 Further Work

All of the antibacterial coatings reported in chapters 3, 4, and 5 utilise cinnamaldehyde as the antibacterial agent. There does however exist a wide variety of bioderived organic compounds found in nature that also exhibit antibacterial activities. Therefore, further work could involve the use of such compounds in combination with polydopamine, tannic acid, tea, and pulsed plasma polymers to produce alternative antimicrobial coatings, with targeted or broad-spectrum activities. In chapter 4, only one type of green tea was utilised. There are of course many other types of teas available (e.g. black tea, white tea, etc.), which could be tested to examine their abilities to form coatings. Also in chapter 4, copper and silver were used in coatings separately, however, it may be possible to combine them to form an alloy coating (i.e. tea–cinnamaldehyde–copper–silver), and examine its antiviral activities. Ultimately, all three of these previous points could be combined, to utilise a range of bioderived antimicrobial compounds, a range of teas, and different combinations of metals, in order to produce a host of antimicrobial coatings. In chapter 5, the monomers used for pulsed plasma polymerisation are all synthetic. There are compounds found in nature that contain polymerisable carbon-carbon double bonds (for example, cinnamaldehyde itself) that could potentially be used to produce plasma polymer thin films, that in turn could be used to form completely bioderived slippery liquid-infused surface coatings. In chapter 6, the pulsed plasma thin film coatings were deposited onto polyethylene as-is. As mentioned in section 6.4, the physical structure of a surface also is important to its anti-biofouling capabilities. Therefore, the pulsed plasma coatings, which are substrate-independent and conformal, could be combined with physically structured anti-biofouling coatings to further enhance their anti-biofouling abilities.

Appendix 1

A1.1 Introduction

'Calixarenes' are a class of cyclic, oligomeric compound, formed from the reaction between a phenol and formaldehyde.¹ Calixarenes appear to be a promising candidate for making antibacterial compounds, owing to their synthetic versatility, i.e. the range of functional groups and compounds that can be added to the basic calixarene structure, and the ease with which they can be added on. One report has previously shown that calix[4]arene with $-\text{CH}_2\text{CH}_2\text{NH}_2$ amine groups attached to the upper-rim have an antibacterial effect against *M. tuberculosis*.² DMAM-calixarene (full name: 5,11,17,23-tetrakis[(dimethylamino)methyl]-25,26,27,28-tetrahydroxycalix[4]arene), Figure A1.1, contains tertiary amine groups on the upper-rim, and has previously been immobilised onto bulk poly(vinylbenzyl chloride).³

In this study, pulsed plasma poly(vinylbenzyl chloride) is deposited onto non-woven polypropylene cloth, and DMAM-calixarene is immobilised onto the surface *via* Williamson ether reaction of the calixarene $-\text{OH}$ with the surface chloride groups, Figure A1.2. The antibacterial activity of this coating is examined.

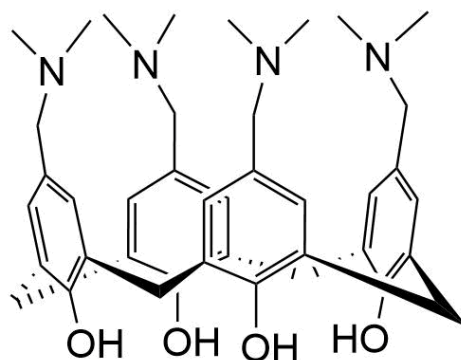


Figure A1.1: Structure of 5,11,17,23-tetrakis[(dimethylamino)methyl]-25,26,27,28-tetrahydroxycalix[4]arene (DMAM-calixarene).

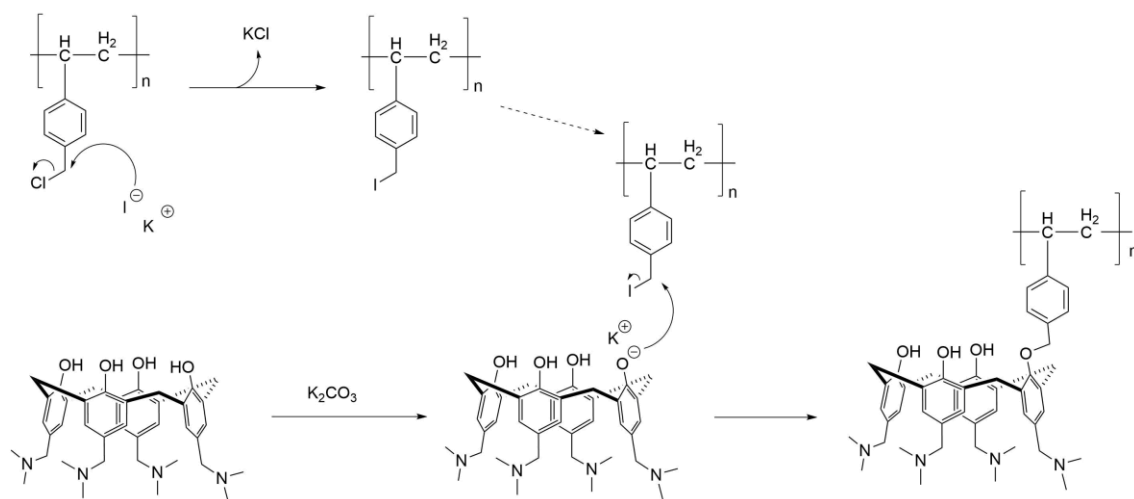


Figure A1.2: Mechanism for the immobilisation of DMAM-calixarene onto poly(vinylbenzyl chloride).

A1.2 Experimental

A1.2.1 Pulsed Plasma Deposition

Pulsed plasma deposition of vinylbenzyl chloride (97%, mixture of 2-, 3- and 4-isomers, Sigma-Aldrich Inc.) on non-woven polypropylene cloth (taken from the middle layer of disposable surgical masks, 80 μm thickness, $5.0 \pm 1.5 \mu\text{m}$ fiber diameter, SD Medical Ltd.) was carried out as described in section 2.1. The fabric was rinsed with ethanol and thoroughly dried in air prior to plasmachemical surface functionalization. Coating was performed on both sides of the cloth in two separate experiments.

A1.2.2 DMAM-Calixarene Immobilisation

DMAM-calixarene (13.4 mg, synthesized by Egemen Ozcelik, Mustafa Karaman, and Mustafa Tabakci (Chemical Engineering Department, Konya Technical University) according to previous literature³), potassium carbonate (27.6 mg, >99.0%, Sigma-Aldrich Inc.), and potassium iodide (43.2 mg, 99+%, Sigma-Aldrich Inc.) and acetone (50 ml, Fisher Scientific Ltd.) were combined in a glass jar. Pulsed plasma poly(vinylbenzyl chloride) coated cloth was cut into quarters (approximately 60 x 70 mm), and one quarter was immersed into the solution. The jar was sealed and left on shaker at 20 °C for 48 h. Samples were removed and washed in acetone for 20 s, followed by high-purity water for 15 min with shaking, and then air-drying.

A1.2.3 Characterisation

XPS of the DMAM-calixarene immobilised cloths was carried out as described in section 2.7. 10 x 10 mm squares were cut out for analysis. Elemental concentrations were calculated using instrument sensitivity (multiplication) factors determined from chemical standards, C(1s) : N(1s) : O(1s) : Cl(2p) = 1.00 : 0.70 : 0.35 : 0.37.

A1.2.4 Antibacterial Testing

Antibacterial testing was carried out as described in section 2.3, with the modification that samples treated with bacteria inoculum were incubated for 16 h, not 4 h.

A1.3 Results

A1.3.1 Characterisation

XPS analysis of poly(vinylbenzyl chloride) coated polypropylene cloth showed good agreement with the theoretical atom percentages expected from poly(vinylbenzyl chloride), Table A1.1. (The small quantity of oxygen likely occurs due to oxidation of the polymer coating in air before it is transferred to the XPS instrument.) DMAM-calixarene immobilised on polypropylene cloth shows an increase in both nitrogen and oxygen, and a decrease in chlorine at the surface, indicating that the DMAM-calixarene has been successfully immobilised on the surface, Table A1.1. The detection of some chlorine atoms is either due to not all of the surface chloride groups reacting, or due to subsurface chlorine atoms being detected.

Table A1.1: XPS compositions for vinylbenzyl chloride (VBC, Theoretical); pulsed plasma deposited poly(vinylbenzyl chloride) (pp-VBC); one unit of vinylbenzyl chloride reacted with one DMAM-calixarene molecule; and pulsed plasma-deposited poly(vinylbenzyl chloride) subsequently functionalized with DMAM-calixarene.

Surface	Composition / atom %			
	C	N	O	Cl
VBC (Theoretical)	90	0	0	10
pp-VBC (Experimental)	90.9 ± 0.5	0	0.3 ± 0.4	8.8 ± 0.2
VBC + DMAM-Calix (Theoretical)	86.0	7.0	7.0	0
pp-VBC + DMAM-Calix (Experimental)	83.7 ± 1.3	3.4 ± 0.9	10.0 ± 1.0	3.1 ± 0.8

It is useful to know how many of the surface chloride groups have reacted with a DMAM-calixarene molecule (i.e. the percentage conversion). An equation relating the fraction of nitrogen atoms, [N], at the surface, to the conversion fraction, x , can be derived as follows:

The fraction of nitrogen will be equal to the amount of nitrogen atoms in the product divided by the total number of atoms in the product. The number of nitrogen atoms can be expressed as the initial amount of chlorine atoms, $[Cl]_0$ (because the calixarene is replacing the chlorine atom on the polymer), multiplied by 4 (because each calixarene contains 4 nitrogen atoms, and therefore each chlorine atom is replaced with 4 nitrogen atoms, assuming only one oxygen atom per calixarene reacts with the surface), multiplied by the conversion factor, x (where a value of 0 means no reaction, and a value of 1 means all chlorine atoms have been replaced). This gives the amount of nitrogen present after reaction as:

$$\text{Amount of nitrogen atoms} = 4x[Cl]_0$$

The total number of atoms present will be equal to the initial number of carbon atoms present, $[C]_0$ (the initial number of carbon atoms is unaffected by reaction), plus the initial number of chlorine atoms present, $[Cl]_0$, plus 47 multiplied by $[Cl]_0$ (this is because each time a Cl atom is replaced by a calixarene (which contains 48 non-hydrogen atoms), the overall increase in atoms is 47), multiplied by x . Therefore, the total number of atoms present in the product can be expressed as:

$$\text{Total amount of atoms} = [C]_0 + [Cl]_0 + 47x[Cl]_0$$

(The derivation of this equation can be also achieved via another slightly different method: the total number of atoms present will be equal to the initial number of

carbon atoms present, $[C]_0$, plus $(1 - x)[Cl]_0$ (since the chlorine atoms are being removed, and must decrease linearly as x increases from 0 to 1), plus $48x[Cl]_0$ (because each time a chlorine is replaced, a calixarene which has 48 non-hydrogen atoms replaces it). This gives the following equation:

$$\text{Total amount of atoms} = [C]_0 + (1 - x)[Cl]_0 + 48x[Cl]_0$$

(Expansion of the brackets and simplification then give the exact same equation as previously derived above.)

The two statements, 'amount of nitrogen atoms' and 'total amount of atoms' can be combined to give the equation for the fraction of nitrogen atoms present at the surface of the sample (and to make it a percentage, the equation is multiplied by 100, as shown):

$$[N](\%) = \frac{4x[Cl]_0}{[C]_0 + [Cl]_0 + 47x[Cl]_0} \times 100$$

Using the atom % values measured with XPS for each sample, the equation can be used to determine the value of x , i.e. the amount of conversion. This can be multiplied by 100 to give percentage conversion. Doing so gives a mean conversion value of 14%. It has been assumed that each calixarene only reacts with one chlorine, when in reality each calixarene may react with two, three or four chlorides. Therefore, this value should only be taken as a rough estimate.

A1.3.2 Antibacterial Testing

DMAM-calixarene immobilised polypropylene cloths were tested for antibacterial activity against *E. coli*, Figure A1.3. The DMAM-calixarene immobilised polypropylene cloths were found not to produce any reduction in the number of bacteria relative to the control. The DMA-calixarene immobilised cloth therefore has no antibacterial properties. (No testing was performed on *S. aureus*).

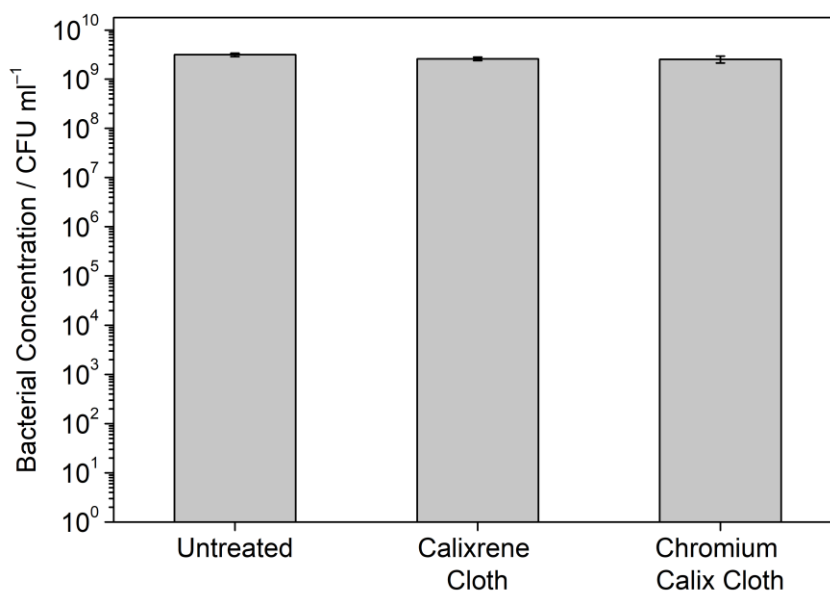


Figure A1.3: *E. coli* bacterial concentrations after treatment with: control untreated non-woven polypropylene cloth; DMAM-calixarene immobilised cloth; and DMAM-calixarene immobilised cloth used for dichromate filtration prior to antibacterial testing.

A1.3.3 Chromium Filtration

The DMAM-calixarene immobilised cloths were used for filtration/removal of toxic Cr(VI) ions (e.g. $\text{Cr}_2\text{O}_7^{2-}$) from polluted water (work performed by Vera Bieber, Durham University).⁴ Since Cr(VI) oxyanions are known to be toxic towards bacteria⁵, DMAM-calixarene immobilised cloth was used to filter water spiked with dichromate (in order to saturate the DMAM-calixarene molecules), and it was examined whether the cloth becomes antibacterial after it had been used for filtration. However, testing against *E. coli* again showed no reduction in bacteria concentration compared to the control untreated cloth, Figure A1.3. The chromium–DMAM-calixarene immobilised cloth was therefore not antibacterial.

A1.4 Conclusions

Pulsed plasma poly(vinylbenzyl chloride) was deposited onto non-woven polypropylene cloth. DMAM-calixarene was reacted with the chloride groups and immobilised onto the surface of the cloths. The DMAM-calixarene immobilised cloths were tested for their antibacterial activity, and were found not to kill *E. coli*. DMAM-calixarene immobilised cloths were used for Cr(VI) filtration and

subsequent antibacterial testing, but the chromium–DMAM-calixarene immobilised cloths were also found not to exhibit any antibacterial behaviour.

A1.5 References

- 1 Gutsche, C. D.; Lin, L. G. Calixarenes 12. The Synthesis of Functionalized Calixarenes. *Tetrahedron* **1986**, *42*, 1633–1640.
- 2 Mourer, M.; Massimba Dibama, H.; Constant, P.; Daffé, M.; Regnouf-De-Vains, J. B. Anti-Mycobacterial Activities of Some Cationic and Anionic calix[4]arene Derivatives. *Bioorganic Med. Chem.* **2012**, *20*, 2035–2041.
- 3 Memon, S.; Tabakci, M.; Roundhill, D. M.; Yilmaz, M. Synthesis and Evaluation of the Cr(VI) Extraction Ability of Amino/Nitrile Calix[4]arenes Immobilized onto a Polymeric Backbone. *React. Funct. Polym.* **2006**, *66*, 1342–1349
- 4 Bieber, V. S.; Ozelik, E.; Cox, H. J.; Ottley, C. J.; Ratan, J. K.; Karaman, M.; Tabakci, M.; Beaumont, S. K.; Badyal, J. P. S. Capture and Release Recyclable Dimethylaminomethyl-Calixarene Functional Cloths for Point-of-Use Removal of Highly Toxic Chromium Water Pollutants. *ACS Appl. Mater. Interfaces* **2020**, *12*, 52136–52145.
- 5 Megharaj, M.; Avudainayagam, S.; Naidu, R. Toxicity of Hexavalent Chromium and Its Reduction by Bacteria Isolated from Soil Contaminated with Tannery Waste. *Curr. Microbiol.* **2003**, *47*, 51–54.

Appendix 2

A2.1 Introduction

In Chapter 1 of this thesis, it was described that quaternary ammonium compounds have an antibacterial effect. Previously, pulsed plasma poly(vinylpyridine) coating quaternised with bromobutane has been shown to produce substrate-independent antibacterial surfaces.¹ There has also been a report where pulsed plasma poly(vinylbenzyl chloride) was reacted with butylimidazole to produce poly(ionic liquid) functional coatings, Figure A2.1.² However, the antibacterial activities of this particular coating have previously not been examined.

In this study, quaternised pulsed plasma poly(vinylbenzyl chloride)–butylimidazole coating is synthesised on non-woven polypropylene cloth, and the antibacterial activities are examined.

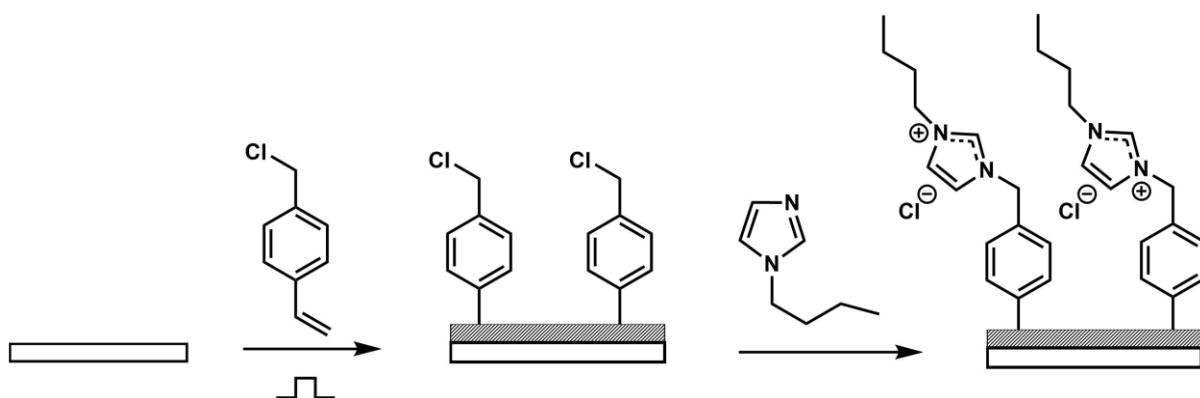


Figure A2.1: Schematic for coating of pulsed plasma poly(vinylbenzyl chloride) and quaternisation with butylimidazole.

A2.2 Experimental

A2.2.1 Pulsed Plasma Deposition

Pulsed plasma deposition of vinylbenzyl chloride (97%, mixture of 2-, 3- and 4-isomers, Sigma-Aldrich Inc.) on non-woven polypropylene cloth (0.41 mm thick, $22.7 \pm 4.4 \mu\text{m}$ fibre diameter, with dimpled structure $0.68 \pm 0.16 \text{ mm}$ separation, spunbond, 70 g m^{-2} , Avoca Technical Ltd.) was carried out as described in section 2.1. The fabric was rinsed with ethanol and thoroughly dried in air prior to plasmachemical surface functionalization. Coating was performed on both sides of the cloth simultaneously in one experiment.

A2.2.2 Quaternization

1-Butylimidazole (4 ml, 98%, Sigma-Aldrich Inc.) and N,N-dimethylformamide (24 ml, HPLC grade, >99.7%, Fisher Scientific UK Ltd.) were combined in a round bottom flask. The poly(vinylbenzyl chloride) coated polypropylene cloth was cut into 15 x 15 mm pieces which were immersed into the solution. A condenser was attached to the flask, and the solution was heated to 70 °C for 16 h. The solution was allowed to cool, then samples were removed, and washed in N,N-dimethylformamide for 5 min with shaking, followed by washing in high-purity water for 5 min with shaking, and then fully air dried.

A2.2.3 Characterisation

XPS of the pulsed plasma poly(vinylbenzyl chloride)–butylimidazole quaternised coated cloths was carried out as described in section 2.7. 10 x 10 mm squares were cut out for analysis. Elemental concentrations were calculated using instrument sensitivity (multiplication) factors determined from chemical standards, C(1s) : N(1s) : O(1s) : Cl(2p) = 1.00 : 0.70 : 0.35 : 0.37.

A2.2.4 Antibacterial Testing

Antibacterial testing of the poly(vinylbenzyl chloride)–butylimidazole quaternised coated cloths was carried out as described in section 2.3, with the modification that samples treated with bacteria inoculum were incubated for 16 h, not 4 h.

A2.3 Results

A2.3.1 Characterisation

XPS analysis of pulsed plasma poly(vinylbenzyl chloride) coated polypropylene cloth showed good agreement with the theoretical atom percentages expected from poly(vinylbenzyl chloride), Table A2.1. (The small quantity of oxygen likely occurs due to oxidation of the polymer coating in air before it is transferred to the XPS instrument.) Quaternized poly(vinylbenzyl chloride)–butylimidazole coated cloths show the presence of nitrogen, indicating quaternisation has indeed taken place, Table A2.1. The detection of some oxygen atoms is likely caused by oxidation of the coating during heating.

Table A2.1: XPS compositions for vinylbenzyl chloride (VBC, Theoretical); pulsed plasma deposited poly(vinylbenzyl chloride) (pp-VBC); one unit of vinylbenzyl chloride reacted with one butylimidazole molecule; and pulsed plasma-deposited poly(vinylbenzyl chloride) subsequently functionalized with butylimidazole.

Surface	Composition / atom %			
	C	N	O	Cl
pp-VBC (Theoretical)	90	0	0	10
pp-VBC (Experimental)	90.9 ± 0.5	0	0.3 ± 0.4	8.8 ± 0.2
pp-VBC–Butylimidazole (Theoretical)	84.2	10.5	0	5.3
pp-VBC–Butylimidazole (Experimental)	86.0 ± 0.3	5.4 ± 0.7	5.3 ± 0.8	3.3 ± 0.3

The percentage of quaternisation can be calculated from the XPS Cl peaks. Upon quaternisation, the Cl peak undergoes a binding energy shift of a few eV since the C–Cl becomes a Cl⁻ ion, Figure A2.2. By taking the ratio of the peak areas of the C–Cl and Cl⁻ peaks, the level of quaternisation can be determined. The quaternisation level was determined to be 47 ± 5%.

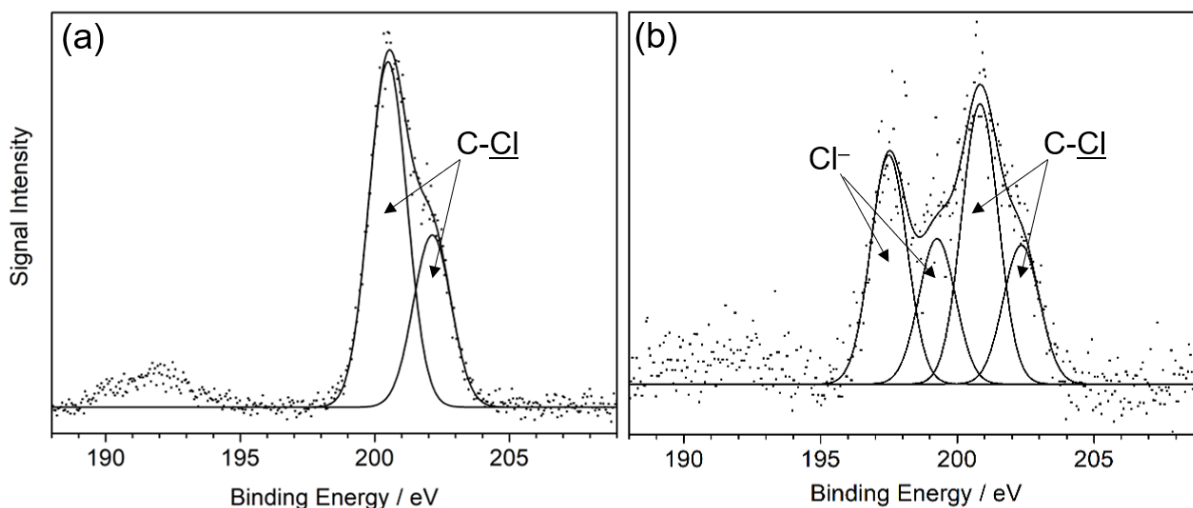


Figure A2.2: XPS spectra Cl fine scans of coatings on polypropylene cloth: (a) pulsed plasma poly(vinylbenzyl chloride); and (b) quaternised pulsed plasma poly(vinylbenzyl chloride)–butylimidazole.

A2.3.2 Antibacterial Testing

Quaternised pulsed plasma poly(vinylbenzyl chloride)–butylimidazole coated polypropylene cloths were tested for antibacterial activity against *E. coli* and *S.*

aureus, Figure A2.3. Against *E. coli*, the cloths had a small effect, Log_{10} Reduction = 0.4 ± 0.1 (59% reduction), and against *S. aureus*, the coating had a slightly stronger antibacterial effect, Log_{10} Reduction = 1.4 ± 0.1 (96% reduction).

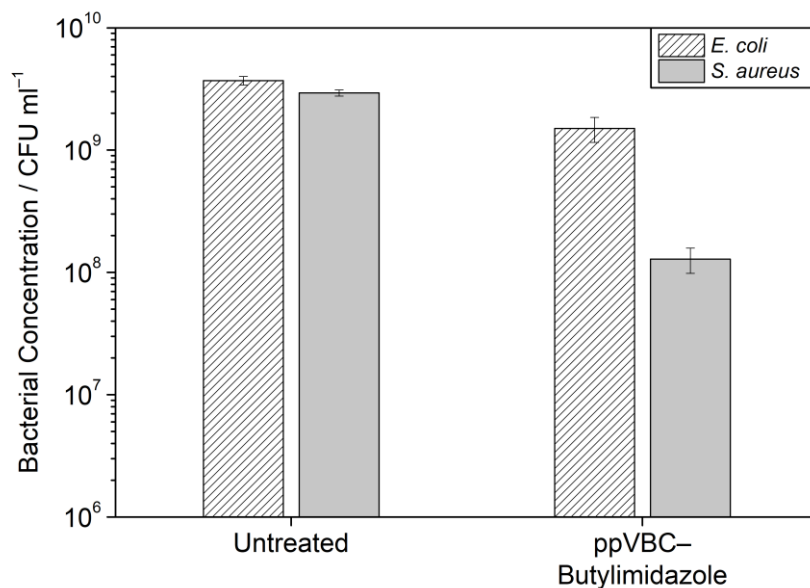


Figure A2.3: *E. coli* bacterial concentrations after treatment with: control untreated non-woven polypropylene cloth; and quaternised pulsed plasma poly(vinylbenzyl chloride)–butylimidazole coated polypropylene cloths.

A2.4 Discussion

The antibacterial efficacy of the quaternised pulsed plasma poly(vinylbenzyl chloride)–butylimidazole coating is not particularly high, for example, when compared to the quaternised pulsed plasma poly(vinylpyridine) coatings, which could achieve Log_{10} Reduction = 4.4 against both *Klebsiella pneumoniae* and *S. aureus*.¹

A2.5 Conclusions

Pulsed plasma poly(vinylbenzyl chloride) was deposited onto non-woven polypropylene cloth, and quaternised with butylimidazole. The coating was found to have a small antibacterial effect against both *E. coli* and *S. aureus*.

A2.6 References

- 1 Schofield, W. C. E.; Badyal, J. P. S. A Substrate-Independent Approach for Bactericidal Surfaces. *ACS Appl. Mater. Interfaces* **2009**, *1*, 2763–2767.
- 2 Wilson, M.; Kore, R.; Ritchie, A. W.; Fraser, R. C.; Beaumont, S. K.; Srivastava, R.; Badyal, J. P. S. Palladium–Poly(Ionic Liquid) Membranes for Permselective Sonochemical Flow Catalysis. *Colloids Surfaces A Physicochem. Eng. Asp.* **2018**, *545*, 78–85.

Appendix 3

A3.1 Introduction

Poly(ethylene glycol) coatings are found in many technological applications including photoinduced microstructures,¹ protein resistant films, piezoelectric materials,² hydrogels,³ biosensors,^{4,5,6} drug delivery,^{7,8,9} proton conducting membranes,^{10,11} thixotropic cell support,¹² cell imaging,^{13,14} photothermal therapy,^{15,16} tissue engineering,¹⁷ antimicrobial coatings,^{18,19} gas separation,^{20,21} and oxygen scavenging.²² Methods used previously to manufacture poly(ethylene glycol) nanocomposite coatings have included photopolymerization,^{1,23,24} dendrimer mediated stabilization,²⁵ suspension polymerization,² coprecipitation,⁵ sol-gel synthesis,^{10,12} and magnetron sputtering.¹⁹ These methods can be time consuming and expensive,^{5,9,25} require multiple steps,^{5,18} lack precision over coating thickness for miniature device applications,²² or suffer from susceptibility to polymer film damage.¹⁹

Plasmachemical deposition is a versatile, solventless method for the fabrication of functional thin films.²⁶ Its inherent advantages are that it is a one-step technique, which provides conformal coatings for both two- and three-dimensional substrates. Past examples of functionalities prepared by this method have included carboxylic acid,²⁷ anhydride,²⁸ amine,²⁹ cyano,³⁰ epoxide,³¹ halide,³² thiol,³³ furfuryl,³⁴ perfluoroalkyl,³⁵ perfluoromethylene,³⁶ and trifluoromethyl³⁷ groups. In order to achieve high levels of structural retention and deposition rate, one approach is to raise the density of the precursor vapour within the reactor (i.e. increase the pressure / flow rate), such that the average plasma power per reactant molecule decreases.^{26,38} However, there exist limitations due to high precursor vapour pressure / flow rates leading to plasma instabilities / inhomogeneity and eventually extinction. Such shortcomings can be overcome by introducing atomized droplets of the precursor into the plasma excitation zone.^{39,40}

In this appendix chapter, poly(ethylene glycol) nanocomposite coatings are prepared by atomised spray plasma deposition (ASPD) using di(ethylene glycol) ethyl ether acrylate precursor mixed with a biocidal additive in order to generate an antimicrobial coating, Figure A3.1. Synergy is achieved by combining poly(ethylene glycol) protein-resistance with antibacterial efficacy of a double

tailed metallosurfactant species containing two C12 chains coordinated to copper (bis(dodecylamine) copper dichloride), Figure A3.2.

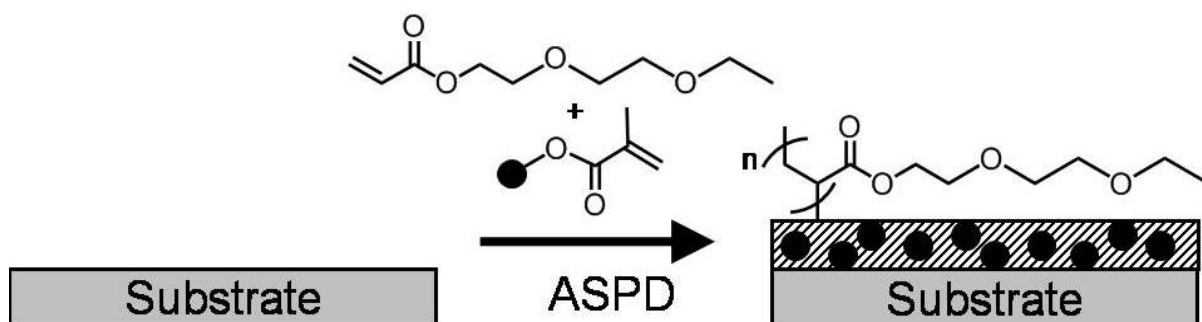


Figure A3.1: Atomized-spray plasmachemical deposited poly(di(ethylene glycol) ethyl ether acrylate) nanocomposite layers with copper (bis(dodecylamine) copper dichloride) metallosurfactant.

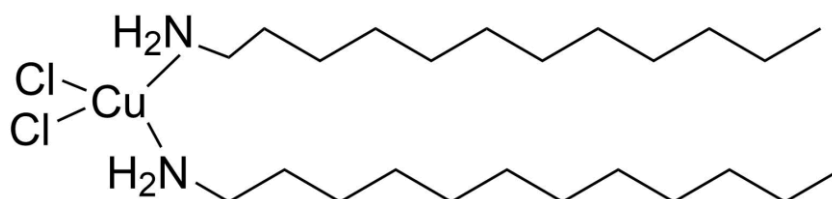


Figure A3.2: Structure of bis(dodecylamine) copper dichloride (Cu(DDA)).

A3.2 Experimental

A3.2.1 Atomised Spray Plasma Deposition of Nanocomposite Layers

For antibacterial coatings, bis(dodecylamine) copper dichloride (CuDDA, 10 mg, synthesised by Preeti Garg and Gurpreet Kaur (Department of Chemistry, Panjab University)) was added to di(ethylene glycol)ethyl ether acrylate (0.5 ml, +90% Aldrich Ltd.), and mixed using an ultrasonic bath for approximately 20 min to ensure full dispersion. Pieces of non-woven polypropylene sheet (0.41 mm thick, $22.7 \pm 4.4 \mu\text{m}$ fibre diameter, with dimpled structure 0.68 ± 0.16 mm separation, Spunbond, 70 g m^{-2} , Avoca Technical Ltd.) were washed in absolute ethanol for 15 min and then dried under vacuum in order to make sure they were sterile and clean (also used as control samples). Both sides of the cloth were coated in separate depositions via atomised spray plasma deposition using the di(ethylene glycol)ethyl ether acrylate–Cu(DDA) precursor mixture, as described in section 2.1.

A3.2.2 Characterisation

Antibacterial testing was carried out as described in section 2.3.

A3.3 Results

Antibacterial testing showed that the control untreated non-woven polypropylene sheet gave *E. coli* and *S. aureus* bacterial counts of $1.97 \pm 0.13 \times 10^9$ CFU ml⁻¹ at 10⁻⁶ dilution ($n = 3$, standard deviation error) and $7.67 \pm 2.87 \times 10^8$ CFU ml⁻¹ at 10⁻⁶ dilution ($n = 3$, standard deviation error) respectively, Figure A3.3.

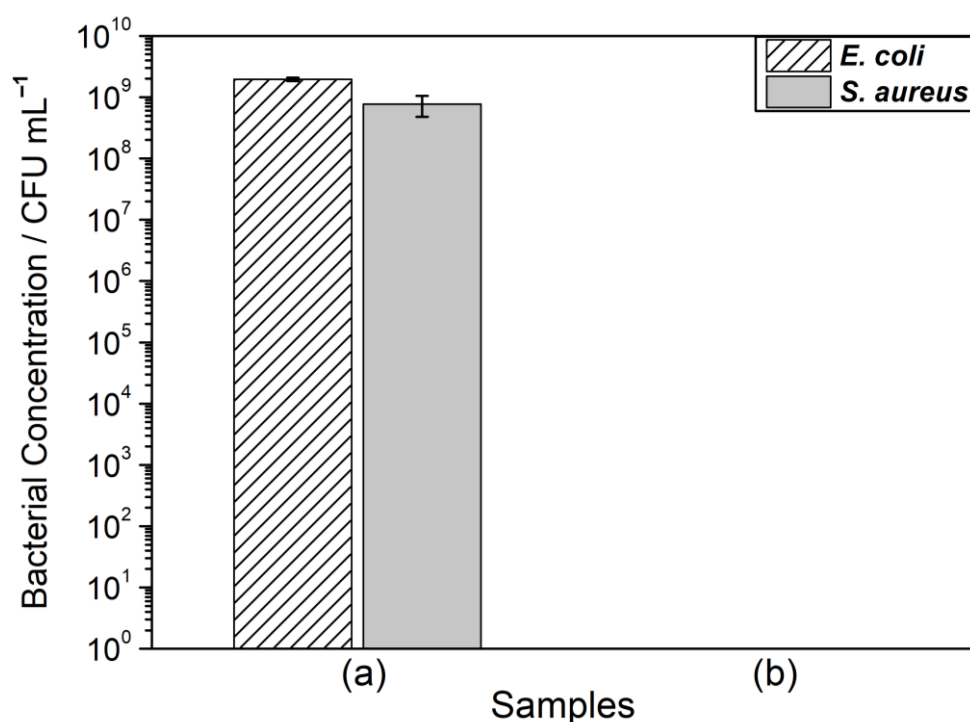


Figure A3.3: Antibacterial activity against *E. coli* (Gram-negative) and *S. aureus* (Gram-positive) bacteria: (a) untreated non-woven polypropylene sheet control; (b) ASPD poly(di(ethylene glycol)ethyl ether acrylate)-bis(dodecylamine) copper dichloride coated polypropylene cloth.

The ASPD poly(di(ethylene glycol)ethyl ether acrylate)-bis(dodecylamine) copper dichloride coated polypropylene cloth showed high activity against both the *E. coli* and *S. aureus*, reducing both bacteria to zero at the 10⁻¹ dilution in 4 h. This equates to Log₁₀ reduction = 8.29 ± 0.03 of *E. coli*, and Log₁₀ reduction = 7.9 ± 0.2 of *S. aureus*.

A3.4 Discussion

ASPD poly(di(ethylene glycol)ethyl ether acrylate)–copper (bis(dodecylamine) copper dichloride) coatings displayed high antibacterial activity (Log_{10} reduction = 8) against both Gram-negative *Escherichia coli* and Gram-positive *Staphylococcus aureus*, Figure A3.3—which easily exceeds the minimal (Log_{10} reduction > 3, in 1 h) set by the US Environmental Protection Agency Office (EPA).⁴¹ A variety of metallosurfactants have been reported in the literature which display a broad spectrum of antimicrobial activities. The antibacterial efficacy can depend on both the head group, as well as the hydrophobic chain.^{42,43} Copper and iron metallosurfactants containing dodecylamine or hexadecyl pyridinium chloride are found to be active against both Gram-positive and Gram-negative bacteria.⁴⁴ Single-chain and double chain chromium(III) metallosurfactant complexes containing dodecylamine and cetylamine have also shown Gram-positive and Gram-negative antibacterial activity combined with antifungal activity.⁴⁵ Double-chain metallosurfactants exhibit greater activity than the single-chain counterparts. The antibacterial mechanism of action of metallosurfactants is reported to be due to interactions between the surfactant tail and the cell membrane, and diffusion of the metallosurfactant into the bacterial cell.⁴⁶ This induces outer membrane damage in *E. coli* and detachment of the plasma membrane from the cell wall in *S. aureus*.⁴⁷ The dependency of antibacterial activity on the type of metal ion includes the metal ion redox chemistry.⁴⁸ Metallosurfactants are also able to interact with and damage bacterial DNA.^{49,50,51}

Whilst previously reported nanocomposite fabrication methods may require multiple steps, removal of solvents or long processing times, atomized-spray-plasma deposition offers the advantages of being one-step, solventless, and fast deposition rates. This makes the nanocomposite coating technique attractive for industrial scale processes such as roll-to-roll for direct conformal application onto electrochemical device components or personal protection equipment.

A3.5 Conclusions

Atomized-spray-plasma deposition has been utilized to deposit poly(di(ethylene glycol)ethyl ether acrylate)–copper (bis(dodecylamine) copper dichloride)

coatings which display high antibacterial activity against both Gram-negative *E. coli* and Gram-positive *S. aureus*.

A3.6 References

- 1 Lavielle, L.; Turck, C.; Loughnot, D.-J. Evolutive Dissipative Structures in Photopolymerized Polyacrylate Films. *J. Phys. Chem. B* **1998**, *102*, 7714–7720.
- 2 Miao, W.; Halloran, J. W.; Brei, D. E. Suspension polymerization casting of lead zirconate titanate, Part II: acrylate system. *J. Mater. Sci.* **2007**, *42*, 8311–8319.
- 3 Wang, Q.; Mynar, J. L.; Yoshida, M.; Lee, E.; Lee, M.; Okuro, K.; Kinbara, K.; Aida, T. High-water-content mouldable hydrogels by mixing clay and a dendritic molecular binder. *Nature* **2010**, *463*, 339–343.
- 4 Gulcev, M. D.; Goring, G. L. G.; Rakic, M.; Brennan, J. D. Reagentless pH-based biosensing using a fluorescently-labelled dextran co-entrapped with a hydrolytic enzyme in sol-gel derived nanocomposite films. *Anal. Chim. Acta* **2002**, *457*, 47–59.
- 5 Chandra, S.; Barola, N.; Bahadur, D. Impedimetric biosensor for early detection of cervical cancer. *Chem. Commun.* **2011**, *47*, 11258–11260.
- 6 Jirimali, H. D.; Nagarale, R. K.; Lee, J. M.; Saravanakumar, D.; Shin, W. Preparation of PEG Tethered Ferrocene Modified Polyacrylic Acid/Silica Composite as an Electroactive Polymeric Platform for Biosensors. *Electroanalysis* **2011**, *23*, 2109–2115.
- 7 Liu, Z.; Robinson, J. T.; Sun, X.; Dai, H. PEGylated Nanographene Oxide for Delivery of Water-Insoluble Cancer Drugs. *J. Am. Chem. Soc.* **2008**, *130*, 10876–10877.
- 8 Lee, J. E.; Lee, N.; Kim, H.; Kim, J.; Choi, S. H.; Kim, J. H.; Kim, T.; Song, I. C.; Park, S. P.; Moon, W. K.; Hyeon, T. Uniform Mesoporous Dye-Doped Silica Nanoparticles Decorated with Multiple Magnetite Nanocrystals for Simultaneous Enhanced Magnetic Resonance Imaging, Fluorescence Imaging, and Drug Delivery. *J. Am. Chem. Soc.* **2010**, *132*, 552–557.
- 9 Chandra, S.; Dietrich, S.; Lang, H.; Bahadur, D. Dendrimer–Doxorubicin conjugate for enhanced therapeutic effects for cancer. *J. Mater. Chem.* **2011**, *21*, 5729–5737.
- 10 Honma, I.; Takeda, Y.; Bae, J. M. Protonic conducting properties of sol-gel derived organic/inorganic nanocomposite membranes doped with acidic functional molecules. *Solid State Ionics* **1999**, *120*, 255–264.
- 11 Chang, H. Y.; Lin, C. W. Proton conducting membranes based on PEG/SiO₂ nanocomposites for direct methanol fuel cells. *J. Membr. Sci.* **2003**, *218*, 295–306.
- 12 Pek, Y. S.; Wan, A. C. A.; Shekaran, A.; Zhuo, L.; Ying, J. Y. A thixotropic nanocomposite gel for three-dimensional cell culture. *Nat. Nanotechnol.* **2008**, *3*, 671–675.
- 13 Lim, Y. T.; Noh, Y.-W.; Cho, J.-H.; Han, J. H.; Choi, B. S.; Kwon, J.; Hong, K. S.; Gokarna, A.; Cho, Y.-H.; Chung, B. H. Multiplexed Imaging of Therapeutic Cells with Multispectrally Encoded Magnetofluorescent Nanocomposite Emulsions. *J. Am. Chem. Soc.* **2009**, *131*, 17145–17154.
- 14 Chan, Y.-S.; Ye, F.; Gallina, M. E.; Zhang, X.; Jin, Y.; Wu, I.-C.; Chiu, D. T. Hybrid Semiconducting Polymer Dot–Quantum Dot with Narrow-Band Emission, Near-Infrared Fluorescence, and High Brightness. *J. Am. Chem. Soc.* **2012**, *134*, 7309–7312.
- 15 Ji, X.; Shao, R.; Elliott, A. M.; Stafford, R. J.; Esparza-Coss, E.; Bankson, J. A.; Liang, G.; Luo, Z.-P.; Park, K.; Markert, J. T.; Li, C. Bifunctional Gold Nanoshells with a

- Superparamagnetic Iron Oxide–Silica Core Suitable for Both MR Imaging and Photothermal Therapy. *J. Phys. Chem. C* **2007**, *111*, 6245–6251.
- 16 Wang, X.; Wang, C.; Cheng, L.; Lee, S.-T.; Liu, Z. Noble Metal Coated Single-Walled Carbon Nanotubes for Applications in Surface Enhanced Raman Scattering Imaging and Photothermal Therapy. *J. Am. Chem. Soc.* **2012**, *134*, 7414–7422.
 - 17 Ma, G.; Yang, D.; Li, Q.; Wang, K.; Chen, B.; Kennedy, J. F.; Nie, J. Injectable hydrogels based on chitosan derivative/polyethylene glycol dimethacrylate/N,N-dimethylacrylamide as bone tissue engineering matrix. *Carbohydr. Polym.* **2010**, *79*, 620–627.
 - 18 Arif Sher Shah, Md. S.; Nag, M.; Kalagara, T.; Singh, S.; Manorama, S. V. Silver on PEG-PU-TiO₂ Polymer Nanocomposite Films: An Excellent System for Antibacterial Applications. *Chem. Mater.* **2008**, *20*, 2455–2460.
 - 19 Chen, Q.; Yue, L.; Xie, F.; Zhou, M.; Fu, Y.; Zhang, Y.; Weng, J. Preferential Facet of Nanocrystalline Silver Embedded in Polyethylene Oxide Nanocomposite and Its Antibiotic Behaviors. *J. Phys. Chem. C* **2008**, *112*, 10004–10007.
 - 20 Patel, N. P.; Miller, A. C.; Spontak, R. J. Highly CO₂-Permeable and Selective Polymer Nanocomposite Membranes. *Adv. Mater.* **2003**, *15*, 729–733.
 - 21 Shao, L.; Chung, T.-S. In situ fabrication of cross-linked PEO/silica reverse-selective membranes for hydrogen purification. *Int. J. Hydrogen Energy* **2009**, *34*, 6492–6504.
 - 22 Xiao-e, L.; Green, A. N. M.; Haque, S. A.; Mills, A.; Durrant, J. R. Light-driven oxygen scavenging by titania/polymer nanocomposite films. *J. Photochem. Photobiol. A* **2004**, *162*, 253–259.
 - 23 Barichard, A.; Galstian, T.; Israeli, Y. Influence of CdSe/ZnS Quantum Dots in the Polymerization Process and in the Grating Recording in Acrylate Materials. *J. Phys. Chem. B* **2010**, *114*, 14807–14814.
 - 24 Barichard, A.; Galstian, T.; Israeli, Y. Physico-chemical role of CdSe/ZnS quantum dots in the photo-polymerization process of acrylate composite materials. *Phys. Chem. Chem. Phys.* **2012**, *14*, 8208–8216.
 - 25 Dietrich, S.; Schulze, S.; Hietschold, M.; Lang, H. Au nanoparticles stabilised by PEGylated low generation PAMAM dendrimers: Design, characterisation and properties. *J. Colloid Interface Sci.* **2011**, *359*, 454–460.
 - 26 Yasuda, H. *Plasma Polymerization*; Academic Press: New York, 1985.
 - 27 Hutton, S. J.; Crowther, J. M.; Badyal, J. P. S. Complexation of Fluorosurfactants to Functionalized Solid Surfaces: Smart Behavior. *Chem. Mater.* **2000**, *12*, 2282–2286.
 - 28 Ryan, M. E.; Hynes, A. M.; Badyal, J. P. S. Pulsed Plasma Polymerization of Maleic Anhydride. *Chem. Mater.* **1996**, *8*, 37–42.
 - 29 Harris, L. G.; Schofield, W. C. E.; Doores, K. J.; Davis, B. G.; Badyal, J. P. S. Rewritable Glycochips. *J. Am. Chem. Soc.* **2009**, *131*, 7755–7761.
 - 30 Tarducci, C.; Schofield, W. C. E.; Badyal, J. P. S.; Brewer, S. A.; Willis, C. Cyano-Functionalized Solid Surfaces. *Chem. Mater.* **2001**, *13*, 1800–1803.
 - 31 Tarducci, C.; Kinmond, E. J.; Badyal, J. P. S.; Brewer, S. A.; Willis, C. Epoxide-Functionalized Solid Surfaces *Chem. Mater.* **2000**, *12*, 1884–1889.

- 32 Teare, D. O. H.; Barwick, D. C.; Schofield, W. C. E.; Garrod, R. P.; Ward, L. J.; Badyal, J. P. S. Substrate-Independent Approach for Polymer Brush Growth by Surface Atom Transfer Radical Polymerization. *Langmuir* **2005**, *21*, 11425–11430.
- 33 Schofield, W. C. E.; McGettrick, J.; Bradley, T. J.; Badyal, J. P. S.; Przyborski, S. Rewritable DNA Microarrays. *J. Am. Chem. Soc.* **2006**, *128*, 2280–2285.
- 34 Tarducci, C.; Badyal, J. P. S.; Brewer, S. A.; Willis, C. Diels–Alder chemistry at furan ring functionalized solid surfaces. *Chem. Commun.* **2005**, 406–408.
- 35 Coulson, S. R.; Woodward, I. S.; Badyal, J. P. S.; Brewer, S. A.; Willis, C. Ultralow Surface Energy Plasma Polymer Films. *Chem. Mater.* **2000**, *12*, 2031–2038.
- 36 Limb, S. J.; Gleason, K. K.; Edell, D. J.; Gleason, E. F. Flexible fluorocarbon wire coatings by pulsed plasma enhanced chemical vapor deposition. *J. Vac. Sci. Technol.* **1997**, *A15*, 1814.
- 37 Wang, J. H.; Chen, J. J.; Timmons, R. B. Plasma Synthesis of a Novel CF₃-Dominated Fluorocarbon Film. *Chem. Mater.* **1996**, *8*, 2212–2214.
- 38 Friedrich, J. Mechanisms of Plasma Polymerization – Reviewed from a Chemical Point of View. *Plasma Processes Polym.* **2011**, *8*, 783–802.
- 39 Ward, L. J.; Schofield, W. C. E.; Badyal, J. P. S.; Goodwin, A. J.; Merlin, P. J. Atmospheric Pressure Glow Discharge Deposition of Polysiloxane and SiO_x Films. *Langmuir* **2003**, *19*, 2110–2114.
- 40 Ward, L. J.; Schofield, W. C. E.; Badyal, J. P. S.; Goodwin, A. J.; Merlin, P. J. Atmospheric Pressure Plasma Deposition of Structurally Well-Defined Polyacrylic Acid Films. *Chem. Mater.* **2003**, *15*, 1466–1469.
- 41 Protocol for the Evaluation of Bactericidal Activity of Hard, Non-porous Copper/Copper-Alloy Surfaces. US Environmental Protection Agency Office. 3rd February 2015.
- 42 Kanazawa, A.; Ikeda, T.; Endo, T. Polymeric Phosphonium Salts as a Novel Class of Cationic Biocides. VII. Synthesis and Antibacterial Activity of Polymeric Phosphonium Salts and Their Model Compounds Containing Long Alkyl Chains. *J. Appl. Polym. Sci.* **1994**, *53*, 1237–1244.
- 43 Colomer, A.; Pinazo, A.; Manresa, M. A.; Vinardell, M. P.; Mitjans, M.; Infante, M. R.; Pérez, L. Cationic Surfactants Derived from Lysine: Effects of Their Structure and Charge Type on Antimicrobial and Hemolytic Activities. *J. Med. Chem.* **2011**, *54*, 989–1002.
- 44 Hafiz, A. A. Crystal Structure of Benzyl Triphenyl Phosphonium Chlorometallate: Some Surface and Biological Properties of Their Metallosurfactant Derivatives. *J. Iran. Chem. Soc.* **2008**, *5*, 106–114.
- 45 Kumaraguru, N.; Santhakumar, K. Synthesis, Characterisation, Critical Micelle Concentration Determination, and Antimicrobial Studies of Some Complexes of Chromium(III) Metallosurfactants. *J. Coord. Chem.* **2009**, *62*, 3500–3511.
- 46 Veeralakshmi, S.; Nehru, S.; Arunachalam, S.; Kumar, P.; Govindaraju, M. Study of Single and Double Chain Surfactant-Cobalt(III) Complexes and Their Hydrophobicity, Micelle Formation, Interaction with Serum Albumins and Antibacterial Activities. *Inorg. Chem. Front.* **2014**, *1*, 393–404.

- 47 Kaur, G.; Kumar, S.; Kant, R.; Bhanjana, G.; Dilbaghi, N.; Guru, S. K.; Bhushan, S.; Jaglan, S. One-Step Synthesis of Silver Metallosurfactant as an Efficient Antibacterial and Anticancer Material. *RSC Adv.* **2016**, *6*, 57084–57097.
- 48 Kaur, G.; Garg, P.; Kaur, B.; Chaudhary, G. R.; Kumar, S.; Dilbaghi, N.; Hassan, P. A.; Aswal, V. K. Synthesis, Thermal and Surface Activity of Cationic Single Chain Metal Hybrid Surfactants and Their Interaction with Microbes and Proteins. *Soft Matter* **2019**, *15*, 2348–2358.
- 49 Sharma, B.; Kaur, G.; Chaudhary, G. R.; Gawali, S. L.; Hassan, P. A. High Antimicrobial Photodynamic Activity of Photosensitizer Encapsulated Dual-Functional Metallocatanionic Vesicles against Drug-Resistant Bacteria *S. aureus*. *Biomater. Sci.* **2020**, *8*, 2905–2920.
- 50 Kanazawa, A.; Ikeda, T.; Endo, T. Polymeric Phosphonium Salts as a Novel Class of Cationic Biocides. VII. Synthesis and Antibacterial Activity of Polymeric Phosphonium Salts and Their Model Compounds Containing Long Alkyl Chains. *J. Appl. Polym. Sci.* **1994**, *53*, 1237–1244.
- 51 Kumar, R. S.; Arunachalam, S. Synthesis, Micellar Properties, DNA Binding and Antimicrobial Studies of Some Surfactant-Cobalt(III) Complexes. *Biophys. Chem.* **2008**, *136*, 136–144.

Appendix 4

A4.1 Introduction

A hydrophilic-oleophobic switchable surface coating has been developed by Angus Ritchie (Badyal group, Department of Chemistry, University of Durham).¹ The coating consists of a polymer–nanoparticle–fluorosurfactant complex; the polymer used is cationic quaternary ammonium compound poly(diallyldimethyl ammonium chloride). Therefore, in this chapter, the antibacterial activities of these switchable coatings are examined.

A4.2 Experimental

A4.2.1 Polymer–Particle–Fluorosurfactant Complex Coatings

Poly(diallyldimethyl ammonium chloride) (4 ml, PDDA; 20 wt% in H₂O, Sigma-Aldrich Ltd.) was diluted with high-purity water (36 ml), and shaken for 2 h. For coatings containing silica nanoparticles, the silica nanoparticles (1.2 g, surface charge: negative, average particle size = 7 nm, Degussa Aerosil® 300) were added to the solution, then sonicated for 1 h, then shaken for 1 h. Anionic fluorosurfactant (0.5 ml, Capstone FS-63, DuPont Ltd.) was diluted with high-purity water (9.5 ml) The fluorosurfactant solution was added dropwise to the polymer solution. Once added, the mixture was shaken for 1 h. Lids were removed from the containers, and the water was allowed to evaporated overnight. The next day, the containers were heated at 110 °C for several hours to drive off any remaining water. The dried solid was rinsed in a minimum amount of water and dried again at 110° for several hours. The resultant solid was weighed out and dissolved in ethanol to give a 1% w/v solution of the polymer–fluorosurfactant or polymer–nanoparticle–fluorosurfactant complex. The coating solution was then applied to non-woven polypropylene cloth (0.41 mm thick, 22.7 ± 4.4 µm fibre diameter, with dimpled structure 0.68 ± 0.16 mm separation, spunbond, 70 g m⁻², Avoca Technical Ltd.) by spray coating using a pressurised spray gun (RG-3L, Anest Iwata Inc.).

A4.2.2 Antibacterial Testing

Antibacterial testing of the poly(diallyldimethylammonium)–anionic fluorosurfactant complex coated cloths and poly(diallyldimethylammonium)–3% w/v silica (7 nm)–anionic fluorosurfactant coated cloths was carried out as described in 2.3, with the modification that samples treated with bacteria inoculum were incubated for 16 h, not 4 h.

A4.3 Results

Poly(diallyldimethylammonium)–anionic fluorosurfactant complex spray coated onto non-woven polypropylene cloth showed excellent antibacterial activities against both *E. coli* and *S. aureus*, showing complete killing of both (Log_{10} Reduction = 8.53 ± 0.04 and 8.39 ± 0.07 respectively), Figure A4.1. The poly(diallyldimethylammonium)–3% w/v silica (7 nm)–anionic fluorosurfactant spray coated onto non-woven polypropylene cloth showed lower antibacterial activity against *E. coli* (Log_{10} Reduction = 5.3 ± 0.4), and complete reduction of *S. aureus* (Log_{10} Reduction = 8.39 ± 0.07).

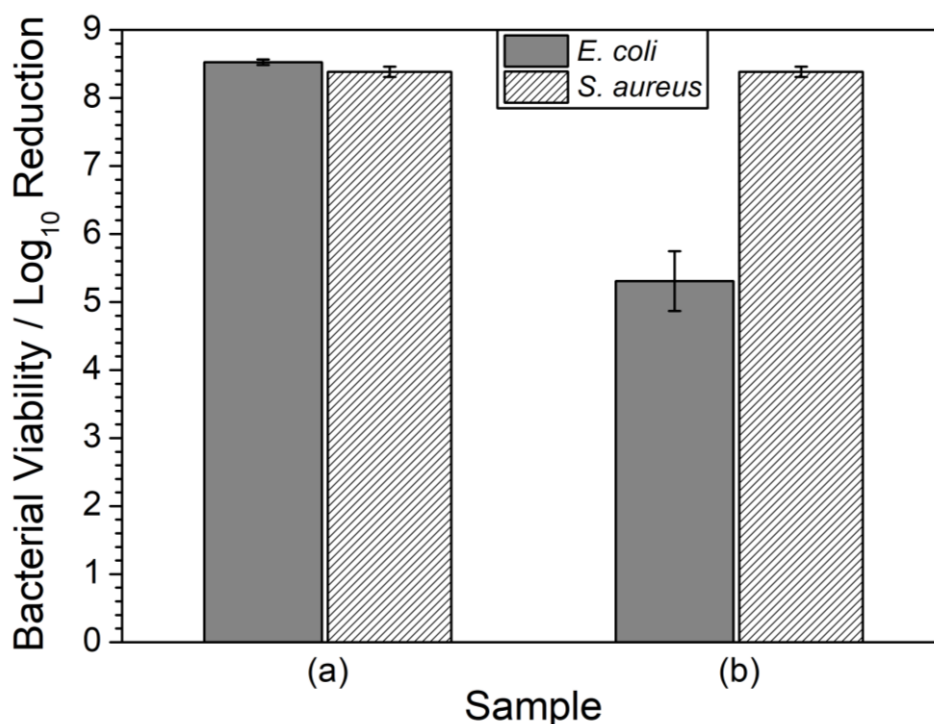


Figure A4.1: Antibacterial activity against *E. coli* and *S. aureus*: (a) poly(diallyldimethylammonium)–anionic fluorosurfactant complex spray coated non-woven polypropylene cloth; and (b) poly(diallyldimethylammonium)–3% w/v silica (7 nm)–anionic fluorosurfactant spray coated non-woven polypropylene cloth. Log_{10} Reduction values are calculated relative to the untreated substrate (mean \pm standard deviation).

A4.4 Discussion

The poly(diallyldimethylammonium)–3% w/v silica (7 nm)–anionic fluorosurfactant complex coating showed lower antibacterial activity against *E. coli* than the poly(diallyldimethylammonium)–anionic fluorosurfactant complex. This may be caused by the silica nanoparticles increasing the surface roughness thus lowering available anchoring points for bacteria attachment (reduction in available area of contact with the bacteria's outer surface²). The differences between *E. coli* and *S. aureus* killing for the poly(diallyldimethylammonium)–3% w/v silica (7 nm)–anionic fluorosurfactant complex coating may be due to the difference in sizes of the bacteria, or the differences in the outer cell structure of the two species.³

A4.5 Conclusions

Poly(diallyldimethylammonium)–anionic fluorosurfactant complex and poly(diallyldimethylammonium)–3% w/v silica (7 nm)–anionic fluorosurfactant complex spray-coated onto non-woven polypropylene cloth show strong antibacterial activities against *E. coli* and *S. aureus*.

A4.6 References

- 1 Ritchie, A. W.; Cox, H. J.; Barrientos-Palomo, S. N.; Sharples, G. J.; Badyal, J. P. S. Bioinspired Multifunctional Polymer–Nanoparticle–Surfactant Complex Nanocomposite Surfaces for Antibacterial Oil–Water Separation. *Colloids Surfaces A Physicochem. Eng. Asp.* **2019**, *560*, 352–359.
- 2 Bagherifard, S.; Hickey, D. J.; de Luca, A. C.; Malheiro, V. N.; Markaki, A. E.; Guagliano, M.; Webster, T. J. The Influence of Nanostructured Features on Bacterial Adhesion and Bone Cell Functions on Severely Shot Peened 316L Stainless Steel. *Biomaterials* **2015**, *73*, 185–197.
- 3 Sonohara, R.; Muramatsu, N.; Ohshima, H.; Kondo, T. Difference in Surface Properties Between *Escherichia coli* and *Staphylococcus aureus* as Revealed by Electrophoretic Mobility Measurements. *Biophys. Chem.* **1995**, *55*, 273–277.